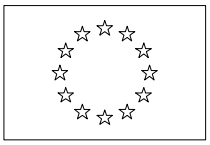

EUROPEAN COMMISSION
5th EURATOM FRAMEWORK PROGRAMME 1998-2002
KEY ACTION : NUCLEAR FISSION

ADS Nuclear Data

FIKW-CT-2000-00107

Final Report of the n_TOF-ND-ADS Project
Deliverable 25

Edited by
A Mengoni (n_TOF-ND-ADS Project Co-ordinator, CERN)

with contributions by
F Käppeler (FZK, Karlsruhe)
F Gunsing (CEA, Saclay)
D Cano-Ott, C Guerrero, and E Gonzalez (CIEMAT, Madrid)
A Plompen (IRRM, Geel)
G Rudolf (IN2P3, Strasbourg)
P Assimakopoulos (University of Ioannina, Ioannina)
R Marques (LIP, Coimbra)
H Leeb (TUW, Vienna)
V Vlachoudis (CERN, Geneva)

Reporting Period: Full

Dissemination level : PU, S/T- 003
PU: Public
S/T: Scientific/Technical reports

PARTNERS of the n_TOF-ND-ADS Project (FIKW-CT-2000-107)

1	**CERN** Co-ordinator	European Organization for Nuclear Research	Switzerland
2	**FZK**	Forschungszentrum Karlsruhe	Germany
3	**IRMM**	Institute for Reference Materials and Measurements – JRC	Belgium
4	**IN2P3**	Institute National de Physique Nucleare et de Physique de Particules – CNRS	France
5	**CEA**	Commissariat a l'Energie Atomique	France
6	**LIP**	Laboratorio de Instrumentacao e Fisica Experimental de Particules	Portugal
7	**INFN**	Istituto Nazionale di Fisca Nucleare	Italy
8	**PVA**	Universita' degli Studi di Pavia	Italy
9	**TUW**	Technische Universitaet Wien	Austria
10	**APC**	Astro-Particle Cosortium (UoI, UoA, NTUA, NSRC, DUTh, AUTh)	Greece
11	**CIEMAT**	Centro de Investigaciones Enrgeticas Mediambientales y Tecnologicas	Spain
12	**CSIC**	Consejo Superior de Investigaciones Cientificas	Spain
13	**UPM**	Universitad Politecnica de Madrid	Spain
14	**USE**	Universitad de Sevilla	Spain
15	**USDC**	Universitad de Santiago de Compostella	Spain
16	**UPC**	Universitad Politecnica de Catalunya	Spain

EURATOM FP5 Project
n_TOF-ND-ADS

Contract No. FIKW-CT-2000-00107

Final Report

Deliverable 25

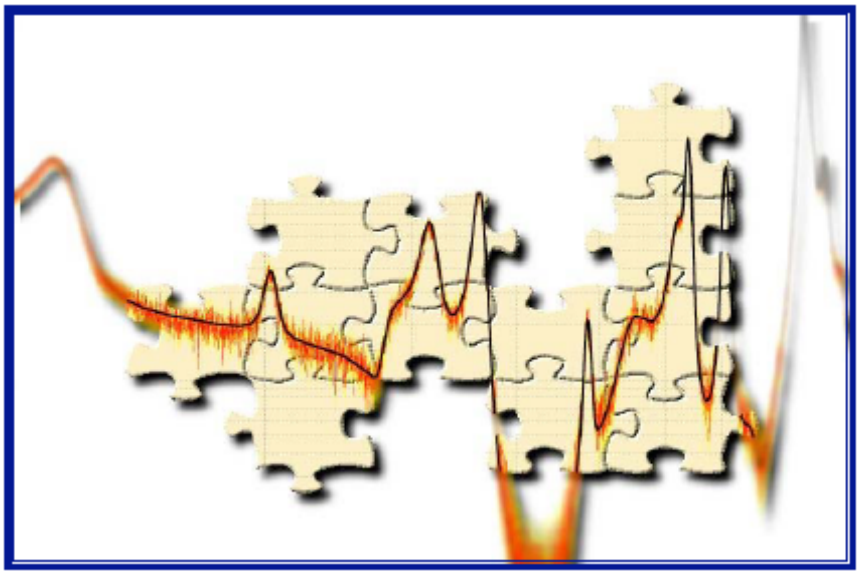

Revision 1.0

February

TABLE OF CONTENTS

Executive Summary

The design of innovative accelerator driven systems (ADS) for incineration of nuclear waste and energy generation requires the complete knowledge of basic cross sections for neutron induced processes. For design purposes, these data need to be derived in a consistent, accurate and cost-effective way, to be evaluated and made available in a way compatible with simulation tools and industry practices in general. The main goal of the n_TOF-ND-ADS Project has been to produce and disseminate high precision cross section data for the majority of the isotopes relevant to the waste incineration and the ADS design. This included capture and fission cross sections for the minor actinides, capture cross sections for the main fission products and (n,xn) reactions for structural and coolant materials. These objectives have been obtained by using three core technologies: an innovative high-energy spallation source built at CERN (the CERN n_TOF facility), high performance detectors and DAQ systems, and state-of-the-art computer engineering.

In this report, a description of the design studies, the realization, and performances of the CERN neutron time-of-flight facility is given together with an overview of all the experimental devices developed for measurements of high-resolution neutron cross section data. A brief account of all the measurements performed at n_TOF in its commissioning phase and in the three experimental campaigns performed in 2002, 2003 and 2004 is given.

The full list of the isotopes for which the neutron cross section measurements have been performed at n_TOF in the framework of the n_TOF-ND-ADS Project is the following:

Capture

^{151}Sm
^{204,206,207,208}Pb, ^{209}Bi
^{232}Th
^{24,25,26}Mg
^{90,91,92,94,96}Zr, ^{93}Zr
^{139}La
^{233,234}U
^{237}Np,^{240}Pu,^{243}Am

Fission

^{233,234,235,236,238}U
^{232}Th
^{209}Bi
^{237}Np
^{241,243}Am, ^{245}Cm

In addition to the n_TOF facility at CERN, facilities already available in Europe have been used for relevant measurements. These facilities included the Institute for Reference Material and Measurements of the Joint Research Center at Geel (Belgium), the Van de Graaff accelerator facility of the Forschungszentrum Karlsruhe (Germany), the Demokritos facility at the National Center of Scientific Research in Athens (Greece), and the Laboratório de Instrumentação e Física Experimental de Partículas at the University of Coimbra (Portugal). Activities performed at these facilities within the framework of the n_TOF-ND-ADS Project included measurements of neutron induced cross sections data and related detector developments, an account of which is presented here.

A description of the nuclear data evaluation tools developed within the framework of the Project and a description of the software platform for the dissemination of the results of the measurements is presented.

The n_TOF-ND-ADS Project involved the direct participation of 16 European research establishments. In addition, a collaboration (“The n_TOF Collaboration”) involving 41

research teams and over 120 researchers has been established around the Project's activities. The teams included participants from the USA and Japan as well as Europeans.

The n_TOF-ND-ADS Project has been an integral part of the BASTRA ("basic studies for transmutation") cluster activities. BASTRA included, in addition to n_TOF-ND-ADS, the HINDAS ("high and intermediate energy nuclear data for accelerator-driven systems"), and the MUSE ("multiplication avec sources externes"). The activity of this cluster spans from experiments devoted to the understanding of the neutronics of sub-critical systems to high-accuracy measurements of neutron cross sections for long-lived fission products and minor actinides as well as the development of reliable nuclear reaction models for the description of high-energy spallation processes, and the generation and dissemination of evaluated nuclear data libraries.

Introduction

The present report provides a description of the means utilized and activities performed to reach the main objectives of the n_TOF-ND-ADS Project. The report is organized as follows: here below a summary of the work packages which constitute the basic project structure are reported. Then, a general description of the CERN n_TOF facility is presented with some details on its main characteristics and experimental equipments. This is followed by a description of the experimental activities performed at CERN n_TOF. The activities performed at other facilities, notably IRMM (Geel, Belgium), FZK (Karlsruhe, Germany), LIP (Coimbra, Portugal), and Democritos (Athens, Greece) are reported in the subsequent section. A brief report on the nuclear data evaluation and dissemination activities are reported before the conclusions.

n_TOF-ND-ADS Project Structure

The n_TOF-ND-ADS project is structured in **19 Work-packages** listed here below (lead Contractor in bracket). A brief summary of the tasks performed for each WP is given in the list. A detailed description of the technical performances of the work performed within the framework of the project for each work-package has been given in the reports submitted to the European Commission during the period November 2000-December 2004.

WP1 (CERN): installation and operation of a high intensity and high resolution neutron beam with low ambient neutron background, and setting-up of the necessary infrastructure for the experimentation with a variety of target and detector configurations. Installation of the counting room for electronics, spare detectors, computers and data acquisition system.

WP2 (APC): realization of a highly flexible and adaptable DAQ that accommodates the various detector requirements without any loss of efficiency, pile-up or dead time, in an effective user-friendly programmable environment.

WP3 (INFN): design and construction of the neutron monitoring detectors necessary for the measurements of the neutron beam characteristics of WP10 and for monitoring the stability of the neutron beam.

WP4 (CIEMAT): design of a neutron time-of-flight beam of well-defined profile, of the experimental area and of the neutron escape line.

WP5 (CEA): design, construction, commissioning and operation of a set of C_6D_6 detectors for the determination of the capture cross-sections.

WP6 (CMBR): Monte Carlo simulation and design of a liquid noble gas prototype detector with development and operation of large-area gaseous photomultipliers with CsI photocathode.

WP7 (FZK): design, Monte Carlo simulations of the detector array, and construction of a total absorption calorimeter.

WP8 (IN2P3): design and construction of a set of 10 PPAC fission detectors.

WP9 (PVA): determine by means of simulations, together with the required accuracy, the relative importance of the different isotopes, in the incineration of nuclear waste different ADS designs and fuels.

WP10 (APC): experimental determination of the quantities characterizing the n_TOF neutron beam and validation of the experimental techniques used in all of the planned cross section measurements.

WP11 (FZK): measurement of the capture cross sections of the isotopes ^{151}Sm, ^{129}I, ^{99}Tc, ^{79}Se, ^{206,207,208}Pb, and ^{209}Bi. The measurement of ^{79}Se could not be performed because of the impossibility to locate a ^{79}Se sample. This measurement has been substituted with the capture cross section measurement of ^{93}Zr for which a suitable sample has been obtained.

WP12 (CEA): determination of the capture cross sections of ^{232}Th, ^{231}Pa, ^{233}U, ^{234}U, and ^{236}U, relevant in the Th-fuel cycle. The ^{232}Th capture cross section measurement has been performed during the 2nd period. The measurement of the ^{231}Pa could not be performed because of the impossibility to obtain a suitable sample. The ^{233,234}U measurements have been performed in 2004 with the n_TOF TAC. The ^{236}U measurement has been performed at GELINA.

WP13 (CIEMAT): determination of the capture cross sections of ^{237}Np, ^{240}Pu, ^{242}Pu, ^{241,243}Am, and ^{245}Cs relevant in the incineration of transuranic waste. These measurements required the 4π total absorption calorimeter and have performed in 2004 after the completion of the n_TOF TAC. A suitable sample of ^{245}Cm for the capture measurement could not be located. The measurements of ^{242}Pu and ^{241}Am could not be performed because of the safety regulations at CERN did not allow the use of the samples obtained for the measurement (the masses of these samples exceeded the amounts permitted). These measurements could be performed in a second experimental area which is in a design phase (2006).

WP14 (IN2P3): measurement of the fission cross sections for the most important transuranic isotopes: ^{237}Np, ^{231}Pa, ^{241}Am, ^{243}Am, ^{244}Cm, and ^{245}Cm and of the relevant isotopes of the Th-fuel cycle: ^{232}Th, ^{233}U, ^{234}U, and ^{236}U. The isotopes related to the Th/U fuel cycle have been measured during the course of the 2003 experimental campaign with two independent setups: the PPAC and FIC (fast ionization chamber) detectors. The measurements of the highly active MA (^{241}Am, ^{243}Am, and ^{245}Cm) has been performed with the FIC setup.

WP15 (IRMM): perform, at GELINA, transmission measurements of the isotopes ^{129}I, ^{237}Np, ^{240}Pu, ^{242}Pu and capture measurements for ^{237}Np, ^{129}I.

WP16 (IN2P3): develop the necessary digital electronics and perform (n,xn) cross section measurements for ^{233}U, ^{239}Pu, ^{241}Pu, and ^{207}Pb at n_TOF and, using the activation technique, for ^{232}Th, ^{237}Np, ^{241}Am, and ^{231}Pa, at other facilities. Attempts to perform (n,xn) cross section measurements at n_TOF have been performed during the 2003 campaign. Measurements at GELINA and at Leuven have been performed during the course of 2004.

WP17 (FZK): perform calibration measurements of fission cross sections, of the capture cross sections of ^{135}Cs and ^{137}Cs using activation technique, as well as the capture cross sections of ^{233}U, ^{79}Se, and ^{151}Sm. These measurements have been performed at FZK with the Karlsruhe setup.

WP18 (TUW): aims at providing the measured n_TOF cross sections to the international nuclear data community and to make the data accessible to the users soon after the measurements, using standard evaluations and modeling procedures. The full evaluation of the experimental data obtained within the framework of the n_TOF-ND-ADS project with its associated critical comparison with existing (when possible) data requires an amount of time and effort which goes beyond the framework established by the project. This work will be done in the frame of international cooperation projects and other initiatives in the years following the completion of the Project.

WP19 (APC/CERN): development and initial operation of a platform for dissemination and easy access by Industry and Academia of evaluated neutron cross section data. A prototype of the n_TOF data dissemination platform is operation and available on the network at the link: http://www.cern.ch/n_TOF. The inclusion of all the information derived and obtained during

the period of the project has started. The database is an open tool which will be more and more complete as the final analysis of the experimental data will be terminated and the related documentation made available.

As mentioned above, a full account of the activities performed within the project framework includes the various publications and reports produced during the project activity. In the following sections we provide detailed information on the most relevant tasks completed during the curse of the activities.

The n_TOF facility & Experimental setup

Overview and Proton Beam Line

The spallation mechanism is a remarkably powerful source of neutrons. At the proton energy of 20 GeV of the CERN PS accelerator, about 300 neutrons are produced per proton within the n_TOF target spallation module. The fact that pulses of up to $7x10^{12}$ protons are delivered to the n_TOF facility at a nominal repetition rate of 0.4 Hz and with a very short pulse width of 7 ns r.m.s. makes up for an extraordinarily prolific neutron source with a tremendous potential for accurate, high resolution time of flight (TOF) measurements covering a unique range in neutron energy from thermal to several GeV.
The neutrons produced by spallation in a lead block surrounded by a water moderator are canalized through an evacuated flight path to an experimental area ~ 185 m downstream of the target, making use of the existing TT2-A tunnel (see Figure 1).

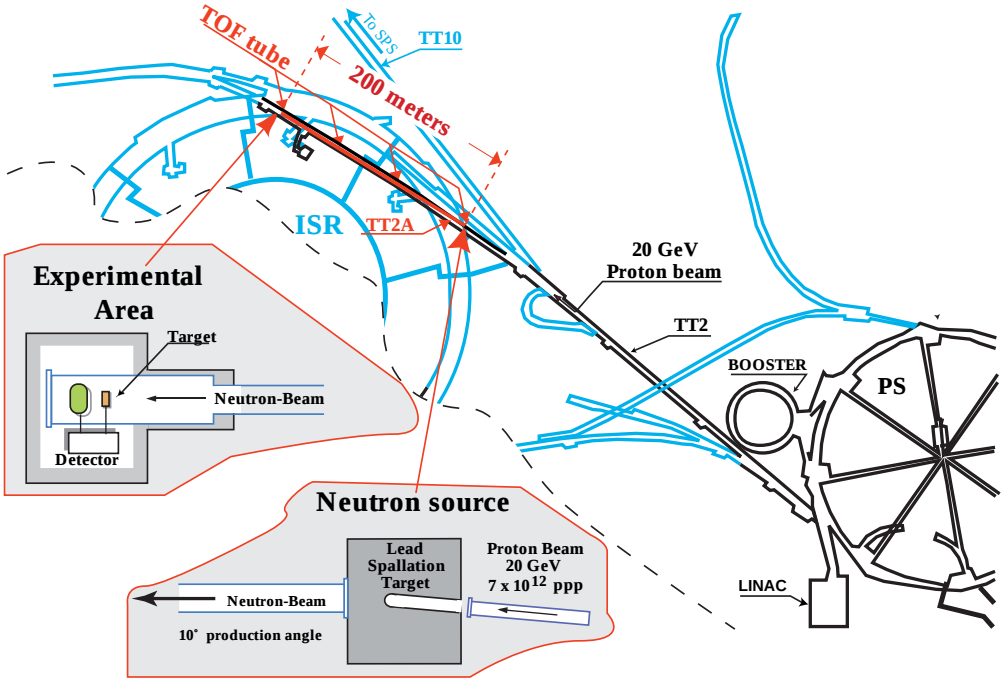

Figure 1: General layout of the experiment. The proton beam is extracted via the TT2 transfer line and hits the lead target. At the end of the TOF tunnel (TT2-A), neutrons are detected about 185 m from the primary target.

The main characteristics of the proton beam are:
- a momentum of 20 GeV/c, corresponding to the maximum attainable energy within a magnetic cycle of 1.2 s of the proton synchrotron (PS);
- proton bunches of $7x10^{12}$ particles with a width of 7 ns r.m.s;
- up to six bunches per supercycle of typically 16.8 s. Of these, up to five bunches per supercycle can be used due to limitations in the maximum power dissipation allowed on the spallation target and in the radiation level in the target area.

The beam is extracted from the PS and sent onto the spallation target by using a fast extraction system. In terms of peak intensity, the proton beam for n_TOF can be considered as a record for the PS thanks to a special compression procedure, by which the original pulse width of 13 ns is reduced to 7 ns (for a technical description see .

The facility can be operated in two ways, in dedicated and – with somewhat reduced intensity - in parasitic mode. In dedicated mode one or more bunches per supercycle are delivered to the n_TOF target with the full nominal intensity of 7×10^{12} protons/bunch. In parasitic mode, the n_TOF bunch is accelerated together with a bunch of much lower intensity, which is slow-extracted at 24 GeV/c to another experimental area. Though the pulse width of the n_TOF bunch could be kept at 7 ns r.m.s by using the fast extraction feature, the intensity is limited to $\sim 4\times10^{12}$ protons/bunch. The advantage is that the parasitic mode is available at almost all times, which leads to a significantly increased efficiency of the n_TOF schedule.

The Spallation target

The choice of the specific geometry of the spallation target is a compromise between several parameters. On one hand, there is the choice between neutron flux and neutron energy resolution, related to fluctuations in the neutron moderation path. On the other hand, the requirements on the dimension of the neutron beam and its halo at the detector station imply strong constraints on the lateral size of the spallation target and on the collimation of the neutron beam. Finally, the energy dependence of the neutron spectrum depends also on the dimensions of the spallation target.

We have performed an overall optimization on the size of a cylindrical spallation target of length h and radius R, followed by a water moderator of thickness d, which is added in order to improve the resolution in neutron energy. All calculations assumed a proton beam intensity of 7×10^{12} ppp at 20 GeV/c.

The spallation cascade is directed forward and spreads out over a large volume. Spallation neutrons emanating from the cascade slow down through isolethargic moderation, which is naturally achieved within a volume of radius R and length h. Since a target with a larger radius would contain a larger fraction of the lateral component of the spallation cascade and its outer layer would act as reflecting cavity, it would also provide a higher neutron flux. A target of smaller radius would produce a smaller neutron flux but with a harder neutron energy spectrum due to the reduced mean moderation path of the neutrons. On the other hand, the influence of the target length, h, on the neutron flux exiting the downstream surface is an interface between the containment of the longitudinal component of the spallation cascade, i.e. the proton to neutron conversion efficiency, and the loss of neutrons due to the reduction in solid angle by the beam-downstream surface of the target.

In both cases, the uncertainty due to the moderation path fluctuations is reduced by the thin water layer in a similar way. However, the smaller target involves shorter moderation paths and consequently a smaller uncertainty. Therefore, a smaller spallation target would provide better precision in the neutron TOF determination at the price of a reduced neutron flux. Hence, the optimization of the target size had to consider the interplay between the resulting neutron flux and the sharpness in determining the neutron energy by TOF.

Good experimental conditions at the detector station require a neutron beam with a well-defined spot of homogeneous neutron flux density and the absence of a penumbra or halo around this beam spot. In particular, for the experiments using a 4π total absorption calorimeter the small size of the neutron beam and the beam penumbra are crucial. In a realistic set-up the size of the penumbra depends directly on the lateral size of the spallation target, vanishing only for a point-like target. For an extended spallation target only a complex system of double collimators can minimize the size of this halo.

By means of the FLUKA [1] and the EA-MC 0 programs, all physical processes were simulated for different sizes of the cylindrical lead target followed by a thin (5 cm) water moderator. The optimum geometry with respect to a high neutron flux and a high neutron energy resolution was found to correspond to a target radius R = 40 cm and to a length h = 40 cm. The optimal thickness of the water moderator is 4 cm. The actual design of the lead spallation target differs slightly from the above values for practical reasons. A detailed description of the properties of the lead spallation target can be found in reference [3].

The simulations for the real geometry of the target provided also detailed information the flux and its spectral function at the exit of the water moderator and in the experimental area at the end if the flight path.

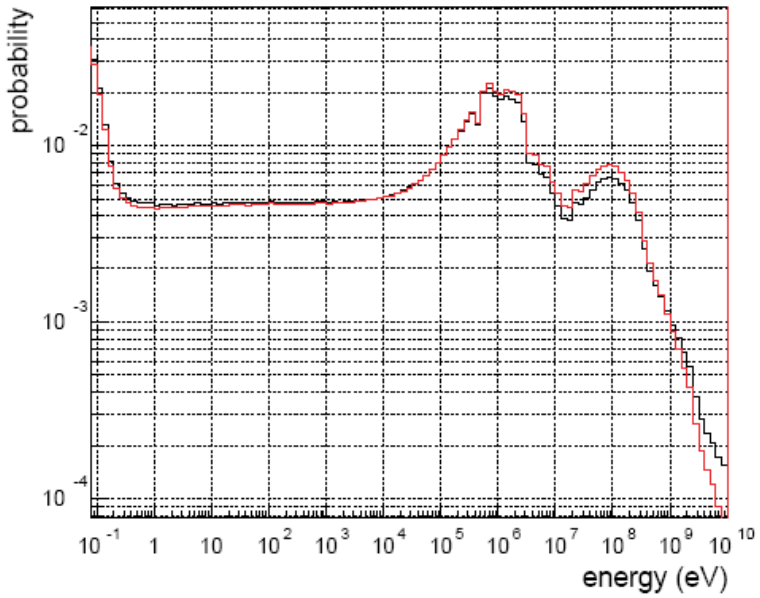

Figure 2: Energy distribution (normalized to unit area) of the neutrons at the exit of the Pb target after the water moderator (black) and at the sample position in the experimental area (red).

Figure 2 shows that 38% of the neutrons emerge from the water moderator with energies below 0.3 eV. The range from 0.3 eV to 20 keV accounts for 23% of all neutrons and evidences an almost exact isolethargic behavior as a consequence of the moderation in the water. However, there is still a significant fraction of 32% of the neutrons having energies between 20 keV and 20 MeV, and a further 7% at neutron energies above 20 MeV. The two spectra in Figure 2 show small deviations in the high energy region. This hard component, the signature of the spallation reactions, differs substantially from those of alternative neutron production mechanisms at other neutron TOF facilities, and has important consequences for the design of collimators and shielding elements.

Target zone

The target zone is the most demanding part of the TOF project since it requires not only the critical coupling of the water moderator with the vacuum of the TOF tube by means of a special window, but also a sophisticated shielding and a highly performing removal procedure. The target zone is surrounded by marble and concrete blocks, some molded and fixed and some removable to give access to the area. Marble has the advantage over concrete in that it becomes less radioactive.

The fixed part of the shielding is made with concrete loaded with 1% of boron in order to capture neutrons outside of the direction of the time of flight tube more efficiently. This shielding is shown in Figure 3. The target is placed and removed from the pool through a vertical shaft 1.3 m in diameter (Figure 4) to a gallery above. After irradiation the target could be placed in a concrete repository located near the top of the shaft or transported to a storage zone to be defined in agreement with the recommendations of TIS (Radioprotection). The

lead target is mounted in a stainless steel support frame (Figure 5), which is an integral part of the whole target assembly.
The lead for the target was taken from the TARC experiment [4]. Pure lead (99.99%) was chosen to ensure that impurities have a negligible effect on the neutron flux. Although the target size optimization favoured a circular cross section in the beam direction, a square shape of 80x80 cm^2 was eventually constructed because of the extreme difficulty to machine lead to a round shape.

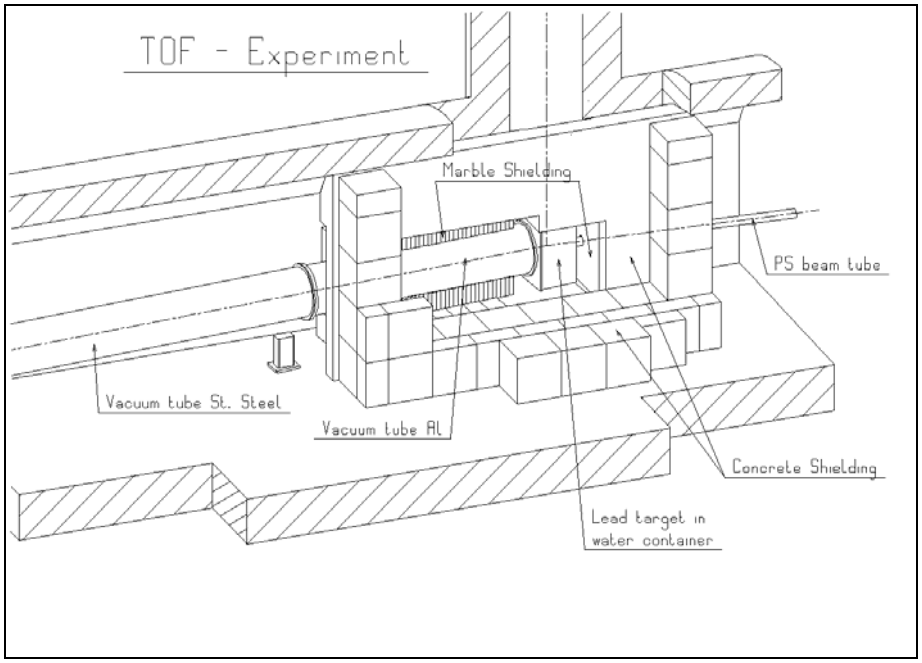

Figure 3: View of the target zone with the different shielding parts.

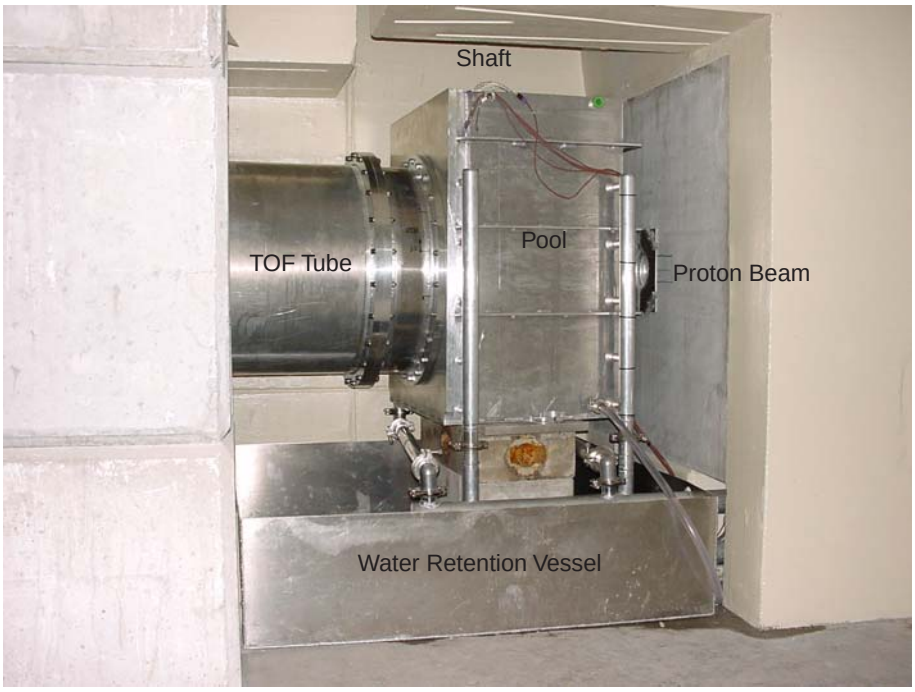

Figure 4: Picture of the target zone.

Figure 5: Picture of the Target Assembly.

Cooling and monitoring of the target

The heat dissipation in the target is expected to reach a maximum of 10 kW if 5 dedicated pulses from the PS reach the lead target during every supercycle of 16.8 s.

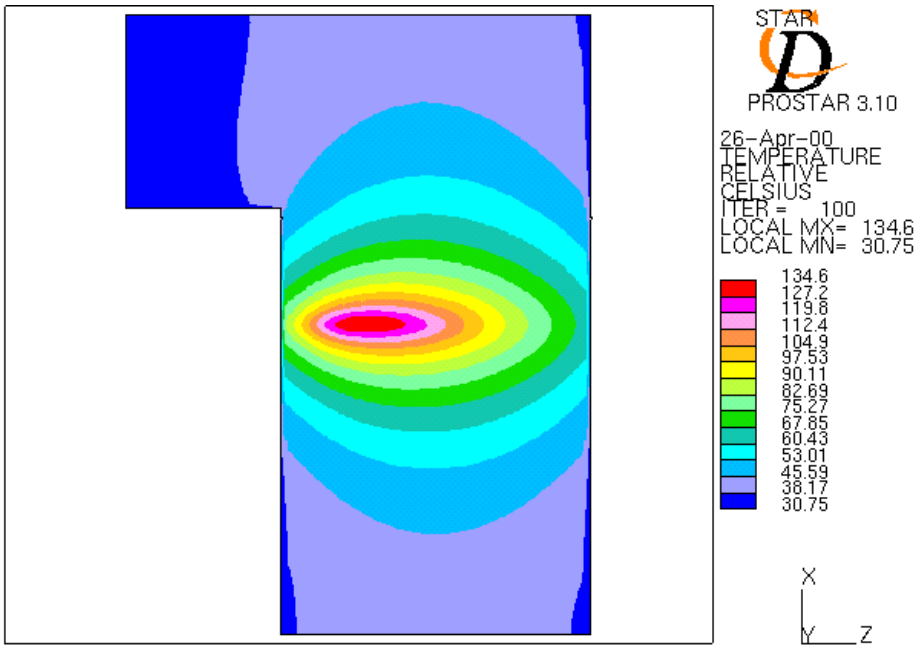

Figure 6: Temperature distribution inside the lead target for a water flow of 6 l/s and a water temperature of 30˚C.

The temperature inside the target and the heat flow on the surface of the target have been simulated, assuming that the demineralized water surrounding the target for cooling and moderation circulated at a rate of 6 l/s at a temperature of 30˚C. The result shown in Figure 6

confirmed that the maximum temperature inside the target does not exceed ~140˚C. To minimize activation, the water tank is made of an aluminum alloy (ISO Al-Si1-Mg-Mn 6082). At the entrance side a cylindrical niche ending with a 2 mm thick window, reduces the proton beam path in water to only 30 mm. At the exit face of the tank the distance between the wall and the lead target is 50 mm, providing the necessary amount of water for the moderation of the neutrons.
The hydraulic circuit consists of a primary loop connected to the cooling circuit for the beam line magnets, a heat exchanger, and a secondary loop connected to the target tank. The differential pressure between the two loops is 8-12 bar with an absolute pressure of 10-14 bar at inlet. The pressure in the secondary loop is about 1 to 1.5 bar, since the target tank is open to the atmosphere to act as an expansion vessel.
A PC based control system monitors and regulates the flow rate in the primary loop in order to maintain the right temperature. A flow meter in the secondary loop ensures the proper flow rate of about 6 l/s. A cut-off differential thermostat prevents that the temperature rises over 50˚C. The control system activates a hardware interlock signal to automatically cut off the proton beam in case of problems.

The beam line window

The window to the evacuated beam line represents a critical part of the project. On one hand it must be solid enough to separate the water from the vacuum reliably (pressure difference = 1.2 bar) and it has to remain flat (maximum depression in the center ≤ 2 mm) in order to guarantee the constant thickness of the water moderator for achieving the required energy resolution. On the other hand neutron absorption and scattering should be as small as possible. Furthermore, it must be made of radiation resistant materials, since the dose rate accumulated in one year could reach a few 10^6 Gray depending on the running period.
In view of these constraints the aluminum alloy (AA 6082) has been chosen for the window instead because the composition of an alternative carbon fiber window could not be obtained. Al alloy has the advantage that the composition and its effect on the neutron spectrum is well known and that its mechanical stability is not influenced by the expected radiation. The window itself is made of a 1.6 mm thick plate, reinforced by a grid 50 mm thick with sides of 100 mm in length. The struts of the grid have a thickness of 5.5 mm. This window is machined in one piece from a thick plate. The “equivalent” total thickness of the Al alloy is 6.17 mm. The face of the window with the grid is mounted towards the vacuum tube. The deformation of the window is limited to 1.96 mm in the centre. Figure 7 shows the design and the coupling to the evacuated flight tube.

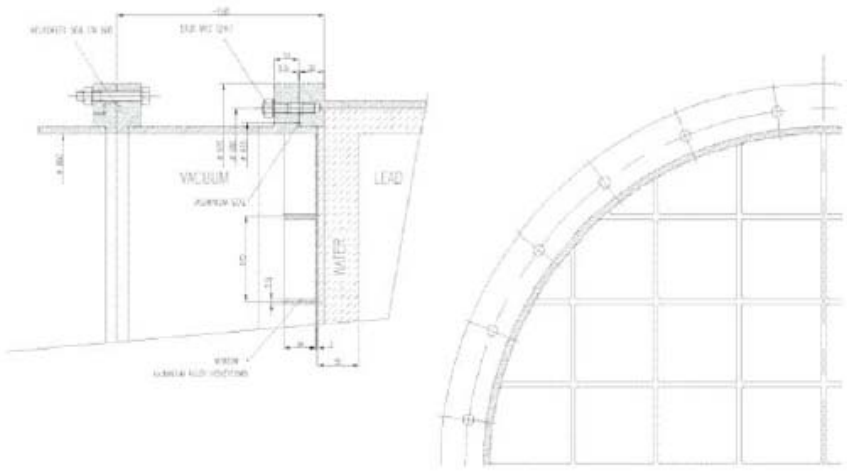

Figure 7: Aluminum alloy window welded to a 250 mm long aluminum alloy tube and fixed on the tank and the time of flight tube. On the right side the grid structure of the window is shown.

The TOF tube

The time-of-flight tube, which starts directly behind the window and ends 200 m away in the escape line, is made of stainless steel. It is divided into the 150 m long, primary section with more restricted access regulations and the secondary section that includes the experimental area. Due to the geometry of the existing tunnel, the tube is not located in the same position in the cross section and has a slope of 1.16% with respect to the flat part of the tunnel. The angle on the horizontal plane between the proton beam axis and the neutron beam is 10° in order to minimize the number of unwanted secondary particles in the experimental area. At the end of the primary section a sweeping magnet is used to remove the remaining charged particles from the beam line.
As illustrated in Figure 8, the diameter of the beam tube is progressively reduced from 800 mm at the target to 600 mm and eventually to 400 mm before the first collimator, which is located at 137 m from the target. In the primary section massive concrete and iron shielding are placed at about 72 m and 140 m .The first 24 m are divided into two parts with vacuum flanges at the end. This allows their removal during shutdown to access the target area with a forklift. Three windows 600 mm in diameter in one of these 12 m sectors are foreseen to insert equipment for measurements at very high neutron flux.

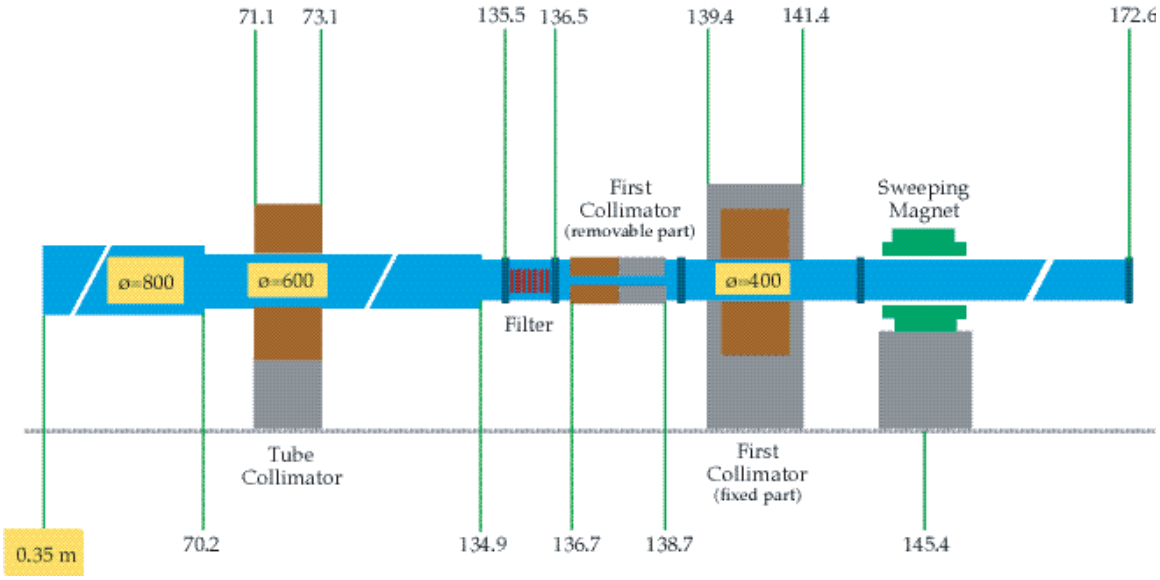

Figure 8: Elements of the TOF Tube in the first 172 m. Distances refer to the centre of the Pb target. This section includes shielding of concrete (grey) and iron (brown) as well as a sweeping magnet, a filter station, and the first collimator.

At the end of the ø=800 mm tube (~ 70 m from the target), a reduction piece of ø=600 mm is welded. Immediately after, an iron shielding with a cross section of 1.80×1.80 m^2 where the left side (seen in the beam direction) is reduced to the available space to the tunnel wall has been constructed. This iron shielding is embedded in 40 cm of concrete.
The first collimator with an inner diameter of 110 mm consists of a 1 m long sections of iron and concrete, both 1.20×1.20 m^2 in cross section. The primary area of the TOF tunnel, which can be accessed through a chicane around the shielding at 140 m, ends at this point. When the facility is in operation, access to this part is closed by a door.

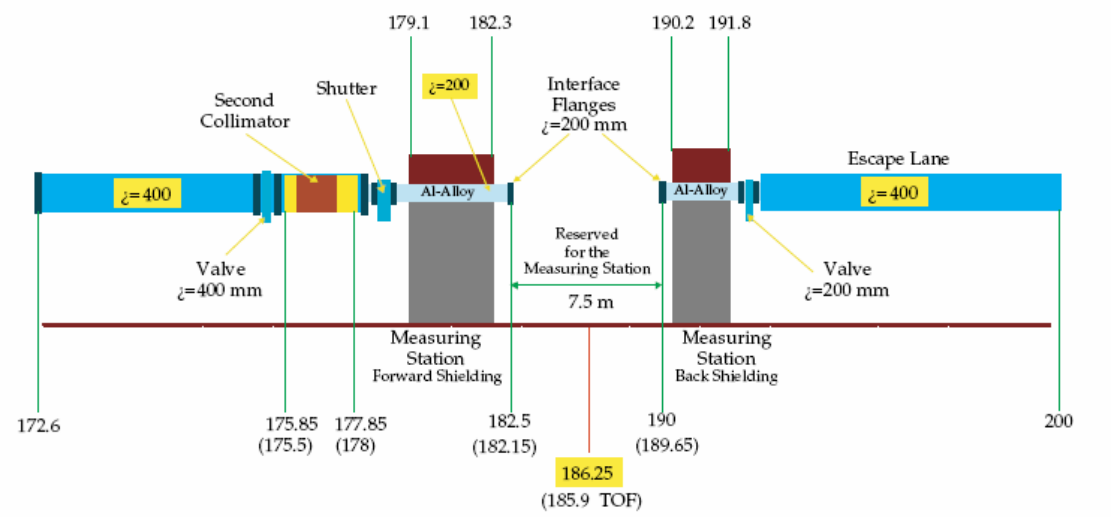

Figure 9: Elements of the TOF Tube after the first 172 m.

In section 2, the beam is cleaned from secondary particles by means of the sweeping magnet and a massive muon shielding, which is located on the side and behind the sweeping magnet and consists of iron and concrete sections, each 3 m in thickness. The iron part covers the entire cross section of the tunnel. In case of an accident the passage of personnel is possible through an open chicane. At a valve at 175 m the diameter of the tube is reduced to 200 mm before the second collimator. Starting from this point the tube is made from an aluminum alloy. Before entering the experimental area the tube crosses a 3.2 m thick concrete shielding, part of which can be removed to allow the passage of a forklift. A chicane equipped with a door is used to connect the secondary section with the experimental area.
The experimental area consists of a 7.5 m long part of the tunnel, where the various experiments are installed, with beam tube flanges 200 mm in diameter on both ends. The shape of the beam tube in between depends on the type of detectors installed. At the exit of the experimental area there is an additional concrete shielding with a simple chicane giving access to the neutron escape line. There, a last valve defines the tube sector in the experimental area. The following 8 m of the tube, which represent the neutron escape line are again made with a diameter of 400 mm.
During operation the TOF tube the required vacuum 1 mbar is established by five rotary pumps installed in three separate vacuum sectors. For safety reasons the two valves defining the experimental area are automatically closed by the control access system if a person enters the area. The pressure value in the three sectors and the status of the valves is permanently monitored in the control room.

The sweeping magnet

This magnet consists of a M200 dipole magnet with a variable gap as it is commonly used in the beam transfer lines of the PS. Given the position of the magnet inside the tunnel and assuming a maximum kinetic momentum $p_{max} = 10$ GeV/c of the charged particles, an integrated magnetic field of the sweeping magnet of

$$(Bl)_{mag} = \theta_{mag} \times (B\rho)_{max} = 1.03\ Tm$$

is required for the deflected particles to reach the tube walls within the next 15 m. This value is well met by the actual integrated field of 1.5 Tm.

The Filter Station

In order to facilitate background corrections in TOF experiments, a filter station with eight positions was installed at 140 m from the neutron target, just in front of the first collimator. Each position can hold a filter consisting of materials with strong neutron resonances. The filters are chosen thick enough that the neutron beam is completely absorbed at the energies of these resonances. Since the filter station cannot be accessed during the runs, it is remotely operated from the control room. The individual filters can be moved in and out of beam by means of pneumatic drives. Their actual positions are monitored by switches at the respective end positions, which are recorded and automatically documented in the software protocols. At present, silver, tungsten, cobalt, molybdenum, and aluminum filters are installed, which are effective at neutron energies of 5.1 eV, 18.8 eV, 45 eV, 132 eV, 35 keV, and 87 keV, respectively.

The Experimental Area

The experimental area is situated 182.5 m downstream of the spallation target and extends up to 190 m. The detectors, the front-end electronics and the necessary auxiliary equipment are mounted in this low background area, called the measuring station. After the measuring station the neutron beam enters in the neutron escape line, which acts as a beam dump.
Since the experimental area is situated in the rising part of the tunnel, a false floor of aluminum grating was installed in order to have a horizontal working area. A central aluminum beam base consisting of two I-beams of 176 mm by 179 mm, which are fixed to the concrete floor, provides a 352 mm wide support for the various detectors. Very massive detectors might require separate supports fixed to the concrete floor for additional stability.
The implementation of the safety system for the TOF facility to ensure personnel and equipment protection follows the standard safety architecture of the PS, except that the supervised access was omitted for financial reasons, because of the very limited number of interventions in the primary section. For access to this zone, an exceptional procedure has been established.

Simulation studies for safety

Since the n_TOF facility is using a high intensity proton beam, a high flux of charged particles, gammas, and neutrons is produced by the spallation process. Thus, one of the main concerns is the radioprotection aspect of such a facility. In this context, detailed simulation studies were performed to calculate the activity and dose at different locations. of the TOF facility. Aspects covered in these simulations concerned the activation of the lead target, the cooling water, and the air in the tunnel as well as of the dose estimates around the target area, near the sweeping magnet, and in the measuring station.
Access to the measuring station is possible only after the proton beam is stopped. The remaining background in the experimental area will be dominated by γ-rays emitted from the lead target and propagating through the TOF tube. The diameter of this tube is restricted 1.8 cm for the capture cross section measurements, and to 15 cm for the fission cross section measurements. Calculations were performed to determine the dose rate in this area and to design the lead shutter to be inserted at the end of the TOF tube.
Considering the dose equivalent rate of 25 Sv/h on the exit face of the target, an estimate of the rate at 187 m gives 0.5 μSv/h by considering the solid angle subtended by a surface 10 cm in diameter. Since this simple consideration does account for the reductions and collimators at different places along the neutron TOF tube, more detailed Monte-Carlo simulations have been made including the complex geometry of the n_TOF line.
After an irradiation period of 1 month, the activity of the lead target saturates around 800 Ci or 2.5×10^{13} γ/s. The photon energy distribution from the whole lead block was obtained from

the integrated activity of the residual nuclei by means of FLUKA using the γ-ray intensities from the ENSDF database [5]. The source photons were then transported with FLUKA from the lead target to the measuring station, taking the detailed geometry of the 200 m long n_TOF tunnel into account. The resulting dose equivalent rate is about 1 nSv/h, much below the crude estimate of 0.5 μSv/h.

Simulated performance of the facility

The simulation of the physical performance of the n_TOF facility was a major task during the design phase. Simulating geometries like the n_TOF tunnel, with a long flight path and with the imposed background conditions, required a difficult and time-consuming effort based on the most advanced computer codes FLUKA [1], EA-MC [2], and MCNPX [6], which have been coupled together by means of special interfaces whenever needed. The accurate representation of the tunnel geometry in the simulation codes was automatically generated from the civil engineering plans by in-house translators, which were specifically designed for this application.

Neutron Flux

The simulation of the neutron flux, one of the most important parameters of the facility, poses a serious difficulty due to the large length of the neutron flight path in the n_TOF tunnel. The solid angle is so small that only one neutron out of $\sim 10^7$ emerging from the lead target will reach the detector station at the end of the TOF tube. Therefore, the problem was treated in two steps: (i) simulation of the spallation target and generation of DST's (Data Summary Tapes) of the neutrons emerging from the aluminum window and entering the TOF tube [7], (ii) transport of the previously collected neutrons through the TOF tube.

For the first step, two simulation codes were used, the intra-nuclear cascade code FLUKA and the Energy Amplifier Monte Carlo code EA-MC, with the detailed geometry of the lead spallation target and of the Al window with the supporting grid. FLUKA was used for the production of spallation neutrons in the lead target and for the transport of the generated neutrons down to the cut-off energy of 19.6 MeV. The transport of neutron with kinetic energy below the cut-off was performed with the EA-MC code, where neutron induced interaction cross sections are available in the nuclear databases. All neutrons traversing the aluminum window with an angle $\vartheta < 20^o$ to the axis of the TOF tube were recorded in a DST file.

In the second step, the previously collected neutrons were transported through the TOF tube towards the measuring station, assuming a perfect collimation system, i.e. particles touching the collimators or the tube were *killed*. In order to enhance the statistics, it was further assumed that the direction of neutrons is isotropic within a small solid angle ($\leq 10^{-7}$ sr). Thus, each particle could be reused several times by tiny changes of its direction, such as to scan an area of a few cm^2 at the sample position in the measuring station. The program was scoring the number of occurrences of particles arriving at the sample without touching any element of the neutron tube and the collimators. The weight of each particle was properly normalized to reflect the number of times that it had been reused. The output histogram of this scanning procedure gave the integrated neutron fluence at the sample position.

The result of the flux simulation using FLUKA and FLUKA/EA-MC are shown Figure 10. The total number of neutrons entering the experimental is plotted in isolethargic units: $dn/dlnE/cm^2/7\times10^{12}$ protons. The same plot shows also the simulation with MCNP-X using a similar procedure, starting from the spallation reactions in the lead target followed by the neutron transport to the measuring station. In general, the three sets are in very good agreement. At high energies, MCNP-X predicts a harder spectrum than FLUKA. The thermal

part appears to be better described by MCNP-X, apart a few non-physical spikes, probably due to a binning affect. The gravitational cut-off due to the geometry of the TOF tube is expected for neutron energies lower than ~0.02 eV.

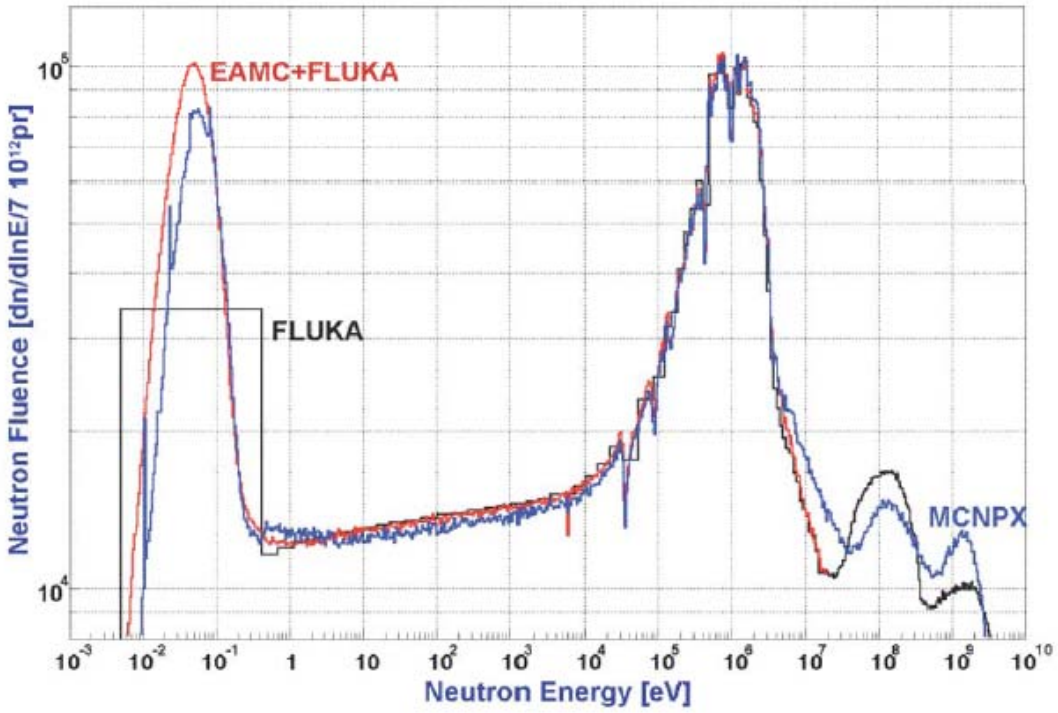

Figure 10: Monte Carlo simulation of the uncollimated neutron flux per cm^2 at 185 m using FLUKA (black), MCNP-X (blue), and the combination FLUKA/EA-MC (red).

Neutron energy resolution

The energy resolution has been evaluated using the relation $\Delta E/E=2\lambda/(\lambda+L)$ between the energy E and the "*effective neutron path* λ" inside the lead target and in the 5 cm thick water moderato. The flight path L is considered to start at the aluminum entrance window of the TOF tube. The effective neutron path λ can be evaluated as $\lambda=v\times t$, where v is the velocity of neutrons entering the TOF tube and t the time elapsed since its creation (Figure 11a). The effective neutron path in the lead target is a few centimeters for the lowest energies. The variance $\Delta\lambda$ has been estimated taking either the r.m.s. of the λ distributions, or the standard deviation from a Gaussian fit of the peaks (Figure 11b).

Neutron beam contaminations

A 20 GeV/c proton beam interacting with a lead target represents a source of many charged and neutral particles [7]. While charged particles are strongly suppressed by the sweeping magnet at 145 m from the spallation target, neutral particles and γ-rays can reach the measuring station. The simulated momentum distribution of the charged particles is shown in Figure 12 together with that of the neutrons.

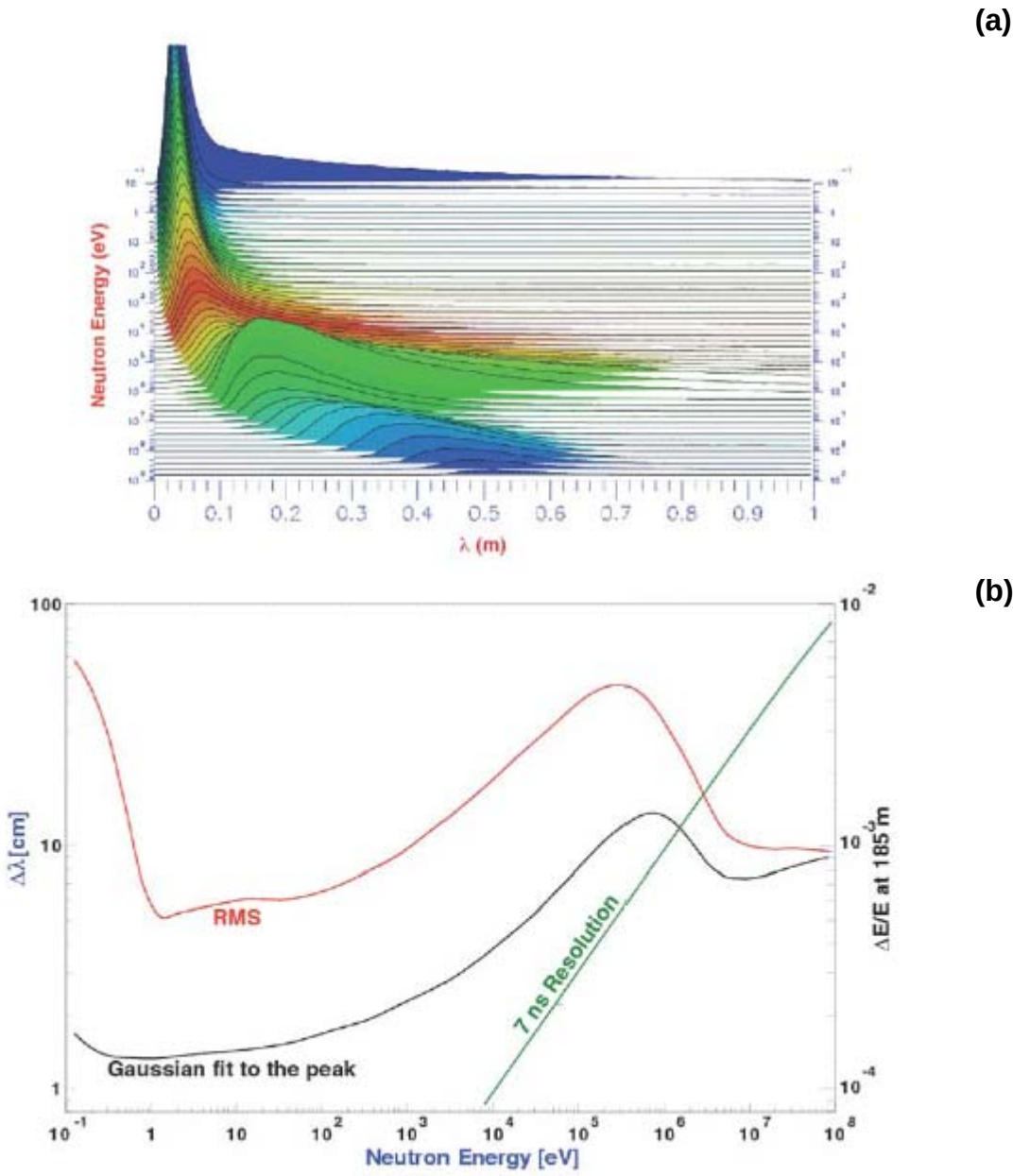

Figure 11: (a) Monte Carlo distribution of the equivalent neutron path inside the moderator, evaluated at the energy of observation; (b) Monte Carlo simulation of the energy resolution at 185 m. The 7 ns resolution due to the proton beam becomes important for neutron energies above a few MeV.

Photons are produced in spallation reactions and during neutron moderation. These photons can be separated into two groups, a "*fast*" component resulting from the spallation process itself with arrival times in the measuring station of < 1 μs, and a "*slow*" component with arrival times between 1 μs and a few 100 μs, mainly due to thermal neutron capture in the moderator and the lead target. The "*fast*" component, which is often called γ-flash, can be used as an accurate measure of the t_o of each pulse.

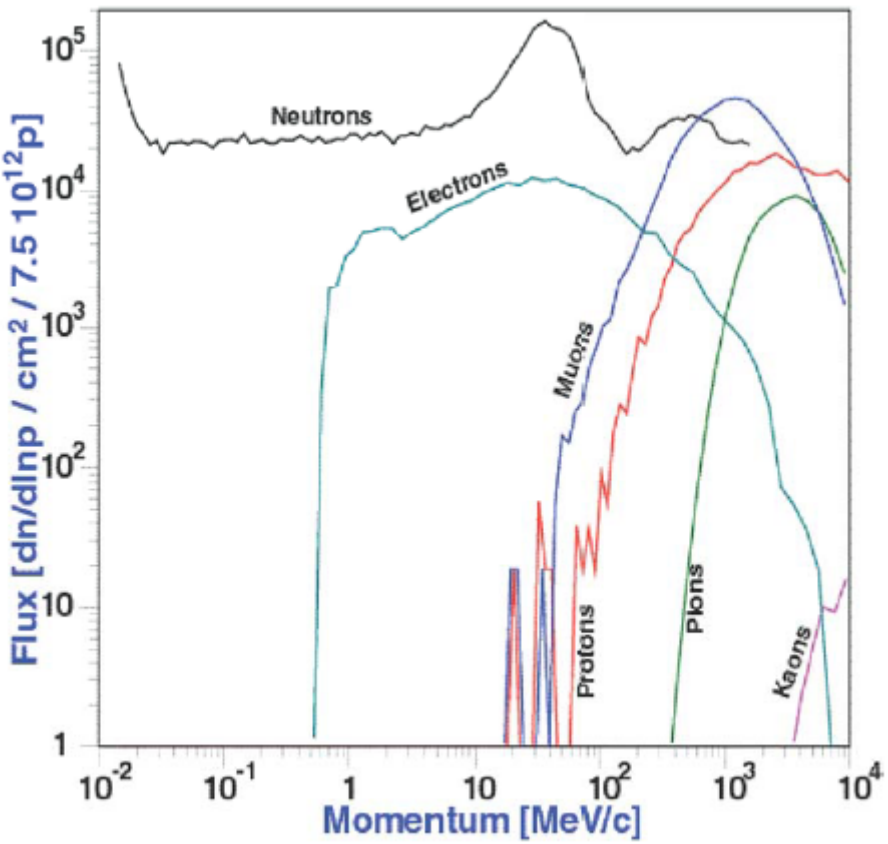

Figure 12: Monte-Carlo simulation of the flux of the charged secondary particles and neutrons produced by the spallation process as a function of their momentum.

The γ-flux of the "*slow*" component arrives at the measuring station along with neutrons having energies of a few keV. Though this γ-flux is more than an order of magnitude lower than the neutron flux (Figure 13a), it represents a severe source of background in capture cross section measurements. From the energy spectrum of these photons (Figure 13b), one finds that 40% are due to the neutron capture on hydrogen producing 2.2 MeV γ-rays. Another 5% contribution comes from photons with energies around 7 MeV resulting from the capture on lead, on the aluminum alloy container and on the iron target support.

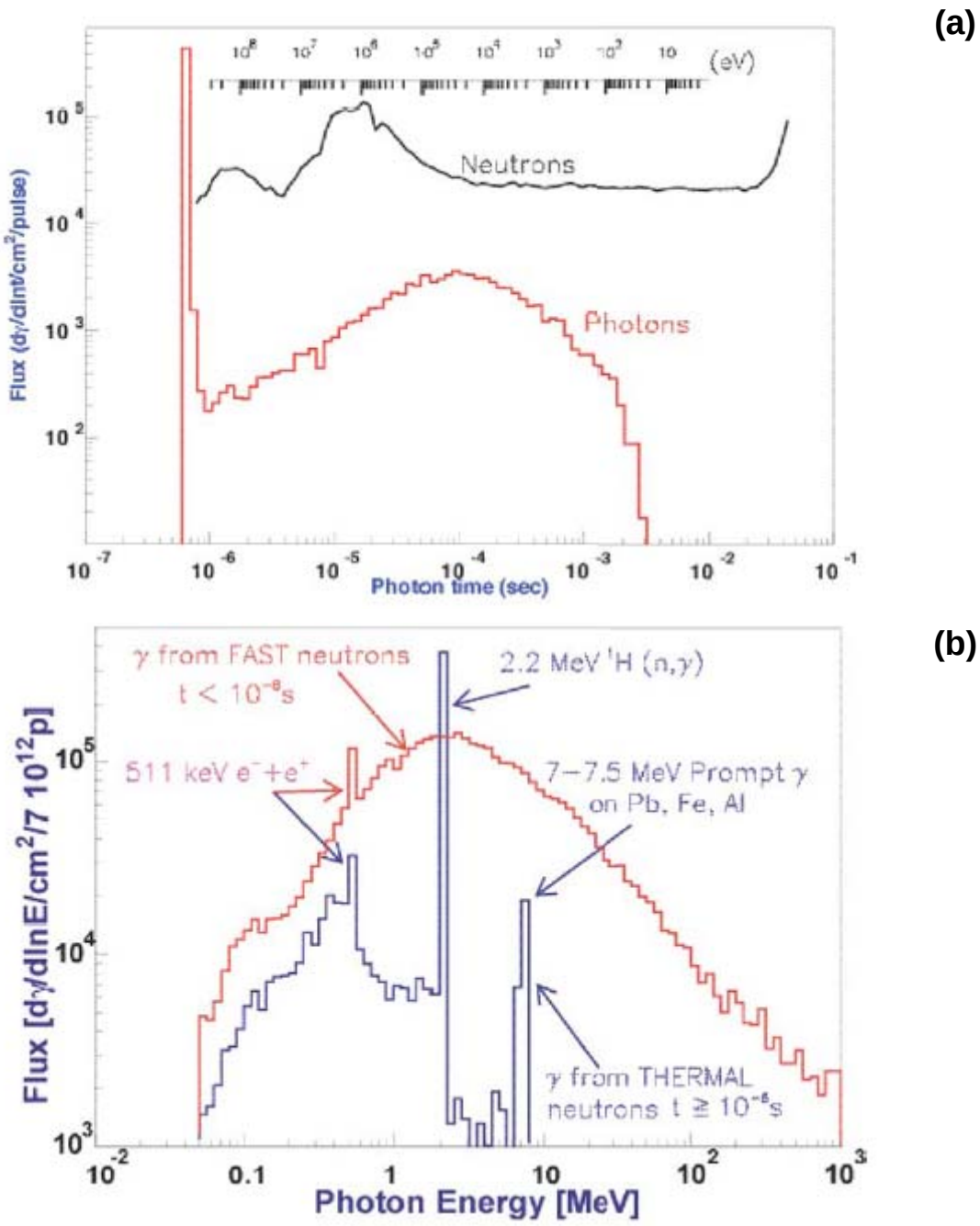

Figure 13: (a) Prompt photon flux at the measuring station versus the arrival time. The neutron fluence and the neutron energy expected at the measuring station is plotted. (b) Energy spectrum of the prompt photons divided into the fast and slow component as discussed in the text.

Experimental equipments

Different detectors and techniques have been used for measuring and monitoring the neutron fluence in the measuring station (experimental area, EAR-1). Such measurements are based on "*standard*" reactions with smooth cross sections, notably $^{10}B(n,\alpha)^{7}Li$ and $^{6}Li(n,\alpha)^{3}H$, which are considered as cross section standards from thermal energies up to 250 keV and 1

MeV, respectively. At higher energies the ^{235}U(n,f) standard cross section was used between 0.15 to 20 MeV. At even higher energies the ^{238}U(n,f) and ^{209}Bi(n,f) cross sections can be used as standards for flux measurements from 1 MeV to 200 MeV and from 35 MeV to 130 MeV, respectively.

The n_TOF MicroMegas detector

MicroMegas [8] is a new gaseous detector based on a simple geometry with planar electrodes developed by Nobel Laureate G. Charpak. It consists of a conversion gap where radiation liberates ionization electrons, and of a thin amplification gap, where the free electrons create an avalanche. The two regions are separated by a thin 5 μm mesh grid. The avalanches produced in the amplification gap can then be collected on printed electrodes of any shape to achieve high spatial resolution. These detectors are also very fast and well suited for high counting rates [9].
In order to use the MicroMegas detector as a neutron beam profile monitor for the n_TOF facility at CERN, an appropriate neutron/charged particle converter has been developed. Since the neutron energy range of the n_TOF facility extends from 1 eV to over 200 MeV, there is no unique choice of an efficient converter. Conversion reactions that are usually employed for slow or fast neutron detection are proton recoil, ^{10}B(n,α)^{7}Be and ^{6}Li(n,α)^{3}H. Recoil protons from elastic neutron scattering on hydrogen are emitted in forward direction and are, therefore, suited for the detection of fast neutrons. The other two reactions can be used for neutron detection at lower energies. A series of test measurements [10] demonstrated excellent background rejection properties and full detection efficiency for the charged particles produced by neutron reactions in the converter. The detector was shown to have a total detection efficiency of up to 0.1% and a spatial resolution of less than 250 μm, perfectly matching the requirements of the n_TOF experiment.
The MicroMegas principle for neutron detection is illustrated in Figure 14. The detector is composed of a drift electrode consisting of a ^{10}B or ^{6}Li converter deposited on an Al foil, a micro-mesh, and an array of anode strips. The charged particles emitted in the (n,α) reactions on ^{10}B or ^{6}Li ionize the filling gas of the detector. After passing the drift gap, the free electrons produce an avalanche in the high field of the acceleration gap behind the micro-mesh, which are then detected by the anode strips.

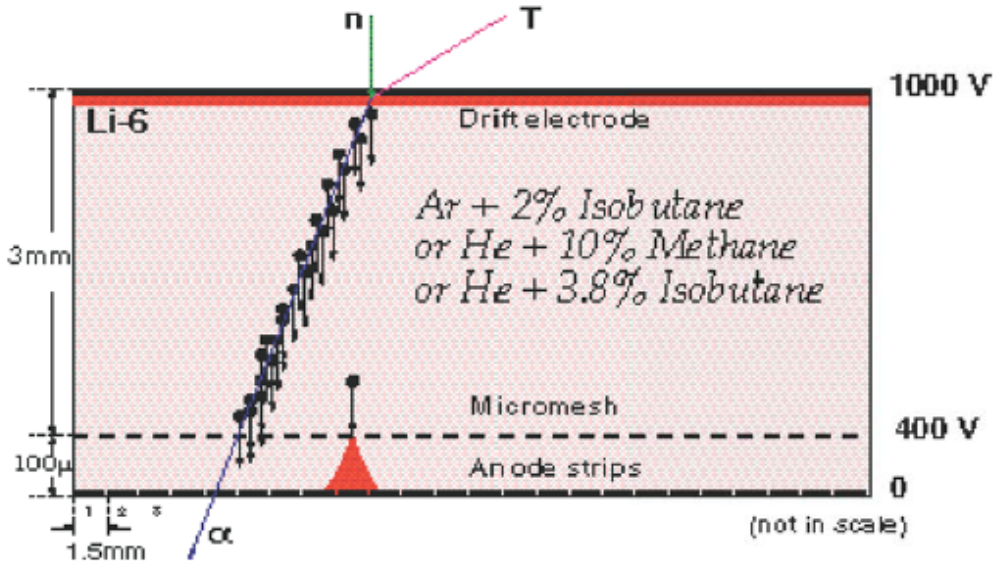

Figure 14: MicroMegas operated as a neutron detector.

The MicroMegas detector was operated inside a vacuum-tight chamber connected to the standard n_TOF tube 200 mm in diameter. The detector is filled with a gas mixture as indicated in Figure 14 at a pressure of the order of 1 bar, separated from the evacuated TOF tube by two Kapton windows. The detector exhibits a fast rise time of about 1 ns, much faster than the 6 ns duration of the n_TOF pulse [10].

Silicon Monitors (SiMON)

For routine neutron beam monitoring a robust and simple system based on Silicon detectors has been developed [13]. Four Silicon detectors are viewing a foil consisting of a pure ^{6}Li layer 200 μg/cm^{2} in thickness and 6 cm in diameter, which is deposited on a substrate of 3 μm thick Mylar. The geometry is designed such that only the ^{6}Li sample is exposed to the neutron flux, whereas the Si detectors are placed inside the carbon-fiber vacuum chamber, but outside of the neutron beam (Figure 15).

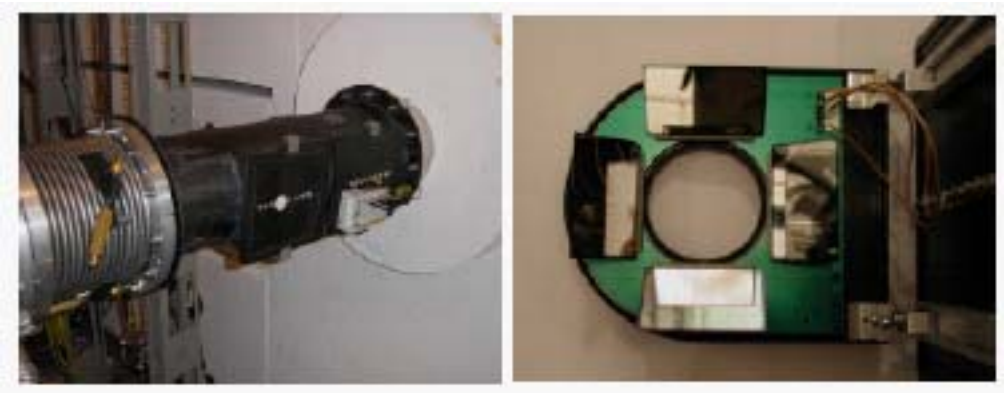

Figure 15: Carbon-fiber chamber (left) and internal geometry of the SiMON detectors (right).

The ^{6}Li deposit is protected by evaporated carbon layers, which are less than 10 μg/cm^{2} in thickness. In this way, the ^{6}Li deposit could be maintained in proper state even after four months of operation and several air/vacuum cycles (venting operations).

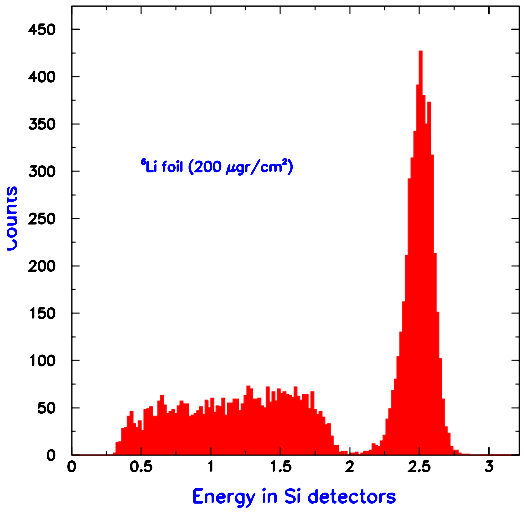

Figure 16: Energy deposited in the Si detectors from the products of the ^{6}Li(n,α)^{3}H reaction in the neutron energy range 1 eV < E_n < 100 keV.

Figure 16 shows the energy spectrum deposited in the Si detectors [25] with the tritons and alpha particles from the $^{6}Li(n,\alpha)^{3}H$ reaction clearly separated. To avoid threshold problems, the neutron flux analysis is performed by selecting only the triton peak with a "banana" gate in the 2D plot of the deposited energy versus neutron energy. The SiMON has been successfully used to monitor the neutron beam throughout all n_TOF capture measurements. As illustrated in Figure 17 the number of counts in the SiMON correlates very well with the number of protons falling on the spallation target as recorded by the n_TOF DAQ (see below).

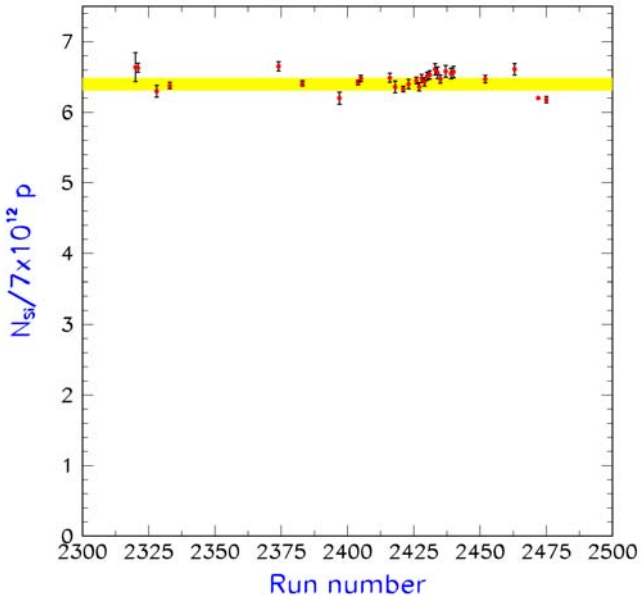

Figure 17: Ratio between the number of protons recorded by the n_TOF DAQ and the number of counts from SiMON. The stability of this ratio over the runs shows the reliability of the monitoring characteristics of SiMON.

The data obtained from the SiMON can also be used to obtain an absolute neutron flux determination. Due to the estimated geometric efficiency and the correction for the angular distribution of emitted tritons, a systematic uncertainty of the order of 10% has to be considered in the determination of the neutron fluence from the SiMON.

BF_3 counters

At the end of the neutron escape line, a polyethylene block of 543×527×528 mm^3 with a set of three BF_3 proportional counters as shown in Figure 18 are placed. Once properly adjusted, comparison of the count rates provides an additional check for the proper alignment of the neutron collimators in the TOF tube.

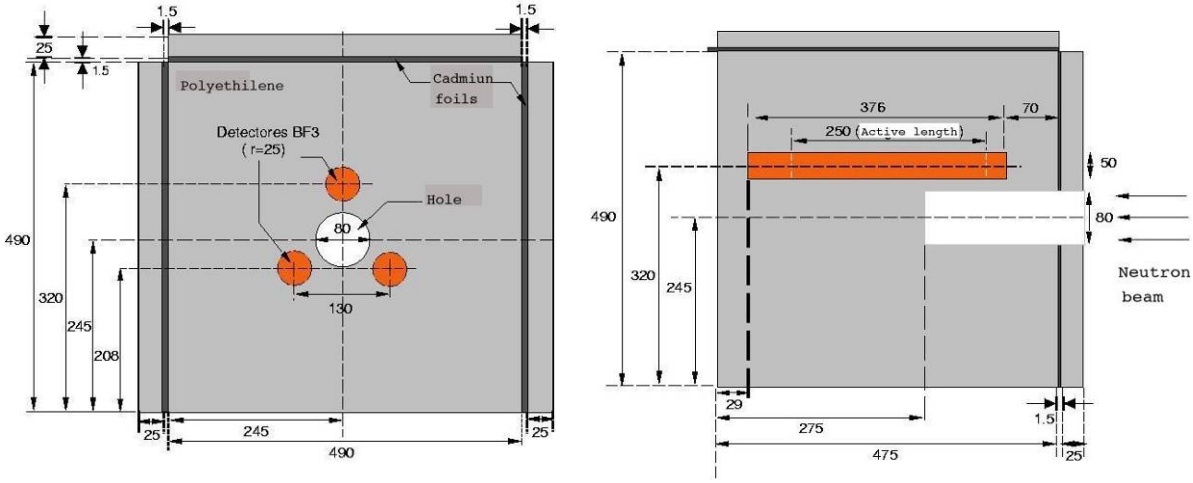

Figure 18: Front face (left) and longitudinal (right) cross section of the BF_3 counter.

C_6D_6 Gamma-ray detectors

Neutron capture experiments with C_6D_6 scintillation detectors for the prompt capture γ-ray cascade [14] rely on the validity of the pulse height weighting technique, by which the detection efficiency becomes independent of the cascade multiplicity. These detectors have low γ-ray efficiency over the range of interest between 0.1 MeV to 10 MeV, and are unique for their very low sensitivity to scattered neutrons as compared to other γ-ray detectors. However, in contrast to a 4π total absorption calorimeter, it is not possible with C_6D_6 detectors to distinguish whether the detected γ rays originate from the (n,γ) reaction, the radioactive background, or from competing reaction channels, e.g. from fission or inelastic scattering.

The quantity determined in a neutron capture experiment is the capture yield, i.e. the fraction of neutrons incident on a sample (with thickness N atoms per barn), which undergo a (n,γ) interaction. The capture yield Y(E), with 0 < Y(E) < 1, for the first interaction can be written as

$$Y(E) = (1 - e^{-N\sigma_T(E)}) \cdot \frac{\sigma_\gamma(E)}{\sigma_T(E)} \approx \begin{cases} N\sigma_\gamma & if\ N\sigma_T << 1 \\ \sigma_\gamma / \sigma_T < 1 & if\ N\sigma_T >> 1 \end{cases}$$

The two limiting cases are approximations for thin and thick samples, respectively. Additional terms must be added to this yield coming from neutrons that are scattered one or more times in the sample and surroundings and subsequently captured. This multiple scattering effect has to be taken into account in the R-matrix analysis code. Since the efficiency and solid angle of the detector do not exceed a few percent, the measured time-of-flight spectra need to be normalized to a well-known isotope. The standard technique is to measure this normalization using a "saturated" resonance. This refers to a resonance, where the thick sample approximation is valid in the peak of the resonance and where the capture yield is no more proportional to the capture cross section but to the ratio of the capture and the total cross section. The measured resonance shape has then a flat top and from this characteristic shape the normalization constant can be extracted. Often an isotope does not have such a large resonance or is not available as a thick sample. In that case the normalization is determined by measuring the first saturated resonance, e.g. of ^{197}Au at 4.9 eV or of ^{109}Ag at 5.1 eV. Since only the strong, saturated resonance needs to be recorded, the normalization measurement with gold or silver lasts in general much shorter than the actual measurement.

For the measurements at n_TOF, optimized C_6D_6 detectors were developed by means of detailed GEANT simulations [23] using GEANT [15] including the library GCALOR [16] for neutron tracking. GCALOR is an interface to the Monte Carlo neutron code MICAP [17]. Particular attention was paid with respect to neutron sensitivity, where previous versions could be significantly improved as illustrated in Figure 19. This achievement is crucial for measurements of resonance dominated cross sections with scattering to capture ratios of 10^4 or more.

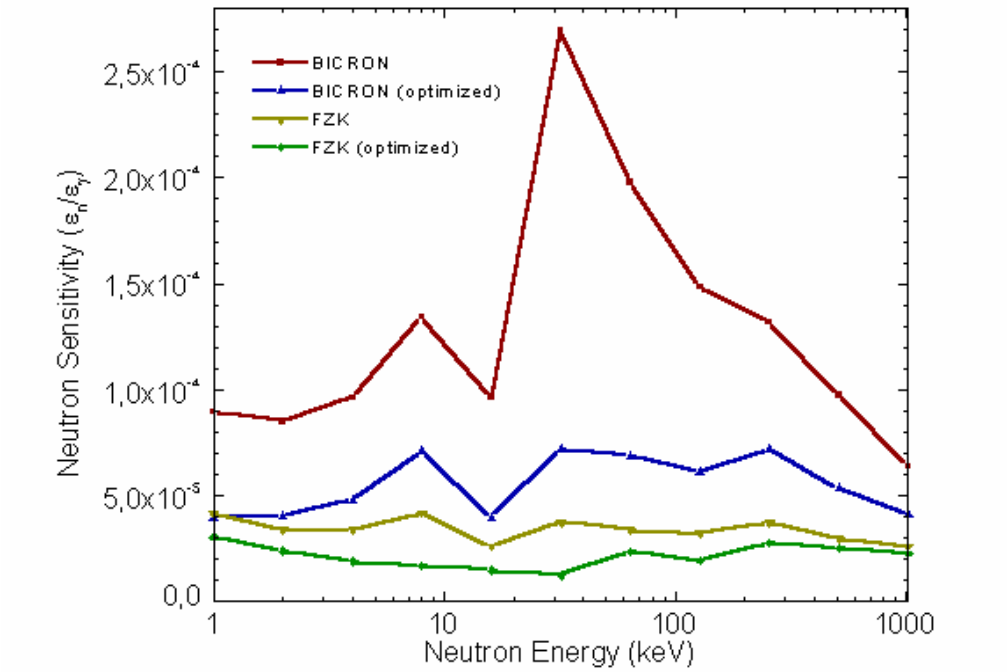

Figure 19: Comparison of the neutron sensitivity of the investigated designs. The neutron sensitivity is given relative to the γ-ray efficiency at 640 keV.

The simulated neutron sensitivity of the optimized version was experimentally verified at the Karlsruhe Van de Graaff accelerator. Figure 20 shows this detector in front of the neutron target. The neutron sensitivity was measured by TOF using a spectrum of $E_n = 30 \pm 20$ keV. The measured neutron sensitivity of $\varepsilon_n = (2.4 \pm 0.3) \times 10^{-6}$ was found in fair agreement with the simulated value of 3.7×10^{-6}, given the fact that the experimental threshold was higher than that assumed in the simulation. A detailed description of simulations and test measurements can be found in reference [14].

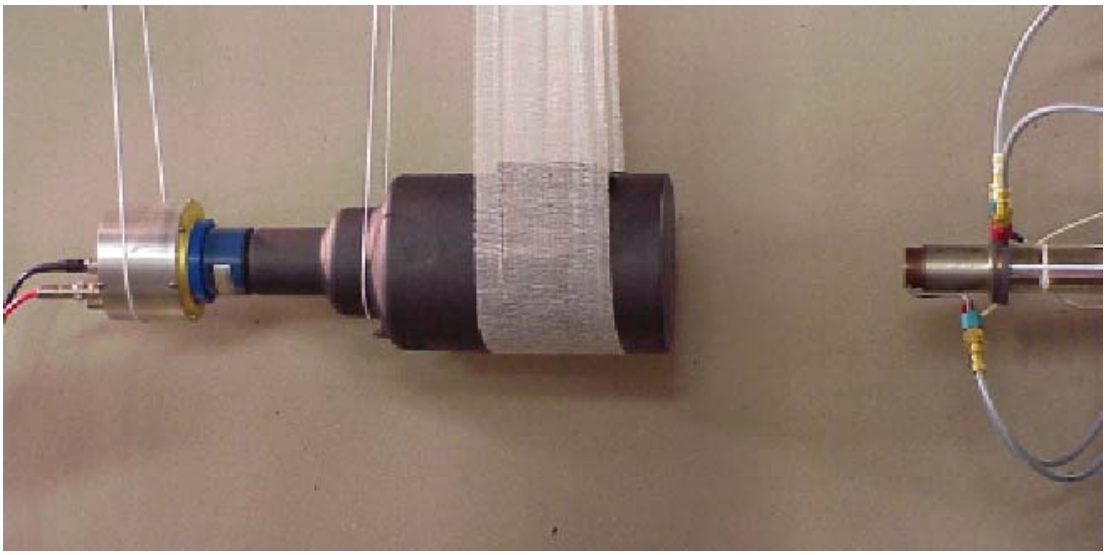

Figure 20: The optimized detector mounted in front of the neutron production target at the Karlsruhe Van de Graaff accelerator. Note the quasi mass-less suspension. The distance to the neutron target in the right part of the figure was 20 cm.

Two optimized detectors have been manufactured and are successfully used at n_TOF. The detectors were mounted in direct contact with the beam line, in close geometry with respect to the sample. This setup allowed one to achieve an overall efficiency for capture events of about 15%. Figure 21 illustrates the arrangement of detectors, beam line and sample changer.

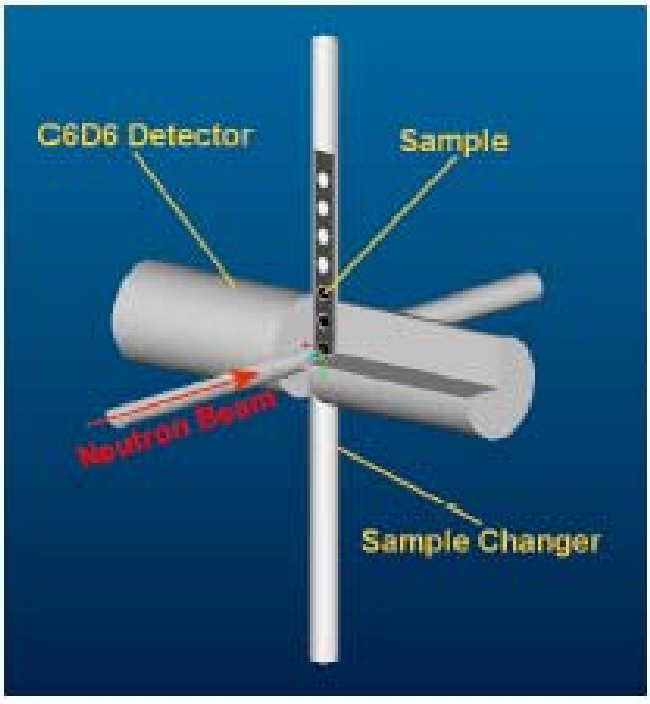

Figure 21: Schematic view of the experimental setup for capture measurements in EAR-1.

The working principle of the C_6D_6 detectors for (n,γ) cross section measurements is the a posteriori manipulation of their γ-response distribution R_{ij} through the introduction of a set of

weighting factors W_i such that the detection efficiency becomes proportional to the γ-ray energy, $E_{\gamma j}$:

$$\sum_i W_i R_{ij} = kE_{\gamma j} .$$

In this way the detection efficiency of the capture cascade becomes proportional to the energy of the cascade, and thus independent of the actual multiplicity (provided that the probability of simultaneous detection of more than one cascade γ-ray is negligible).
The accuracy of this method depends strongly on the accuracy with which the responses can be determined. Historically, and due to the difficulty to obtain mono-energetic γ-ray sources in the energy range of interest, the detector responses were initially obtained by Monte Carlo simulations. It turned out, however, that the so obtained result for the well-known resonance at 1.15 keV in ^{56}Fe showed a serious discrepancy compared to the value deduced from transmission measurements. This discrepancy could be reduced but not resolved even after thorough attempts to determine the weighting function on the basis of experimental investigations [18] and by improved Monte Carlo simulations [19] using the EGS4 [20] code. The existing data were eventually reconciled by an extensive n_TOF study with the simulation package GEANT3[15] to calculate the response for the respective detector set-up including the effect of the sample itself [24].
Figure 22 shows the comparison of the simulated experiment with the measurement for different samples. On one hand the dispersion of the experimental values illustrates the limitation of the experimental weighting function, but the fact that the simulation reproduces the behavior of the experimental points provides strong evidence for the accuracy of the Monte Carlo simulations. This success confirms the necessity of using the appropriate weighting function for each specific (n,γ) set-up, which can only be obtained by Monte-Carlo simulations.

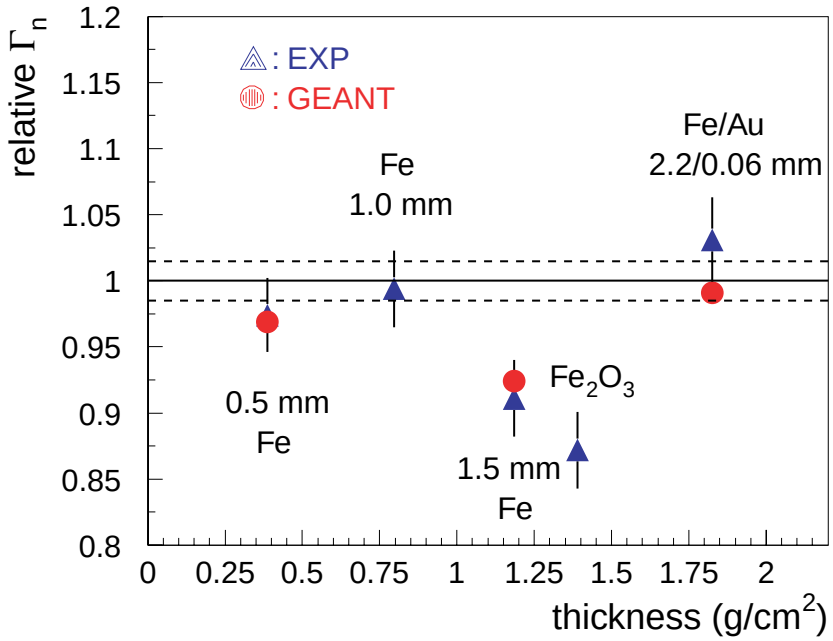

Figure 22: Comparison of measured [18] and simulated neutron width for the 1.15 keV resonance of ^{56}Fe obtained with the pulse height weighting technique for various sample thicknesses and compositions. The values are normalized to the transmission value.

The 4π Total Absorption Calorimeter (TAC)

The best identification of neutron capture events is provided by the total energy of the capture γ-cascade. This requires a large solid angle detector that operates as a calorimeter. With a γ-ray efficiency of better than 90% in the entire energy range below 10 MeV, capture events can be registered with almost 100% probability. A high efficiency together with good resolution in γ-ray and neutron (TOF) energy is essential for an accuracy of better than 3%, which is typically achieved in cross section measurements with such detectors.
When an (n,γ) reaction occurs, a cascade of γ-rays is promptly emitted. Depending on the atomic mass of the nucleus, there can be from $\sim 10^2$ to $\sim 10^4$ possible de-excitation channels with γ-multiplicities averaging around 3 or 4. The cross section of the process can be determined by counting the number of events in the sample irradiated with a known neutron flux and assuming that the detector efficiency is also known. The efficiency is measured in a calibration experiment with ^{197}Au as a target. The most important feature of such measurements is that capture events have to be detected independent of the multiplicity of the respective gamma-ray cascades. The desirable features of a calorimeter type γ-ray detector for use in neutron capture cross section measurements are

- high efficiency for the detection of a capture event, independent of the particular γ cascade,
- high granularity,
- low sensitivity to the scattered neutrons,
- fast time response,
- low background and ease of shielding.

These requirements are well satisfied by a $4\pi BaF_2$ array. The performance of such a calorimeter depends critically on its sensitivity to scattered neutrons, since the scattering cross sections are on average about 10 times larger than the capture cross sections. The first detector of this type at FZ Karlsruhe is used at a comparably short flight path of about 80 cm and with neutron spectra in a limited energy range. In this particular case, most of the delayed background from scattered neutrons can be discriminated by time-of-flight. At moderated neutron sources, however, this background must be reduced by other means. In addition to a central absorber containing ^{6}Li, simulations have shown that this background can be further reduced by a ^{10}B layer surrounding each scintillator module.
Neutron captures studies on radioactive isotopes are difficult because of background radiation due to the activity of the sample. In addition, suited samples are not easily available and often excluded because of safety regulations. The n_TOF facility at CERN is best suited for measurements on radioactive samples, owing to the unique combination of high neutron intensity and small duty cycle. From the detector side, the decay time of the scintillation light plays a capital role with respect to the allowed mass of the radioactive sample and consequently to the systematic and the statistics of the measurements. The mass of radioactive samples is constrained by the requirement of a manageable pileup level. In this respect the use of the fast component of BaF_2 (620 ps at 200 nm) with UV-sensitive photomultipliers seems to be very promising. This high performance γ-detector can also be used for measuring the capture cross sections of fissile samples, because capture and fission events can be separated by their different γ-ray patterns.
For reasons of compatibility, it was decided to follow the Karlsruhe design of a 42-fold geometry with 12 pentagonal and 30 hexagonal BaF_2 modules, but to adapt this design to the specific n_TOF situation. The corresponding differences include a central neutron absorber with ^{6}Li, carbon fiber capsules around the BaF_2 crystals, which were loaded with ^{10}B, modified and less massive mechanical parts, optimized voltage dividers as well as a data acquisition system with flash ADCs.

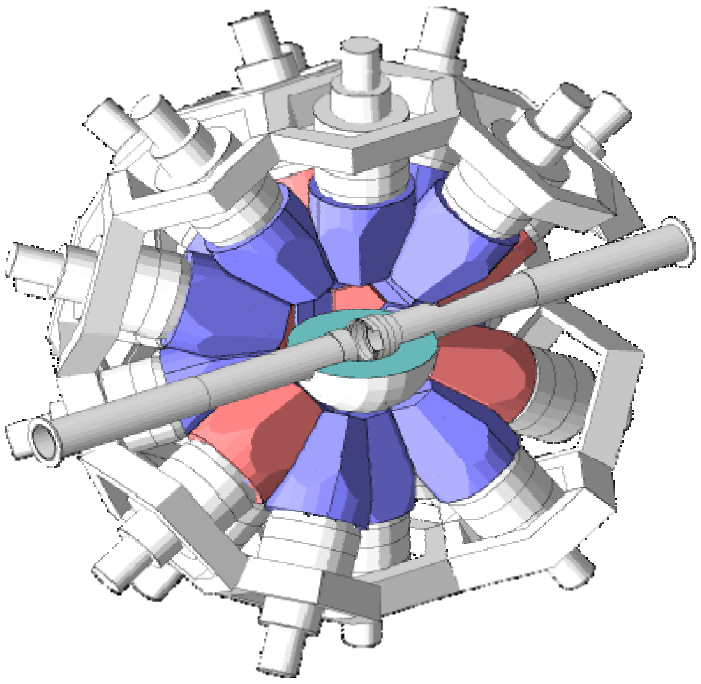

Figure 23: The total absorption calorimeter is composed of 42 BaF_2 detector modules forming a spherical shell of 20 cm inner diameter and 15 cm thickness. The neutron beam line is indicated with the mount of the sample in the center and with the lower half of the neutron absorber. The array itself is separated into two hemispheres, which can be moved apart for access of the sample.

Given the density of 4.88 g/cm^3 the detector exhibits an absolute γ-ray efficiency of better than 90% in the energy range up to 10 MeV. This means that γ-ray cascades following neutron capture can be detected with an efficiency of ≥ 95%. Other important features of this detector are a resolution in γ-ray energy ranging from 14% at 662 keV to 6% at 6.13 MeV and a time resolution of 500 ps.
For a full computer simulation of the performance, the complex geometry of the detector was modeled in detail, including the light reflectors, the cladding materials of the BaF_2 crystals, and the support structure. These simulations were carried out with the GEANT package [15]complemented by the GCALOR software [16] for following neutron energies down to very low energies. The simulations were verified by comparison with experimental data obtained with the Karlsruhe array, which could be perfectly reproduced.
Figure 24 shows the response of the detector array to a gold sample. The open part of the spectra corresponds to true capture events in gold, while the hatched part illustrates the background due to neutrons scattered in the sample and captured in the scintillator. While of no concern in the eV range, this background becomes increasingly disturbing at higher energies. Therefore, the sample is surrounded by a 5 cm thick neutron absorber. The best material for the central absorber is ^{6}LiH by the combined effect of the hydrogen (which acts as a moderator) and the ^{6}Li (which absorbs neutrons via the ^{6}Li(n,α)T reaction without producing any γ-rays).
With such a LiH absorber the signal to background ratios in the spectra of Figure 24 could be improved by factors of 40, 19, and 6 for energies ranging from 0.1-1 keV, 1-10 keV and 10-100 keV respectively.

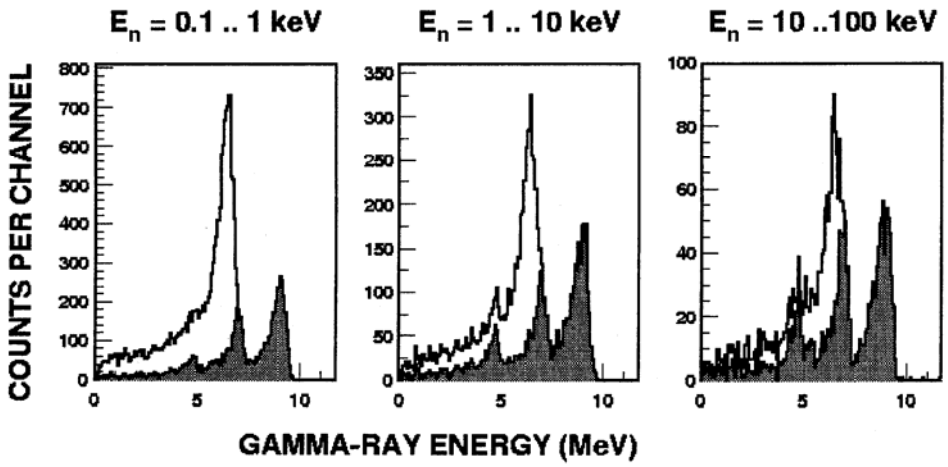

Figure 24: GEANT simulations of the response of the 4π BaF_2 calorimeter to a gold sample. The contributions from true capture events are indicated by the open parts, while the hatched parts correspond to background from scattered neutrons. This background can be reduced by factors of 40, 19, and 6 (from left to right) surrounding the sample with a 6 cm thick layer of ^{6}LiH.

Since the use of ^{6}LiH was, however, denied because of security arguments, an alternative solution has been adopted. Based on GEANT simulations with the criteria that the absorber should not produce γ-rays and should not contain elements heavier than oxygen (which would disturb the γ-spectra emitted by capture events in the sample), the lithium salt of the dodecanedioic acid

$$HOOC(CH_2)_{10}COOH + {}_6Li_2CO_3 \rightarrow {}_6LiOOC(CH_2)_{10}COO_6Li + H_2O + CO_2,$$

was found to constitute an acceptable solution. Chemically, this compound is inert, inflammable, and suited for unlimited storage. For better mechanical stability the absorber is encapsulated in an 0.5 mm thick, welded aluminum canning adapted to the geometry inside the TAC. The absorber consists of two symmetric modules, one for each of the TAC hemispheres.

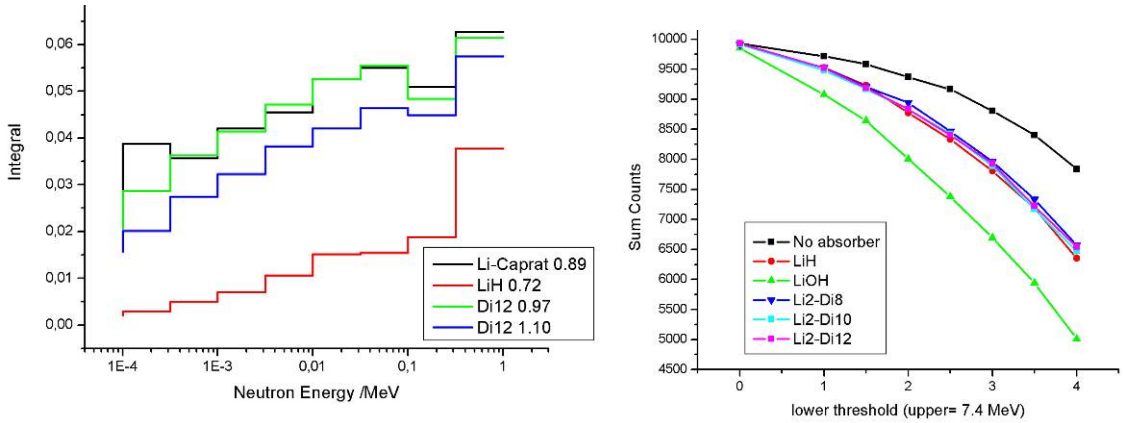

Figure 25: Comparison of the neutron transmission through a 5 cm thick layer of different neutron absorbers. Compared to ^{6}LiH the efficiency of the investigated Li salts of the fatty acids (capric acid and dodecanedioic acid) are less efficient (left panel), but exhibit similar γ-ray transmission (right panel).

The TAC was commissioned in time for the n_TOF campaign 2004 and was successfully used for neutron capture cross section measurements on a series of actinide samples as described in a section below.

HPGe detectors

Germanium detectors are mandatory for γ-ray spectroscopy because of their high energy resolution. However, their use at n_TOF is not straightforward because of the high flux and the very low frequency of the beam. Indeed, the neutrons corresponding to (n,*x*n) reactions, for example, have energies between 6 and 250 MeV and appear between 1 and 5 μs after the impact of the proton beam so that the effective time per burst is 4 μs only. This yields a total effective time of some tens of seconds per year per burst. The measurement of (n,*x*n) cross sections is nevertheless possible, but the method has to be adapted to these extreme conditions. The solution proposed, which is based on a digitalization of the preamplifier signal with a 12 bit, 100 MS/s flash ADC and a segmentation of the detectors, has been developed in several test experiments. The main problem was due to the intense flash from the n_TOF target, which blocked the detectors for more than 120 μs, even at a large distance from the target. The origin of this blocking was attributed to the high muon flux in the experimental room, which has been strongly reduced since then. Similar tests with the same set of detectors at GELINA (IRMM Geel) and at the cyclotron of Louvain-la-Neuve opened interesting opportunities for measurements at these facilities and initiated major steps towards the applicability of the method at n_TOF. A very significant, but not fully sufficient improvement was achieved at CERN by using a new preamplifier, in which a current opposite to the signal is injected and resets the preamplifier. In this test, where the detector was located 70°cm from the beam tube, data could be taken already 2°μs after the flash, corresponding to neutron energies lower than 50 MeV. When the detector was set as close as 12°cm from the sample, it recovered after less than 25 μs. Its behavior suggested that an energy between 10 MeV and 40 MeV is deposited in the detector during each flash. From these observations, it appears that there is still a large flux of muons in a narrow zone around the beam pipe. FLUKA simulations will be performed in order to understand the energy deposit in the detector at time t=0, and to find solutions to lower it to acceptable values,
Possibly by an additional iron shielding that may suppress the problem with the flash completely. In summary, HPGe detectors can already now be used at n_TOF below about 1 MeV, i.e. for studying (n,γ) reactions. Further progress for applications at higher energies is anticipated by a segmentation of the detectors and by an improved shielding against the residual muon flux.

Fission detectors

PTB Chamber

Two identical parallel plate ionization chambers (Figure 26a) with fissile deposits of ^{235}U and ^{238}U have been used with the main objective to determine the neutron flux over a wide energy range. These detectors are inter-comparison instruments and were provided by the (from the Physikalisch-Technische Bundesanstalt at Braunschweig, Germany (PTB). A full description of the detectors can be found in Ref. [24].The detectors consist of five platinum plates with fissile deposits on both sides separated by 5 mm of the electrodes made of tantalum. The thickness of the electrodes is about 0.125 mm. The circular plates are 86 mm in diameter, and the fissile deposits have a diameter of 76 mm. The fission chambers are operated under atmospheric pressure with a mixture of 90% Ar and 10% CF_4. The 0.15 mm-thin windows are made of tantalum.

The total mass of ^{235}U and ^{238}U is 201.56 ± 0.60 mg and 197.78 ± 0.60 mg, respectively, corresponding to 444 μg/cm^2/plate for the ^{235}U and 436 μg/cm^2/plate for the ^{238}U chamber. The isotopic purity is about 99.9% for both materials. The detection efficiency is a slowly decreasing function of energy, which varies from about 95% at low energies to 91% for energies of 150 MeV (Figure 26b).

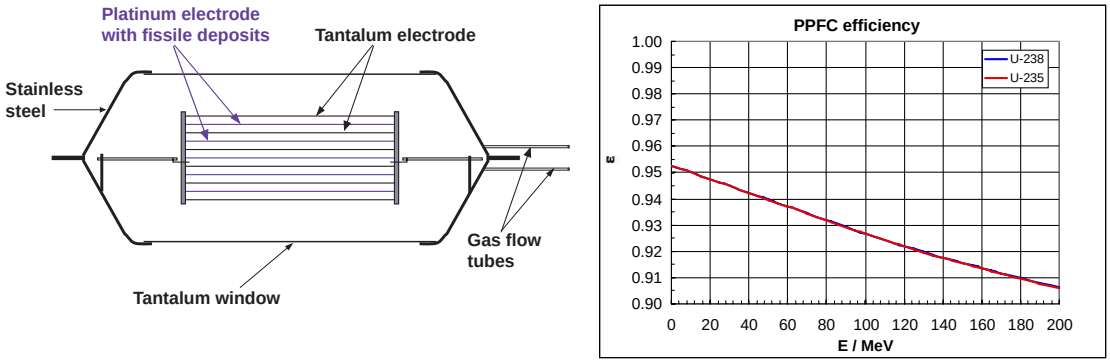

(a) (b)

Figure 26: a) The multi-plate fission chamber from PTB. b) Fission chamber efficiency.

Parallel Plate Avalanche Counters

Parallel Plate Avalanche Counters (PPACs) have been known for many years as a precise timing instrument but were scarcely used before the development of heavy ion physics. A PPAC consists of two thin parallel stretched foils with a very low gas pressure in between. Particles traverse the detector perpendicular to the planes. The principle of operation is the same as a multi-wire proportional chamber. The gap between the foils must a few millimeters only, in order to maintain a high electric field for reducing the time spread and for achieving good time resolution. The electric field has to be uniform to insure the same operating regime on the whole active surface of the detector. Time information is obtained from the central anode made of a 1.5 micron thick aluminized mylar foil with a resolution of 250 ps. The cathodes on both sides of the anode consist of 1.5 μm thick mylar foils with 2 mm wide aluminum strips, which are connected to a delay line with 5 ns resolution/cell, corresponding to a spatial resolution of better than 2 mm.

Due to the high specific ionization of fission fragments, these detectors are operated at low pressures of a few mbar and at a relatively low bias voltage far from the sparking limit. The advantages of PPACs are that they are the thinnest available detectors with excellent time and good position resolution, they can be built in large dimensions, are insensitive to radiation damage, and can be operated at high count rates of more than 2 MHz.

The PPAC detector built for fission cross section measurements at n_TOF is sketched in Figure 27. The samples are typically 300 μg/cm^2 thick and a few cm in diameter. They are deposited on a thin substrate to allow the coincident detection of both fission fragments. Two 20 × 20 cm^2 PPACs are mounted on both sides of each sample at a distance of 15 mm. Apart from the neutron TOF information, the position of an event and the emission angle of the fragments can be reconstructed from the PPAC signals to determine the overall detection efficiency. The detector chamber holds up to 10 samples, including standard samples of ^{235}U, ^{238}U, and ^{209}Bi for normalization of the relative fission yields as well as for flux monitoring.

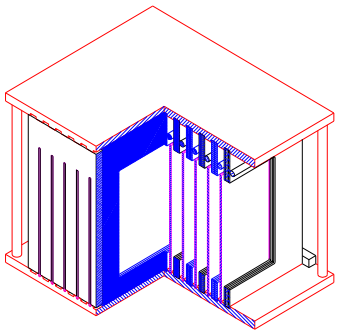

Figure 27: A schematic sketch of the PPAC detector setup for fission measurements at n_TOF. Up to 10 samples can be mounted in the detector chamber.

Fission Ionization Chamber

An optimized fission ionization chamber (FIC) has also been built for cross section measurements at the n_TOF facility as illustrated in Figure 28. Apart from the 125 µm thick Kapton windows, in a first version all metal parts were made of aluminum or aluminum alloy. For safety reasons, two later versions were completely made of stainless steel. The FIC is directly mounted in the TOF neutron beam tube.

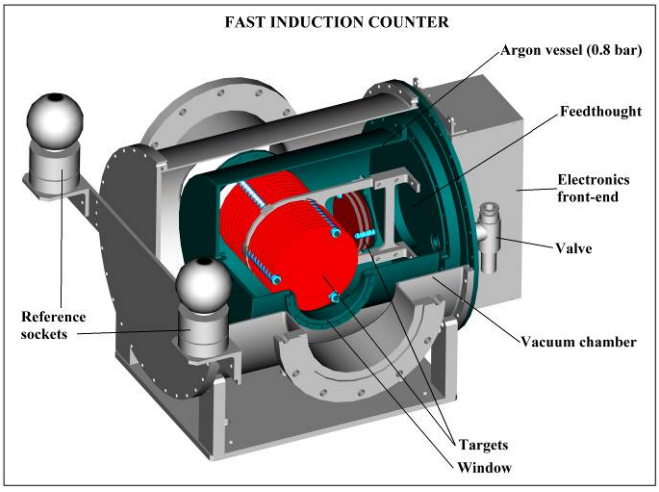

Figure 28: A schematic view of the FIC detector.

The detector is operated without gas circulation using 90% Ar and 10% CF_4 at 0.72 bar. A total of 16 samples and 18 electrodes are stacked in the neutron beam with 5 mm spacings. A smaller stack of three reference samples and four electrodes is mounted outside of the beam to evaluate the background by scattered neutrons. In both stacks one place is reserved for an empty support without deposit.

Figure 29 shows the pulse height distribution of ^{235}U event is plotted in, showing the clear separation between fission fragments and background due to alpha particles and noise. Based on the corresponding pulse height distributions the discrimination threshold was carefully chosen for every channel individually.

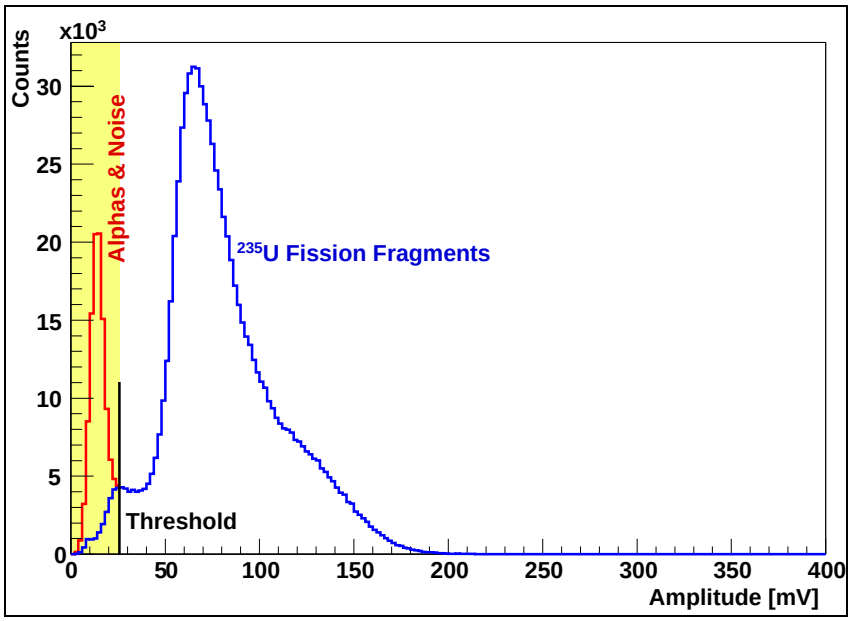

Figure 29: Pulse height distribution of ^{235}U fission events. The discrimination threshold is also indicated.

Data Acquisition Systems

Two independent data acquisition systems have been developed, which match the specific characteristics of the n_TOF neutron beam.

DAQ-A

This innovative, general purpose Data Acquisition System (DAQ) has been designed [25] to match the CERN n_TOF beam repetition rates, the expected event rates, and the characteristics of the detector signals in a most flexible and user-friendly way. The system has the novel feature to sample and store the full analogue waveform of the detector signals for each channel and beam burst by using fast Flash ADCs . Efficient data reduction is achieved by on-line zero-suppression and by recording the data in compressed "tar" file format as illustrated in Figure 30 for the C_6D_6 detector signals from different samples and for the Silicon Monitor.

The hardware specifications of the digitizer modules, the "slow control" and the networking features are presented in references [25] and [26]. The architecture of the DAQ system has been extensively described [25]-[29] and will be addressed only by a brief update. During the n_TOF campaign 2004 the system had reached a capacity of four data streams equipped with 48 digitizer channels feeding 4 PCs and a fifth stream containing 2 PCs for the "slow control" data and the relevant beam information provided by the PS control system. This equipment was situated next to the experimental area, and the data were transferred to the n_TOF control room by an optical Gigabit switch (Figure 31). Three PC Workstations are installed in the control room for the run control, event monitoring, and on-line analysis, and 10 PCs connected to the CERN LXPLUS cluster are installed in offices for further data analysis.

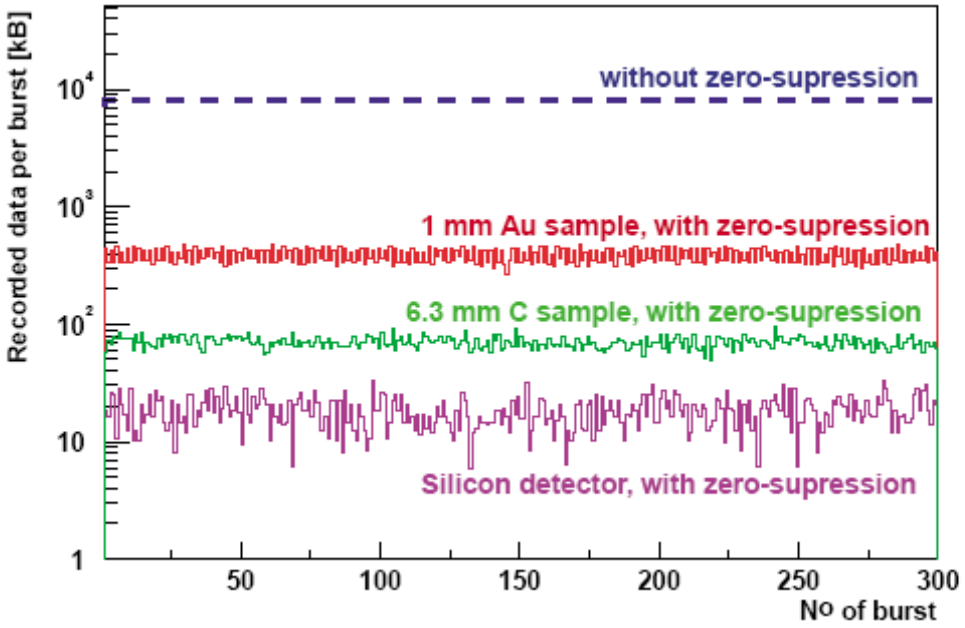

Figure 30: Data reduction efficiency obtained by zero-suppression of the FADC signals illustrated for the signal rates from the C_6D_6 detector. The comparison shows the examples of a 1 mm thick gold sample with ~ 350 signals per burst, of a 6.3 mm thick C sample with ~ 70 signals per burs, and of the Silicon Monitor with ~ 10 signals per burst.

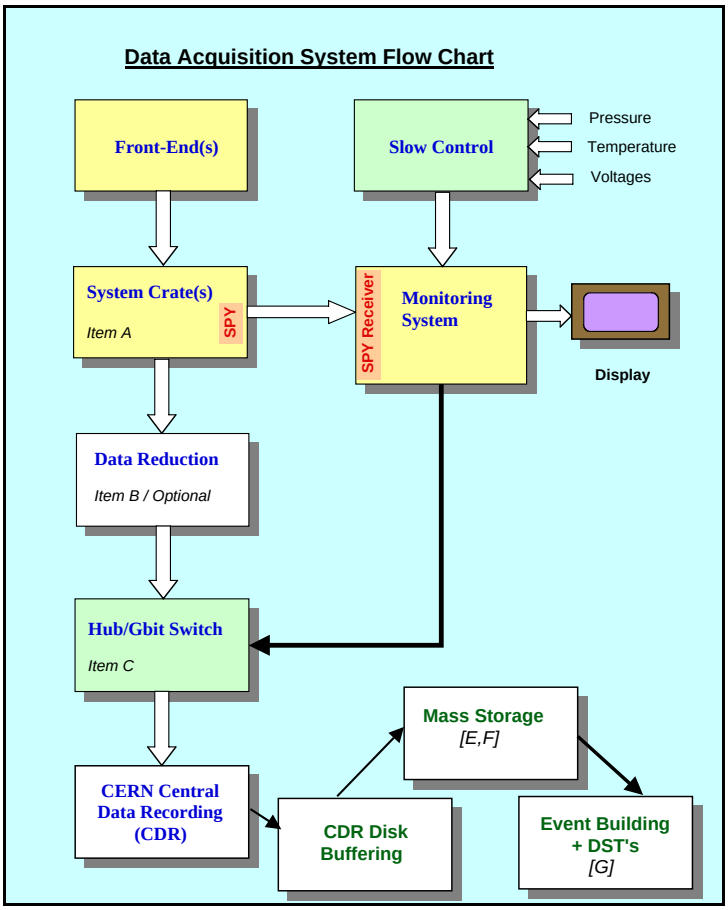

Figure 31: The architecture of the n_TOF data acquisition system.

DAQ-B

During the commissioning phases of the n_TOF facility a second, multi-purpose data acquisition system was developed [29], which has proven to be very robust. Due to its versatile and user-friendly features it is well suited as a general-purpose acquisition system that can be adapted to a variety of experimental requirements. The system was successfully used for the determination of the neutron fluence with the PTB fission chambers, for the measurement of the temperature behavior of the lead target, for investigating the neutron background generated by muons [30], and the activation of the air in the experimental area [31].
In the actual data campaigns at n_TOF it was employed in the fission cross section measurements with the FIC detector. Apart from the n_TOF measurements, the second DAQ was also used in experiments at the PTB neutron facility and for gamma spectroscopy with HPGe detectors.

References

[1] A. Ferrari and P.R. Sala, *Intermediate and High Energy Physics Models in FLUKA: Improvements, Benchmarks and Applications*, Proc. of Int. Conf. on Nuclear Data for Science and Technology, NDST-97, ICTP, Miramare, Trieste, Italy, (19-24 May 1997).

[2] Y. Kadi et al., *The EA-MC Monte Carlo Code Package*, Proc. Of the 5th Meeting on Shielding Aspects of Accelerators, Targets and Irradiation Facilities (SATIF5), Paris (18-21 July 2000).

[3] S. Andriamonje et al., *Neutron TOF facility (PS213) Technical Design Report*, CERN/INTC/2000-004, Editor: E. Radermacher.

[4] A. Abánades et al., *Results from the TARC experiment: spallation neutron phenomenology in lead and neutron-driven nuclear transmutation by adiabatic resonance crossing*, Nuclear Instruments and Methods in Physics Research, A **478** (2002) 577-730.

[5] J.K. Tuli, *Evaluated Nuclear Structure Data File – A Manual for Preparation of Data Sets*; T.W. Burrows, *The program RADLST*, National Nuclear Data Center, Brookhaven National Laboratory, Upton, NY 11973, (29 February 1988).

[6] H.G. Hughes et al., *MCNPX for Neutron-Proton Transport*, Mathematical and Computation Topical Meeting, American Nuclear Society, (27-30 September 1999), Madrid, Spain.

[7] V. Vlachoudis *et al*., *Particle distribution entering the vacuum tube from a 80x80x60 cm^3 lead target*, SL-Note-2000-029 (EET), (30 March 2000). See also the MC-2000 Conference Proceedings, Lisbon (23-26 October 2000).

[8] Y. Giomataris, *et al*., *Micromegas: a high granularity position sensitive gaseous detector for high particle-flux environments*, Nucl. Instr. and Methods A **376** (1996) 29-35.

[9] G. Charpak *et al*., *First beam test results with Micromegas, a high-rate, high-resolution detector*, CERN-LHC/97-08 (EET), DAPHNIA-97-05.

[10] S. Andriamonje et al., Experimental studies of a MICROMEGAS neutron detector, Nucl. Instr. & Methods A 481 (2002) 36-45.

[11] U. Abbondanno *et al.* (The n_TOF Collaboration), *Performance Report*, CERN, INTC-2002-037.

[12] n_TOF-02, *Determination of the neutron fluence, the beam characteristics and the backgrounds at the CERN-PS TOF Facility*. CERN/INTC 2000-016, (2000).

[13] S. Marrone, *et al.*, *A low-mass neutron flux monitor for the n_TOF facility at CERN*, Nuclear Instruments and Methods A **517** (2004), p. 389.

[14] R. Plag, M. Heil, F. Kaeppeler, P. Pavlopoulos, R. Reifarth, and K. Wisshak. *An optimized C_6D_6 detector for studies of resonance-dominated (n,γ) cross sections*, Nuclear Instruments and Methods A 496 (2003), p. 425.

[15] GEANT, *Detector description and simulation tool*, CERN Program Library W5013 (1994).

[16] T. Handler, *et al*., *Unix Version of CALOR89 for Calorimeter Applications*, SDC-92-00257 (May 1992).

[17] J.O. Johnson and T. A. Gabriel, *A User's Guide to MICAP: A Monte Carlo Ionization Chamber Analysis Package*, ORNL/TM-10340 (January 1988).

[18] F. Corvi, G. Fioni, F. Gasperini, P. B. Smith, *The weighting function of a neutron capture detection system*, Nuclear Science & Engineering **107** (1991), 272.

[19] F. G. Perey, J. O. Johnson, T. A. Gabriel, R. L. Macklin, R. R. Winters, J. H. Todd, and N. W. Hill, *Response of C_6D_6 and C_6F_6 gamma-ray detectors and the capture of the 1.15 keV resonance of ^{56}Fe*. Proceedings of the International Conference on Nuclear Data for Science and Technology, Mito, Japan, 30 May-3 June 1988, p. 379 (1988).

[20] EGS4: Monte Carlo Simulation of the Coupled Transport of Electrons and Photons, SLAC-PUB-6499.
[21] J. L. Tain *et al.*, *Accuracy of the pulse height weighting technique for capture cross section measurements*, Journal of Nuclear Science and Technology, Supplement **2** (2002) p. 689.
[22] K. Wisshak, *et al*., Nuclear Instruments Methods A **292**, 595 (1990).
[23] M. Heil, *et al*., Nuclear Instruments and Methods A **459**, 229 (2001).
[24] D.B. Gayther, *International Intercomparison of Fast Neutron Flux-Rate Measurements Using Fission Chamber Transfer Instruments*. Metrologia **27** (1990), p. 221-231.
[25] The n_TOF Collaboration, n_TOF Technical Report, CERN/INTC 2000-018, (3 November 2000).
[26] H. Wendler *et al.*, The n_TOF General Data Flow, n_TOF Note 200502, (May 2000).
[27] D. Cano-Ott *et al.*, The n_TOF data access package, n_TOF Note 210402, (April 2000).
[28] U. Abbondanno *et al.* (The n_TOF Collaboration), *The data acquisition system of the n_TOF facility at CERN*, Nuclear Instruments and Methods A, in press.
[29] V. Vlachoudis, *A multi purpose DAQ system developed for the n_TOF commissioning*, in Proceedings of CHEP 2001, Edited by H.S. Chen, Science Press New York, pg. 562, (2001).
[30] The n_TOF Collaboration, *Study of the Background in the Measuring Station at the n_TOF Facility at CERN: Sources and Solutions*, CERN/SL/Note 2001-046, CERN/INTC 2001-038.
[31] V. Lacoste, *Gamma Background Measurement in the n_TOF Experimental Area*, Internal Note, CERN/SL/EET 2000-006.

Capture Cross Sections of long-lived fission product nuclei, coolants, and structural materials

Contributed by *F Käppeler* (FZK, Karlsruhe)

Introduction

Neutron capture cross sections of long-lived fission products (LLFP) represent a key issue for concepts of nuclear incineration. So far, these data were rather poorly known and figured prominently in the "High Priority Nuclear Data Request List" of the Nuclear Energy Agency (NEA/OECD), where a 5% accuracy is requested for these data in the entire energy region from thermal to 20 MeV. The experimental determination of these cross sections is difficult because of enhanced backgrounds due to the radioactivity of the samples, the radiotoxicity of the sample material, or simply by the fact that sufficiently large samples were not available. Thanks to the efforts at GELINA, the electron linear accelerator at Geel, and at the n_TOF facility at CERN, these difficulties could be solved, thus allowing for the successful measurements on ^{151}Sm and ^{93}Zr (see also measurements on ^{129}I and ^{99}Tc at GELINA (see pag. 95). The excellent sensitivity of these measurements is best illustrated by the fact that the ^{151}Sm cross section could be measured at n_TOF with a sample containing only about 150 mg of this isotope. Note that ^{93}Zr was investigated in place of the originally planned ^{79}Se, for which it was impossible to find a suited sample.

The previously reported neutron capture cross sections of the Pb isotopes and of ^{209}Bi showed large systematic uncertainties because of the experimental difficulty in treating the unfavorably large scattering to capture ratios in a proper way. While the small capture cross sections dictated the use of fairly bulky samples, the large scattering cross sections led to correspondingly large backgrounds due to capture of scattered neutrons in the γ-ray detectors used. This dilemma could be greatly reduced at the n_TOF facility. Thanks to the very high luminosity of this neutron source, which results from the combination of a high neutron flux and the very low repetition rates, it became possible to perform measurements on much smaller samples. And by the development of detectors with minimal neutron sensitivity, the uncertainties due to backgrounds from scattered neutrons became negligibly small.

The measurements on the stable isotopes of Mg, Zr, and on ^{139}La were carried out partly because this information was needed for data analysis (the ^{93}Z sample was enriched to only 20%) and partly because these isotopes represent relevant structural materials and/or fission products.

This section corresponds essentially to work package 11, for which all deliverables are completed. The capture cross sections of ^{151}Sm, ^{129}I, ^{99}Tc, ^{207}Pb, and ^{209}Bi, have all been published in detailed reports or in refereed journals. The papers describing the measurements on the Pb cross sections are well advanced and will soon be submitted.

Capture measurements on ^{151}Sm

The samarium isotopes are of relevance for nuclear reactor studies, and in particular for transmutation projects. In particular, the neutron capture cross section of ^{151}Sm is important in the design of any "traditional" nuclear reactor as well as for the development of advanced devices

for waste incineration schemes such as those based on accelerator driven systems (ADS). This fission product isotope is, in fact, produced in the nuclear fuel during the operation of a reactor with a sizeable fission yield of ~0.4%. Due to its large thermal capture cross section, ^{151}Sm represents a neutron poison in thermal reactors as it absorbs a certain fraction of the neutrons necessary to sustain the fission chain. In fast reactors and in ADS, ^{151}Sm affects the neutron balance, because it has one of the largest capture cross sections in the intermediate energy region. In both scenarios, the neutron capture cross section is of key interest in order to obtain reliable information on the amount of this unstable isotope ($t_{1/2}$ = 93 yr) produced during the fuel cycle.
The transmutation of ^{151}Sm is currently being considered in all incineration schemes. Although the high neutron absorption rate may compromise the necessary criticality of an ADS system, the main attention is focused on the consequences for the interim storage facility due to the high toxicity and the large production yield of this isotope.
In view of the above motivations, it is mandatory for any ADS project to know the capture cross section of ^{151}Sm with high accuracy. A specific request for this data has been included in the NEA "High priority nuclear Data Request List", 4.D.28. Apart from the thermal value, no capture cross section measurements have been performed so far, mostly due to the difficulty associated with the radioactivity of the sample. In this respect, the n_TOF facility is perfectly suited for such a study due to its innovative features, in particular the very high instantaneous neutron flux and the low repetition rate, that allows to greatly improve the signal-to-background ratio.

Experimental procedures

The ^{151}Sm(n,γ) measurement was performed in May 2002, soon after the final commissioning of the n_TOF facility. The experimental apparatus consisted in the low neutron sensitivity C6D6 (deuterated benzene) liquid scintillator cells, specifically designed with carbon-fibre container to further minimize the neutron sensitivity [1]. The sample used in the measurement consisted of 206 mg Sm_2O_3 powder, compressed and sealed inside a low-mass titanium can of natural composition 1 cm in diameter. This sample was prepared by Oak Ridge National Laboratory. It was mounted on a low-mass sample changer, together with reference samples of Au, C, Pb, and an empty Ti can. The data were recorded with the n_TOF acquisition system based on fast Flash ADCs from Acqiris [2]. The Pulse Height Weighting technique was used to correct for the dependence of the detection efficiency on the energy and multiplicity of the de-excitation cascade following neutron capture [3]. Detailed Monte Carlo simulations of the experimental setup were used to determine the weighting functions, which are important for achieving the required linear dependence of the detection efficiency with γ-ray energy.

Interpretation

The measurement allowed to extract the capture yield in the full energy range from 1 eV to 1 MeV, i.e. covering the resolved and unresolved resonance regions in a single experiment. Figure 32 shows the yield measured with the Sm_2O_3 sample together with the overall background. The ^{151}Sm capture cross section in the unresolved resonance region was determined after careful subtraction of the different background components, estimated with dedicated measurements and Monte Carlo simulations. Corrections for dead time, multiple scattering and self-absorption were applied, and the contribution of contaminant isotopes was subtracted. The Au capture data were used to determine the absolute neutron flux. The overall uncertainty was estimated to be 6%. The present results are in perfect agreement with a parallel measurement [4] using the 4π BaF_2 array at FZK (see WP17). Among the previous evaluations the JEF data base was found to be in fair agreement with the measured cross sections.
In the resolved resonance region, the resonance parameters (energy, neutron and capture width) were determined by analyzing the capture yield with the R-matrix analysis code

SAMMY. Approximately 500 resonances could be analysed up to 1 keV thanks to the high resolution of the n_TOF neutron beam. With these results the previous information from a transmission measurement of the total cross section could be substantially extended and allowed for a much more accurate evaluation of the level density parameter. The cross section analysis was part of a dissertation at the University of Bari .
The results of the ^{151}Sm(n,γ)^{151}Sm cross section measurement have been published in Physical Review Letters [5]. A detailed description of the experiment, the analysis and the results are the subject of an extended paper that has been accepted by Physical Review C[6]. Furthermore, the results of this measurement have been presented at several international conferences.

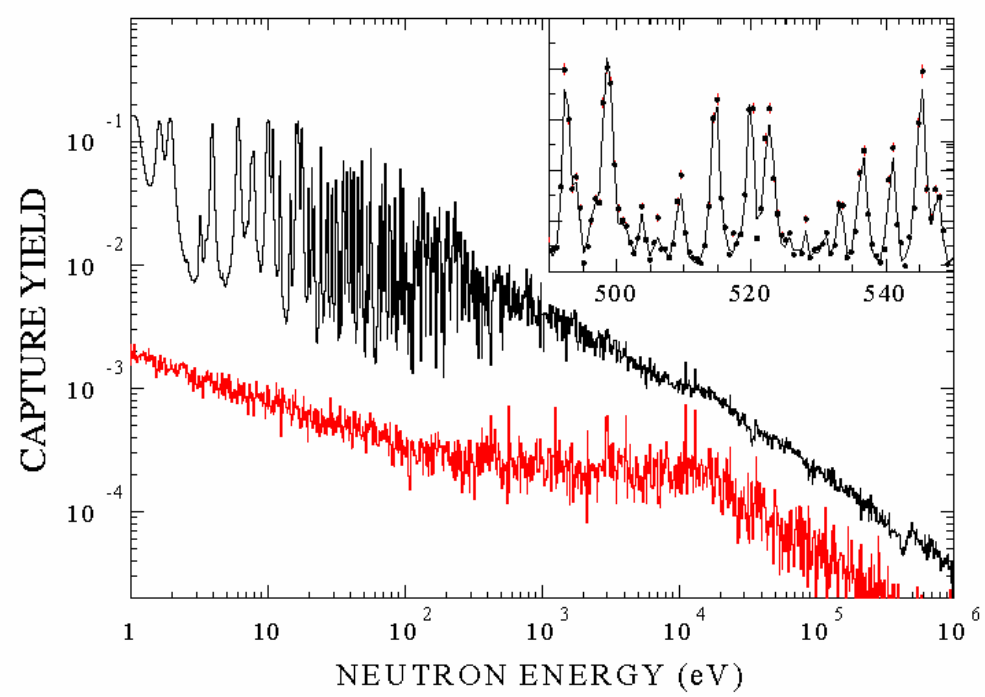

Figure 32: Measured capture yield of ^{151}Sm. The overall background is also shown in the figure. The insert shows a SAMMY fit of the resonances around 500 eV.

Deliverables

A paper has been published in Physical Review Letter [5]. Tables with resonance parameters and cross sections in the unresolved resonance region are included in a second paper being submitted to Physical Review C [6]. Inclusion of the results in EXFOR is in progress.

References

[1] R. Plag *et al.*, Nuclear Instruments and Methods A **517**, 389 (2002)
[2] U. Abbondanno *et al* (The n_TOF Collaboration), Nuclear Instruments and Methods A **538**, 692 (2005)
[3] U. Abbondanno *et al* (The n_TOF Collaboration), Nuclear Instruments and Methods A **521**, 425 (2004)
[4] K. Wisshak *et al.*, Report FZKA 6996, Forschungszentrum Karlsruhe (2004), and accepted by Physical Review C
[5] U. Abbondanno *et al.* (The n_TOF Collaboration), Physical Review Letters **93**, 161103 (2004)
[6] S. Marrone *et al* (The n_TOF Collaboration), accepted by Physical Review C

Capture measurements for ^{93}Zr

The measurement of the capture cross section of ^{93}Zr was decided to replace the measurement on ^{79}Se. Though originally included in the deliverable list it turned out impossible to find the necessary ^{79}Se sample. The unstable isotope ^{93}Zr ($t_{1/2}$ = 1.5x10^6 yr) is one of the major long-lived fission products, since it is situated in the maximum of the fission yield distribution. It, therefore, needs to be included in any incineration scheme with ADS. In the "High Priority Nuclear Data Request List" of the Nuclear Energy Agency (NEA/OECD), a 5% accuracy is requested for the ^{93}Zr(n,γ) cross section in the entire energy region from thermal to 20 MeV. Mainly for this reason, an improved measurement of this cross section was adopted in the n_TOF_ND_ADS project.
Furthermore, the cross sections of the stable zirconium isotopes are also of interest for reactor technology. Due to its small capture cross section as well as its favorable chemical and mechanical properties, this element is an important component in alloys used for structural materials in nuclear reactors, e.g. for cladding of fuel elements for all reactor types, including pressurized water reactors (PWRs), boiling water reactors (BWRs), and natural uranium reactors (CANDU). With the present research programs on reactors with fast neutron spectra, including ADS, there is a growing demand for the determination of precise capture cross sections for fast neutrons, aimed at improving the rather uncertain information contained in the Nuclear Data libraries.

Experimental procedures

The measurement was performed in two steps. In 2003, the cross sections of all stable isotopes were measured using samples with high isotopic enrichments. In August 2004, after obtaining the permission from the Safety Division of CERN, the unstable ^{93}Zr isotope was finally measured. The experimental apparatus is similar to the one employed in capture measurements for other LLFP isotopes. It consisted of two C_6D_6 detectors with minimized neutron sensitivity. The signals from these detectors were recorded with fast Flash ADCs for further off-line analyses. The Pulse Height Weighting technique was applied with weighting functions determined for each sample individually. The weighting functions were determined by detailed Monte Carlo simulations. The sample consisted of 4.461 g ZrO_2 powder with an isotopic enrichment in ^{93}Zr of 20%. The sample was pressed into a pellet 22 mm in diameter and encapsulated in a titanium can. Reference samples of C, Pb, and Au as well as an empty can were also measured in order to estimate the various background components and to determine the absolute normalization factor.

Interpretation

The analysis of all stable isotopes is complete. A total of approximately 400 resonances, some of which not observed in previous measurements, have been analysed with the R-matrix code SAMMY, using the n_TOF resolution function. On average, the strength of the resonances was found to be 10% to 20% lower than previously reported [1-3]. The analysis of the ^{93}Zr(n,γ) ^{94}Zr cross section is progressing. The yield (left panel of figure 1) shows a large number of well resolved resonances up to almost 10 keV, thanks to the high resolution in neutron energy of the n_TOF facility. All resonances belonging to stable isotopes have been identified (see, for example, the right panel of figure 1). The remaining resonances, attributed to ^{93}Zr, are being analysed with SAMMY. The accuracy of the present measurement, mostly associated to the weighting function technique and to the flux determination, is typically around 5%. A comparison with the only previous measurement of the capture cross-section is being performed [4]. From the present data we expect a significantly improved accuracy for this isotope as a consequence of the accurate determination of the cross sections for all stable zirconium isotopes, which constitute the isotopic impurities. Furthermore, the high resolution of the n_TOF beam allows to extend the region of resolved resonances.

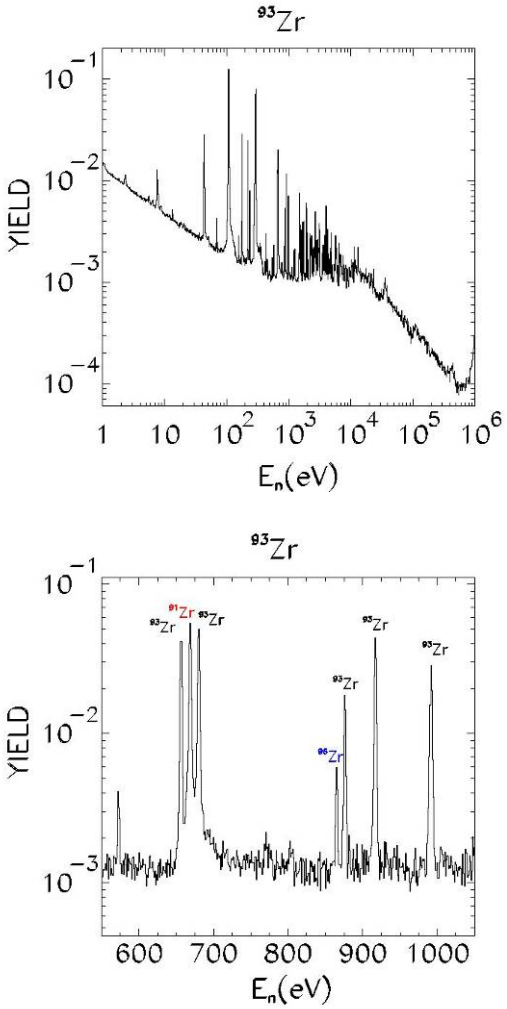

Figure 33: Measured capture yield of ^{93}Zr. In the left panel, the yield in the whole energy region between 1 eV and 1 MeV shows the high resolution achieved in the measurement. In the right panel, the analysis around 1 keV shows several well identified resonances of ^{93}Zr together with contaminations from other isotopes.

Deliverables

The resonance analyses of all investigated Zr isotopes have been completed and the publication in a refereed journal is in preparation. The deduced resonance parameters and average cross sections will be included in the EXFOR data base.

References

[1] Z.M. Bartolome et al., Nuclear Science and Engineering **37**, 137 (1969)
[2] J.W. Boldeman et al., Nuclear Physics A **246**, 1 (1975)
[3] G. Leinweber et al., Nuclear Science and Engineering **134**, 50 (2000)
[4] R.L. Macklin, J.A. Harvey and N.W. Hill, Nuclear Science and Engineering **92**, 525 (1986).

Capture measurements on bismuth and lead isotopes

The capture cross sections of bismuth and of the lead isotopes are very important with respect to modern transmutation concepts for nuclear waste. The design of an Accelerator Driven System (ADS) using a lead-bismuth eutectic as spallation target and coolant requires accurate capture cross sections for these isotopes, since they represent a large fraction of the mass of the device and have, therefore, a strong effect on the neutronics of the system. Capture on bismuth determines also the radiotoxicity of the spallation target represented by a long term component via the production of the isomer ^{210m}Bi with a half life of $t_{1/2}=3\times10^6$ yr and a short term component via the decay product ^{210}Po with $t_{1/2}$=138 d.

From the experimental point of view, these measurements are hampered by the very small cross sections, resulting in long measuring times and critical background problems. Under these conditions, systematic uncertainties due to background from sample scattered neutrons are particularly crucial. Since previous cross section measurements were clearly suffering from this type of systematic uncertainties, new measurements with an improved setup were called for. At n_TOF an optimized setup was developed using detectors of low efficiency made of deuterated benzene (C_6D_6), which contained a minimum amount of dead materials [1]. In this way, the corrections for scattered neutrons became negligibly small in most cases or were at least reduced by an order of magnitude.

The use of such low efficiency detectors for the prompt capture γ-rays requires the application of the so called Pulse Height Weighting Technique (PHWT). Since the accuracy of this technique had been questioned In the past [2] a series of dedicated measurements was performed at n_TOF. These have shown that a precision of better than 2% can be achieved if the detector response is carefully modeled by detailed Monte Carlo simulations [3].

Measurements

The measurements have performed during the n_TOF campaign of 2002. The setup included two C_6D_6 detectors of the type mentioned above. The detectors were placed at about 125° with respect to the neutron beam in order to reduce the background caused by in-beam photons scattered on the sample and to minimize the effect of γ -ray angular distributions. The disk-shaped samples were 20 mm in diameter and consisted of pure, natural ^{209}Bi and of isotopically enriched Pb. The respective sample masses and enrichments as well as the total number of protons employed for each isotope are listed in Table 1. Compared to previous studies the sample masses were significantly reduced in order to minimize the sample-related corrections and the corresponding systematic uncertainties.

Additionally, a ^{197}Au sample was measured for normalization of the total number of neutrons using the saturated resonance method. The data acquisition system developed at n_TOF is based on Acqiris digitizers [4]. During all measurements the neutron beam intensity was continuously monitored using the SiMON detector [5].

Table 1: Sample characteristics and integrated proton beam intensities

Isotope	Enrichment (%)	Mass (g)	Number of protons (in units of 10^{17})
^{204}Pb	99.708	4.039	6.79
^{206}Pb	99.76	8.123	4.1
^{207}Pb	92.40	8.000	4.0
^{208}Pb	98.5	12.531	5.51
^{209}Bi	100	18.905	6.16

Results

The publication of ^{209}Bi is submitted [6] and the resonance analyses of the Pb cross section using the R-matrix code SAMMY [7] are completed. In this context a new method was developed for obtaining reliable weighting functions for application of the PHWT to thick samples [8]. Fig. 1 shows a comparison between our more accurate results with current evaluated data files. The obvious discrepancies are clearly calling for an update of the evaluations.

Deliverables

Final publications for refereed journals have been or are being finalized. Data files for diffusion in EXFOR format are in preparation. Part of these measurements were subject of a PhD thesis [8].

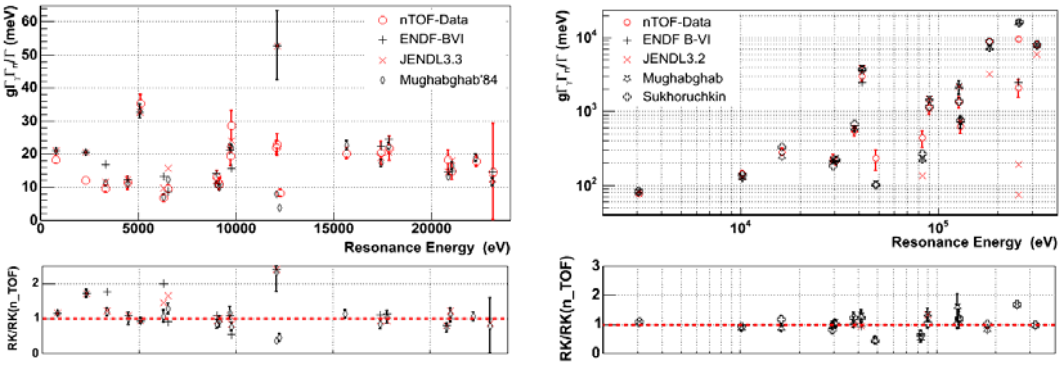

Figure 34: Comparison of the present radiative capture kernels RK = gΓγΓn/Γ with evaluated data files for the examples of ^{209}Bi (left) and ^{207}Pb (right).

References

[1] R. Plag et al., Nucl. Instrum. and Meth. A **496** (2003) 425.
[2] J.L. Tain et al., J. Nucl. Sci. and Techn., Supplement 2 (2002) 689.
[3] U. Abbondanno et al., Nucl. Instrum. and Meth. A **521** (2004) 454.
[4] U. Abbondanno et al., Nucl. Instrum. and Meth. A **538** (2005) 692.
[5] S. Marrone et al., Nucl. Instrum. and Meth. A **517** (2004) 389.
[6] C. Domingo-Pardo et al., submitted to Phys. Rev. C.
[7] N.M. Larson, SAMMY-M6, ORNL/TM-9179/R6 (2003).
[8] C. Domingo-Pardo, PhD Thesis, Univ. of Valencia, Spain, Feb. 28, 2005.

Capture measurements on ^{24,25,26}Mg

Within the n_TOF-ADS_ND project these measurements were not listed among the deliverables, but reliable cross sections for the Mg isotopes are desirable as magnesium plays an increasingly important role as a structural material. Since the small cross sections of these light isotopes are difficult to measure the few available data suffer from severe systematic uncertainties. With the excellent resolution and the high flux of the CERN n_TOF facility the experimental techniques are significantly improved resulting in a new and promising access to these persistent problems. Apart from this immediate relevance as a structural material, the measurement of these cross sections has a pilot function for the investigation of small, resonance-dominated cross sections.
The available experimental data for ^{24,25,26}Mg are essentially based on a single measurement that was carried out at the electron linear accelerator in Oak Ridge [1] Though fairly small uncertainties are claimed for the resulting cross sections, the setup used at that time turned out to be rather sensitive to scattered neutrons. This problem led to discrepancies of factors two to four in case of the ^{208}Pb and ^{209}Bi cross sections, which are similarly dominated by relatively few resonances [2]. Recent activation studies on ^{26}Mg [3] have indeed reported three times smaller resonance contributions, thus confirming this severe problem of the existing data.

Measurements

The measurements have been performed using isotopically enriched oxide samples of ^{25,26}Mg as well as a natural metal sample. Capture events were detected with two C_6D_6 detectors that had been optimized for minimal neutron sensitivity [4]. Otherwise, the experimental conditions were similar to the situation during the Pb/Bi measurements described before.

Results

A detailed R-matrix analysis using the SAMMY code [5] has meanwhile been completed. ??I have asked Paul and Shawn for the status……??

References

[1] H. Weigmann, R. Macklin, and J. Harvey, Phys. Rev. C **14**, 1328 (1976).
[2] Z.Y. Bao, H. Beer, F. Käppeler, F. Voss, K. Wisshak, and T. Rauscher, Atomic Data Nucl. Data Tables **76**, 70 (2000).
[3] P. Mohr {\it et~al.}, Phys. Rev. C **58**, 932 (1998) and Phys. Rev. C **60**, 017603 (1999).
[4] R. Plag et al., Nucl. Instr. Meth. A **496** (2003) 425.
[5] N.M. Larson, SAMMY-M6, ORNL/TM-9179/R6 (2003).

Capture Cross Sections of the Th-cycle isotopes: ^{232}Th, and ^{233,234,236}U

Contributed by *F Gunsing* (CEA, Saclay)

Introduction: The thorium fuel cycle

In the currently operating nuclear fission reactors the spent fuel elements account for the largest part of the nuclear waste in terms of radiation activity. In addition to uranium, the waste consists of fission products and isotopes of plutonium and minor actinides like neptunium, americium and curium. After a cooling period of the spent fuel necessary to diminish the activity due to the shorter lived fission products, the remaining material is considered as waste (after a possible extraction of the uranium and plutonium which can be re-used as fuel). The high activity and long lifetimes of several isotopes present in the nuclear waste necessitates long term storage under safe conditions on a very long time scale, reaching several hundreds of thousand of years. Transmutation of these isotopes by means of neutron capture or fission could considerably reduce the radiotoxicity inventory.

A different approach is to reduce the amount of nuclear waste, notably the higher actinides, by using a fuel cycle based on ^{232}Th. The isotope ^{232}Th itself is not fissile but after neutron capture followed by β-decay, the fissile isotope ^{233}U is formed. An interesting advantage from the point of view of production of radioactive waste in using the ^{232}Th/^{233}U-based fuel cycle as compared to the classic uranium cycle is related to its low production in of higher mass actinides. The lower atomic number of thorium with Z = 90, instead of Z = 92 for uranium, reduces significantly the build-up of heavy transuranium isotopes, in particular plutonium and curium.

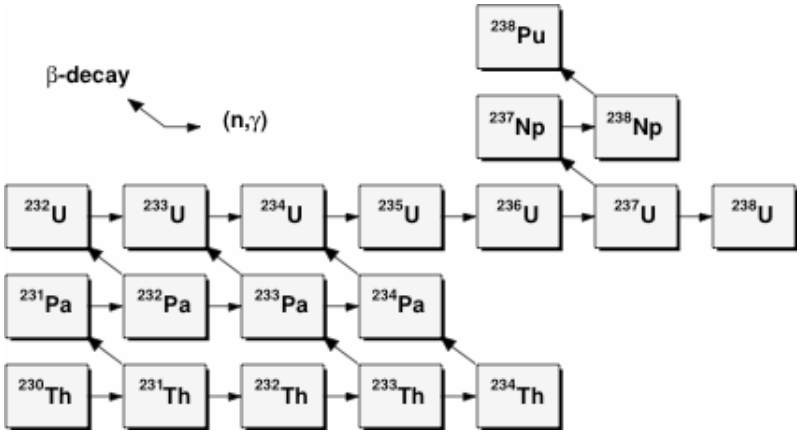

Figure 35: Schematic view of the actinide build-up chain of the thorium cycle.

The build-up of the higher actinides, especially americium and curium, is strongly suppressed due to the lower atomic and mass number of thorium, as is shown in Figure 35. In addition other arguments play a role. The natural abundance of thorium is three times larger than that of uranium so extends potentially the existing fuel resources. Also the number of neutrons produced after absorption of a neutron in a reactor environment is larger for ^{233}U than for ^{235}U or ^{239}Pu for thermal neutrons, opening the possibility, although technically still quite complicated, for a "thermal breeder".

Several experimental projects using thorium have already been worked out in the past on critical assemblies (Molten Salt Reactor, CANDU-Th, High-Temperature Gas Reactor). Due to encountered technical problems but also overshadowed by the rapid industrialized production of uranium-based reactors, a long history of research and development has been

focused on the uranium based cycle, which is nowadays the standard for all operating power plants, and is at present missing for thorium.

The objective of Work Package 12 is the determination of the capture cross sections of the isotopes ^{232}Th, ^{231}Pa, ^{233}U, ^{234}U, and ^{236}U, relevant in the Th-fuel cycle. The following table gives a summary of the performed measurements which will be described in more detail below.

isotope	Status
^{232}Th	Measurement done at CERN in 2002 with C_6D_6 detectors
^{231}Pa	Sample unavailable
^{233}U	Measurement done at CERN in 2004 with BaF_2 TAC
^{234}U	Measurement done at CERN in 2004 with BaF_2 TAC
^{236}U	Measurement done at GELINA in 2004 with C_6D_6 detectors

The measurement of the ^{232}Th(n,γ) cross section at CERN n_TOF

The measurement of the ^{232}Th(n,γ) cross section was performed at the CERN n_TOF installation using two C_6D_6 detectors placed perpendicular to the neutron beam. The samples were placed in a remotely controlled sample changer. The distance from the center of the beam was 2.9 cm and the detectors were placed 9.2 cm backward from the center of the sample in order to reduce the scattered photon background. Two disc-shaped thorium samples with a total mass of 2.8 grams and a diameter of 1.5 cm have been measured together at CERN. The thickness of sample is such that some low-energy resonances are saturated from which the absolute normalization can be obtained. In addition to these samples, we used a natural lead sample to estimate the scattered photon background and a gold sample to verify the analysis procedure. The purity of Th sample was 99.5% according to the specifications.

The recorded events were processed from the DST files and the amplitude and time-of-flight information for the C_6D_6 detectors and the silicon detectors was extracted. A pulse height weighting function, calculated from simulated detector responses to mono-energetic gamma rays, was applied to the C_6D_6 data to obtain a detector efficiency independent from the gamma-ray cascade following neutron capture. For the calibration of the pulse height distribution of the C_6D_6 detectors we measured the response to radioactive sources of ^{137}Cs, ^{60}Co and a composite source of ^{238}Pu together with ^{13}C.

The use of flash ADCs limits the effective dead time in the order of a few tens of nanoseconds, related to the software pulse extraction. Its effect is often negligible, except at large local count rates, like in large resonances. In the event processing, we therefore applied a fixed dead time of 30 ns, for which the count rate can be corrected exactly. All spectra are normalized to the number of counts in the in-beam silicon flux monitor, which is supposed to be proportional to the number of incident neutrons.

Several components contribute to the background. The radioactivity of the sample has been measured with the neutron beam switched off. The gamma-ray spectrum of the ^{232}Th samples have gamma-ray energies going up to 2.6 MeV originating from the beta decay of the daughter product ^{208}Tl. This presents a constant background in time and is visible as a decreasing line when represented as a function of the equivalent neutron energy. With the

high instantaneous flux of the n TOF installation this background is relevant only at low neutron energies and can be easily subtracted or fitted with the data.

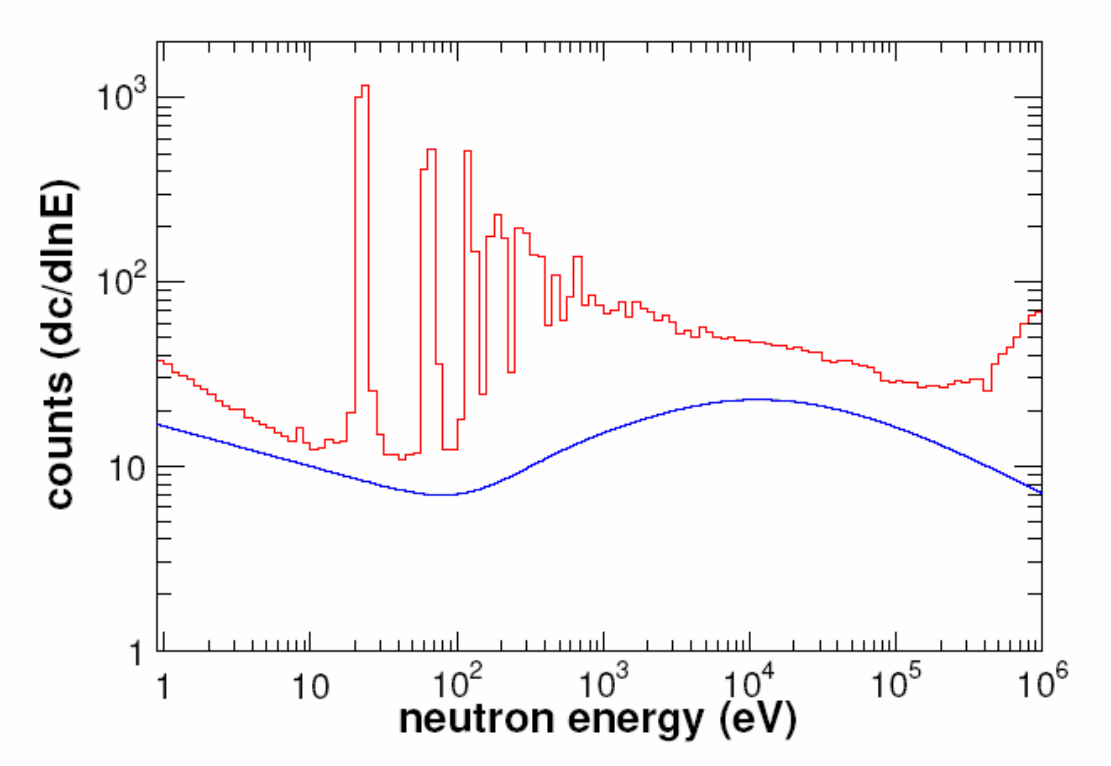

Figure 36: the count rate of the thorium spectra together with its background.

The main source of background in the keV region comes from in-beam gamma rays scattered from the sample and detected in the C_6D_6 detectors. Measurements have been taken of the thorium sample with and without neutron filters in the beam. The neutron filters remove the neutrons at specific energies, corresponding to large resonances of the filters with zero transmission, the so-called black resonances. We have used measurements with a 30 mm thick aluminum filter. The level of the background in the measurements with filters corresponds to the valleys of the black resonances. But the neutron filter also attenuates the in-beam photons that are scattered from the sample. In order to obtain the level of the background in the measurements without filters, we have corrected for the attenuation of the in-beam gamma-rays by the filters. The general shape of the background as a function of the time of flight was modeled by the sum of three components. The background subtracted spectra were normalized by the saturated resonances at low energy to provide the absolute normalization.

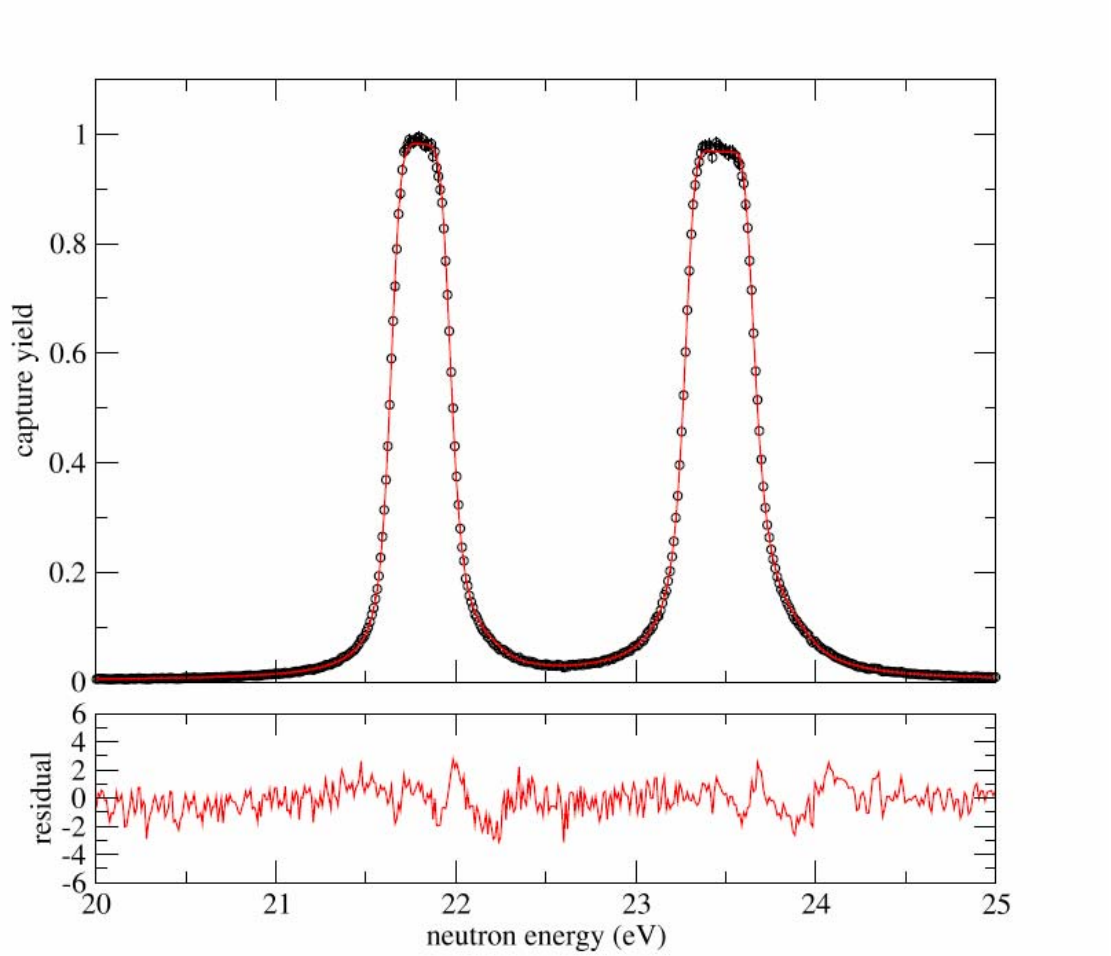

Figure 37: R-matrix fit of the saturated resonances in thorium in order to derive the absolute normalization.

From the experimental spectra we derived the capture yield, which is the experimental result of this experiment. The relation between the capture yield and cross section requires further analysis which is divided in two regions: the resolved resonance region (RRR) and the unresolved resonance region (URR). In the URR the capture yield is corrected for self-shielding effects and for the energy dependent incident neutron beam fraction. This resulted in the capture cross section in the energy range from 5 keV to 1 MeV. At lower energies in the RRR were resonances are resolved, the cross section is parameterized in R-matrix resonance parameters.

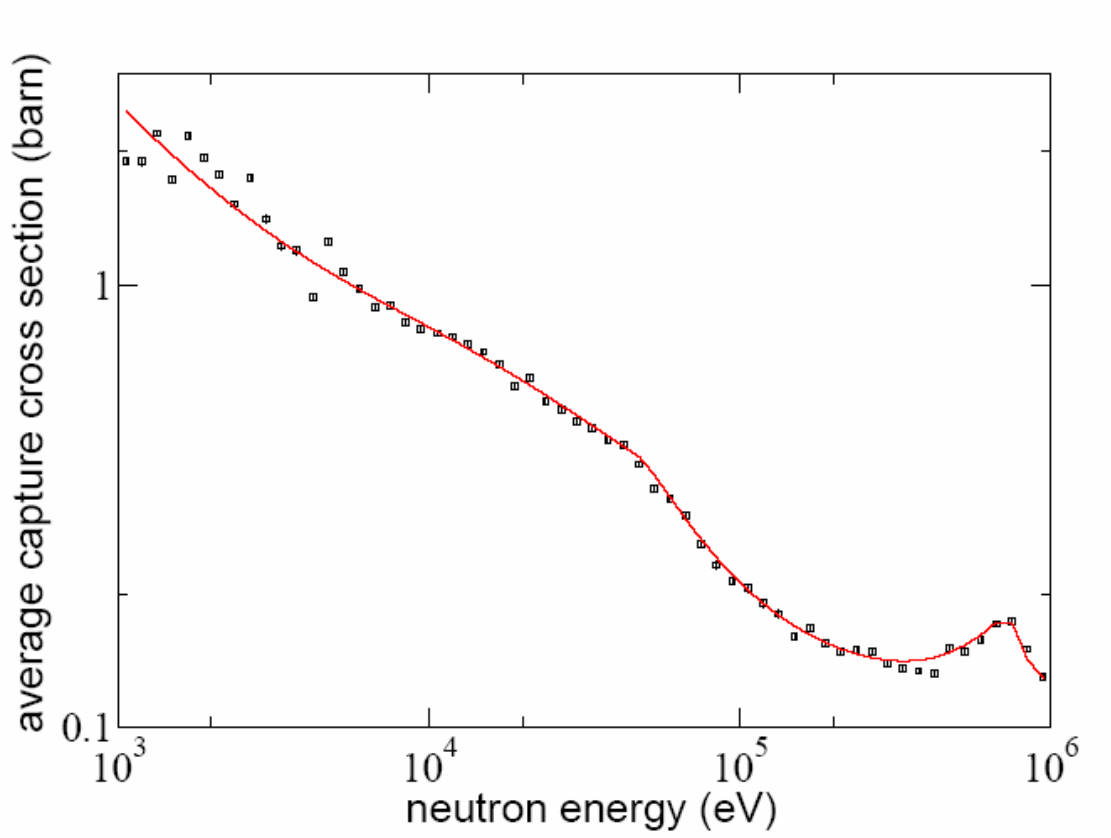

Figure 38: The capture cross section of thorium from 1 keV to 1 MeV together with a fit of the average resonance parameters.

The measurement of ^{233}U(n,γ) and ^{234}U(n,γ) with the TAC at CERN

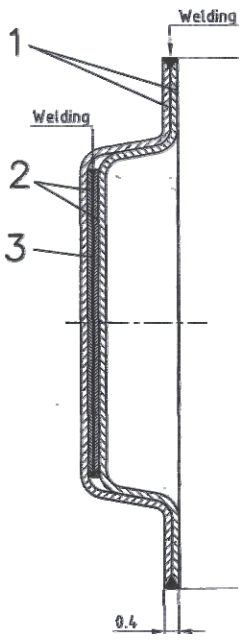

In order to be allowed to measure these radioisotopes at CERN, samples had to be ISO-2919 compliant (sealed source). In order to fulfill this rule both samples (3) were surrounded by an about 0.02 mm thick aluminum foil (2), and encapsulated by a 0.17 mm thick titanium GOST 19807 foil (1) above and below the radioactive spot. The source diameter is 15 mm, for a 10 mm active diameter. These samples were delivered by the IPPE Obninsk, Russia.

^{233}U sample

The ^{233}U sample consists of a 10 mm diameter disk containing 10.8 mg of enriched U_3O_8 giving 9.1 mg of ^{233}U. The isotopic purity (in atomic %) is: ^{233}U-99.01, ^{234}U-0.74, ^{235}U-0.23, ^{238}U-0.04. The sample activity is 3.565 10^5 Bq/mg.

^{234}U sample

The ^{234}U sample consists of a 10 mm diameter disk containing 38.7 mg of enriched U_3O_8 giving 32.7 mg of ^{234}U. The isotopic purity (in atomic %) is higher than 99% for ^{234}U. The sample activity is 2.31 10^5 Bq/mg.

Experimental set-up

Both experiments were performed using the newly installed Total Absorption Calorimeter (TAC) at CERN. In order to avoid low energy scattered neutrons, a neutron absorber was surrounding the sample. The signal of each individual crystal was digitized during 16 ms. For each event the time of flight, the deposited energy in each BaF_2 crystal and an α-γ discrimination flag were determined by using a sophisticated pulse shape analysis routine. In order to identify the detected reaction, one reconstructs the total energy deposited in the calorimeter during a coincidence window of about 10 ns. The calorimeter is calibrated in energy response and resolution, and in efficiency by studying its response to radioactive sources of ^{137}Cs, ^{60}Co, ^{88}Y, ^{24}Na and a composite source of ^{238}Pu (acting as an α source) together with ^{13}C. A drift in energy is observed and monitored by using the intrinsic α activity of each BaF_2 crystal.

Preliminary results of the ^{233}U neutron capture measurement

Figure 6 shows the count rate in the TAC for a total deposited energy in the TAC from 1 MeV to 7.5 MeV, the neutron separation energy for ^{233}U being 6.843 MeV, as a function of the neutron incoming energy. The blue line corresponds to the measurement without any sample in the beam. Red line represents the measurement with an empty titanium canning. Finally the black line gives the measurement with the ^{233}U sample in the beam. All measurements with the beam are scaled to the same number of incident protons. Below one keV neutron incident energy, one can clearly see resonances attributed to neutron capture and to neutron induced fission on ^{233}U, except for the small resonance at about 5 eV which is due the small ^{234}U impurity inside the ^{233}U sample. Below one keV the background is mainly due the sample radioactivity. Above this energy the main contribution to background comes from the titanium canning as can be seen in the Figure 39. Due to the high background level in this region, mainly due the canning, the cross section will be probably difficult to determine with a high accuracy. Work is currently under way to distinguish between capture and fission events.

Figure 7 shows the count rate in the TAC for a total deposited energy in the TAC from 1 MeV to 6.5 MeV, the neutron separation energy for ^{234}U being 5.192 MeV, as a function of the neutron incoming energy. The blue line corresponds to the measurement without any sample in the beam. Red line represents the measurement with an empty titanium canning. Black line gives the measurement with the ^{234}U sample in the beam and finally the pink line corresponds to the ^{234}U measurement without any beam. All measurements with the beam are scaled to the same number of incident protons. Furthermore the empty canning measurement is also normalized to the ^{234}U measurement by the canning mass ratio between the two samples. Activity measurement is scaled to the ^{234}U neutron capture measuring time.

Below one keV one can clearly see resonances attributed to neutron capture on ^{234}U. Below few hundreds eV the background is mainly due the sample radioactivity. Above this energy the main contribution to background comes from the titanium canning as can be seen in Figure 36. As for the ^{233}U case, the signal induced by canning may limit the accuracy of the cross section determination in the unresolved resonance region.

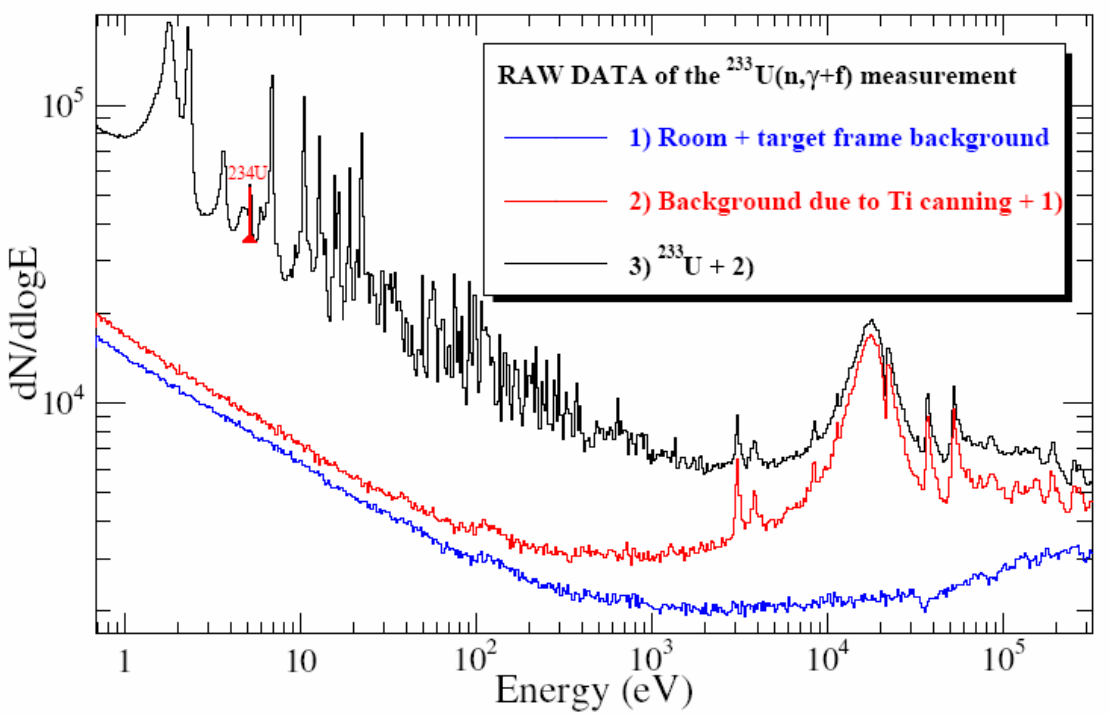

Figure 39: Count-rate for the ^{233}U sample measurement as a function of the neutron incident energy.

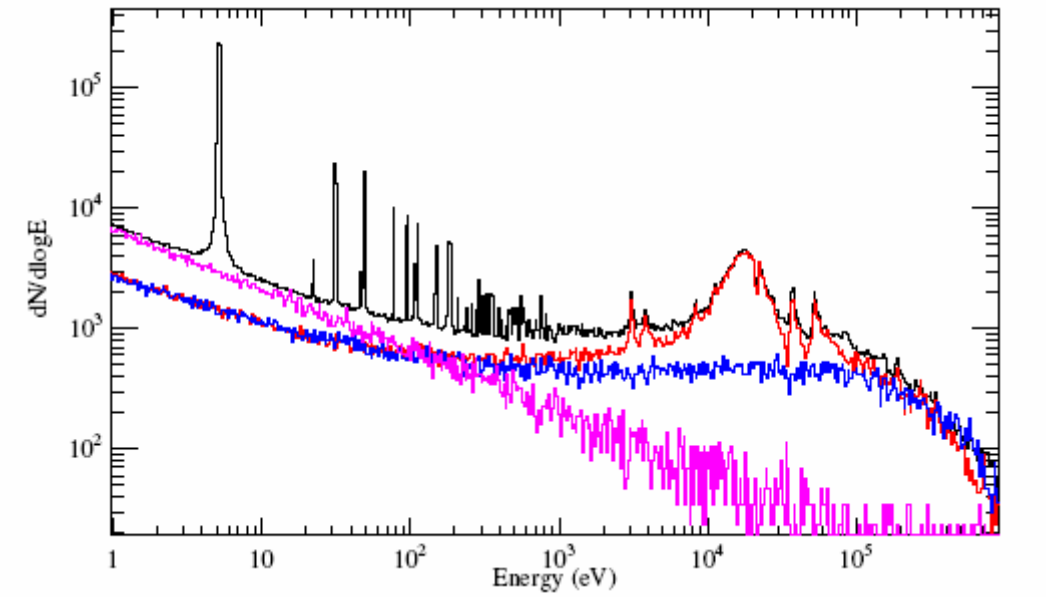

Figure 40: Count-rate for the ^{234}U capture measurement.

The measurement of the $^{236}U(n,\gamma)$ cross section at GELINA

A capture sample with about 300 mg ^{236}U has been prepared by IPPE-Obninsk through JINR-Dubna. The radioactive uranium oxide has been pressed into a pallet and packed in a thin high purity aluminum container sealed by means of epoxy glue. In this form the sample is sealed in a practical way avoiding contamination and the surrounding material is limited to a minimum of well known material. For neutron capture measurements on radioactive powder samples this is the best suited form for an experiment. However, this sealing is not ISO-compliant which has been a reason for the CERN safety authorities to refuse the measurement at the last moment in 2003. We have therefore transported the sample to GELINA neutron time-of-flight facility. This laboratory has more experience with radioactive samples and after a careful study of the case, the sample was allowed for a measurement in 2004. The details of the experiment are described on page 60.

Related publications

[1] F. Gunsing et al., *Measurement of the neutron capture cross section of ^{232}Th, ^{231}Pa, ^{234}U and ^{236}U*. Technical Report, CERN/INTC 2002-010, CERN, 2002 (proposal).

[2] U. Abbondanno et al., Neutron capture measurements at the CERN-n_TOF facility for ADS applications. In J. Kvasil, P. Cejnar, and M. Krticka, editors, Capture Gamma-Ray Spectroscopy and Related Topics, pages 460–466, World Scientific, 2003.

[3] G. Aerts, E. Berthoumieux, F. Gunsing, and L. Perrot. *Weighting functions for the neutron capture measurements performed at n_TOF-CERN in 2002-2003*, Technical Report DAPNIA-04-106, CEA/Saclay, 2004.

[4] G. Aerts, E. Berthoumieux, F. Gunsing, and L. Perrot. *The capture yield of the $^{232}Th(n,g)$ reaction measured at n_ TOF-CERN*, Technical Report DAPNIA-04-125, CEA/Saclay, 2004.

[5] G. Aerts et al., *Measurement of the ^{232}Th neutron capture cross section at the CERN n_ TOF facility*. Proc. Int. Conf. Nuclear Data for Science and Technology, Santa Fe, September 28-October 1, 2004. In press, 2005.

Capture Cross Sections of TRU (^{237}Np, ^{240,242}Pu, ^{241,243}Am, ^{245}Cm)

Contribted by *D Cano-Ott, C Guerrero, and E Gonzalez* (CIEMAT, Madrid*)*

Introduction

Nuclear waste is one the main problems for the public perception of the nuclear energy production and for the sustainability of this energy source. Although a deep underground repository seems to be a scientifically proven and technologically viable solution for the nuclear waste for the first thousands of years, this option presents difficulties for social acceptability. For this reason, nuclear waste transmutation has been proposed as a way to reduce substantially (in a factor of 1/100 or more) the inventory of the long lived component of the nuclear waste, mainly the trans-uranium actinides.

Actinide transmutation is proposed to take place by fission in nuclear systems like critical reactors or sub-critical Accelerator Driven Systems (ADS). In most of the scenarios, the use of fast neutron energy spectra and specific fuel compositions, highly enriched in high mass trans-uranium actinides, are proposed. In addition, the transmutation of Long Lived Fission Fragments has also been proposed using neutron absorption (mainly by radioactive capture) normally in thermal and epithermal neutron energy spectra.

The actual knowledge on the neutron cross sections of actinides is mainly related to the exploitation of the U-Pu cycle in nuclear reactors with a thermal neutron spectrum and the design and operation of experimental fast U-Pu nuclear reactors. In addition, the currently existing nuclear databases can be used for the conceptual design of the transmutation oriented nuclear devices – critical reactors or ADS – and for the first order evaluation of the impact of the transmutation technology in the nuclear waste management.

However, the detailed engineering designs, safety evaluations and the detailed performance assessment of dedicated transmutation ADS and critical reactors (i.e. with fuels highly enriched in transuranic isotopes) require more precise and complete basic nuclear data.

Of crucial importance is the composition of the fuels proposed for transmutation devices, with a large concentration of minor actinides and high mass plutonium isotopes. These isotopes with little relevance for the operation of present reactors will play an important role in the neutronics of the transmuters. Figure 41 shows the strong differences in the fuel composition of nuclear plants – including the typical PWR fresh and irradiated fuels – and the fuel for the typical transmutation devices for two scenarios: the equilibrium cycle in a version of the double strata and a scenario for the phase-out of the nuclear electricity production.

A selection criterion based on the impact on the transmuter neutronics and availability of capture cross section data allows for setting a lower priority to the capture measurements of ^{239,241}Pu. In addition, the extreme difficulties involved in the capture measurements of the highly radioactive isotopes like ^{238}Pu ($T_{1/2}$ = 87.74 a) and ^{244}Cm ($T_{1/2}$ = 18.1 a) reduces further the list of possible measurements to ^{237}Np, ^{240,242}Pu, ^{241,243}Am and ^{245}Cm.
As a particular scenario, the Th fuel cycle has been proposed as an alternative to the nuclear energy production based on the U/Pu fuel cycle. The main reactions involved in the Th fuels are the neutron capture in ^{232}Th that, after fast series of radioactive decays breeds ^{233}U, which finally undergoes neutron induced fission and provides the necessary neutron multiplication. ^{232}Th has a smaller nuclear mass than ^{238}U. As a consequence, its neutron irradiation produces mainly uranium isotopes and much less trans-uranium actinides (protactinium is also produced), which results into a better tractable nuclear waste.

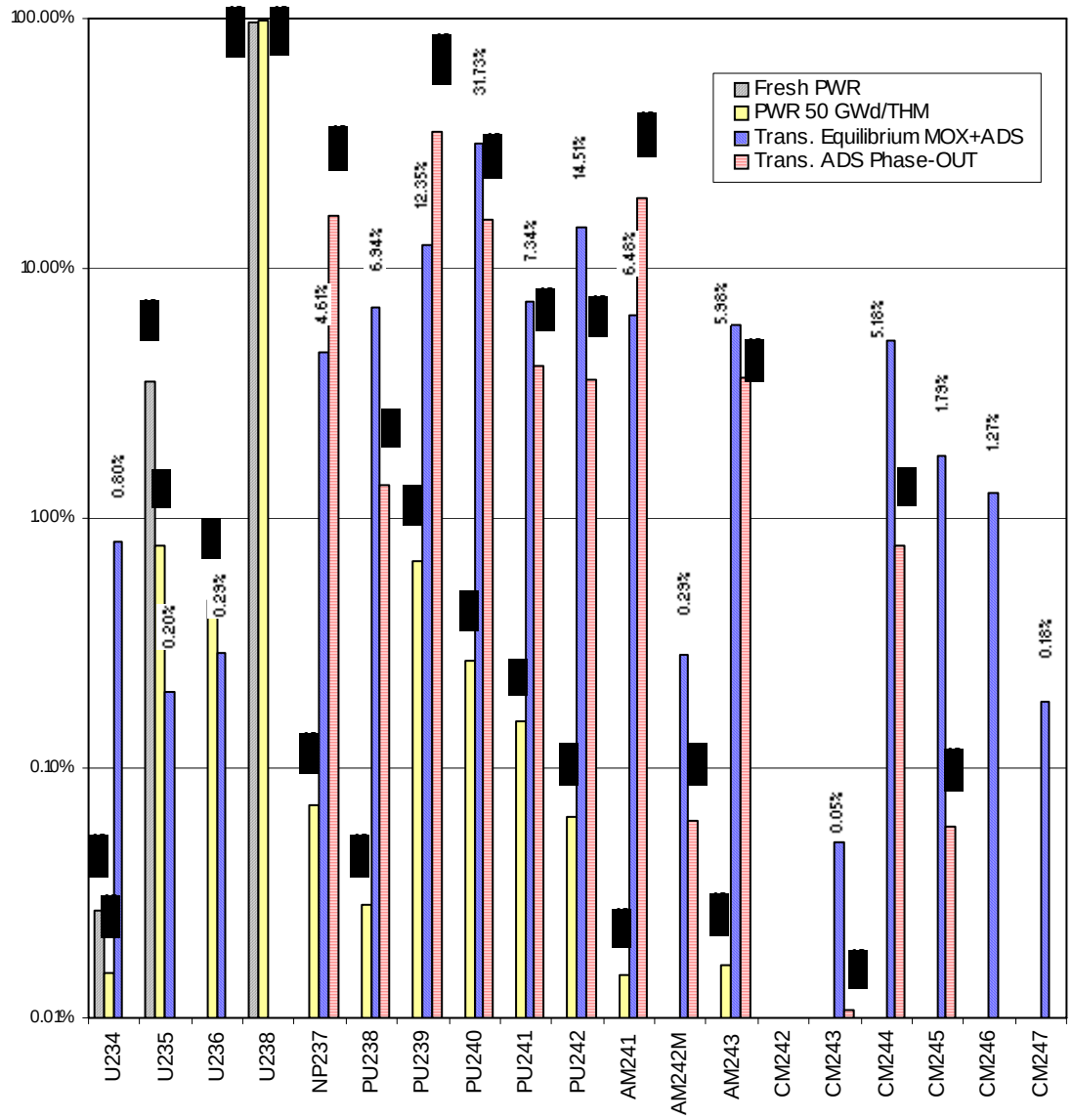

Figure 41: Comparison of the composition of the fuels for different nuclear plants: PWR (fresh and irradiated fuels) and for two Transmutation devices.

Not only the isotope list but also the energy range in which the capture cross sections has to be measured needs to be extended. For the U/Pu fuel cycle, the knowledge on the capture cross sections is mainly focused at thermal and epithermal neutron energies.

On the contrary, in a fast reactor or ADS core, the neutron captures of fast neutrons play an essential role. Figure 43 shows the cumulative capture rate in several isotopes of interest for transmutation as a function of the neutron energy. A typical ADS neutron energy flux spectrum was adopted for the calculation. As it can be observed in the figure, energies up to 1 MeV have to be considered in order to take into account up to 99% of the neutron captures in the ADS core.

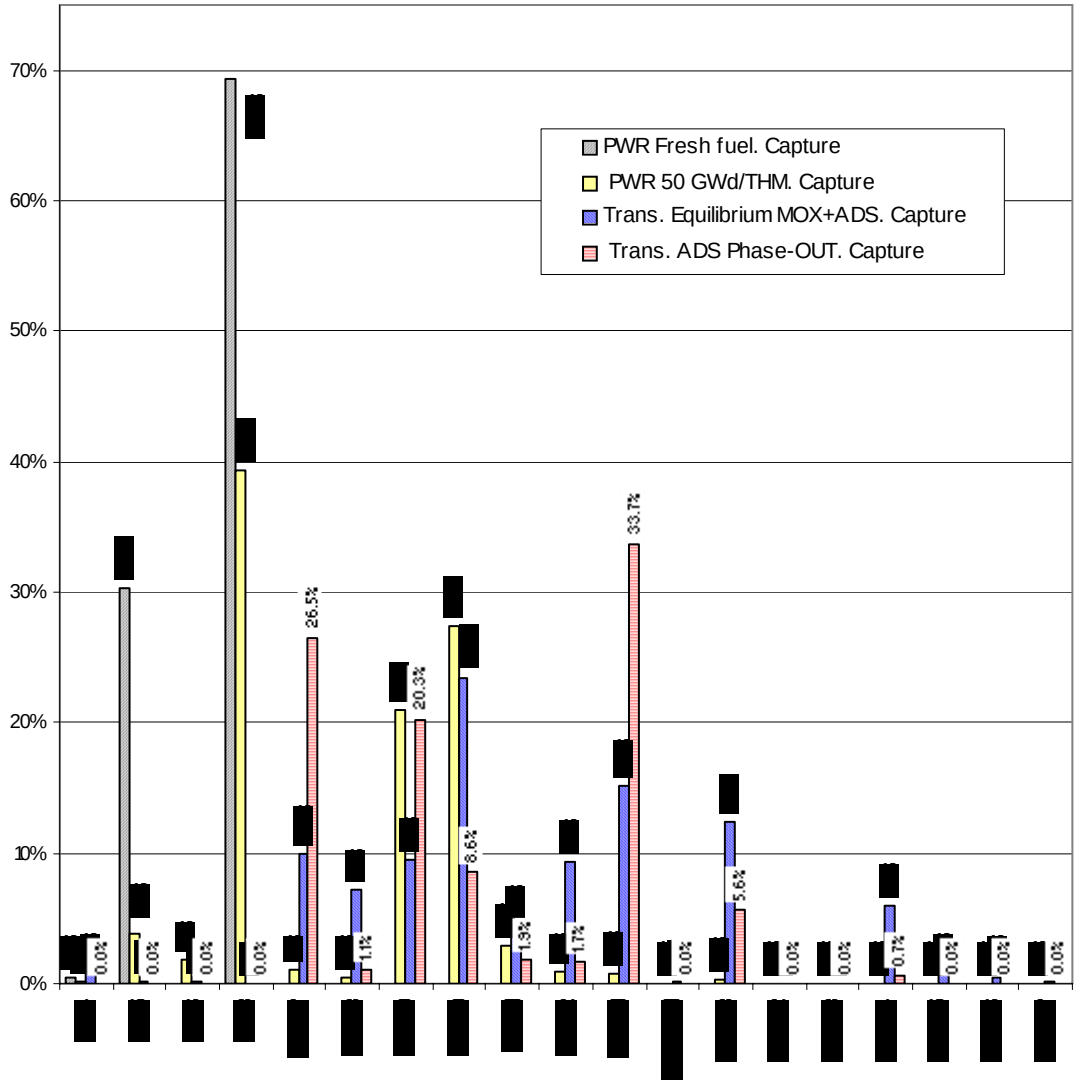

Figure 42: Contribution to capture from the isotopes present in the fuels for different nuclear plants: PWR (fresh and irradiated fuels) and for two Transmutation devices.

Neutron sensitivity analysis evidence the need of determining the neutron capture cross sections of the isotopes listed above with an accuracy of better or equal than 5% in the energy range from thermal energies up to 1 MeV. In addition, a neutron sensitivity analysis allows to establish the dependence of several physical quantities describing the behavior of a transmuter on a large number of reaction channels. Thus, the overall uncertainties in such quantities can be largely reduced by performing highly accurate and targeted measurements of specific isotopes and reaction channels.
In addition, deterministic calculations based on multigroup cross sections are evidencing problems in describing changes in the neutron flux spectrum in the reflector of an ADS core. Such problems are attributed to the poor knowledge on the shape of the cross sections in the unresolved resonance region up to 1 MeV. Data with enough resolution, of about 5% or better, are needed in order to determine more accurately the shape of the cross sections at high energies.

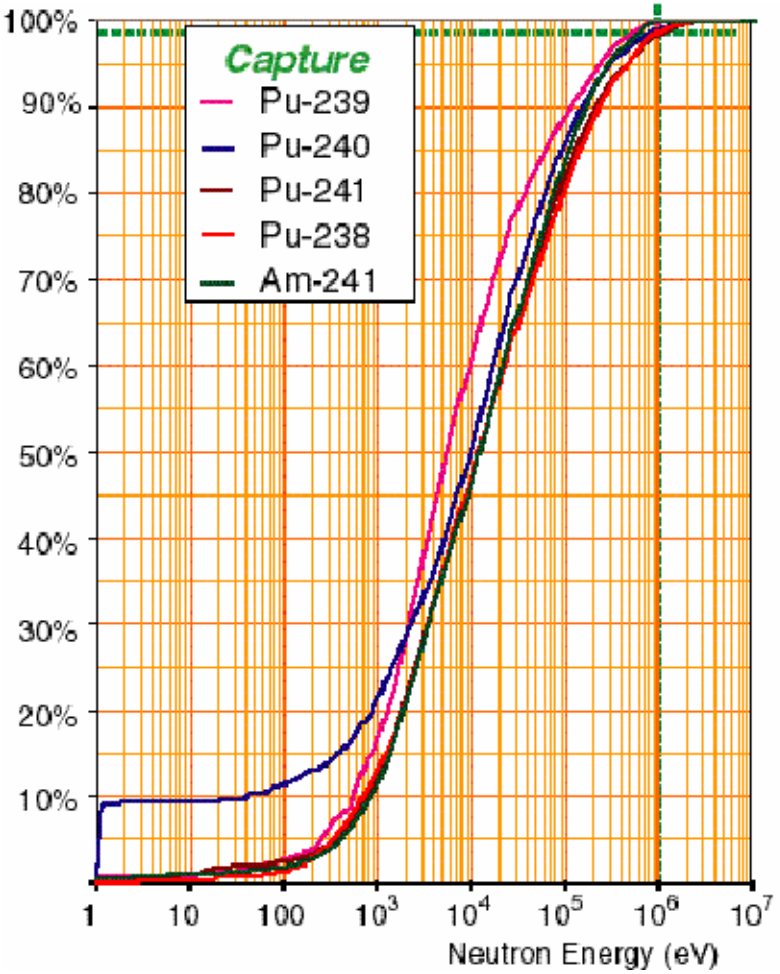

Figure 43: Capture energy range of interest in transmutation devices (Th-based fast ADS). To reach 99% of the full capture rate neutron energy has to be integrated up to 1 MeV.

For understanding why the available capture cross sections on ^{233}U, ^{237}Np, ^{240,242}Pu, ^{241,243}Am and ^{245}Cm are not sufficient for the optimization of a transmutation device, one has to consider the two steps previous to the release of the corresponding evaluated files. First, the available data sets for ^{233}U, ^{237}Np, ^{240,242}Pu, ^{241,243}Am and ^{245}Cm are not accurate enough, are incompatible in some cases, do not cover the necessary neutron energy range and the resolution provided is not sufficient. Second, the available evaluated cross section files do not agree between themselves as well. More often than it would be desirable the evaluators are forced to question and re-investigate the accuracy of specific data sets in order to reach a self-consistent result in their evaluation for all the reaction channels. Thus, the result on the evaluation depends strongly on the decisions adopted by the evaluator. More accurate measurements are necessary in order to constrain the parameters (such as level densities or optical potential parameters) of the physics models applied.

Measurements

The neutron capture cross sections of ^{237}Np, ^{240}Pu and ^{243}Am have been measured at n_TOF in the range from 0.08 eV up to 100 keV. The measurements were performed in the period between August and October 2004 with the barium fluoride Total Absorption Calorimeter and the Data Acquisition system based on flash ADCs.

The neutron capture cross section measurements ^{242}Pu, ^{241}Am and ^{245}Cm could not be performed because no provider for ^{242}Pu and ^{245}Cm targets could be identified in time for the measurements. Several institutions from the Russian Federation and the Oak Ridge target laboratory were contacted but none of them had the necessary amount of material available.

The measurement of the ^{241}Am(n,γ) has not been approved by the radioprotection authorities at CERN. The target ^{241}Am was delivered together with the ^{237}Np, ^{240}Pu and ^{243}Am targets and manufactured in the same way: canned inside a sealed Ti container fulfilling the ISO 2919 norm. However, the radioprotection authorities at CERN did not authorize the measurement arguing an excessively high risk associated with the strong activity of the sample.

In addition to the TRU measurements, a set of reference measurements necessary for the relative cross section determination – the ^{197}Au(n,γ) cross section – as well other for determining the different background components – like ^{nat}C and ^{nat}Pb targets and an empty Ti canning – were performed as well.

The capture cross sections were measured in different neutron energy ranges by varying the sampling rates of the flash ADCs. The lowest sampling rates allowed to increase the time of flight window in which the DAQ was acquiring, thus, allowing to record capture events of lower energy neutrons:

- The neutron energy range between 0.7 eV and 100 keV was covered at a sampling rate of 500 MSamples/s for the ^{237}Np and ^{240}Pu measurement. The high intrinsic activity of the ^{243}Am target forced to reduce the amount of data generated by the DAQ by lowering the sampling rate of the flash ADCs to 250 Msamples/s.

- The neutron energy range between 0.08 eV and 100 keV was covered at a sampling rate of 100 MSamples/s for all three isotopes.

The of ^{237}Np, ^{240}Pu and ^{243}Am targets (defined as the assembly of the sample and its container) have been provided by the Institute for Physics and Power Engineering (Dubna, Russia) and were delivered to CERN during spring 2004. All targets were weighted, sized and characterized by means of a gamma ray spectrometry at CERN (TIS).

The technical characteristics of all samples, including both TRU and reference samples are given in Table 2.

Table 2: Characteristics of the TRU and reference targets

Sample	Total mass (mg)	Isotopic Purity (% in mass)	Activity (MBq)
^{237}Np (NpO_2)	49.5	99.9	1.14
^{240}Pu (PuO_2)	58.0	92.6	425.68 (very low energy gamma rays)
^{243}Am (AmO_2)	11.3	97.0	73.13
^{197}Au	185.4	pure	stable
^{12}C	70.0	natural abundance	stable
^{nat}Pb	171.1	natural abundance	stable

All samples, both TRU and the reference ones, had a disc shape with 1 cm diameter. In addition, each TRU (i.e. radioactive) sample had to be encapsulated inside a sealed canning

fulfilling the ISO 2919 norm. The cannings were all identical and made of a sandwich of two 0.17 mm thick titanium layers.

As it is shown in Figure 44 ach sample was mounted between two Kapton foils, with a thickness of 20 μm, attached to a circular PCB structure.

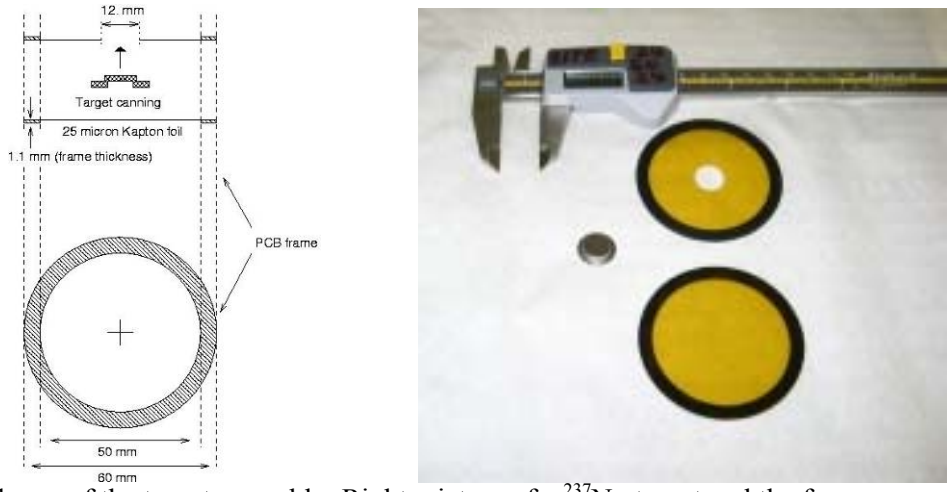

Figure 44: Scheme of the target assembly. Right: picture of a ^{237}Np target and the frame.

Such a simple construction allowed to place and remove the targets easily and quickly in the centre of the calorimeter, by sliding the PCB frame into the previously aligned vacuum pipes, and therefore without the need of continuous alignments for each sample change.

Due to the high activity of the targets, a protocol for its manipulation and operation at the n_TOF facility had to be defined:

- The access to the n_TOF experimental area was restricted to authorized personnel only.
- An extra access gate with electronics locks had to be installed at the entrance of the n_TOF tunnel.
- The radioactive targets had to be mounted and dismounted inside the calorimeter under the supervision of the radioprotection division officers.
- All actinide targets had to be stored at a radioactive sources repository when not being measured at n_TOF.
- All target transports had to be escorted and supervised by CERN's fire brigade.

The Total Absorption Calorimeter (TAC)

A new Total Absorption Calorimeter (TAC) has been used for neutron capture cross section measurements at n_TOF. The TAC consists of 12 pentagonal, 28 hexagonal shaped BaF_2 crystals and two holes at 180º for the entrance and exit point of the neutron beam. Both types of crystals are 15 cm long and are placed at 11 cm from the geometric centre of the TAC. Such a configuration covers 95.2% of the total solid angle.

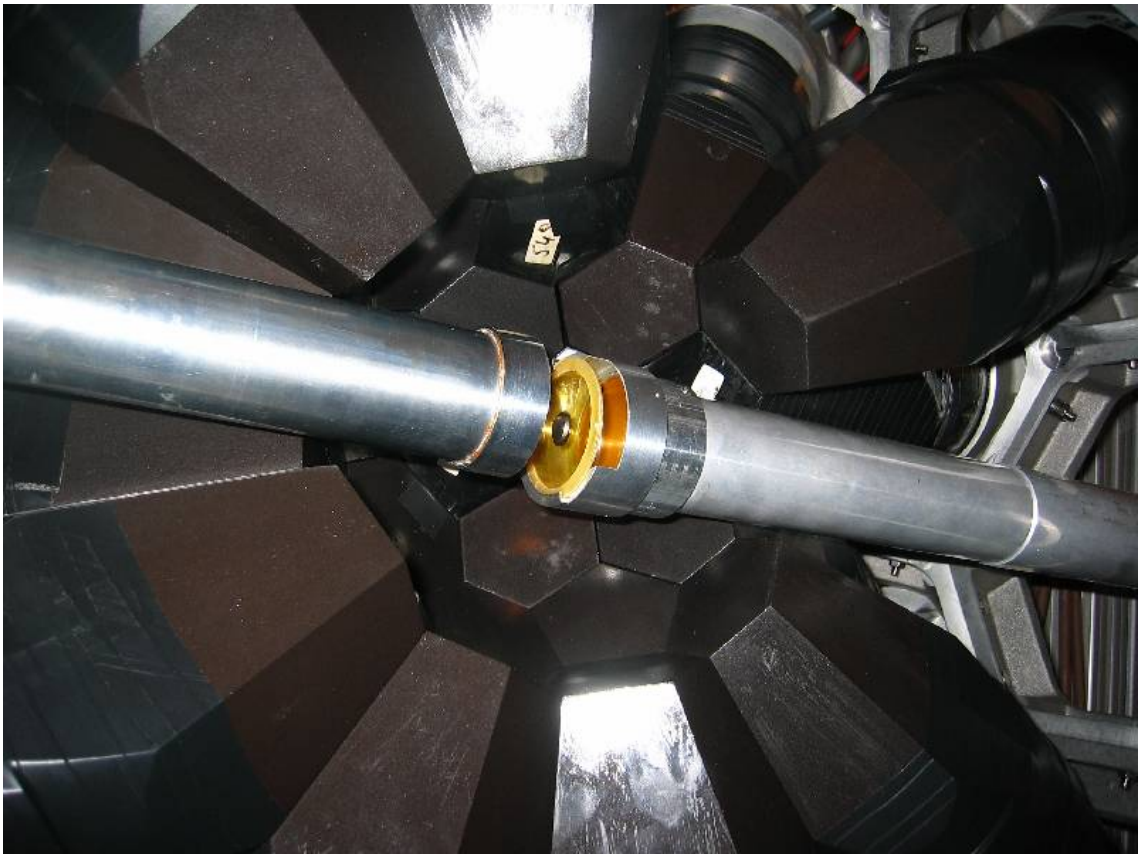

Figure 45: Picture of the inner part of the TAC, the two parts of the aluminium pipe and a sample placed on its centre.

As it is shown in Figure 45, two aluminium pipe segments crossed the TAC through the two entrance and exit holes, leaving a 4 cm gap of air right in the middle of the TAC. The targets were placed there in air, exactly at the centre of the TAC, by sliding them into a target holder fixed to one of the pipe segments. The pipes and the sample holder were carefully aligned with respect to the neutron beam at the beginning of the measurements and the positions fixed.

With this standard configuration, the commissioning of the detector was performed during June 2004. The commissioning included the mounting of the crystal on the structure and the fine tuning of the electronics and data acquisition system (DAQ). The TAC showed an average energy resolution of 14.9% at the standard energy of 662 keV in the decay of ^{137}Cs. Other standard gamma ray sources such as ^{24}Na (1369 and 2754 keV), ^{60}Co (1173 and 1332 keV), ^{88}Y (898 and 1836 keV) and a Pu/C (6131 keV) were used for characterizing the energy resolution, efficiency and response function of the TAC at various energies and gamma ray multiplicities.

The efficiency of the TAC has been calculated by means of Monte Carlo simulations with the GEANT-4 code. As it is shown in Figure 46, a very detailed geometry of the TAC has been modeled inside the simulation package.

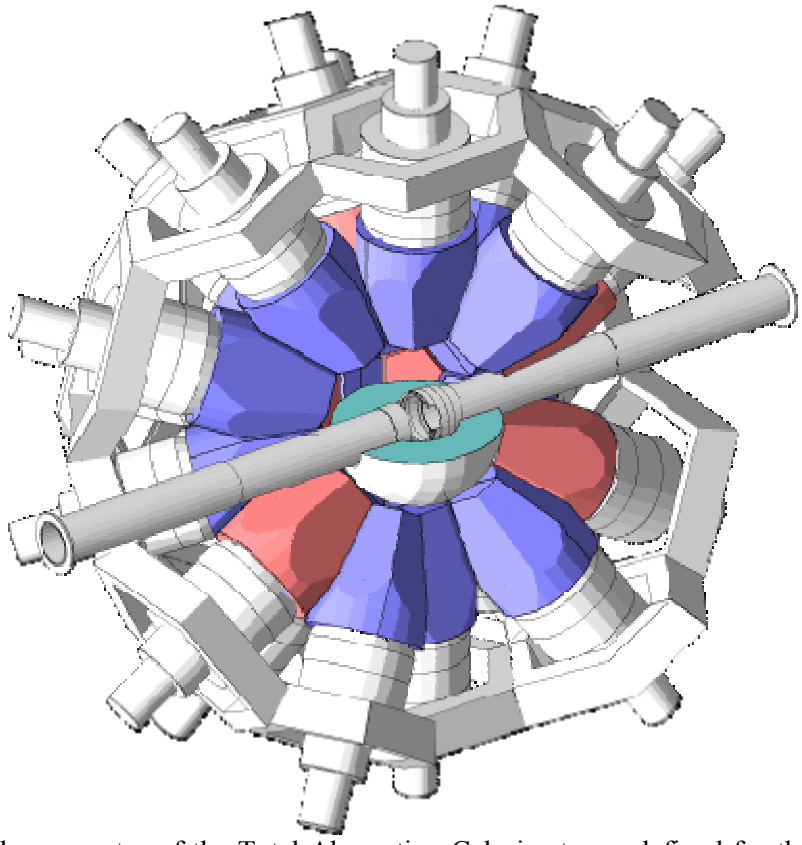

Figure 46: The geometry of the Total Absorption Calorimeter as defined for the simulations with GEANT 4.

All the neutron capture cross section measurements, reference and background measurements were performed neutron absorber inside the TAC for minimizing its neutron sensitivity. It moderates and captures the neutrons scattered by the targets that otherwise could be captured in the detector and surrounding materials, leading to background signals that can be misidentified with real capture events. The neutron absorber is a spherical shell of 10 cm external radius made of a ($^{6}LiOOC(CH_2)_{10}COO^{6}Li$) H and ^{6}Li enriched compound. It was placed inside the TAC and surrounding the targets

Due to high activity of the ^{243}Am target, a 1mm thick, 9 cm long and 3,2 cm radius cylindrical lead shielding had to be placed around the Am target holder, in order to absorb the low energy gamma rays.

The response of the detector in each of this configuration has been studied using all the calibration sources available.

The data acquisition system (DAQ)

The configuration of the n_TOF Data Acquisition system used for the TRU measurements with the calorimeter consisted of 49 flash ADC channels: 40 for the BaF_2 crystals, 4 for the silicon flux monitor (SiMon), 4 for a fission detector monitor and 1 for the proton accelerator signal. The FADC modules used were the DC270 and DC240 8 bit resolution models manufactured by Acqiris. The DC270 offer four data inputs plus one trigger input, a maximun sampling rate of 1GHz and a bandwidth of 250 MHz. The DC240 modules offer only two

data inputs plus one trigger input but a maximum sampling rate of 2 GHz and a bandwidth of 500 Mhz. Every channel was configured with 8 Mbytes memory.

Each detector was coupled to a corresponding FADC channel. The output produced by each detector was digitized by the flash-ADC over a time window of 16 ms at a sampling rate of 500 MS/s or 80 ms at a sampling rate of 100 MS/s. The DAQ was triggered signal produced by the impact of the proton beam on the target. The data was transferred via cPCI/PCI adapters into the readout PCs. These linux PCs compressed the data and transferred it over Gigabit links to a disk server. From there the data was transferred to CERN's tape pool CASTOR and stored permanently on tape.

Once the raw data was written on tape, it was read-out by the Data Processing Software. The relevant signal parameters such as time, energy and quality factors such as pile-up, baseline were extracted from the pulse shape and formatted and saved as Data Summary Tapes (DSTs) by means specific algorithms developed in C/C++ for every type of detector used. In this way, we the size of the amount of data to be analysed was reduced significantly. The data reduction factors in the DSTs depended on the detector type and ranged from 10 to 100.

The amount of raw data measured was huge: a total of 138.4 TBytes as Raw data and 2.7 TBytes as DSTs (average reduction factor of 50), which represents a data rate of 2.5 Tbytes/day over a period of 2 months. A summary of the data taking statistics for the different configurations is found in Table 3.

Table 3: Raw and DST data for each measurement.

	Raw data size (GBytes)	DST data size (GBytes)	Configuration	Sampling rate
Calibration sources: ^{137}Cs, ^{60}Co, ^{88}Y, ^{24}Na and ^{16}O	11,442	131	with and without neutron absorber	500 MS/s, 250 MS/s and 100 MS/s
PCB + Kapton frame	4,436	40	with neutron absorber	500 MS/s, 250 MS/s and 100 MS/s
Empty canning (Ti alloy GHOST 19807)	7,639	62	with neutron absorber	500 MS/s, 250 MS/s and 100 MS/s
^{nat}C (graphite)	2,831	21	with neutron absorber	500 MS/s, 250 MS/s and 100 MS/s
^{nat}Pb	4,350	30	with neutron absorber	500 MS/s, 250 MS/s and 100 MS/s
^{197}Au	25,896	214	with neutron absorber	500 MS/s, 250 MS/s and 100 MS/s
^{237}Np	20,292	297	with neutron absorber	500 MS/s and 100 MS/s
^{240}Pu	21,832	219	with neutron absorber	500 MS/s and 100 MS/s
^{243}Am	43,006	1,778	with neutron absorber and Pb shielding (1 mm)	250 MS/s and 100 MS/s

The capture cross section data

The raw data obtained from the capture cross section measurements on ^{237}Np, ^{240}Pu and ^{243}Am are presented in this section. The measurements have covered the neutron energy range between 0.08 eV and 100 keV. Those values are limits imposed by the experimental conditions. In fact, two different effects limit the neutron energy range that could be covered in one measurement:

- At higher energies, the prompt flash of ultra-relativistic particles that travel at speed of light from the spallation target to the experimental area inside the n_TOF beam line. All detectors suffer saturation on the arrival of the flash and are ready for the detection only after being recovered. For the case of the BaF_2 modules, neutron energies as high as a 100 keV can be reached.
- At low energies, the time window set in the flash ADCs and resulting from the fixed memory size of 8MBytes and the variable sampling rate. Thus, for a sampling rate with 100 MSamples/s, neutron energies as low as 0.08 eV can be reached with a time window of about 80 ms.

The data are shown with a normalization defined by the total number of counts in the silicon flux monitor (SiMon). Since the neutron source at n_TOF is a spallation, a normalization given by the total number of neutrons, counts in the monitors or number of protons put on the target are equivalent. However, a better accuracy is achieved if the normalization given by the SiMon is used.

The ^{237}Np(n,γ) cross section measurement

The sample of ^{237}Np had a mass of 43.3 mg and was very pure at the time of the measurement. It was measured in two different configurations depending on the energy range to be studied:

A configuration with a sampling rate of 500 Msamples/s and a 16 ms time of flight window covered the neutron energy range from 1 eV to 100 keV. A total of $70.2 \cdot 10^{16}$ protons was allocated to this measurement. The corresponding data are shown in Figure 47 and in an enlarged view in Figure 48.
A configuration with a sampling rate of 100 Msamples/s allowed to extend the time window to 80 ms and thus to cover a neutron energy range between 0.08 eV and 100 keV. A total of $4.1 \cdot 10^{6}$ protons was allocated to the measurement with this configuration.

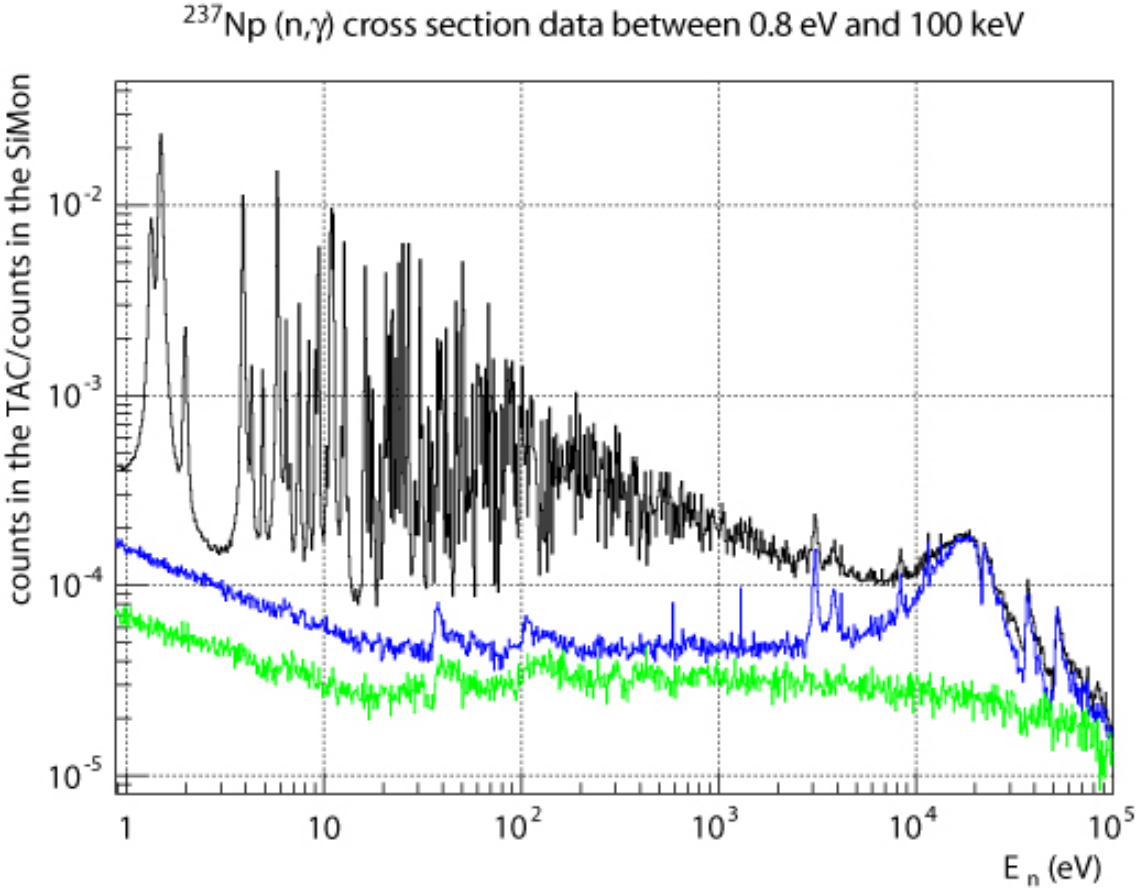

Figure 47: Counting rate of the TAC as a function of the neutron energy in the range between 0.8 eV and 100 keV: for the ^{237}Np target (black), due to the titanium container (blue) and without any target (green).

The ^{237}Np data are, up to date, the best neutron capture data ever obtained for this isotope. The intrinsic radioactivity of the target did not represent any mayor drawback due to the high instantaneous flux of the n_TOF facility and the large segmentation of the TAC. Due to the high resolution of the n_TOF facility, resolved resonances have been observed up to a few tens of eV and well isolated resonance groups up to a few hundred eV. A clear capture signal was observed in the neutron energy region between 1 keV and 10 keV, thus allowing to

extract the neutron capture cross section after a careful background subtraction. The cross section in the neutron energy region between 10 keV and 100 keV will be obtained only if the very important background due to the Ti canning can be subtracted properly during the analysis.

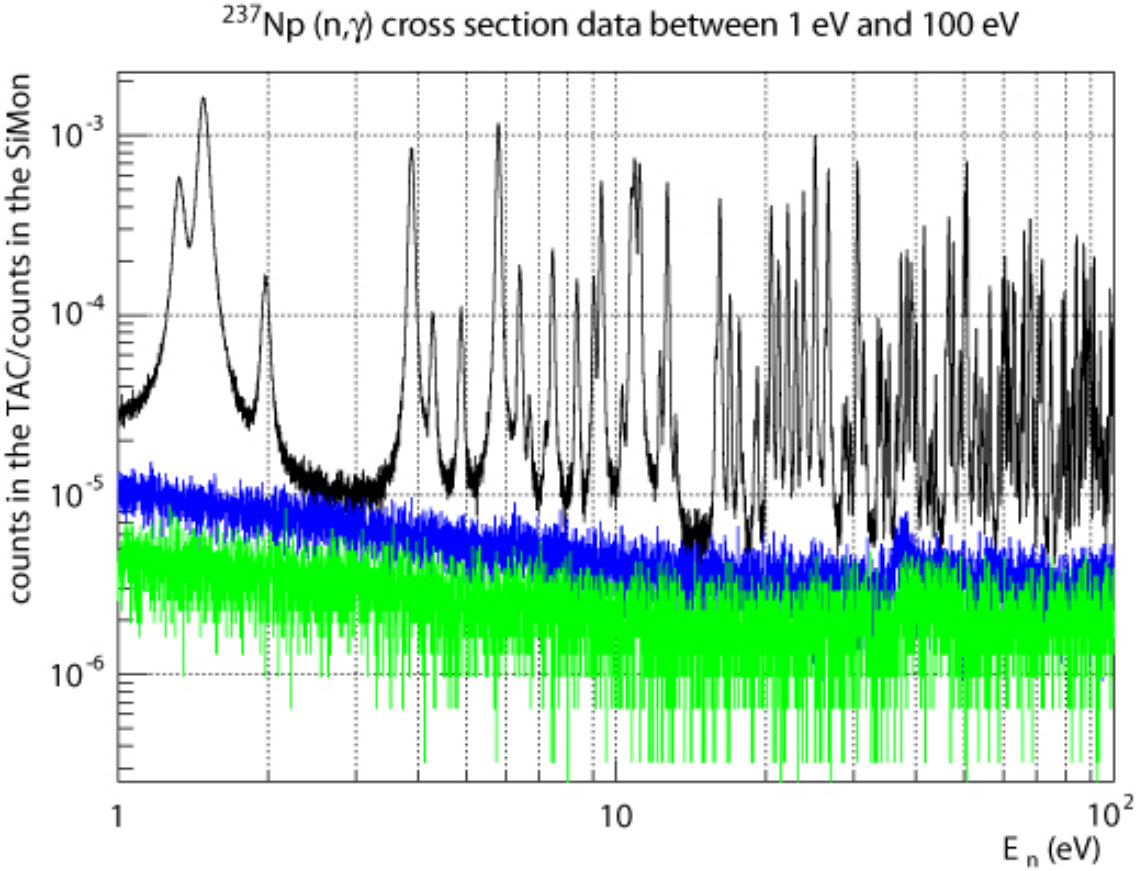

Figure 48: Counting rate of the TAC as a function of the neutron energy in the range between 1 eV and 100 eV: for the ^{237}Np target (black), due to the titanium container (blue) and without any target (green).

The ^{240}Pu(n,γ) cross section measurement

The ^{240}Pu target had a mass of 51.1 mg and an unexpected 7.5% contamination of ^{239}Pu. It was measured with the same two DAQ configurations as the ^{237}Np. A sampling rate of 500 MSamples/s covered the neutron range from 1 eV to 100 keV and a total number of $108.7 \cdot 10^{16}$ protons were used. The corresponding data are shown in Figure 49 and in an enlarged view in Figure 50. With a sampling rate of 100 MSamples/s the neutron energy range between 0.08 eV and 100 keV has been covered with a total number of $3.5 \cdot 10^6$ protons.

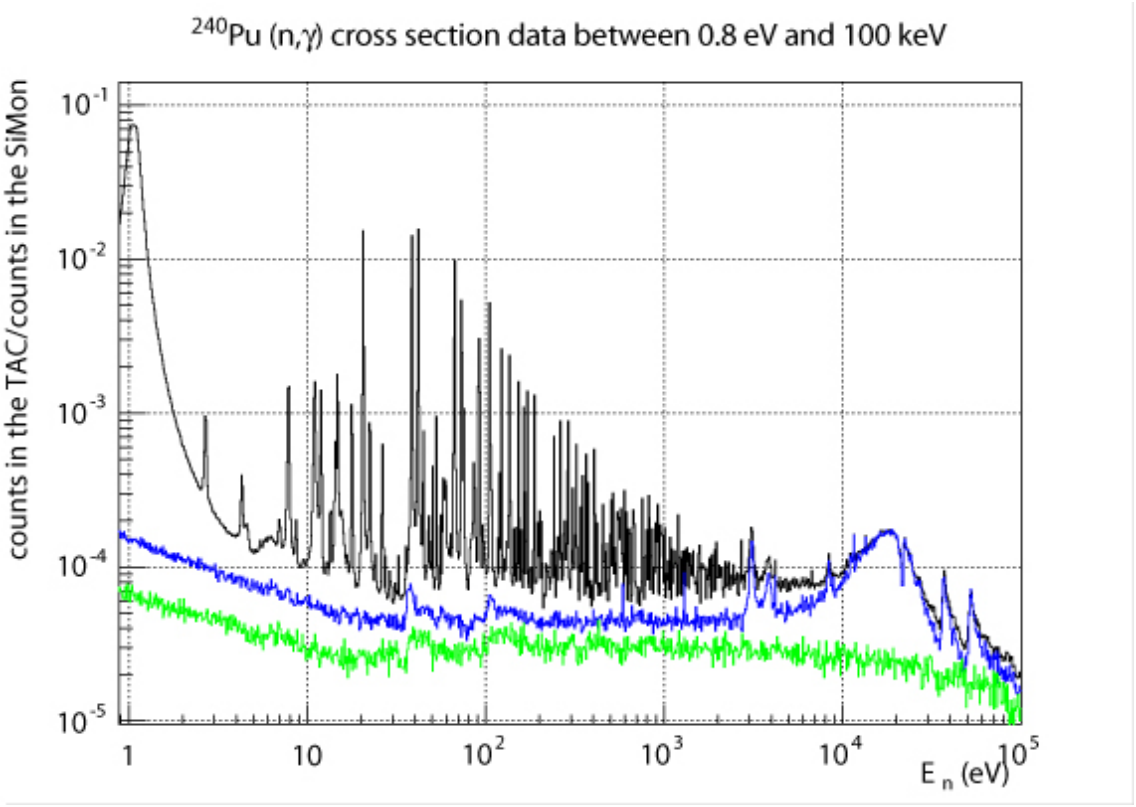

Figure 49: Counting rate of the TAC as a function of the neutron energy in the range between 1 eV and 100 eV: for the ^{240}Pu target (black), due to the titanium container (blue) and without any target (green).

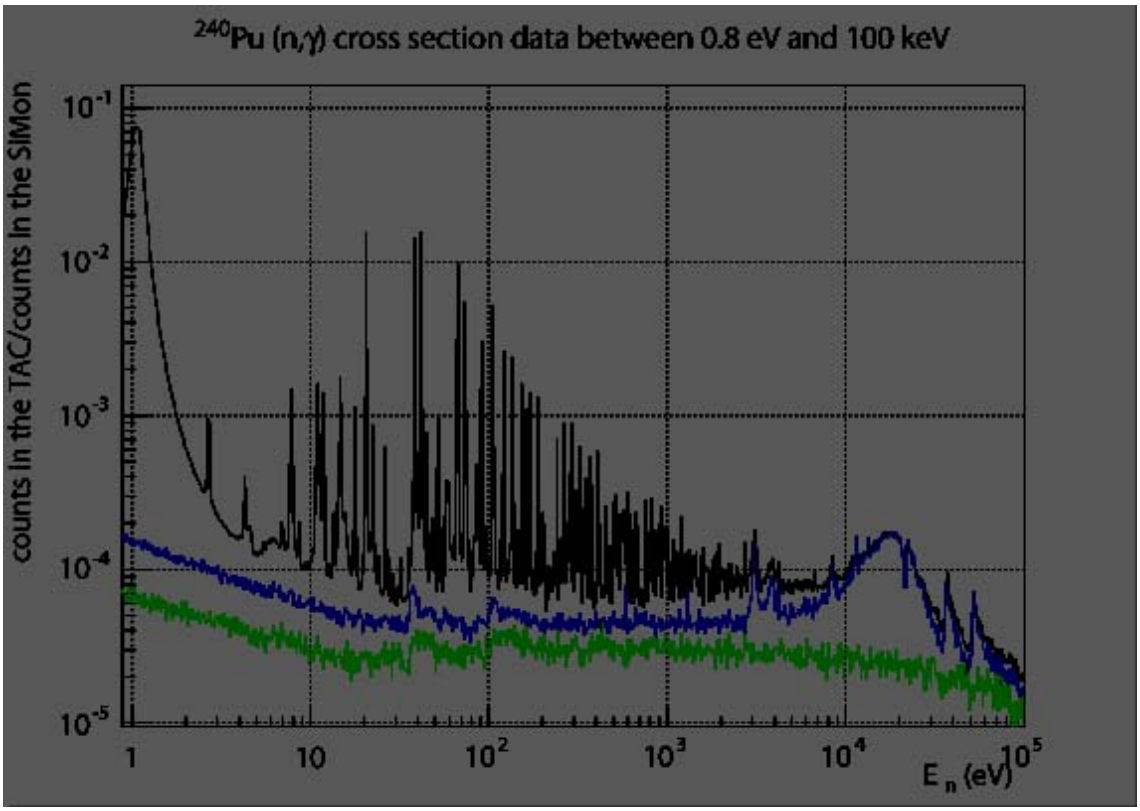

Figure 50: Counting rate of the TAC as a function of the neutron energy in the range between 1 eV and 100 eV: for the ^{240}Pu target (black), due to the titanium container (blue) and without any target (green).

The ^{243}Am(n,γ) cross section measurement

The ^{243}Am was by far the most difficult neutron capture measurement performed at n_TOF due to its low mass and high energy intrinsic radioactivity. The Am target had to be shielded with a 1 mm thick lead shielding for lowering the trigger rate of the TAC and eve then, the rate in the TAC was so high that the sampling rate of the flash ADCs had to be lowered to 250 MSamples/s for reducing the data throughput. Furthermore, a technical stop of the CERN PS for a period longer than 20% of the total yearly beam time forced to shorten the measurement to 1/10 of the beam time requested initially.

Even though the difficulties and the lack of statistics, the measurement was successful and is on its own, a proof of the unique features of the n_TOF facility and its excellent performance. The ^{243}Am(n,γ) data shown in Figure 51and Figure 52correspond to the first successful time of flight measurement in the resolved resonance region ever. The resonances observed have been unambiguously identified as ^{243}Am resonances observed in previous transmission measurements.

Like for the other TRUS, the neutron capture cross section was measured in two different neutron energy regions:

- With a sampling rate of 250 MSamples/s in the neutron range from 1 eV to 100 keV and a total number of $153 \cdot 10^{16}$ protons. The corresponding data are shown in Figure 51 and in an enlarged view in Figure 52.
- With a sampling rate of 100 MSamples/s in the neutron energy range between 0.08 eV and 100 keV with a total number of $1.96 \cdot 10^{16}$ protons.

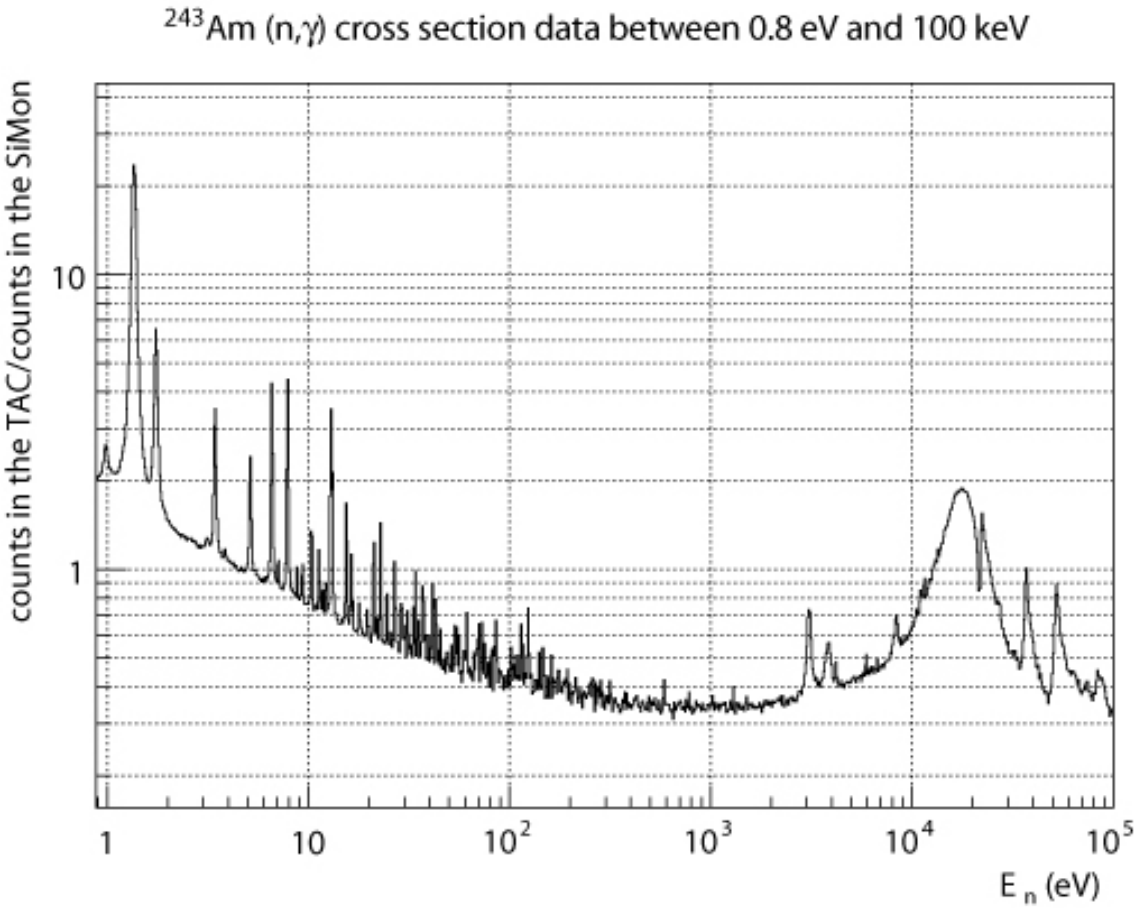

Figure 51: Counting rate of the TAC as a function of the neutron energy in the range between 0.8 eV and 100 keV for the ^{243}Am target.

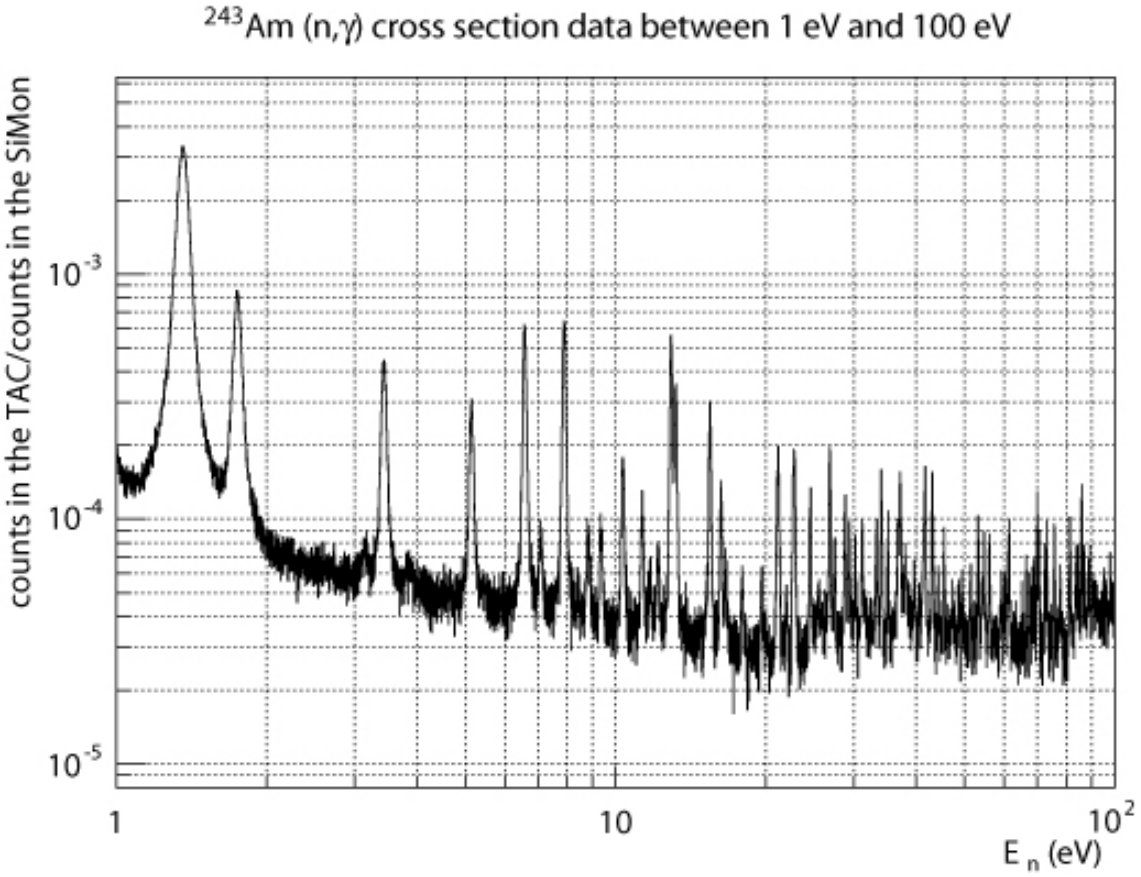

Figure 52: Counting rate of the TAC as a function of the neutron energy in the range between 1 eV and 100 eV for the ^{243}Am target.

Reference Samples

The neutron capture cross section of ^{197}Au was the most massive one –185.4 mg – and measured in the same conditions as the TRU ones over the energy range between 0.08 eV and 100 keV. Since it is the reference cross section to which all other data will be normalized, it was measured with about ten times more statistics than all others: $79 \cdot 10^{16}$ protons with 500 MSamples/s, $17 \cdot 10^{16}$ protons at 250 MSamples/s and with the lead shielding, and at last $2.16 \cdot 10^{16}$ protons for the measurement at 100 MSamples/s in the low energy range.

Other targets measured where a 70 mg ^{nat}C sample, an empty Ti canning used to encapsulate the TRU and an empty frame used to place all the targets in the sample holder at the centre of the TAC. In this way, the main background components were determined experimentally and will be used during the data analysis.

Fission Cross Sections of the Th-cycle isotopes (^{232}Th, ^{233,234,236}U)
*(in charge: **L Tassan-Got**)*

Neutron Induced Fission Cross-Section Measurements with FICs Detectors

Contributed by *V Ketlerov* (IPPE, Obnisk)

FIC construction

FIC (Fast Ionization Chamber) detectors have been used for the measurements of the neutron induced fission cross-section [1]. There were three detectors (FIC0, FIC1 and FIC2) built. They have different design of the body but the same internal configuration, which is a stack of several parallel-plate ionization chambers with 5 mm spacing between electrodes and operating with argon-tetrafluormethane (90%Ar+ 10%CF4) at 700 mbar pressure. High-voltage of 400 V was applied to the targets while intermediate electrodes were connected to the ground. The design and construction of the detector body were carried out according to the recommendations of the ISO 2919 standard in order to comply with safety requirements. FIC detector set-up is shown in Figure 53. Up to 16 targets can be installed in one detector. This means that the fission cross-section of several isotopes can be measured simultaneously.

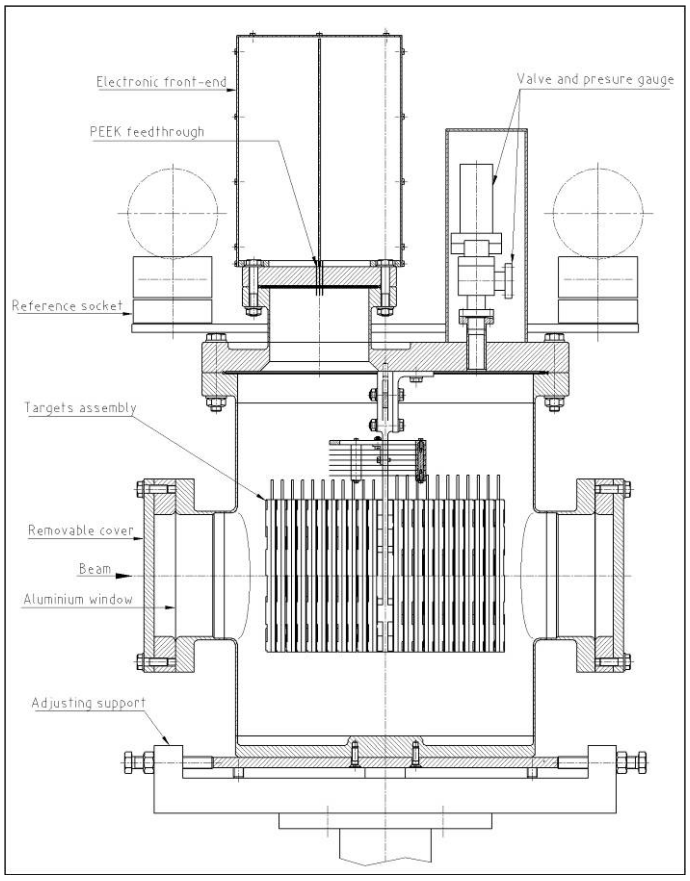

Figure 53: FIC detector setup.

Targets

30 targets were specially made for these measurements. One target consists of a stainless steel holder and backing with very thing layers of substance on both sides. The backing is made of 100 μm thick aluminum foil. A spot of substance with 80 mm in diameter was deposited on

the backing using painting technique, which consists of about 200 iterations of painting and baking in an oven. All targets were tested by alpha-spectrometry with a silicon detector in order to determine the mass and impurities [2]. In spite of the fact that all initial substances were chemically cleaned from impurities and decay products just before the preparation, traces of these have been observed. The list of targets is presented in Table 4.

Table 4: list of targets in the FICs detectors.

Nuclide	Ring label	Mass, mg	Uncertainty, %	Nuclide	Ring label	Mass, mg	Uncertainty, %
Th-232	1	1.92E+04	1.4	U-236	15		
	2	1.90E+04	1.2		16	5.82E+03	1.3
	3	1.94E+04	1.4		17	5.33E+03	1.4
	4	1.82E+04	1.3		18	5.25E+03	1.4
U-233	5	8.04E+03	1.2		19	4.95E+03	1.4
	6	7.45E+03	1.2	U-234	8	5.46E+03	5
	7	7.49E+03	1.3		7	5.00E+03	5
	8	5.86E+03	1.1		6	5.17E+03	5
U-235	9	1.67E+04	1.1		5	5.17E+03	5
	10	1.89E+04	1.1		4	5.46E+03	5
	11	1.52E+04	1.4		3	5.28E+03	5
	12	1.66E+04	1.3		2	5.40E+03	5
	13	6.47E+03	1.1		1	5.41E+03	5
	14	6.32E+03	1.1	U-238	209	10E+03	10
U-238	20	1.18E+04	1.3	U-238	210	10E+03	10
	21	1.15E+04	1.4	U-238	211	10E+03	10
	22	1.28E+04	1.4	U-235	78	5E+03	10
	23	1.26E+04	1.4	Am-243 (Am-241)	38	5.56E+02	1.2
	24	1.34E+04	1.2		39	5.85E+02 (1.48E+01)	1.3 (1.2)
	25	1.37E+04	1.4		40	6.13E+02	1.3
	26	1.28E+04	1.4		41	6.31E+02	1.3
	27	1.24E+04	1.4		42	5.37E+02	1.2
Am-241	30	2.34E+02	1.1		43	5.58E+02	1.2
	31	2.30E+02	1.2		44	5.95E+02	1.3
	32	2.80E+02	1.2		45	7.10E+02	1.2
	33	2.79E+02	1.2	Cm-245 (Cm-244)	46	3.67E+02 (2.43E+01)	1.3 (1.1)
	34	3.04E+02	1.2		47	5.38E+02	1.2
	35	3.36E+02	1.2		48	4.07E+02	1.3
	36	3.21E+02	1.2		49	3.99E+02	1.3
	37	2.77E+02	1.2	Np-237	28	6.34E+03	1.0
	37 (1)	2.82E+02	1.2		29	6.48E+03	1.1
	37 (2)	2.46E+02	1.2				

Electronics

In order to transfer fast electronic signals at a distance of about 100 m, custom electronic modules were designed and made keeping in mind that there are 16 independent ionization cells inside one detector. The FIC electronics setup is shown in Figure 54. The front-end board was mounted on the flange of the detector body and consists of three parts: current sensitive preamplifiers, fast linear amplifiers and twisted pair drivers. The outputs of linear amplifiers could be connected directly to Acqiris digitizers inputs, while twisted pair drivers

were used to transfer signals for additional analog processing. Twisted pair receiver was used on the other end of cable in this case. The signal was split by fan-out and connected to two different modules: FADC and TDC. FADC is 40 MHz 10 bits fast (flash) analog-to-digital converter with 4k samples memory that is equal to 100 μs of waveform, which in turn corresponds to neutron energy range down to about 20 keV. TDC is 0.8 ns resolution time-to-digital converter with list-mode memory. It was configured to cover time range from 0 to 100 ms, which corresponds to neutron energy range from 0.01 eV to maximum. But due to oscillations in the electronic channels just after the proton pulse this simple the TDC approach cannot provide data for neutron energy higher than 1 MeV. Thus, we have to different types of data with an overlap in neutron energy range from 20 keV to 1 MeV where they could be cross-checked.

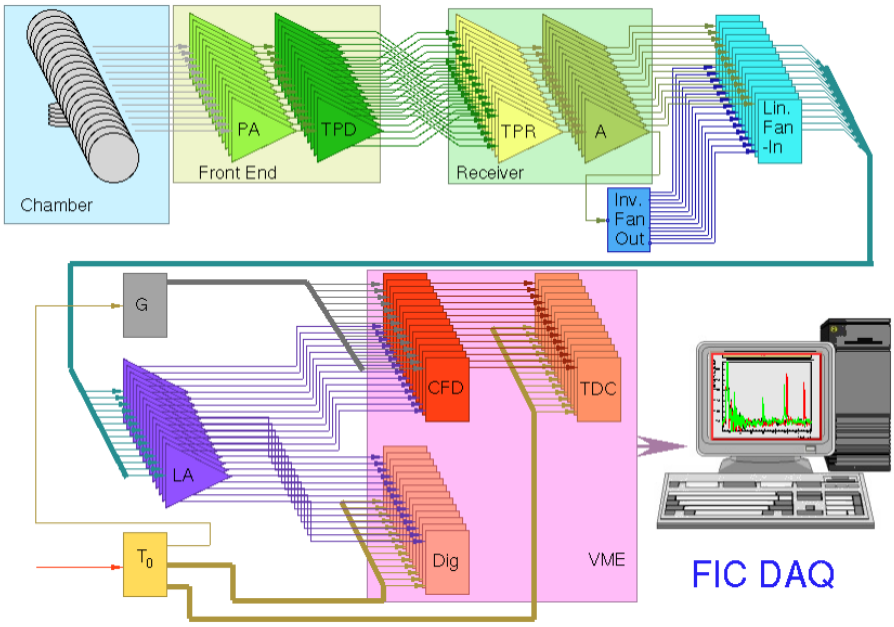

Figure 54: FIC electronics setup.

TDC data

TDC data processing is divided into two groups of activities: a) filtering and conversion of raw data into counting rates for each channel; b) determination and application of corrections in order to get cross-section. Special computer codes were developed to perform all the necessary steps. The presence of 16 electronic channels allows to create noise filter based on the fact that noise signals must appear simultaneously in different channels. After the tuning of noise filtering parameters (which were found to be: time window of 20 ns and majority level of 3 channels), we obtained noise-free data. An example is shown in Figure 55, where counts are plotted versus approximate neutron energy.

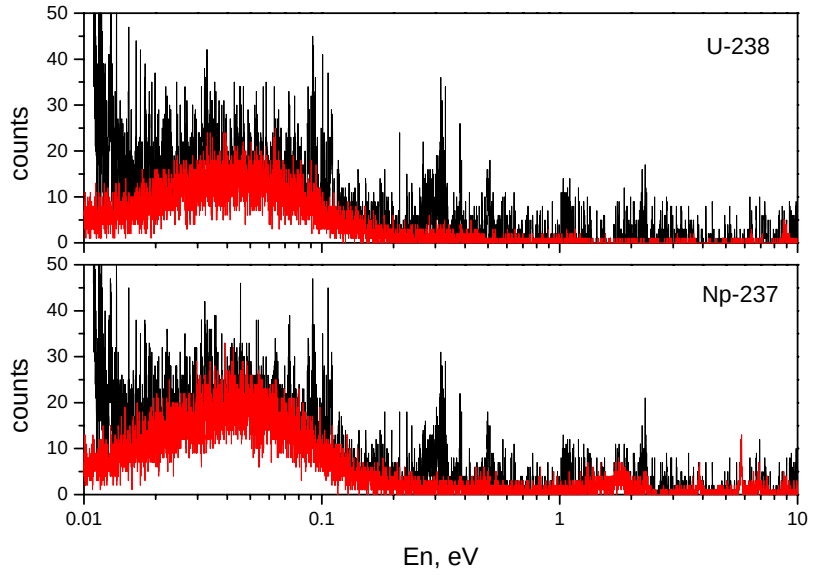

Figure 55: TDC data noise filtering. Black curve (before filtering), and red curve (after filtering) are shown for comparison.

The results of previous step were used for the determination of time-to-energy conversion parameters: a) flight-path for thermal neutrons; b) flight-path correction for neutrons with energy higher than thermal. For both cases a comparison of resonance positions of our data with ENDF/B-VI data was used. Figure 56 shows the value of flight-path correction that has to be introduced to have the resonance positions matched. It is seen that behaviour of this value in case of U-233 is absolutely strange. It could be the result of bad quality of neutron energy resonance data in the ENDF/B-VIlibrary for U-233. Figure 57 shows the flight-path correction versus time-of-flight used in our data processing.

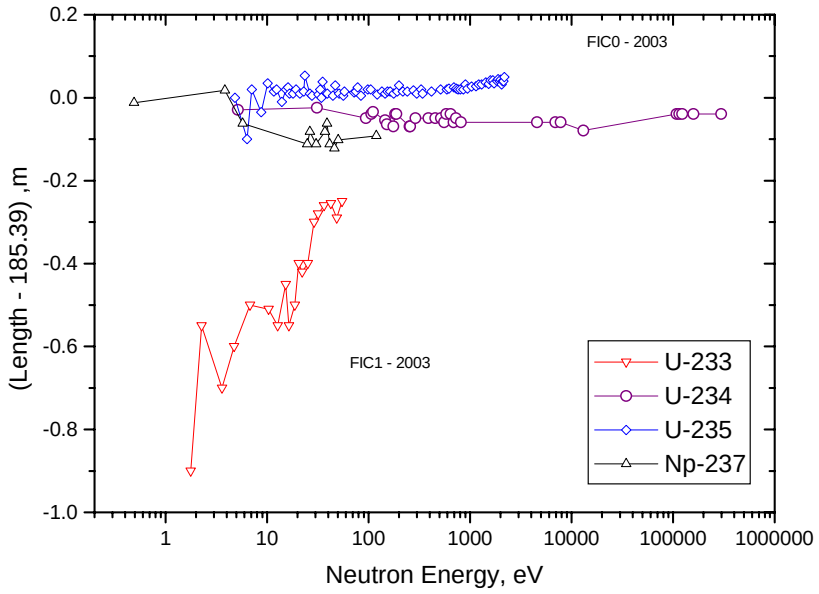

Figure 56: Determination of the flight-path correction from position of known resonances. Points for U-234 plotted for verification of applied correction.

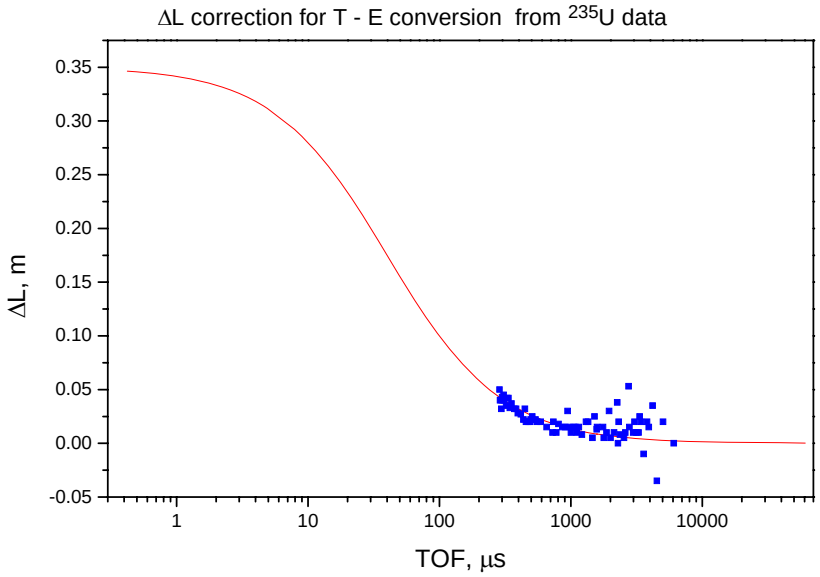

Figure 57: Extrapolated flight-path correction versus time-of-flight.

A first comparison of our data with other experiments taken from EXFOR is presented in Figure 58. From the measured data and using the cross section data from the evaluated nuclear data library ENDF/B-VI it is possible to deduce the neutron flux at the sample position. Although the distance between different targets mounted inside one detector is not more than 180 mm we have found that the deduced neutron flux is different for different targets (note that the position of the n_TOF spallation module is 185 m away from the detector position). There are two reasons for that: a) beam divergence; b) aluminium backings and intermediate electrodes.

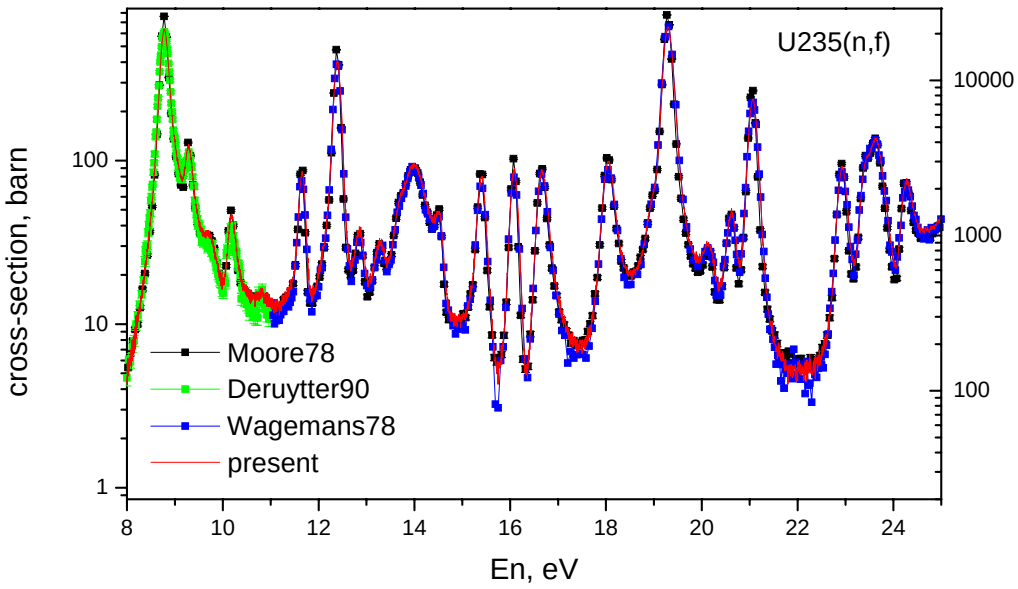

Figure 58: Comparison of present count rate data with other experimental data.

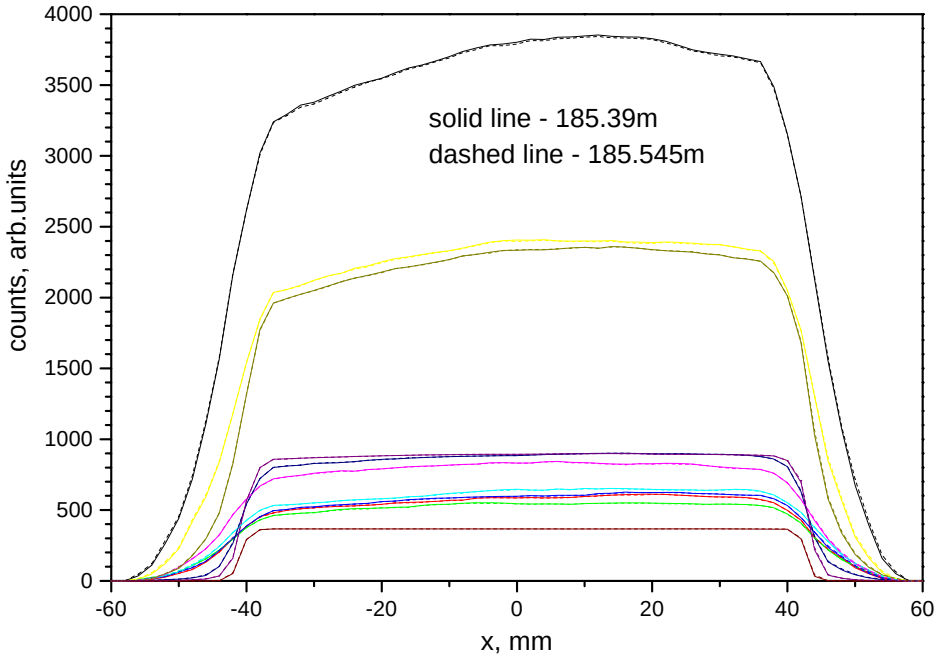

Figure 59: Simulated beam profile for different neutron energies for two targets spaced by 155 mm.

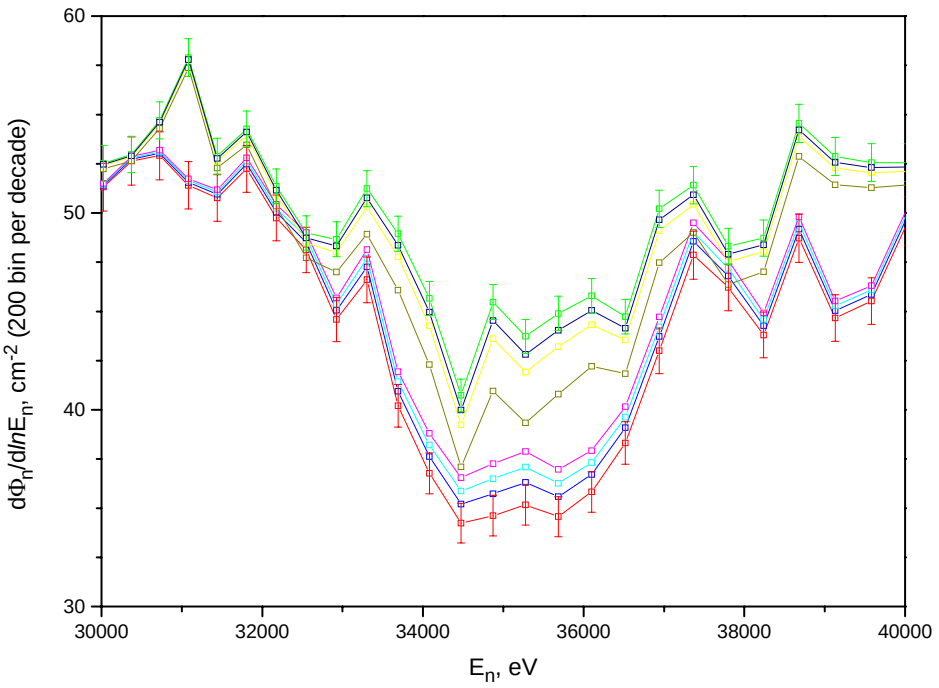

Figure 60: Difference in the counting rate of two U-235 targets because of the aluminium backings and the electrodes. Total amount of aluminum is 1.5 mm. Simulated count rates for intermediate positions are also shown.

According to beam profile simulations, we have a negligible difference of 0.01% in the beam shape for the last two targets in the stack (see Figure 59). The influence of the aluminum backings and electrodes was obtained from comparison of count rate for two U-235 targets mounted in position 2 and position 14 (see Figure 60). For the last case we have 1.5 mm of aluminum in between the targets. Unfortunately, it is impossible to make targets free from impurities, so we have to subtract counts, which could be attributed to these. In the case of U-234, U-236 and U-238 the most important impurity is U-235. Even very small amount of this isotope shows a number of counts comparable with the isotope under investigation. The result of the subtraction of U-235 counts is shown in Figure 61.

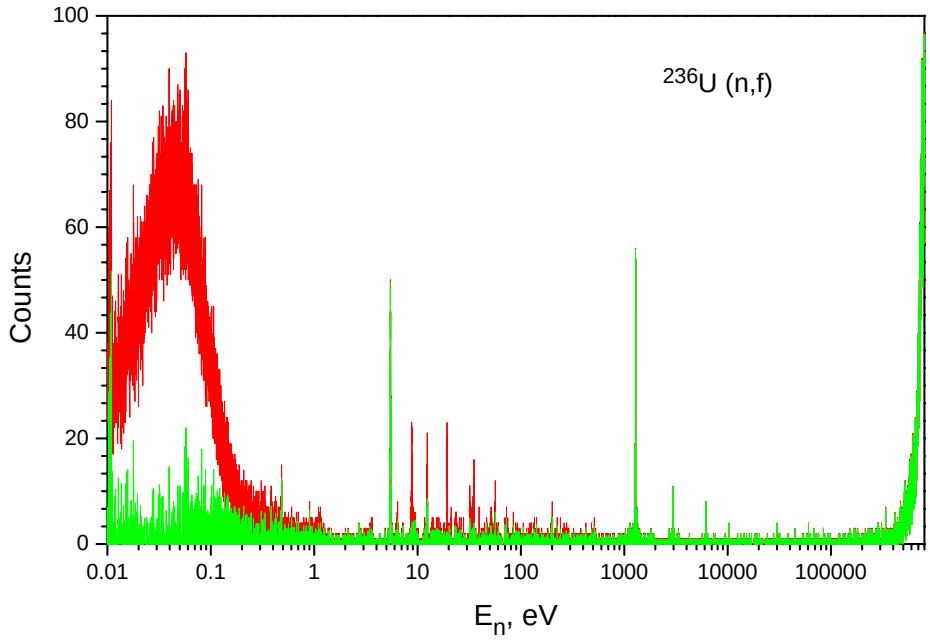

Figure 61: Subtraction of U-235 counts from original counts of U-236 target. Admixture of U-235 is only 0.047%. Red line - before subtraction, green line - after subtraction.

The neutron induced fission cross-section relative to U-235 using formula (1) or absolute cross-section using formula (2).

$$\sigma_f = \frac{N}{N^{ref}} \cdot \sigma^{ref} \frac{M \cdot m^{ref}}{m \cdot M^{ref}} \qquad (1)$$

$$\sigma_f = \frac{N \cdot M}{\Phi \cdot m \cdot N_A} \qquad (2)$$

FADC data

Waveforms recorded with FADC have almost full information about pulses from ionization chambers, namely time tag and amplitude. In order to extract this information a special computer code was developed. This code was tuned and tested by processing data from the FIC2 detector, which was installed in the escape lane during the capture campaign of the year 2004. An example of the typical waveform is shown in Figure 10. The position of the gamma-flash is regarded as T0. It is seen that oscillations in the beginning of the waveform are only slightly higher than the noise level, but they could still affect dramatically the counting rate in this region. To fight against these oscillations their image was created as an average of almost all waveforms (see Figure 62, red line) keeping in mind possible jitter of T0.

As a first step of the FADC data processing the subtraction of the oscillation image from the original waveform was performed. The resulting waveform was smoothed by median filter in order to remove sharp spikes, which could affect the differentiation. Then, the residue was

differentiated. The positions of differential threshold crossing were taken as possible fission fragment pulses and a fitting procedure was applied. As a result of the successful fitting we had time tag, amplitude of the pulse and goodness of fit (see Figure 63).

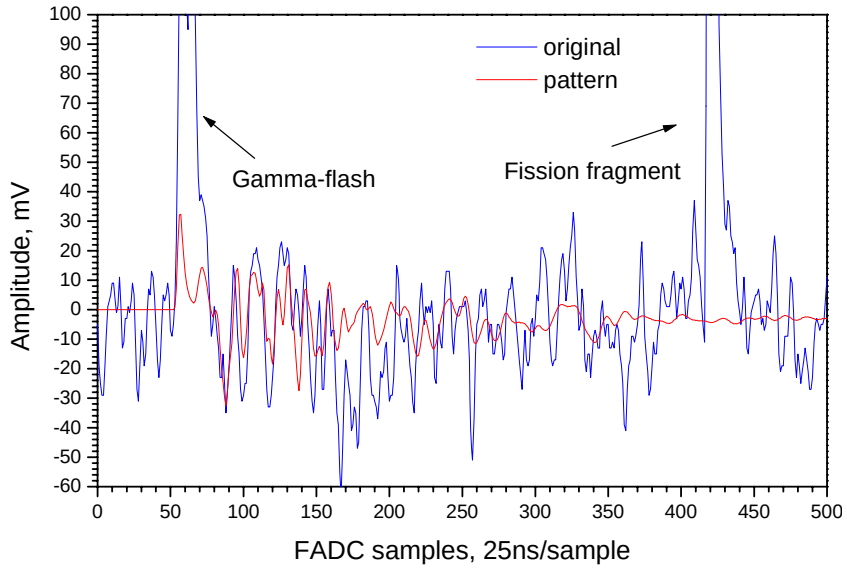

Figure 62: Typical waveform recorded during from FIC2 detector during capture campaign of the year 2004.

These parameters for each identified pulse were stored for further histogram making. In order to collect the correct counting rate versus neutron energy histogram, a threshold for the pulse height must be defined after analysis of double dimensional histogram, pulse amplitude versus neutron energy (see Figure 64 and Figure 65). It is seen that there are a lot of small amplitude pulses in the high neutron energy region. They are the results of fragmentation rather than fission of nuclei and have to be cut by the threshold.

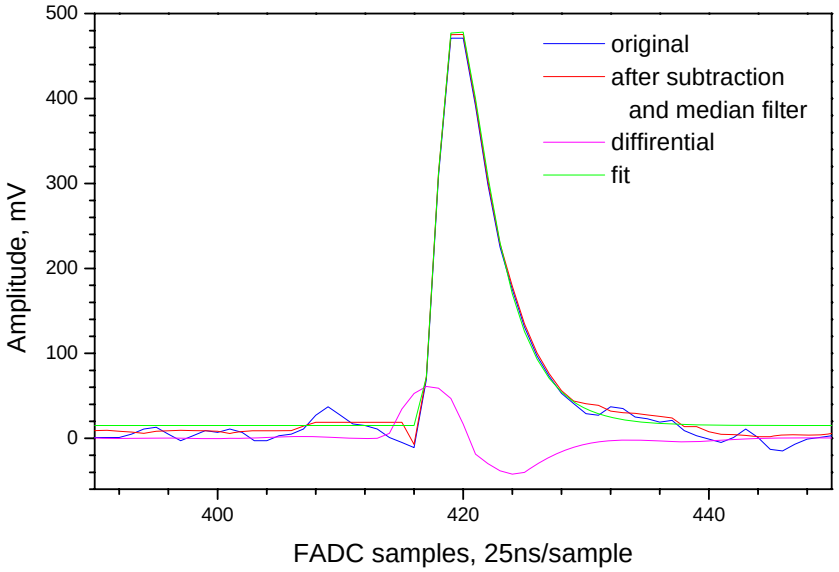

Figure 63: Fit of the fission fragment pulse.

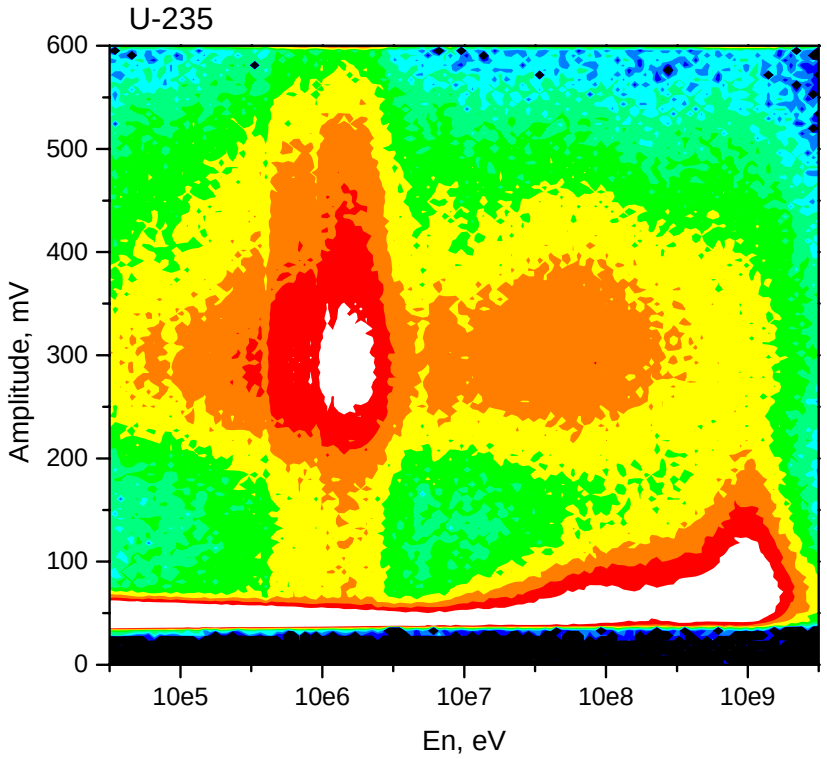

Figure 64: Double dimensional histogram of the pulse fit parameters.

The analysis of the pulse height histograms in the neutron energy region from 20 keV to 1 MeV gave us the efficiency of fission fragment registration, which is about 94.5% (see Figure 66). The comparison of FADC and TDC data shows a very good agreement (see Figure 67). The effect of oscillations is very pronounced in case of TDC data.

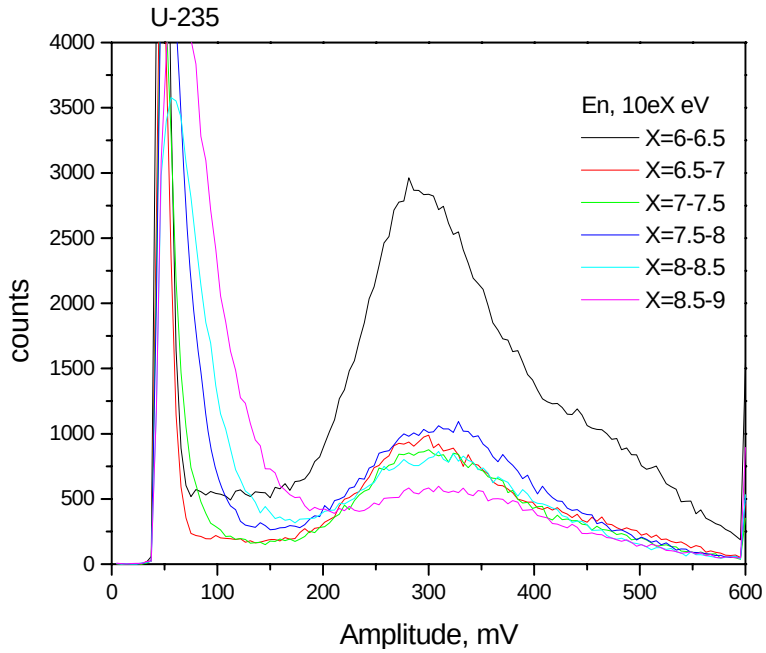

Figure 65: Pulse height amplitude histograms for different neutron energy regions.

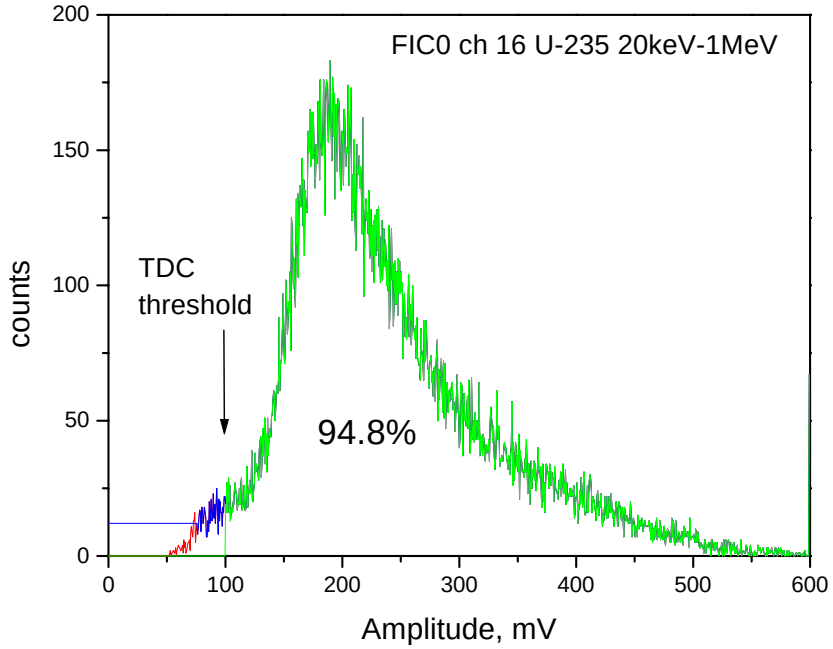

Figure 66: Fission fragment registration efficiency obtained from pulse height histogram.

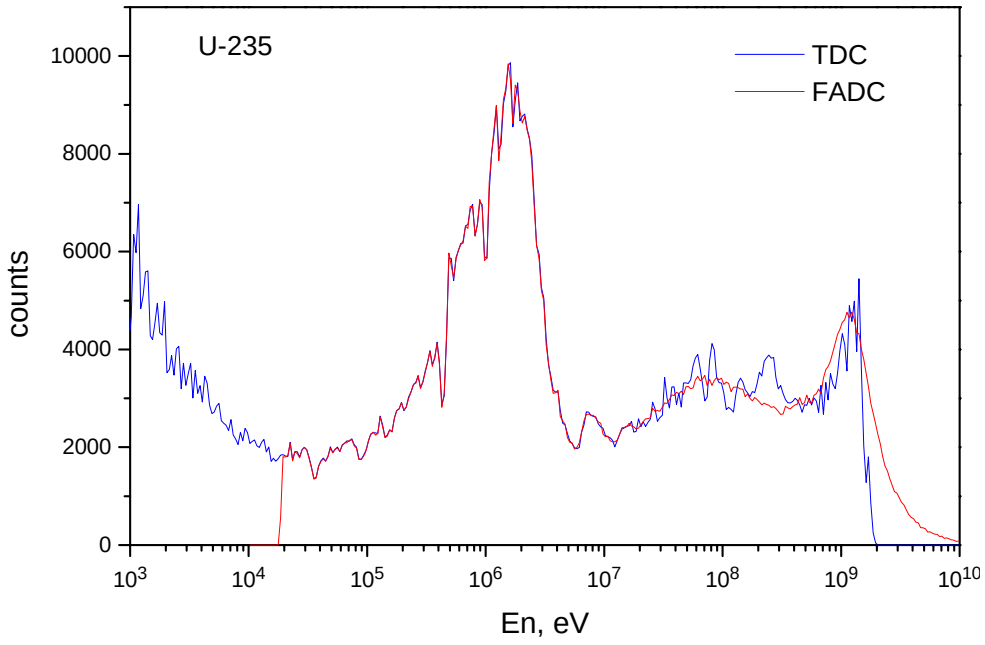

Figure 67: Comparison of TDC and FADC count rates.

Analysis of the uncertainties

Several factors affect the uncertainty of the fission cross-section data. Here below we provide a brief description of each uncertainty component.

a) the statistical uncertainties in the count rate were determined as usual, $\Delta N_i = \sqrt{N_i}$

b) the uncertainties connected with background subtraction and isotopic dilution method have been treated as follows. The background from the constant-in-time alpha pile-ups and admixture of U-235 in the sample was fitted using MINUIT code with the function:

$$N_i^{BG} = \frac{m}{m^{ref}} A \cdot N_i^{ref} + cE_i^{-b^2}$$

The MINUIT code provides the errors (one standard deviation) of each parameter *A, b, c*. Due to complicated fitting function, in practice it is better to calculate the value of the function with all parameters larger (or lover) the estimated the standard deviation of each of them and then take this value as uncertainty of the background counts. Beside that, due to smallness of parameter *A* (usually about 10^{-4}) the uncertainty of the mass ratio and reference count is omitted. So,

$$\Delta N_i^{BG} = \frac{m}{m^{ref}} \left((A + \Delta A) \cdot N_i^{ref} + (c + \Delta c) E_i^{-(b+\Delta b)^2} - (A - \Delta A) \cdot N_i^{ref} + (c - \Delta c) E_i^{-(b-\Delta b)^2} \right)$$

c) the flux is derived from the U-235 count rate:

$$\Phi_i = \frac{N_i^{ref}}{\sigma_{(n,f)}^{ref}(E_i)}$$

The uncertainty of the standard cross-section is taken from ENDF-B/VI estimation, which is shown in Table 5.

Table 5: Estimated uncertainties of the ^{235}U fission cross-section.

Energy (keV)	Estimated Uncertainty (%)
2.53E-05	0.2
150-600	1.5
600-1000	1.6
1000-3000	1.8
3000-6000	2.3
6000-10000	2.2
10000-12000	1.8
12000-14000	1.2
14000-14500	0.8
14500-15000	1.5
15000-16000	2.0
16000-17000	2.5
17000-19000	3.0
19000-20000	4.0

Following this procedure, the estimated uncertainty on the neutron flux is given by

$$\Delta\Phi_i = \Phi_i \sqrt{\frac{1}{N_i^{ref}} + \left(\Delta\sigma_{(n,f)}^{ref}(E_i)\right)^2}$$

d) the mass of target was derived from alpha-spectrum with uncertainties from 1% to 5% for different isotopes (see Table 1).

e) the uncertainty of fission fragment registration efficiency was determined from pulse-height spectra of the fission fragments and given threshold for each registration channel. The resulting uncertainty values for each target and are listed in Table 6.

Table 6: Fission fragment registration efficiency.

Channel	Isotope	Mass, mg	Efficiency	Uncertainty
1	Th-232	38.2	0.958	0.005
2	U-235	35.6	0.962	0.002
3	U-236	11.15	0.972	0.003
4	Np-237	12.82	0.967	0.002
5	U-236	10.2	0.971	0.003
6	U-238	23.3	0.966	0.003
8	U-238	25.4	0.966	0.003
9	Th-232	37.6	0.953	0.005
11	U-234	5.46	0.976	0.003
12	U-234	5.28	0.981	0.003
13	U-234	5.4	0.981	0.003
14	U-235	5	0.965	0.003
15	U-238	20	0.959	0.003
16	U-235	12.79	0.957	0.002

All these uncertainty components were taken in to account for the determination of final results.

Results

The results of the fission cross sections derived from the measurements at n_TOF are shown in the Figure 68, Figure 69, and Figure 70 below for the U-234, U-236, Np-237 target respectively. A comparison between the cross section data of the ENDF/B-IV nuclear data library (blue line) and the n_TOF data (red line) of neutron induced fission cross-sections of Th-232, U-234, Np-237, and Cm-245 in selected energy ranges are presented in Figure 71, Figure 72, Figure 73, and Figure 74.

The numerical values of these cross sections will be made available in the n_TOF dissemination web interface on the n_TOF web server (http://www.cern.ch/ntof). The data will be compiled into the EXFOR format and included in this database as well.

Finally, the most important result of the measurements with FIC2 is ratio of neutron induced fission cross-sections of U-238 and U-235 (see Figure 75). Our data points are located around level of Sherbakov's data, which is about 15% lower than Lisowski's data.

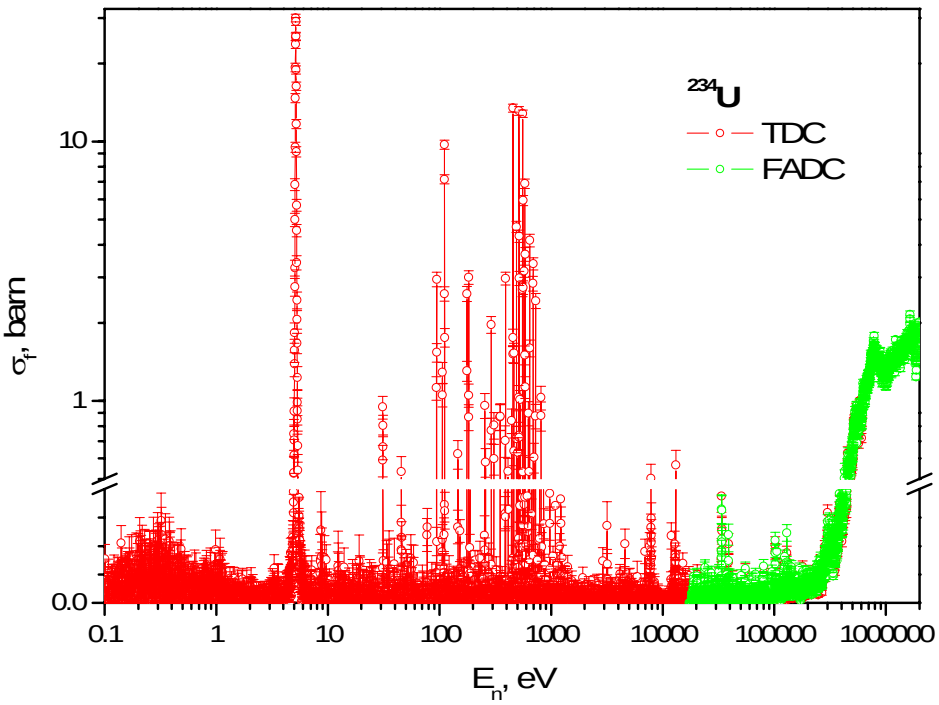

Figure 68: Neutron induced fission cross-section of U-234.

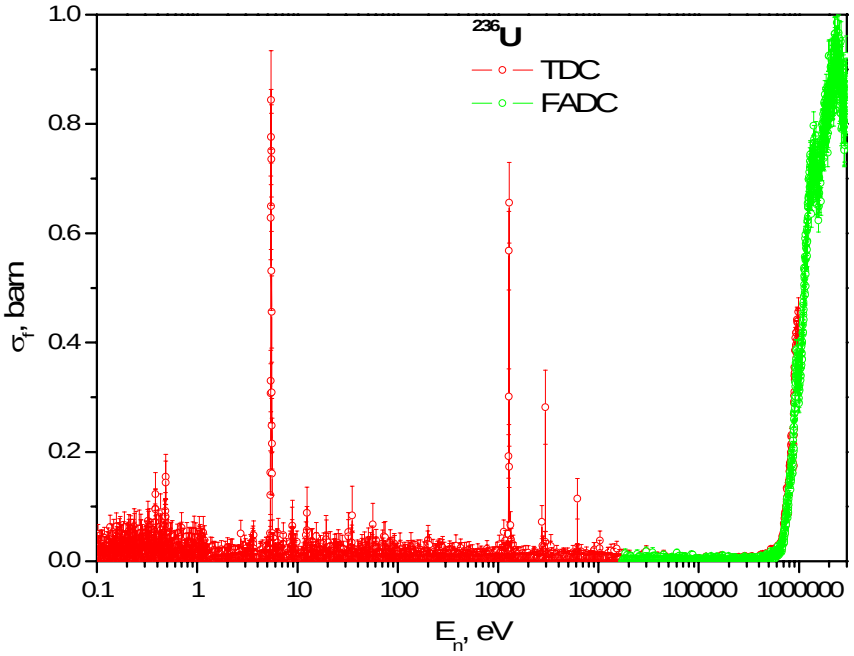

Figure 69. Neutron induced fission cross-section of U-236.

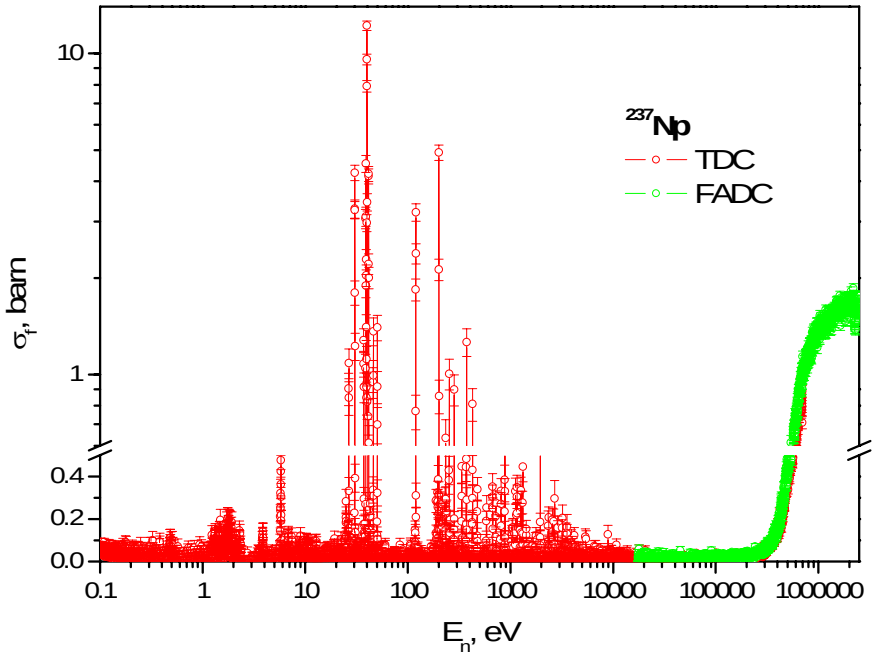

Figure 70: Neutron induced fission cross-sections of Np-237.

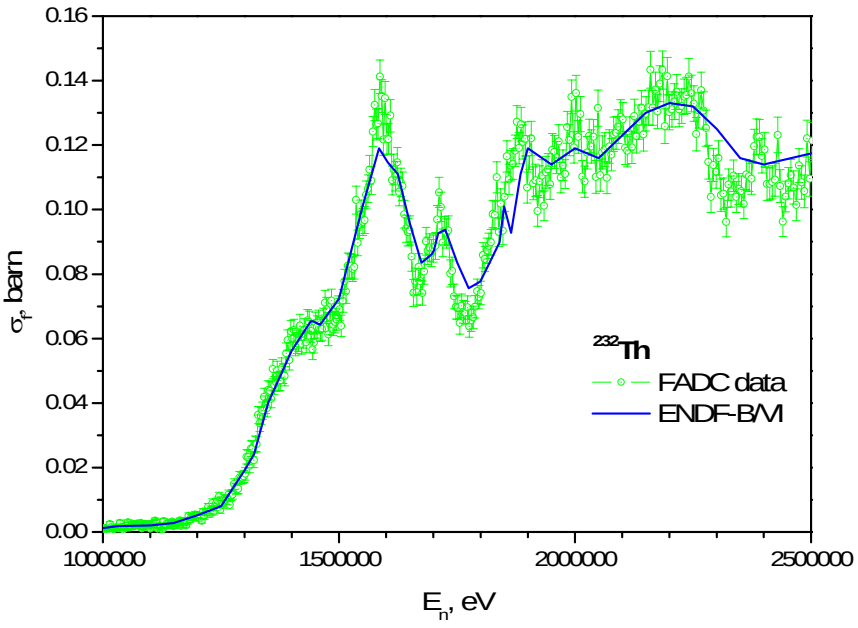

Figure 71: Neutron induced fission cross-section of Th-232.

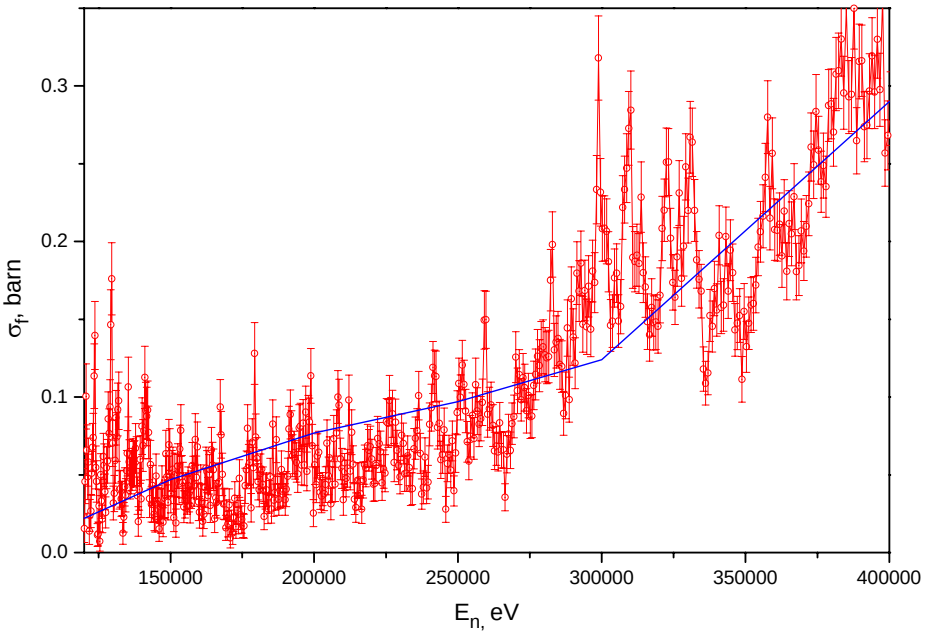

Figure 72: ENDF-B (blue line) and our data (red line) of neutron induced fission cross-sections of U-234.

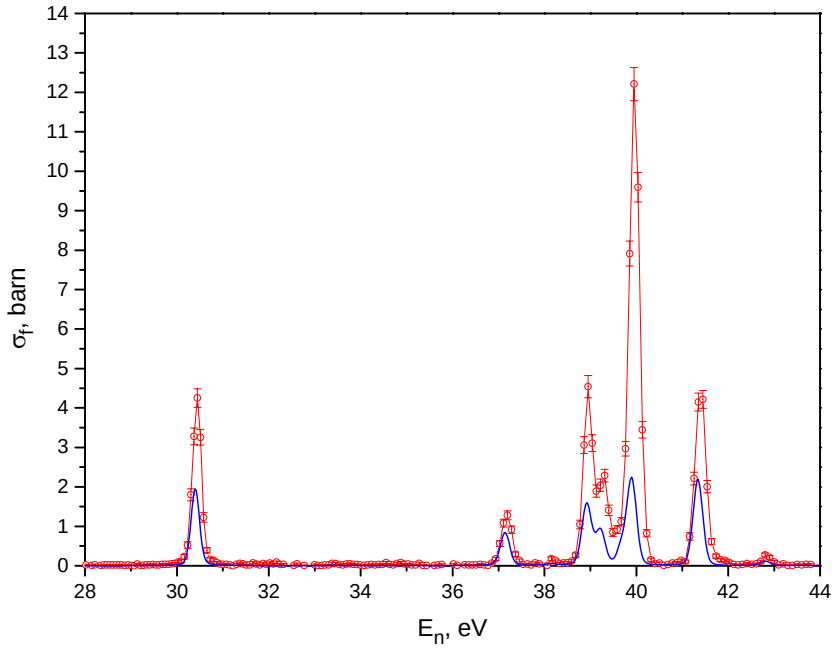

Figure 73: ENDF-B (blue line) and present data (red line) of neutron induced fission cross-sections of Np-237.

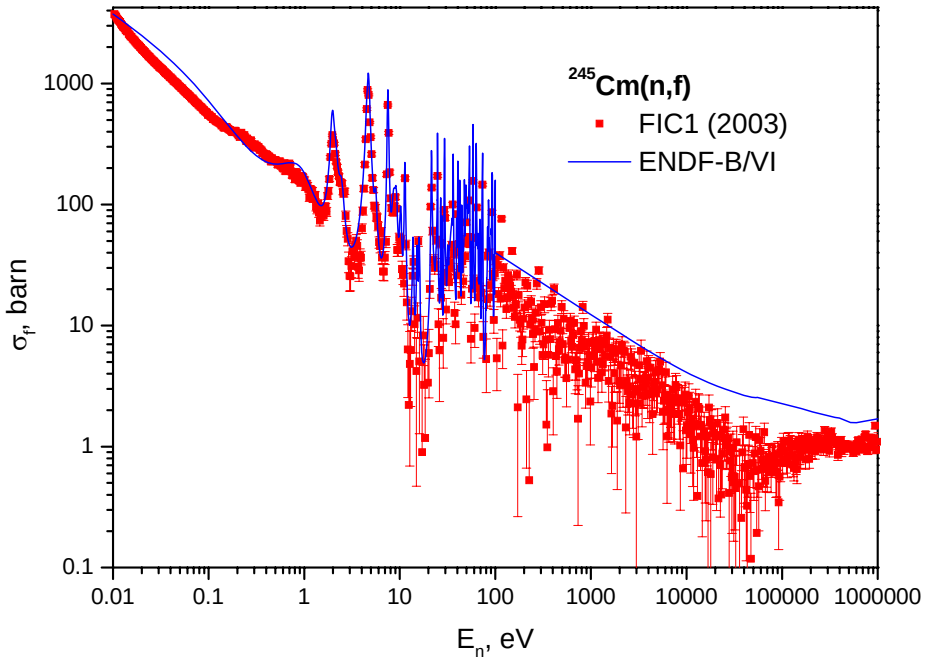

Figure 74: ENDF-B (blue line) and preliminary present data (red points) of neutron induced fission cross-sections of Cm-245.

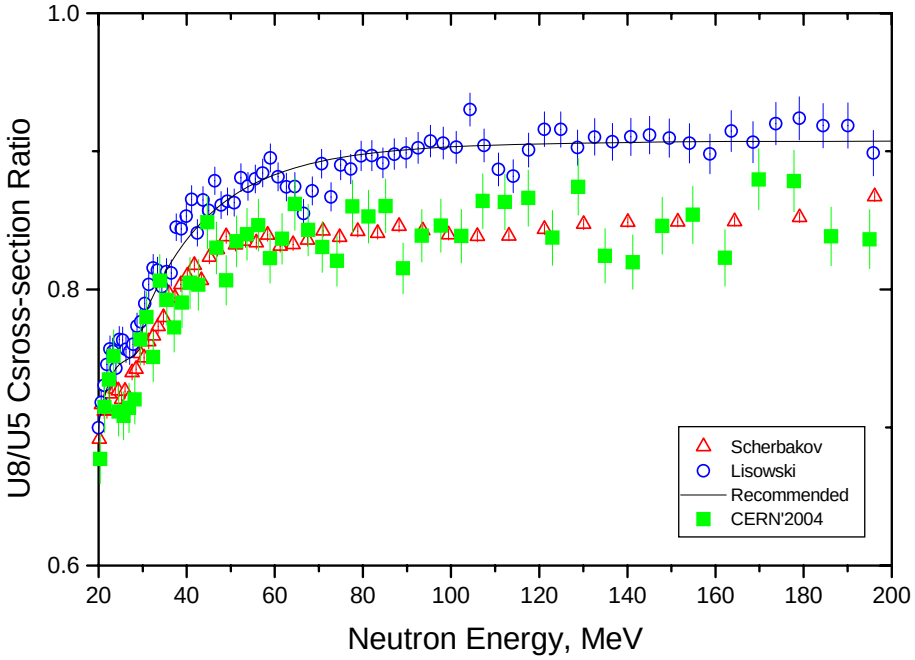

Figure 75: Ratio of neutron induced fission cross-sections of U-238 and U-235.

Measurements performed at IRMM

Contributed by *A Plompen* (IRMM, Geel)

At IRMM transmission, capture and (n,xnγ) measurements were carried out, together with some detector tests. For the most part these are described below. Capture measurements for ^{99}Tc are described elsewhere as well as the ^{207}Pb(n,2nγ)^{206}Pb cross section measurements. All work was carried out at the pulsed white neutron source Gelina.

^{240}Pu and ^{242}Pu transmission measurements

With regard to the renewed interest in Pu recycling and reactor fuel with high Pu content, the large resonances of ^{240}Pu (1.056eV) and ^{242}Pu (2.68eV) are of major importance for the determination of temperature coefficients in modern reactors. Both resonances have a small natural resonance width resulting in a large contribution of the Doppler broadening to the total width. Total cross section measurements have been performed with highly enriched Pu samples at the GELINA facility of the IRMM. For both isotopes, measurements were performed at three different temperatures. The resonance shape analysis was carried out using the R-matrix code SAMMY in which the treatment of Doppler broadening is included by means of a crystal lattice model (CLM).

Experimental procedures

The experiments were performed at flight path 2 of the pulsed neutron source GELINA of the IRMM. This flight path views the water moderator of 36 mm thickness at an angle of 81 degrees with respect to the electron beam. The neutron beam is collimated to a size of 40 mm diameter. Samples are inserted at 10 m from the neutron source and the detector is placed at 26.45 m. A lithium-glass scintillator (NE912), enriched in ^{6}Li and with a thickness of 1.27 cm was used. It was viewed by two 5`` EMI9823 photo-multiplier tubes which were placed orthogonal to the beam axis and out of the neutron beam.
Samples were produced by mixing PuO_2 powder with graphite powder, adding alcohol and filling the copper sample container. After pressing, the samples were dried for several days and sealed. For the sample-out position equivalent dummy samples were made containing only graphite.
The samples were placed on a sample changer inside a cryostat so that both sample-in and sample-out positions are cooled. The cryostat uses the Gifford-McMahoon cycle. Temperatures were measured with two Pt100 temperature sensors and stabilized with a PID-loop to within 0.5 K at each temperature (see Table 7).
The electronic setup was based on a combination of the amplitude and the time of the anode signal from both photomultiplier tubes. A valid time signal was generated when the sum of both signals falls within a preset amplitude window as well as in a narrow time window with both independent signals. This signal was registered with a multi-hit time coder of 0.5 ns resolution that is started by the pulse derived from an induction loop signaling the arrival of the electron burst. A PC based data acquisition system controls the measurement, iterating over sample-in and sample-out runs and monitoring the total dead time of the setup. A separate PC was available for controlling and monitoring of the sample temperatures.

Data were taken at 100 Hz and 40 Hz repetition rate. At 100 Hz a Cd filter suppresses low energy neutrons from the previous cycle. This filter was not used for the measurements at 40 Hz. Here the small contribution of the overlapping neutrons was extrapolated and corrected for in the analysis. A set of black resonance filters was used to measure the neutron background at the measurement station. Na was used as a permanent filter whereas Cd, Au, and Co were used only for dedicated background runs. For the reduction of the gamma-flash, coming from the neutron producing target, a high purity lead disk with 5 mm thickness was placed continuously in the beam.
Further details of the experimental conditions are given in Table 7 and further information about this setup can be found in Ref. [1].

Table 7: Experimental conditions for the neutron transmission measurements PuO_2.

Experiment	GELINA	Temperatures	Sample (enrichment, thickness)	Energy range
^{240}Pu (run1)	100 Hz, 1ns	15K 300K	98.47%, 8.75*10-5 at/b	0.3 eV – 1 keV
^{240}Pu (run2)	40 Hz, 1 ns	15K 77K 294K	98.47%, 8.75*10-5 at/b	0.013 eV – 1 keV
^{242}Pu	100 Hz, 1 ns	12K 77K 300K	99.93%, 2.50*10-5 at/b	0.3 eV – 1 keV

Data Processing

The transmission measurements were performed for each sample and for each temperature in cycles with a preset number of counts and data were stored as TOF spectra in histogram mode. Sample-in and sample-out measurements were interchanged with cycle times of about 20 minutes. By this, the influence of the neutron flux instabilities was minimized. At the same time the neutron flux was monitored continuously by two BF_3 detectors and recorded for each cycle. Before summing the corresponding transmission spectra, a visual check on the data and the reporting files was performed to ensure the general integrity of the data with regard to system- and/or accelerator failure. Moreover the stability of the cryostat was verified and cross checked with the transmission data.
The data analysis was performed using the program package AGS. This includes:

- corrections for time offset
- corrections for dead-time (assuming a step behavior)
- determination and subtraction of background
- normalization to the neutron flux
- calculation of transmission factors
- determination of uncertainties

The time offset in the setup was measured by determining the arrival time of the gamma-flash. A calibration of the sub-thermal neutron energies was performed by analyzing the Bragg-edges in the total transmission curves due to Bragg-scattering at 180^0 from the lattice plane in the micro-crystals of graphite.
For the determination of the background a power function $Y = a + bt^c$ with 3 free parameters (a,b,c) and t as time-of-flight was fitted to the black resonance dips. The obtained function was used to subtract the background from the measurements. The observed neutron background was of the order of 0.5% below 100 eV for the 100 Hz runs and even lower for the 40 Hz measurements. The contribution of overlap neutrons was determined by linear

extrapolation of the thermal and sub-thermal neutron flux to the next accelerator burst. This contribution was then subtracted from the spectra as well (Figure 76).
After the normalization of the sample-in and sample-out spectra, the transmission factors were determined. The use of short sample-in and sample-out cycles in combination with a stable neutron flux allowed for the data handling to be applied to the summed spectra instead of treating the individual cycles independently.

Results

The data from the transmission measurements for ^{240}Pu and ^{242}Pu are available as ASCII data files for each isotope and temperature given in Tab. 4.1.1. The transmission factors for Pu are given as function of neutron energy together with the corresponding uncertainty. They cover the neutron energy range from 0.013 eV (at 40 Hz) and 0.3 eV (at 100 Hz) up to neutron energies around 100 keV where the influence of the gamma flash became visible. However, for the resonance shape analysis the range was restricted to about 1 keV due to the energy resolution becoming larger than the resonance width.

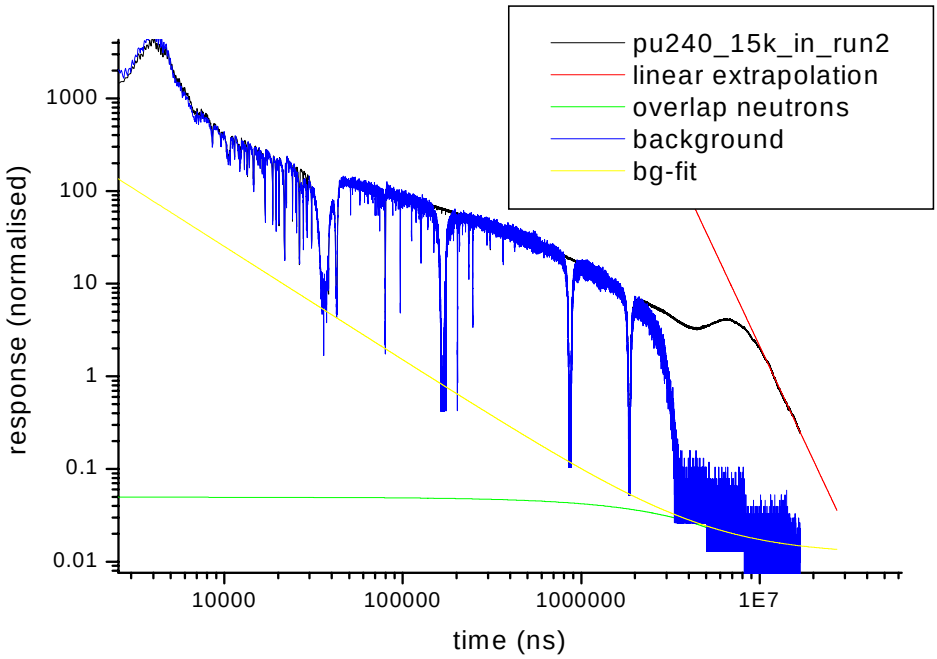

Figure 76: Response of the neutron detector as function of TOF for the determination of the background and the correction of the overlap neutrons.

For the resonance shape analysis the R-matrix analysis code SAMMY [2] was used including the crystal lattice model for the treatment of the Doppler broadening. The following input parameters had to be determined:

- resonance parameter files (prior input)
- user defined resolution function
- phonon spectrum for PuO_2

For the prior information necessary for the Bayesian fitting procedure tabulated resonance parameters were taken either from ENDF or from literature [3,4].
For the determination of the GELINA resolution function the program code REFIT was used, which includes a parametrization based on Coceva´s calculations [5]. Recently, detailed simulations [6] using MCNP revealed a very good agreement between both approaches. The

obtained resolution function includes the detailed description of the neutron target, moderator and the Li-glass detector.
The calculation of the Doppler broadening based on the crystal lattice approach depends on the exact knowledge of the phonon distribution in the crystal under investigation. Up to now only the phonon spectrum for UO_2 was used in the analysis of actinide-oxides. Only a few experimental data were available and only recently the phonon spectra for Pu and PuAl alloys was obtained experimentally. No data for PuO_2 exist.

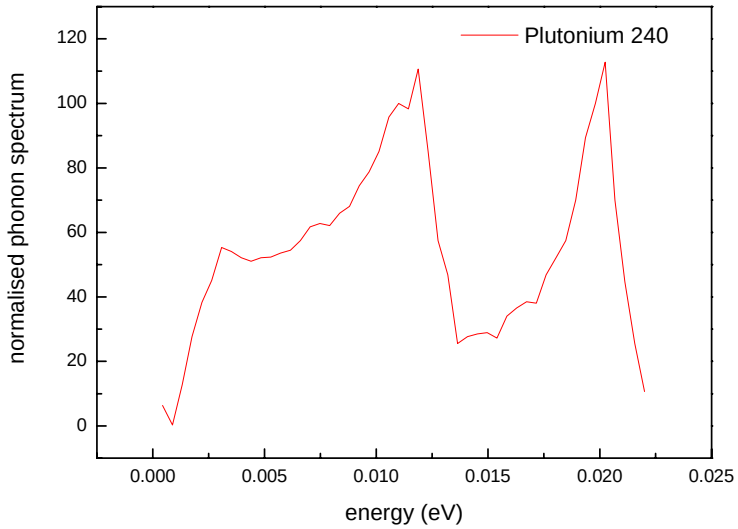

Figure 77: Component of the vibration of the Pu atoms in the phonon spectrum of PuO_2.

By using GULP [7], a program package designed to perform a variety of tasks related to 3-dimensional solids, it was possible to extract phonon spectra for a number of actinide compounds. Based on bulk parameters from Korzhavyi et al. [8] the first phonon density of states for PuO_2 was calculated. The component of this spectrum corresponding to the vibration of the Pu atoms in the PuO_2 lattice was included in the input file for the SAMMY code (Figure 77).

^{240}Pu: Due to the higher sample thickness the first resonance of ^{240}Pu at 1.056 eV was nearly black and has a high uncertainty in the peak of the resonance due to statistics and the subtraction of the background. Preparations of thinner samples failed due to the appearance of 'holes' in the distribution of the Pu in the graphite matrix. As a consequence the analysis of the first resonance was hampered and a fit with E_n, Γ_n, and Γ_γ as free parameters revealed a Γ_γ which was too high compared with the values from the data file and the other resonances in this measurement. For the first resonance, Γ_γ was fixed and the other parameters varied. The obtained Γ_n agrees with the documented resonance parameters. The analysis of the other resonances up to 100 eV gives a good description with Γ_γ as free parameter. As a general trend, the crystal lattice model gives a much better description when compared with the free gas model (FGM). Moreover, the resonance parameters are nearly independent from the temperature, whereas in the FGM an unphysical temperature dependent offset is obvious. The thermal and sub-thermal cross sections could be reproduced with the documented parameters in this first approach.

^{242}Pu: The fit of the first resonance of ^{242}Pu was considerably more straight forward than for the saturated resonance of ^{240}Pu (Figure 78). By using the CLM model, the temperature dependence was much lower than compared to the FGM and moreover the quality of the fit was improved. The values of Γ_γ obtained in the analysis with the CLM differ with those reported previously. A similar conclusion was reached by A. Courcelle for the case of ^{238}U

[9]. Interestingly, the value of Γ_n=1.25 meV for the first resonance agrees better with the value of 1.22 meV in the compilation of Mughaghab [3] than that in ENDF-B6 (2.325 meV).

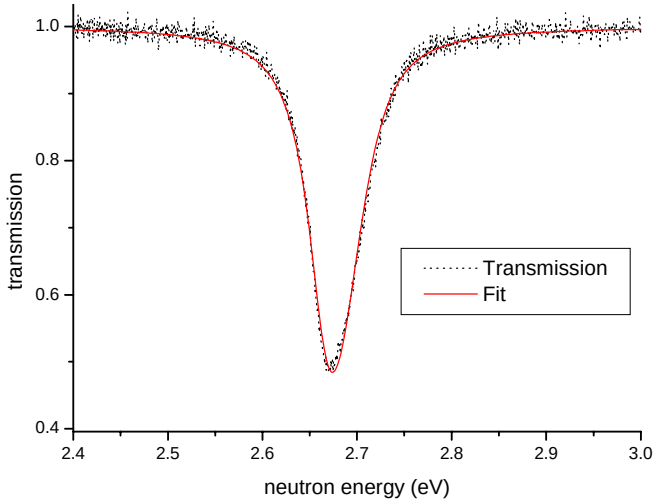

Figure 78: Fit to the 2.68 eV resonance of ^{242}Pu at 12K using the CLM and the calculated phonon spectrum.

An EXFOR file of the experimental data is in preparation together with a JEFF report documenting the experimental procedure.

[1] P. Siegler, K. Dietze, P. Ribon, Proc. Int. Conf. On Nuclear Data for Science and Tech. Tsukuba, Japan, (2001), p. 936
[2] N.M. Larson, ORNL-TM9179 (Rev. 1, Rev. 2)
[3] S. F. Mughabghab, Neutron Cross Sections, Vol. 1 part B, Academic Press, USA
[4] O. Bouland et al. Nucl. Sci and Eng. 127, 105-129 (1997)
[5] C. Coceva et al., Resolution Rotary Target, IRMM report GE/R/ND/06/96
[6] M. Flaska, et al., Nucl. Inst. Meth. A, 531, 392-406, (2004)
[7] J.D. Gale, JCS Faraday Trans., 93, 629 (1997)
[8] P.A. Korzhavyi et al., Nature Materials, 225-228 (01 Apr. 2004) Letters
[9] A. Courcelle, CEA Cadarache, Oct. 2003, working document, private communication.

^{127}I and ^{129}I capture and transmission measurements

Four hundred kg of the long-lived ^{129}I ($T_{1/2}$=1.57 10^7 years) is produced yearly in power reactors in the EU. Iodine is difficult to isolate for long periods of time as it readily dissolves in water and easily moves through the ecosystem. This makes ^{129}I one of few fission products that is considered for transmutation. The various scenarios proposed for transmutation require accurate cross sections in the thermal and epithermal region for assessment of their effectiveness and the interpretation of semi-integral transmutation experiments [1,2,3].
Within the framework of a collaboration between CEA Cadarache and IRMM, the capture and transmission measurements were performed in the energy range from 0.5 eV to 100 keV at the GELINA pulsed neutron source using the time-of-flight technique.
The sample was obtained from a 210 l spent fuel solution with 1.3 g/l of iodine and other products. As a result of the complex chemistry of iodine, as well as the volatility and reactivity of I_2 the material had to be precipitated as PbI_2 [4]. About 140 g of sample material was obtained with a complex composition of PbI_2, elemental Pb, sodium sulfate and some nitrate. The final composition was determined from ICP-MS for the isotopic ratio of ^{129}I/^{127}I,

fast neutron activation analysis for the content of ^{127}I and Pb and Neutron Resonance Capture Analysis for all isotopes of interest except ^{14}N. A separate chemical analysis was carried out at PSI. The final accuracy on the ^{129}I content was better than 3%. Since the ratio of ^{129}I to ^{127}I is about 5, natural samples of PbI_2 were prepared as well in order to separate the contributions from the two isotopes. The sample powder was compacted and canned in cylindrical Al containers of different sizes. For both the transmission and the capture measurements a thin and a thick sample were prepared to cover the low and the high energy region, respectively.
The transmission detector is a ¼" thick Li-glass (NE912) placed at 49.34 m in an Al sphere with white reflective $BaSO_4$ coating and viewed by a 5" EMI 9823 KQB Quartz photomultiplier situated perpendicular to and out of the beam. The sample was placed at 23.7 m. The beam was collimated to 4.5 cm diameter. Black resonance filters (W, Mo, Co, Na, S and Bi) were used to determine the background which was fitted with a simple function and subtracted. For the 800 Hz runs a ^{10}B overlap filter was used whereas a Cd filter was used for the 100 Hz runs.
Capture measurements based on the total energy principle were performed at 28.67 m using two C_6D_6 detectors at 90^o for detection of the gamma-rays. The pulse-height weighting technique was applied to eliminate the dependence on the gamma spectrum. A ^{10}B ionisation chamber was used for the determination of the energy dependence of the neutron flux.
Resonance shape analysis was performed using the codes REFIT [5] and SAMMY [6] using resolution functions obtained from Monte Carlo simulations [7]. Reich-Moore parameters were obtained for all resonances up to 10 keV for both isotopes. For ^{129}I (^{127}I) the fit included 400 (719) resonances, whereas for JENDL3.3 one finds 127 (374) resolved resonances going up to 3 (4.2) keV. Mean resonance parameters obtained from a statistically meaningful set of identified s-wave resonances are presented in Table 8.
For the range from 3.5 keV to 100 keV the average cross sections were analysed using the Hauser Feshbach formalism as implemented in the FITACS option of the SAMMY code. Correction factors for width fluctuations and multiple scattering were obtained with the code SESH [8]. Contributions from s, p, d and f waves were included in the analysis. The results for s-waves are presented in
Table 9 and are consistent with those of Table 8.

Table 8: Average s-wave resonance parameters from a statistical analysis of the resolved resonance region. S0 is the neutron strength function, D_0 the mean s-wave level spacing in eV, $<\Gamma_\gamma>$ the mean radiation width in meV and R_0^∞ is the s-wave distant level parameter.

Parameter	^{127}I	^{129}I
$10^4\ S_0$	0.72±0.06	0.54±0.07
D_0	12.5±0.3	27.3±0.9
$<\Gamma\gamma>$	100±23	106±15
R_0^∞	0.19±0.01	≈0.18

Table 9: Average s-wave resonance parameters from a Hauser-Feshbach analysis of the unresolved resonance region.

Parameter	^{127}I	^{129}I
$10^4\ S_0$	0.779±0.009	0.584±0.004
$<\Gamma\gamma>$	112.4±0.1	108.3±0.9
R_0^∞	0.195±0.001	0.166±0.002

Resonance region (file2) endf formatted files have been produced for both isotopes that have been processed into ACE and ERANOS format for estimates required by the EFFTRA and PROFIL experiments. Currently these files are being integrated into the new JEFF3.1 library. Exfor files were prepared and submitted to the NEA databank and the results of the work have been described in a JEFF report [9]. A refereed journal paper is in preparation.

[1] D. Wootan et al., Trans. ANS **64**, 125 (1991)
[2] E. Gonzalez, Proc. 5th Information Exchange Meeting, Mol, Belgium (1998)
[3] B.Ya. Galkin et al., Radiochemistry **44**, 174 (2002)
[4] C. Ingelbrecht et al., Nucl.Instrum.Meth., **A480**, 204 (2002)
[5] M.C. Moxon and J.B. Brisland, GEEL REFIT, CBNM/ST/90-131/1 (1990)
[6] N.M. Larson, Sammy-M6, ORNL/TM-9179/R6 (2003)
[7] A. Brusegan et al., Proc.Int.Conf. Nuclear Data for Science and Technology, 7-12 October 2002, Tsukuba, J.Nucl.Sci.Tech. **S2**, 685 (2002).
[8] F.H. Froehner, Rept. Gulf General Atomic GA-8380 (1968)
[9] G. Noguere et al., JEFDOC-986, NEA, Issy-les-Mouineaux, France (2005).

^{236}U capture measurements

Capture cross section measurements for ^{236}U have been performed at the neutron time-of-flight spectrometer GELINA of the Institute for Reference Materials and Measurements (IRMM) at Geel in Belgium. A capture sample with about 300 mg ^{236}U has been prepared by IPPE-Obninsk through JINR-Dubna. The radioactive uranium oxide has been pressed into a pallet and packed in a thin high purity aluminum container sealed by means of epoxy glue. In this form the sample is sealed in a practical way avoiding contamination and the surrounding material is limited to a minimum of well known material. For neutron capture measurements on radioactive powder samples this is the best suited form for an experiment. However, this sealing is not ISO-compliant which has been a reason for the CERN safety authorities to refuse the measurement at the last moment in 2003. We have therefore transported the sample to GELINA neutron time-of-flight facility where the sample was allowed for a measurement in 2004

The measurements were performed at a 30 m flight-path, at 0° with respect to the normal of the water moderator. Fast neutrons were eliminated by means of a shadow bar. The accelerator was operated at 800 Hz and 70 μA average electron current, providing electron pulses of 1 ns with 100 MeV average electron energy. The moderated neutron beam was collimated to about 20 mm in diameter at the sample position. A 0.013 at/b thick ^{10}B anti-overlap filter was installed to eliminate the influence of slow neutrons from a previous accelerator cycle. We performed two different measurement campaigns. One with a fixed S filter and one with a fixed Na filter to monitor continuously the background at 2.85 keV and 102.71 keV, respectively. Both campaigns lasted about 3 weeks.

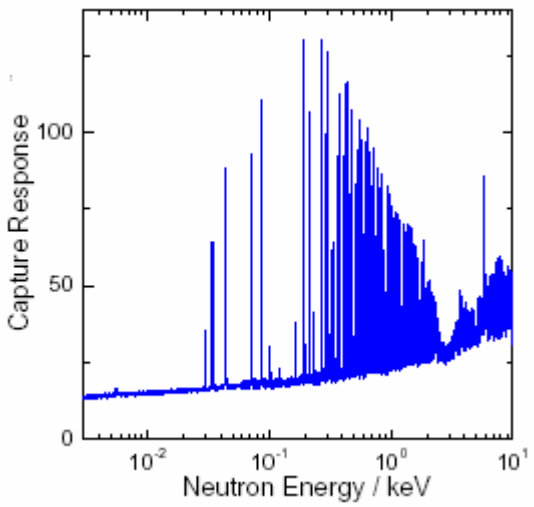

Figure 79: The response of the C_6D_6 detection system as a function of neutron energy.

The gamma rays, originating from the neutron capture reaction, were detected by a pair of C_6D_6-based liquid scintillators (NE230) of 10 cm diameter and 7.5 cm length, which were oriented perpendicularly to the neutron beam direction. Each scintillator was coupled to an EMI9823KQB photomultiplier through a quartz window, reducing the neutron sensitivity of the detectors as much as possible. Such a detection system is suitable to apply the total energy detection principle in combination with the pulse-height weighting technique. In Figure 79 we show the response of the capture detection system, expressed as counts per time interval, for the measurements with the fixed Na background filter.
Two BF_3 proportional counters were used to monitor the stability of the accelerator and to normalize the spectra to the same total neutron intensity. The shape of the neutron spectrum was measured with a double Frisch-gridded ionization chamber placed 50 cm before the sample. This chamber has a cathode loaded with two back-to-back layers of about 40 μg/cm^2 ^{10}B each. The background for the flux measurements was derived from the saturated resonance dips of Ag, W, Co, Na, and S filters.
All experimental data have been sent to CEA Saclay. In addition, we provided all experimental details which are required to determine an accurate capture yield and to perform a resonance shape analysis in the resolved resonance region.
Preliminary accounts of these measurements were presented at the ND2004 conference and the NEMEA-2 workshop [1,2]

[1] A.J.M. Plompen, Proc.Int.Conf. on Nuclear Data for Science and Technology, 26 Sep. – 1 Oct., Santa Fe, NM, USA (2004).
[2] A.J.M. Plompen, Proc. Int. Workshop on Neutron Measurements, Evaluations and Applications -2, 5-8 November, Bucharest (2004).

Transmission measurements for ^{99}Tc and ^{237}Np

All experiments were carried out at the pulsed white neutron source GELINA of the Institute for Reference Materials and Measurements at Geel, Belgium and the measurements and data analysis were carried out by CEA Saclay in a collaboration with IRMM [1]. The linear accelerator was used to provide electron bursts of 100 MeV average energy with a pulse width of 1 ns, a repetition rate of 800 Hz and an average beam current of 60 μA. In the case of investigating low energy cross sections in the eV region, a 100 or 200 Hz repetition rate was used with a pulse width of 15 ns. The fast neutron spectrum produced in the rotary uranium target was moderated into a white spectrum by means of two water moderators of 36 mm thick, canned in beryllium and placed beneath and above the uranium target. The partially thermalized neutrons scattered from the moderators were collimated into the flight paths through evacuated aluminum pipes of 50 cm diameter with several collimators consisting of borated wax, copper, and lead. A shadow bar made of copper and lead was placed in front of the uranium target, preventing fast neutrons and gamma rays produced in the rotary target from reaching the sample-detectors area. Several flight paths are normally in use at the same time for different experiments, in this way optimizing the time of data taking which is typically in the order of 700 hours for a complete capture or transmission experiment.
For the transmission measurements we used an NE912 lithium glass of 1/4 inch thick with a diameter of 6 inches placed in an aluminum sphere with an inside coating of a seven layer $BaSO_4$ light reflector. The sphere is connected to a 5 inch EMI9823KQB photomultiplier, installed orthogonally and out of the neutron beam. The raw time-of-flight counting spectra were corrected for dead time and backgrounds and converted to a capture yield or transmission factor which is the required input for the analysis programs.

Measurement of the total cross section of ^{99}Tc

For ^{99}Tc both transmission and capture experiments were performed with three different sample thicknesses for each experiment resulting in 6 data sets covering the energy range from 3 eV to 150 keV. From the transmission measurements, performed at a flight distance of 49.3 m, a number of 659 resonances have been resolved up to 10 keV. Experimental data for capture and transmission between 2 and 3 keV are shown in Figure 80 on the left. For this nucleus, the radiation width is rather constant in this energy range since a large number of partial radiation widths contribute to the total radiation width, but the neutron widths show large variations due to the Porter-Thomas fluctuations. Between 10 and 150 keV the cross section was parametrized in terms of average level parameters. Details of these transmission measurements can be found in Refs. [2,3]. The capture experiments were done at a distance of 28.4 m. Due to the shorter distance and consequently the lower resolution, the analysis of the resolved resonances is feasible up to 5 keV. The unresolved energy range for the capture measurements has been analyzed [4].

Measurement of the total cross section of ^{237}Np

Two types of transmission measurements were performed: the first was the standard one, done at a flight distance of 49.3 m on samples kept at room temperature, from which the parameters of 571 resonances up to 500 eV energy were derived [5,6]. A second series of measurements was then carried out at a flight distance of 26.5 m and with samples kept at three different temperatures of T =15, 50 and 290 K: the objective here was to study the influence of solid state effects on the Doppler broadening of neutron resonances in the frame of a scientific programme which has been carried out at GELINA also for other nuclides. Results of the transmission measurements are shown in Figure 80 on the right together with the capture data.
The measurements have been analyzed using the R-matrix code REFIT, which includes a detailed description of the resolution function and the recently developed Doppler broadening model DOPUSH. Comparison with previous work shows that, apart from some local discrepancies, the parameters are on average in rather good agreement. The average radiation width and the s-wave strength function are consistent within the quoted uncertainties with previous work. For the average level spacing there is more variation but our present value is in the range of existing values in the literature. From our results one can conclude that the resonance part of ^{237}Np is presently known with an accuracy of 3 to 4%.

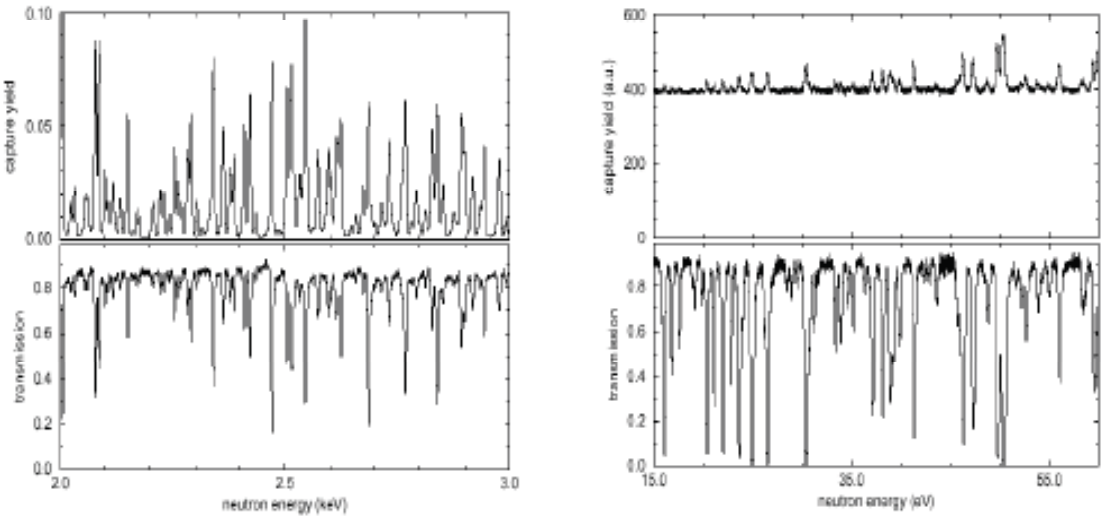

Figure 80: Spectra of capture and total cross section measurements of ^{99}Tc (left) and ^{237}Np (right).

[1] F. Corvi, F. Gunsing, C. Bastian, A. Brusegan, N. Herault, J. Gonzalez, V. Gressier, A. Leprêtre, E. Macavero, C. Mounier, G. Noguère, C. Raepsaet, and P. Siegler. Neutron data measurements for waste transmutation at Gelina. J. Nucl. Sci. Techn., Sup. 2, (2002) 1067.
[2] Caroline Raepsaet "Nouvelle détermination expérimentale des paramètres de résonances neutroniques de ^{99}Tc", PhD thesis, Universtity of Marseille, (1997).
[3] F. Gunsing, A. Leprêtre, C. Mounier, C. Raepsaet, A. Brusegan, and E. Macavero. Neutron resonance spectroscopy of ^{99}Tc from 3 eV to 150 keV. Physical Review C, 61 (2000) 054608.
[4] F. Gunsing, A. Leprêtre, C. Mounier, C. Raepsaet, C. Bastian, F. Corvi,and J. Gonzalez. Stellar neutron capture cross section of ^{99}Tc. NuclearPhysics, A688 (2001) 496c.
[5] Vincent Gressier "Nouvelle détermination expérimentale des paramètres de résonances neutroniques de ^{237}Np en dessous de 500 eV", PhD thesis, Universtity Paris XI, (1999).
[6] A. Leprêtre, A. Brusegan, N. Herault, G. Noguère, P. Siegler, "Determination des paramètres des résonances neutroniques du neptunium 237, en dessus de 500 eV, et obtention des matrices de covariances statistiques et systématiques entre les paramètres de ces résonances", Internal Report DAPNIA-02-374, CEA/Saclay 2002.

(n,xn) Cross Sections measurement by prompt gamma-ray spectroscopy

Contributed by *G Rudolf* (Institut de Recherches Subatomiques, Strasbourg, France)
gerard.rudolf@ires.in2p3.fr

The importance of (n,xn) reactions

Reactions with a threshold become important in reactors with a fast spectrum, and especially in ADS. On the other hand, their cross sections are often badly known. For reactions on actinides, the data bases rely mostly on models.

The best example is ^{233}U(n,2n). This is the reaction which competes with the fission of ^{233}U in the fast Thorium cycle. It produces ^{232}U, the decay chain of which ends at ^{208}Pb and produces a 2.6 MeV γ emission. Its cross section determines therefore in part the needed shielding in a facility running on this cycle, but also the possibility of proliferation. It turns out that three main data bases disagree (Figure 81) strongly on this cross section. This is due to the fact that not a single measurement has been performed up to now.

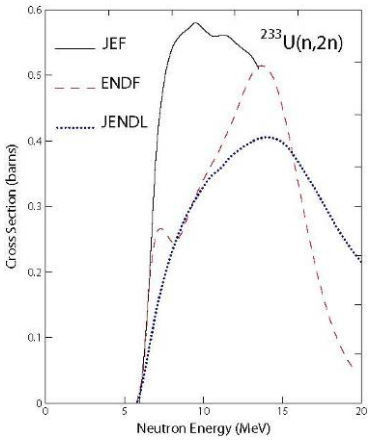

Figure 81: The ^{232}U(n,2n) cross section in three data bases.

The methods to measure (n,xn) cross sections

Two methods have been used generally to measure (n,xn) cross sections: activation and direct detection of the neutrons. They require a mono-energetic beam. Its instantaneous intensity must be large enough so that the counting rate due to the reaction competes with that of the sample, when it is active. The energy range must cover at least the 6 to 20 MeV region. No facility exists meeting these three characteristics. n_TOF meets the two last ones, but it is not mono-energetic.

Therefore we have chosen a method which has been used since less than a decade with the white beam of WNR (Los Alamos): the prompt γ spectroscopy. However the conventional technique which was employed is not applicable if the beam has a frequency as low as n_TOF. Thus the first step has been to develop a new acquisition system to adapt the method to the CERN beam.

In-beam γ spectroscopy has another important advantage: it allows to measure (n,n') reactions. These are actually (n,xn) reactions with x=1. Their cross section can also be measured by direct detection of the neutrons, but even in apparently simple cases the accuracy of this method is not very good. A spectacular example is the (n,n') reaction on ^{208}Pb (Figure 82). It has been estimated that the errors on the inelastic cross sections on the three isotopes of lead –which is an essential material in ADS- imply an uncertainty of 2% on the criticality of such a reactor!

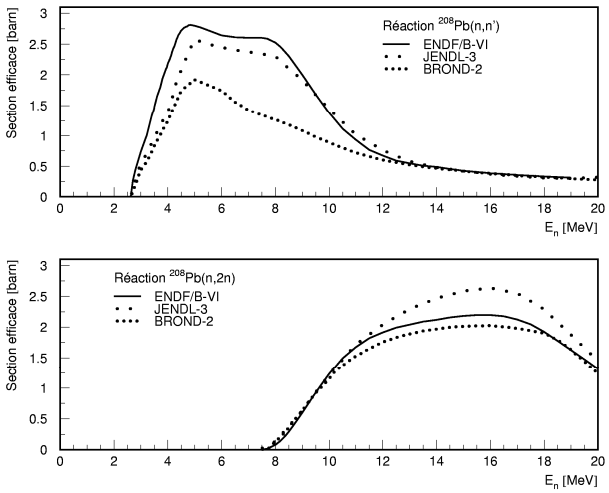

Figure 82: The ^{208}Pb(n,n') and ^{208}Pb(n,2n) cross sections in three data bases.

The acquisition system developed at IReS

High purity Germanium (HPGe) detectors are used to obtain the high energy resolution needed to select the lines corresponding to given transitions in the final nucleus. Such detectors are slow: the rise time of the signal produced by the crystal varies between 100 and 300 ns according to the thickness. State-of-the-art electronics need a shaping of this signal to obtain the good energy resolution. This introduces a dead time of a few tens of μs during which a second γ ray would pile-up with the preceding one. It determines two limitations

- the instantaneous counting rate, which is generally limited to a few kHz
- the highest possible energy of the neutron beam if there is a strong γ flash. Indeed, with a white beam, this energy is measured by the time-of-flight method. At a flight path of 200m as at n_TOF, a γ ray coming from the γ flash arrives 2.5 μs only before a 20 MeV neutron. This is much less than the dead time introduced by conventional electronics.

We have found the solution in digital electronics. However, the digitizers bought by the n_TOF collaboration are not suited for HPGe detectors. Indeed their 8 bits are not sufficient to obtain the needed energy resolution, but their sampling rate of 1GS/s is beyond necessity.

Instead, we have first bought commercial 12 bits, 60 MS/s digitizers from the Signatec Company. These allowed us to perform various tests and to develop the algorithms to extract the physical quantities from the oscillograms. However, they cannot be used at Gelina, where it was finally necessary to perform our first measurement. Indeed the frequency of the beam is 800 Hz. This makes it impossible to store oscillograms during months, as was done at CERN. Instead, one has to perform the extraction on-line. Therefore, we have developed our own digitizers.

The first digitizers developed at IReS had 14 bits, 65 MS/s (Figure 83). The present day generation reaches 100 MS/s. Implemented in their Field Programmable Gate Array (FPGA) are the algorithms which perform the data processing equivalent to a Fast Timing Amplifier and a Constant Fraction Discriminator for the time measurement, and the algorithm to obtain the energy resolution.

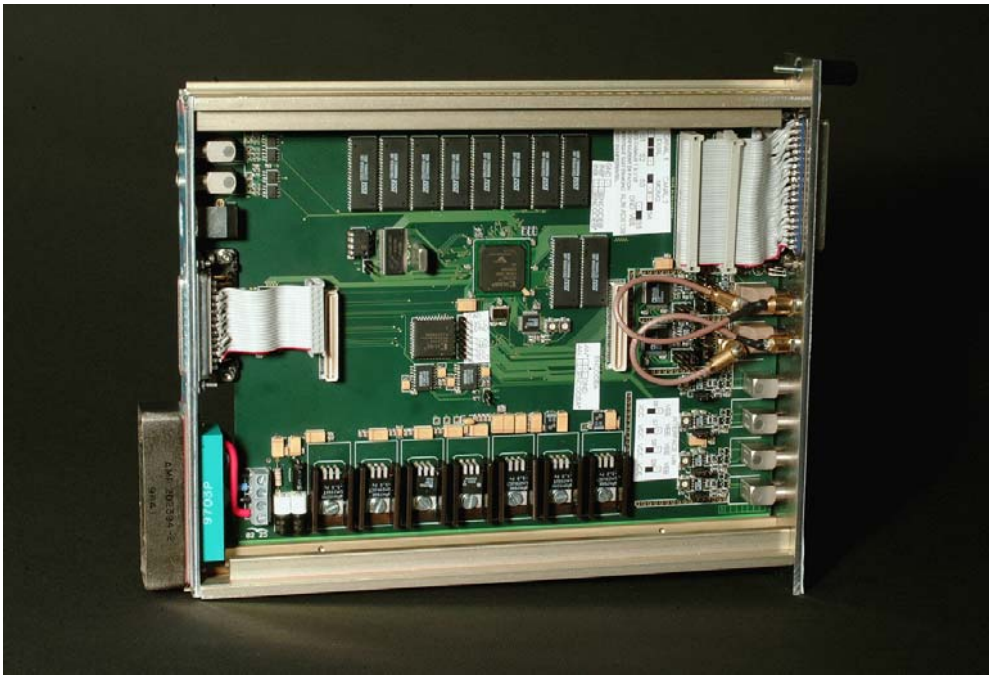

Figure 83: The acquisition card developed at IReS. It is composed of two 14 bits 65 MS/s digitizers, and a FPGA in which the data processing is performed on-line.

Measurement at Gelina

From May to July 2004, this method has been used to measure the cross sections of the ^{207}Pb(n,2n) reaction. The set up consisted in two HPGe detectors from IRMM Geel, placed at 110 and 150° so as to be able to correct angular distribution effects through Gaussian quadrature. The sample was a 90 g disk of lead enriched to 92% in ^{207}Pb, on lease from ORNL. The flight path was 200 m. The flux was monitored by a ^{235}U fission chamber.

As seen in Figure 84, at least three lines due to transitions in ^{207}Pb appear clearly at low bombarding energies. Well above the threshold of the (n,2n) reaction, six lines due to transitions in ^{206}Pb can be seen. The energy resolution is 4 keV for the 803.1 keV line measured by a 100% coaxial detector. The intensity of the γ flash is demonstrated by Figure 84. The time resolution is limited to 25 ns by the 65 MS/s sampling rate of the prototype digitizers. This will be improved in the new generation, but is by far sufficient to reach the desired 1 MeV resolution at E_n=20 MeV.

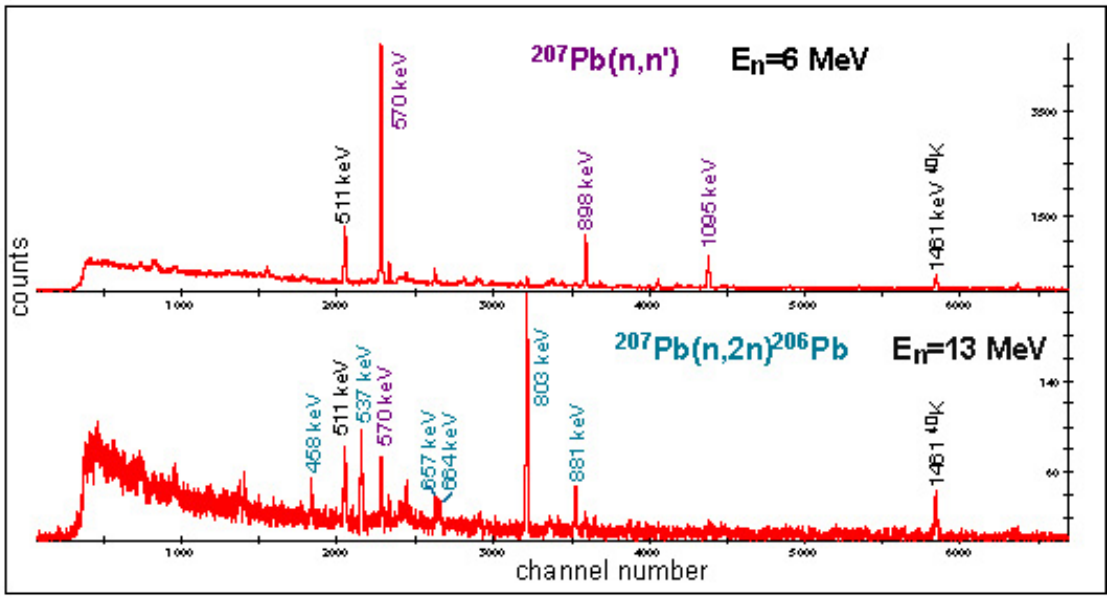

Figure 84: Prompt γ spectrum obtained with a 100% coaxial HPGe detector and a digital acquisition system developed at IReS. If a flight time corresponding to E_n=6 MeV is selected, transitions in ^{207}Pb fed by the inelastic scattering of neutrons are strongly populated (top). If E_n=13 MeV is selected, one sees essentially transitions in ^{206}Pb fed by the ^{207}Pb(n,2n) reaction (bottom).

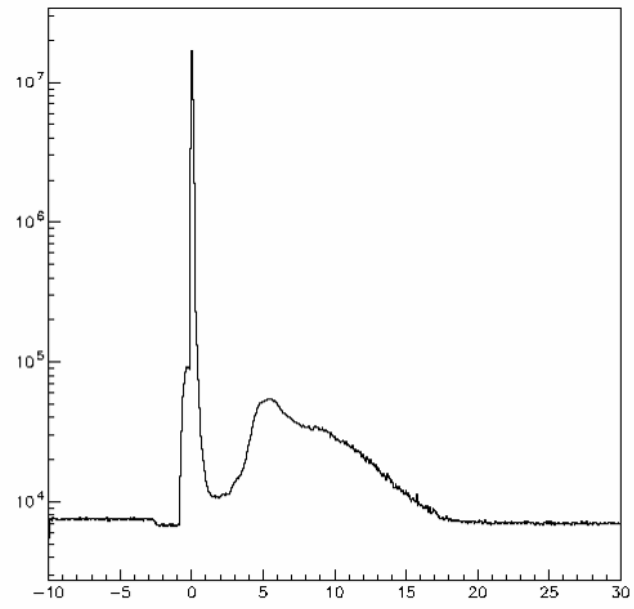

Figure 85: Time spectrum at the flight path of 200 m at Gelina. The delay between the intense flash and the fast neutrons is 2.5 μs. The time resolution is 25 ns for a 70% coaxial detector.

The fact that several lines corresponding to the same reaction are observed is quite important. Indeed, a model has to be used to transform the (n,xnγ) cross section into a (n,xn) one. In actinides, the correction is of the order of 10% when the lowest transitions are observed. In the case of Pb isotopes, it is of the order of 50% because the first excited states have energies

of several hundreds of MeV. In any case, models are severely tested by the relative intensity of several lines, which makes the correction safer.

Figure 86 shows the excitation function for the 803 keV transition in ^{206}Pb, and Figure 87 that of the 570 keV transition in 207Pb. Please note that the absolute normalization in these preliminary results is arbitrary. In the model calculations, one has to take the influence of isomeric states into account.

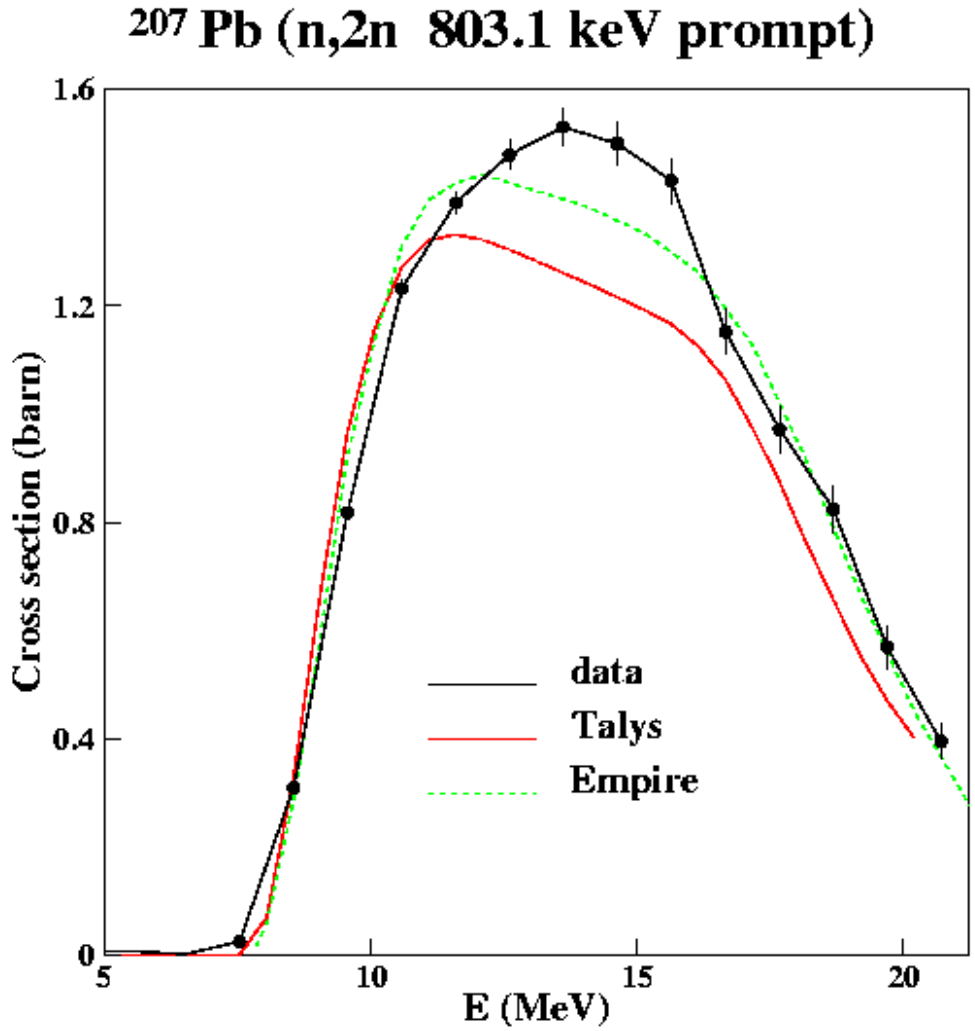

Figure 86: Cross section to the 803 keV state in ^{206}Pb. The results are very preliminary, the absolute normalization is arbitrary. The predictions of the Talys and Empire codes are quite close. Here the two curves differ because the trapping in the isomeric state at 1633 keV is entirely subtracted in the case of Talys, while it is not for the transitions for which the branching ratio is unknown in the case of Empire.

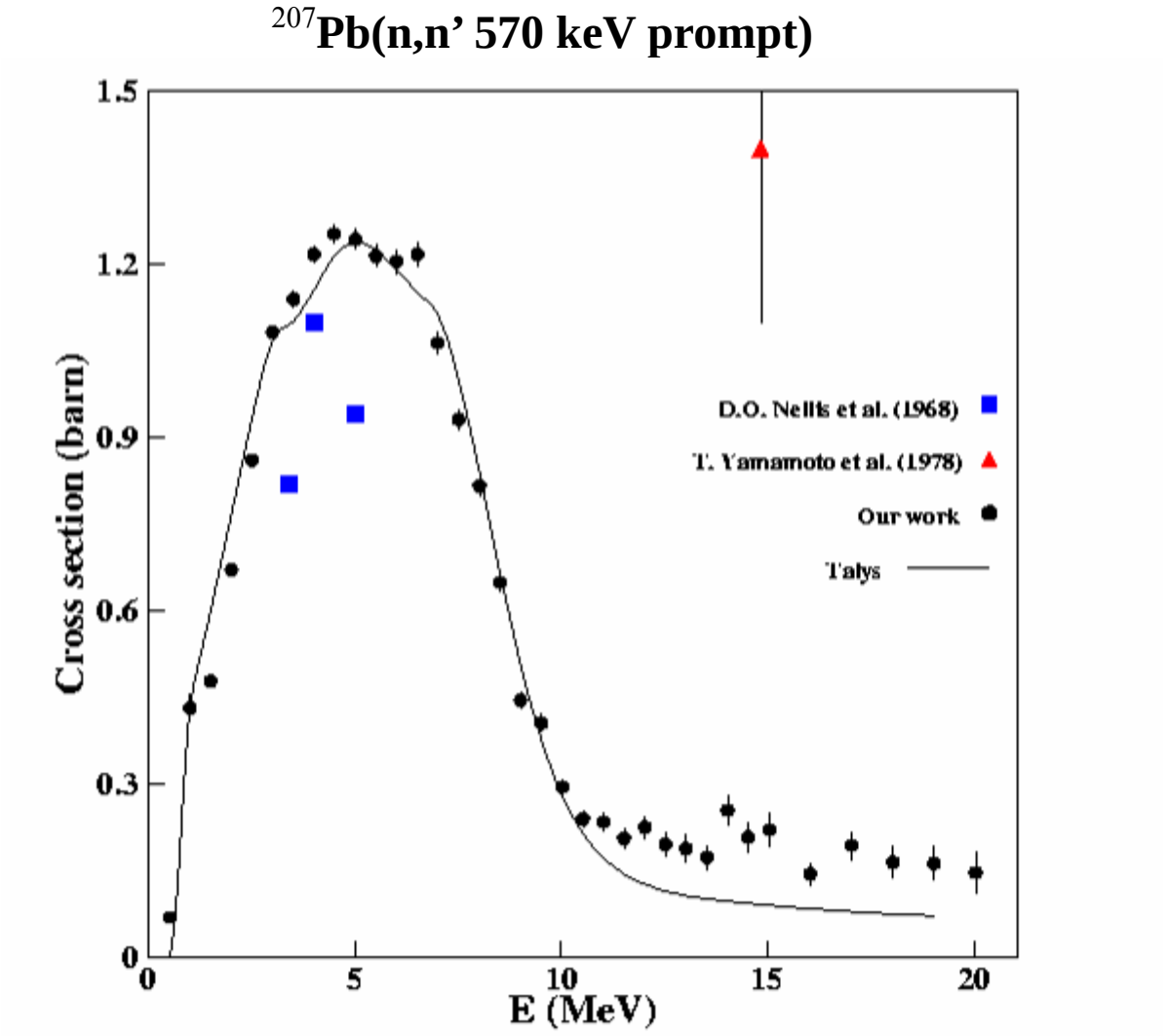

Figure 87: Cross section to the 570 keV state in ^{207}Pb. The normalisation is arbitrary. Only statistical errors are taken into account in our data. Data from the literature are very scarce and imprecise.

The other lines will be analysed too. At Gelina, the method is now working routinely. During 2005, we plan to measure ^{206}Pb(n,n'), for which data exist only up to a few MeV and differ strongly, as well as ^{208}Pb(n,n'), ^{208}Pb(n,2n) and ^{208}Pb(n,3n).

Tests at n_TOF

No measurement has been possible at n_TOF. The detectors are blinded at time 0 by a strong electromagnetic radiation which saturates the signal (Figure 88).

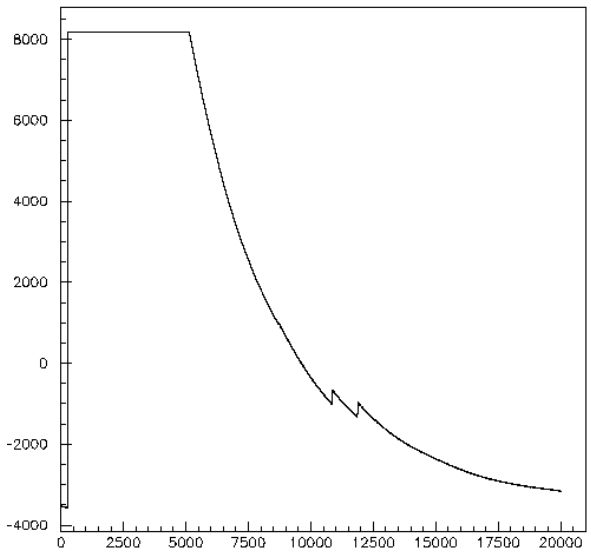

Figure 88: Example of an oscillogram of the signal at the output of the preamplifier at n_TOF. Here the saturation corresponds to an energy of 3.5 MeV. It lasts 75 μs. One sees also two γ-rays of about 100 keV which have been detected at a larger time.

The situation has actually evolved during the four years of the contract. The first year the saturation was observed even when the detector was surrounded completely by several cm of lead, and at any place in the experimental room. Since the detector was a thin (1.5 cm) planar essentially sensitive to small γ rays, this demonstrates that the radiation originates from very penetrating particles and is not an electromagnetic radiation coming from the neutron source. Extrapolating the decay of the signal to time t=0 (Figure 88) showed that the energy deposit in the HPGe could amount up to 150 MeV. Thus the detector was blocked for times up to ms. We modified the preamplifier of the detector so as to inject in it a current opposite to the one produced by the flash, which allowed to reduce the blocking time to about 20 μs, still longer than the 2.5 μs corresponding to neutrons of 20 MeV.

The successive transformations of the shielding made by CERN were efficient, confirming probably the presence of muons. The last test in October 2004 showed that in most cases less than 40 MeV are deposited in the detector, even at some 20 cm from the beam (Figure 89).

The challenge is to measure γ energies of 100 to 200 keV with a resolution of the order of 1 keV, 2.5 μs at most after the flash. This has been realised at GELINA, where the γ rays from the flash have an energy rarely exceeding 2 MeV, but not yet at n_TOF.

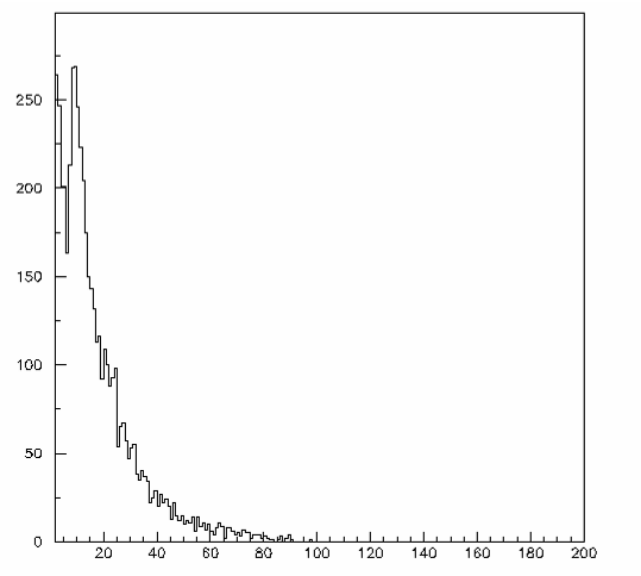

Figure 89: Energy spectrum of the flash at n_TOF, obtained by extrapolating the exponential decay of the signal (see Figure 94) to time 0, as measured in 2004.

Other measurements

We have measured the ^{232}Th(n,5n) reaction in Louvain-la-Neuve. The set up consisted in two planar detectors placed at 110 and 150°. The sample was placed at 3.3 m from the neutron source. It was a disk of 12 g of ^{nat}Th. Six different values of the energy of the primary proton beam were chosen so as to cover the 30 to 50 MeV range where the (n,5n) cross section was supposed to reach its maximum.

Because the frequency of the beam is too high, it is not possible to decrease the background by a time selection as at Gelina. Indeed, two successive bursts are separated by 50 ns only, while the time resolution of our HPGe detector is of the order of 10 ns. Thus a very large statistics has to be measured. Moreover, one has to alternate measurements with and without beam in order to subtract the background due to the natural activity of Th and to the build up of fission fragments.

Since the flight path is too short, the time of flight technique cannot be used. Therefore, the beam should be mono-energetic. It has actually a mono-energetic component, but also a continuous one which cannot be separated with the help of the time information. Therefore, we have measured in great detail not only the flux, but also its time structure at each bombarding energy. This has been achieved with the set of dedicated detectors from PTB Braunschweig.

Despite all these difficulties, the first results are encouraging.

Conclusions

We have adapted a method allowing to measure (n,xn) cross sections on targets which are out of the scope of the other existing methods, and is applicable at facilities where the beam is pulsed.

It necessitated the development by IReS of a new acquisition system which is able to register oscillograms of the signals as the one used at CERN, but is also able to treat them on line so as to reduce drastically the amount of stored data.

The different steps of its application have been tested, and two measurements have been performed. At Gelina, the flight distance is similar to that of n_TOF and the γ flash is fairly strong. There we have measured the ^{207}Pb(n,2n) and the ^{207}Pb(n,n') reactions up to 20 MeV.

In Louvain-la-Neuve, the high frequency of the beam is not favorable to the measurement of active targets. Nevertheless, we were able to measure the (n,5n) reaction on ^{232}Th, a target which is active and fissions. This result is highly interesting to test models, since Thorium has a level scheme representative of all actinides. It is also the fertile element of the Th/U cycle.

Thus all elements of measurement of (n,n') and (n,2n) reactions on actinides at a facility like n_TOF are checked. Nevertheless, we have not been able to perform a measurement there because of the existence of a very strong radiation arriving at the precise time when (n,xn) reactions are produced. As shown by the progress realized by enhancing the shielding in the tunnel, solutions certainly exist to decrease it to acceptable levels.

Capture cross section measurements at FZK (^{135}Cs, ^{151}Sm)

Prepared by: F Käppeler (FZK, Karlsruhe)

Neutron capture studies on unstable ^{135}Cs for nucleosynthesis and transmutation*

N. Patronis[1], S. Dababneh[2,3], P. A. Assimakopoulos[1], R. Gallino[4], M. Heil[2], F. Käppeler[2], D. Karamanis[1], P.E. Koehler[5], A. Mengoni[6], R. Plag[2], and the n_TOF collaboration
[1] Nuclear Physics Laboratory, Department of Physics, The University of Ioannina, 45110 Ioannina, Greece
[2] Forschungszentrum Karlsruhe, Institut für Kernphysik, 76021 Karlsruhe, Germany
[3] Faculty of Applied Sciences, Al-Balqa Applied University, Salt 19117, Jordan
[4] Instituto di Fisica Generale, Universita di Torino and Sezione INFN di Torino, I-10125 Torino, Italy
[5] Physics Division, Oak Ridge National Laboratory, Oak Ridge, Tennessee 37831, USA
[6] CERN, 1211 Geneva 23, Switzerland

The neutron capture cross section of the unstable isotope ^{135}Cs was measured relative to that of gold by means of the activation method. The sample was produced by ion implantation in a high resolution mass separator and irradiated with quasi-monoenergetic neutrons at 30 keV and 500 keV, using the ^{7}Li(p,n)^{7}Be reaction. An additional irradiation with thermal neutrons has been carried out for defining the sample mass and for an improved measurement of the half-life of ^{136}Cs. The neutron capture cross sections were determined as 164 ± 10 mbarn and 34.8 ± 3.0 mbarn at 30 keV and 500 keV, respectively. As shown in Figure 90 these values represent the first experimental data for this cross section and were used to normalize the theoretically derived cross section shape. Based on the present results, refined statistical model calculations were performed to obtain the (n,γ) cross sections of the short-lived isotopes ^{134}Cs and ^{136}Cs as well. Updated Maxwellian averaged capture cross sections of all unstable Cs isotopes were calculated for a range of thermal energies characteristic of helium burning scenarios for an improved *s*-process analysis of the Xe-Cs-Ba region. During this experiment, the half-life of ^{136}Cs was measured to be 13.04 ± 0.03 d, in fair agreement with a recent compilation [3], but in contradiction with the latest experimental value [3].

* Published in Phys. Rev. C **69** (2004) 025803

[1] http://www.nndc.bnl.gov/nndc/endf/endfintro.html
[2] A.A. Sonzogni, Nuclear Data Sheets **95** (2002) 837
[3] T. Katoh, S. Nakamura, H. Harada, Y. Hatsukawa, N. Shinohara, K. Hata, K. Kobayashi, S. Motoishi, and M. Tanase, Nucl. Sci.Tech. **34** (1997) 431

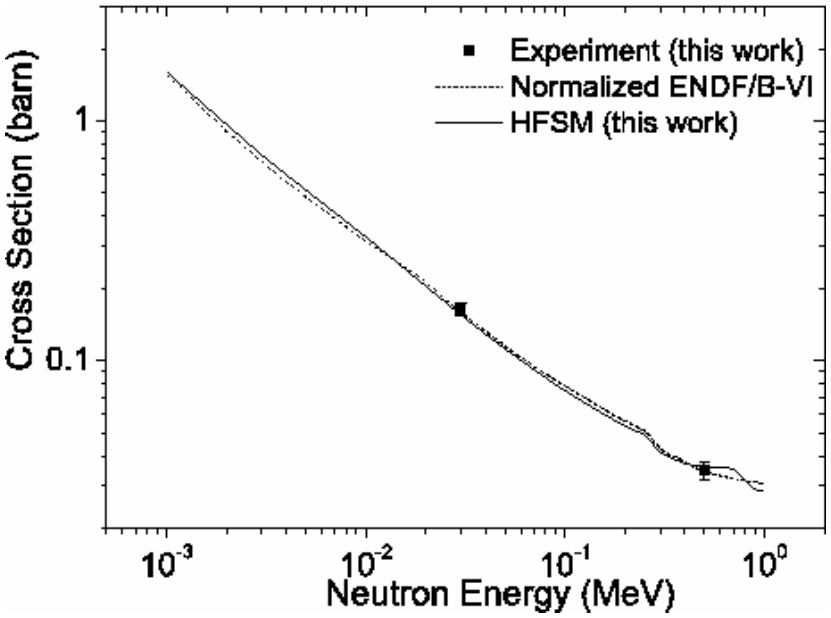

Figure 90: The experimental and the evaluated results for the $^{135}Cs(n,\gamma)^{136}Cs$ cross section. The evaluated data [1] have been normalized to the experimental points.

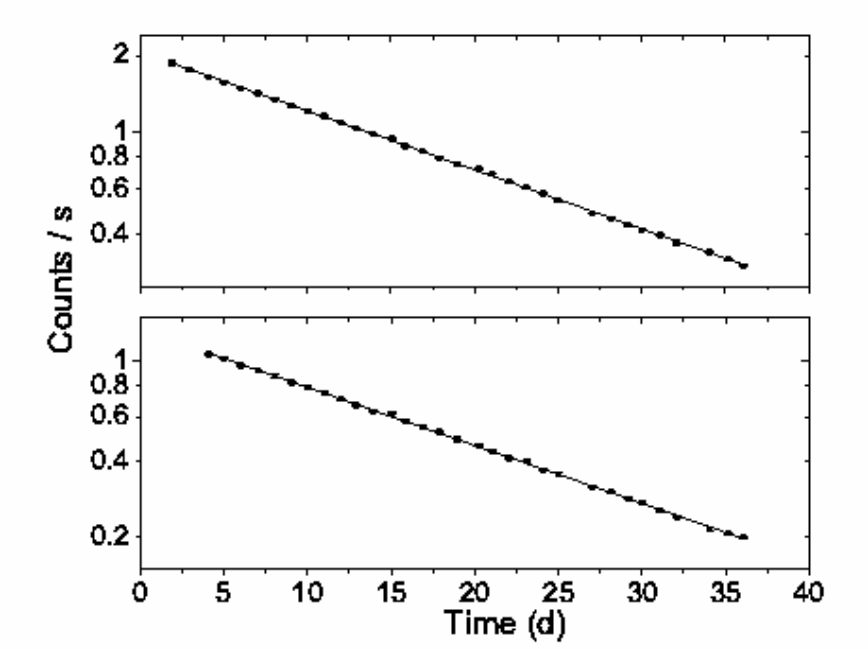

Figure 91: The decay curve of ^{136}Cs obtained from the counting rates of the transitions at 819 keV and 1048 keV (upper and lower panel, respectively).

Stellar neutron capture cross section of the unstable *s*-process branching point ^{151}Sm*

K. Wisshak[1], F. Voss[1], F. Käppeler[1], M. Krticka[2], S. Raman[3], A. Mengoni[4], and R. Gallino[5],
[1] Forschungszentrum Karlsruhe, Institut für Kernphysik, Postfach 3640, D-76021 Karlsruhe, Germany
[2] Faculty of Mathematics and Physics, Charles University, CZ-180 00 Prague, Czech Republic
[3] Oak Ridge National Laboratory, Oak Ridge, TN, 37831-6354, USA (deceased)
[4] CERN, CH-1211 Geneva 23, Switzerland
[5] Dipartimento di Fisica Generale, Universita di Torino and Sezione INFN di Torino, Via P. Giuria 1, I-10125 Torino, Italy

The neutron capture cross sections of the radioactive isotope ^{151}Sm and of natural samarium have been measured in the energy range from 3 keV to 225 keV at the Karlsruhe 3.7 MV Van de Graaff accelerator via the time-of-flight technique. Neutrons were produced via the ^{7}Li(p,n)^{7}Be reaction by bombarding metallic Li targets with a pulsed proton beam (pulse width 0.7 ns, repetition rate 250 kHz, average current 2 μA). Capture events were registered with the Karlsruhe 4π Barium Fluoride Detector that allowed to achieve a detection efficiency of 95%. The cross sections were determined relative to the gold standard using a 206 mg sample of samarium oxide with 90% enrichment in ^{151}Sm. Over most of the measured energy range uncertainties of 2% to 3% could be obtained. As shown in Figure 92, these results are in perfect agreement with the parallel measurement by the n_TOF collaboration, but are two times more accurate. Maxwellian averaged neutron capture cross sections of ^{151}Sm were calculated for thermal energies between kT = 8 keV and 100 keV and were found to be systematically larger than all previous theoretical calculations. With these results the analysis of the *s*-process branching at ^{151}Sm with respect to the temperature at the stellar site could be significantly improved. In addition the ^{152}Gd abundance could be decomposed into the respective *s*- and *p*-process contributions.

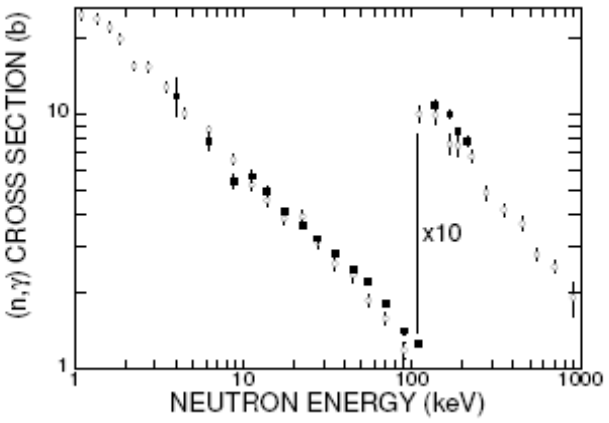

Figure 92: Comparison of the cross sections obtained in this work and in a parallel experiment by the n_TOF collaboration.

* Published as Report FZKA-6996, Forschungszentrum Karlsruhe (2004); to be submitted to Phys. Rev. C (February 2005).

Development of a module for a γ-ray detector based on Liquid-Xe

Contributed by *R Herreira-Marques* (LIP, Lisbon)

The recent development of the liquid noble gas detectors such as Ar, and Xe shows the high performance of this type of photon detector concerning the efficiency related to the high resolution. Moreover, the discrimination between gamma and neutron interactions represents an important feature of these detectors in TOF applications. Therefore we have performed the design and construction of a liquid Ar/Xe calorimeter prototype module, in order to determine the photon and neutron response and establish the rejection factor of neutrons and photons with such a set-up for capture cross section measurements. This module will be in-beam tested and will serve for cross section measurements of known elements and isotopes with known cascade multiplicity.

Introduction

Liquid xenon is known to be an excellent medium for efficient detection of γ-rays. It has high atomic number (Z=54) and relatively high density (about 3 g/cm^3). It scintillates at the wavelength of 178 nm and has three decay time constants 3 ns, 27 ns and 45 ns. The scintillation light yield is similar to that of NaI(Tl). Compared to LXe, liquid argon has the advantage of having very small cross section for neutron capture. Liquid argon is also a good scintillator but emitting the light at shorter wavelength (127 nm) and with longer decay time (fast component is 5 ns while the slow component is about 0.9 μs). Its light output is somewhat lower. However, these drawbacks of LAr can be surmounted by adding a small percentage of xenon due to the fact that in the mixture LAr + few % Xe the initial excitation of argon is transferred to xenon atoms with high efficiency. The atomic number of argon is Z=18 and the density is about 1.43 g/cm^3. Consequently, in order to provide similar detection efficiency, a LAr γ-ray detector must have a significantly larger volume than a LXe one.

Preliminary Monte Carlo simulation of detection efficiency

A Monte Carlo simulation has been carried out to determine optimum detector dimensions with respect to detection efficiency for γ-ray cascades due to neutron capture reaction in a ^{197}Au target. The cascades were pre-generated using a statistical model for 100 keV neutrons. The outputs of the program are: i) absorbed energy spectrum, ii) detection efficiency for a cascade, understood as the probability of detection of at least one γ-photon from a cascade, ε_c (ε_c=1-P_m, where P_m is the probability to miss a cascade), and iv) the probability of detection of all γ-rays emitted in a cascade, P_w (in this case, whole cascade energy is deposited in the detector).

The detector was assumed to have the shape of a double-wall cylinder with dimensions D_1×D_2×L oriented along the neutron beam, with the target at its centre as shown in Figure 93.

Various detector dimensions were simulated, with the internal cylinder diameter, D_1, fixed at 30 cm (determined by the beam line size). The external cylinder diameter, D_2, varied between 60 cm and 90 cm for liquid xenon (60 cm and 230 cm for liquid argon). For the detector length, L, values of 100 cm, 150 cm and 200 cm were used. Some examples of spectra simulated for a 150 cm long detector are shown in Figure 94. The energy resolution at 1 MeV was assumed to be 15% for argon and 10% for liquid xenon varying with γ-ray energy as $1/E^{1/2}$.

It is observed that rather high detection efficiency for a cascade (ε_c=98%, P_m=2%) can be obtained even with 15 cm of liquid argon (with D_2=60 cm), although only 3.6% (P_w) of the cascades deposit the whole energy in the detector. If the same detector volume is filled with liquid xenon, both numbers (missed cascades and events with full energy deposit) improve by an order of magnitude, up to P_m=0.23% and P_w=48.7%. This leads to quite significant differences in the spectra obtained with LXe and LAr of similar thickness (compare Figure 94-a and Figure 94-b). On the other hand, Figure 94-a and Figure 94-c require the detector

thickness to be increased to 50 cm (i.e., to D_2=130 cm) in order to obtain similar parameters with argon. From Figure 94-d, -e and -f one concludes that 20 cm of liquid xenon are equivalent to 70 cm of liquid argon.

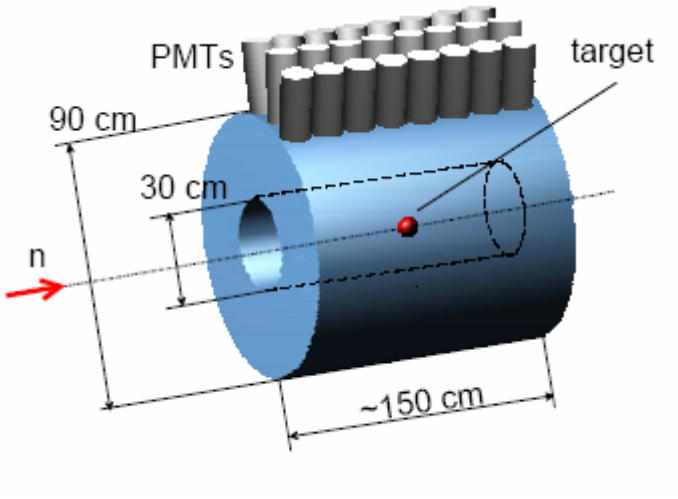

Figure 93: Simulated geometry of the liquid γ-ray calorimeter

Pondering all the above reasons, we conducted our main effort to the investigation of the liquid xenon option.

Design and construction of the liquid xenon prototype module

A liquid xenon prototype module has been designed and produced at the LIP-Coimbra workshop with that purpose. Its layout is shown in Figure 95 together pictures of assembling stages. The liquid xenon chamber is a stainless steel cylindrical vessel (∅200 mm, 278 mm high) with thickness of 0.4 mm for the lateral wall and 6 mm for the bottom. For thermal insulation, this vessel is housed inside another cylinder kept under vacuum. The outer cylinder is made of aluminum, 0.8 mm thick, reinforced with ~3 mm of carbon fiber epoxy glued on the outer surfaces.

The active volume of liquid xenon (about 1.2 liter) is defined by PTFE reflectors arranged to form a cylinder, ∅163 mm and 55 mm high. The bottom of this cylinder is a 4 mm thick PTFE sheet, whereas the lateral surface and the top disk (with 7 openings for the PMTs) have a thickness of 1 mm. The active volume is viewed by an array of 7 photomultipliers (Hamamatsu R2154) in direct contact with the liquid xenon, whose entrance windows are immersed in order to maximize light collection. The photomultipliers have 2 inch quartz window and bialkali photocathode. Metal fingers are deposited under the photocathode to reduce its resistivity at low temperature. The PMT photocathodes are kept at ground potential. The tubes were selected by the manufacturer to have quantum efficiency above 20% at the xenon scintillation wavelenght. The quantum efficiency of the supplied PMTs varied from tube to tube between 21% and 25%, at room temperature.

Xenon is introduced into the chamber through an inlet stainless steel tube, which passes through the volume under vacuum and the aluminum flange of the outer chamber. The condenser consists of a helix gas tube in good thermal contact with a massive copper block connected by a thick copper rod to a liquid nitrogen container. The condenser was filled with alcohol to improve the heat transfer and ensure a more uniform temperature along the helix.
High purity commercial xenon gas was purified in a portable purification system, specially designed for tests at the neutron beam (see Figure 96). Prior to condensation into the chamber,

the xenon gas was passed several times through an Oxisorb column. The chamber and all connections to the purification system were primarily pumped down to ~10^{-6} mbar under heating during several days. The connecting tubes are heated to a temperature of about 200 ºC, though the chamber is kept at 70 ºC, the maximum storage temperature quoted for the PMTs. Then, xenon is introduced into the hot chamber. For the next several days, xenon gas is kept circulating through both the chamber and the Oxisorb column, at room temperature.

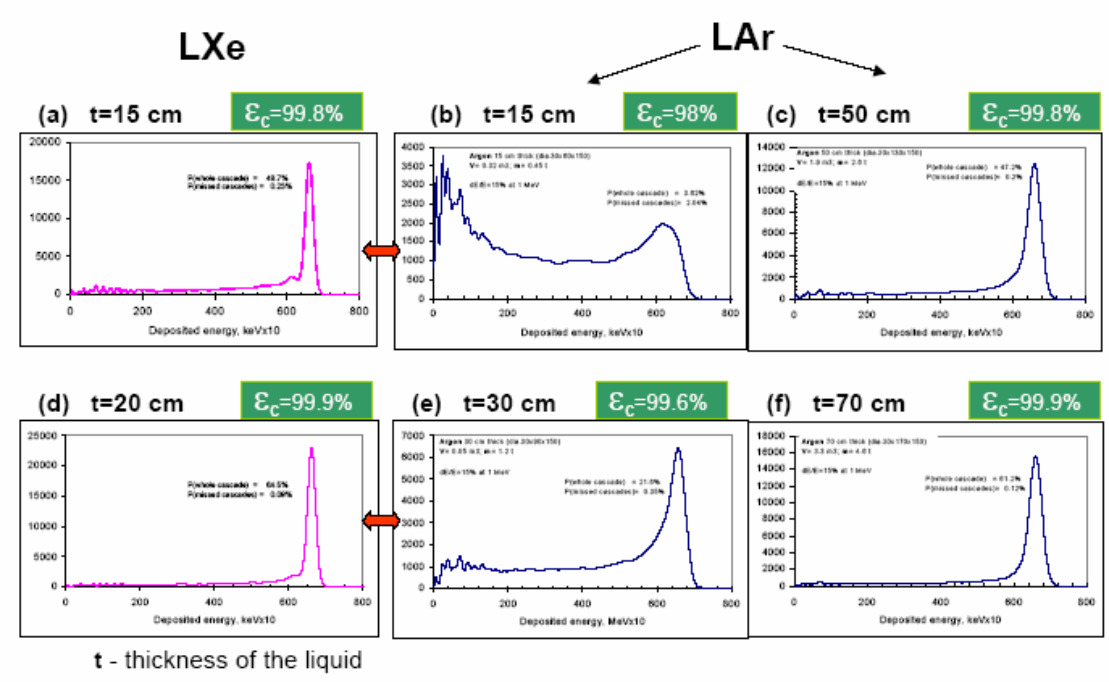

Figure 94: Simulated gamma-ray spectra

Bench tests

Bench tests of the liquid xenon module were carried out at the LIP-Coimbra lab. The tests aimed at: a) development of the cooling, liquefaction and operation procedures; b) test of the front-end electronics and the data acquisition systems; c) measurement of the VUV light collection efficiency and uniformity in the active volume, d) measurement of the time resolution; e) test of the position reconstruction algorithm; f) comparison of the experimental data with the predictions of the Monte Carlo simulation, which takes into account propagation of the scintillation light in the chamber, and adjustment of relevant parameters such as reflectivity of PTFE and absorption and scattering lengths for the scintillation light in the liquid xenon.

The tests were done either with a ^{57}Co γ-ray source (122 keV) or a ^{22}Na positron source, which emits both annihilation γ-rays (511 keV) and γ-rays with an energy of 1.2 MeV. The ^{57}Co γ-ray source was placed in the vacuum insulation volume below the chamber bottom. It can be moved from the outside with a magnet and put under any of 7 PMTs in a fixed position or hidden in a small lead container. The ^{22}Na source was placed outside the chamber assembly so that the chamber was irradiated from the lateral side. A ∅2×2 inch BaF_2 scintillation detector was used for the measurements with the ^{22}Na source, in order to select pairs of 511 keV γ-rays.
The chamber is cooled down by the liquid xenon itself, as it condensates in the helix condenser (see Figure 95) and drops into the chamber under gravity. The evaporated xenon gas is returned into the condenser through the chamber outlet, in a closed cycle. Once the

chamber bottom reaches the liquid xenon temperature, about −90 ºC at vapor pressure of 2.5 bar, the condensation of gas is started.

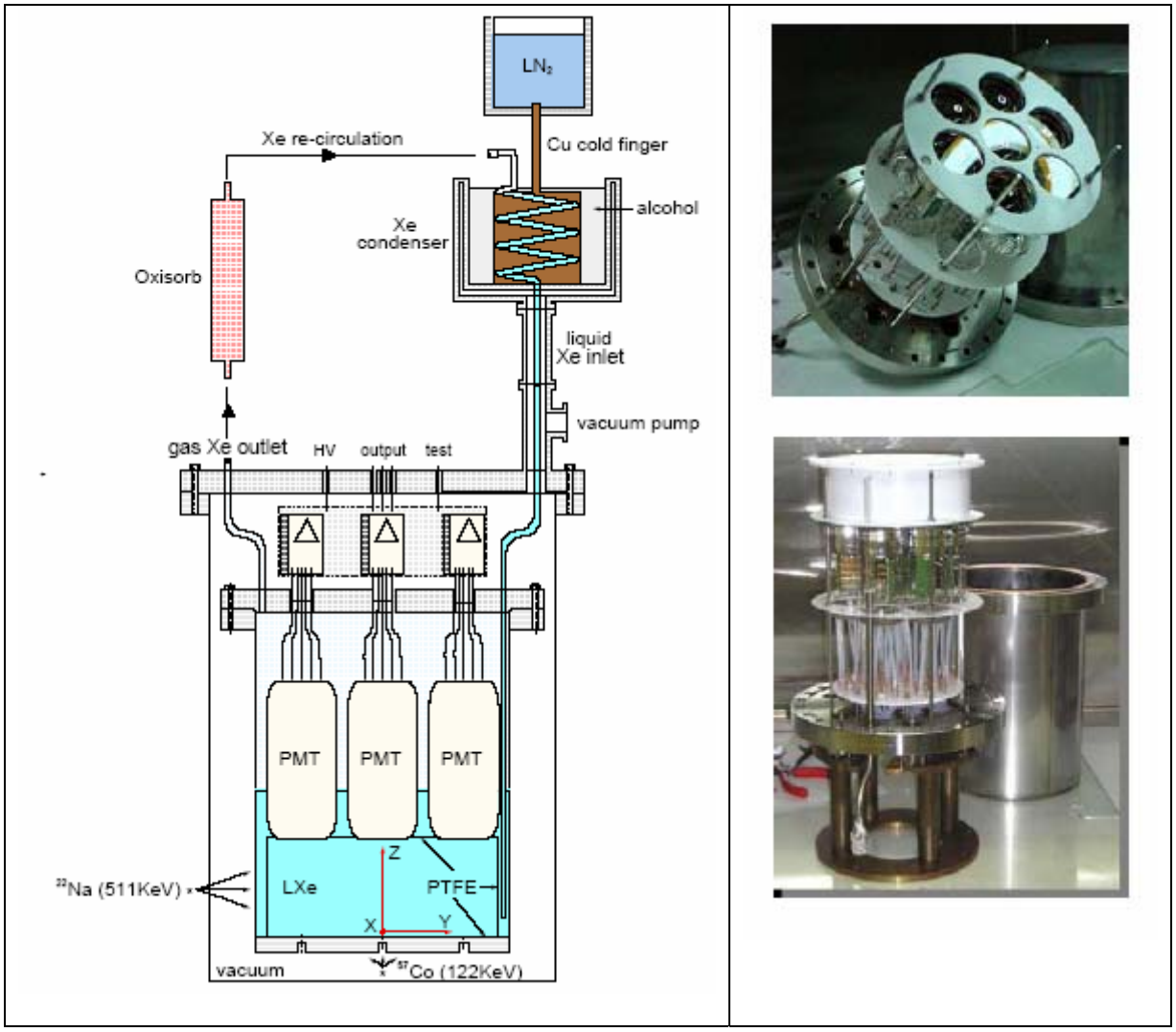

Figure 95: Layout of the liquid xenon test module with the condensing and re-circulation system (left). View of the PMT array (right-top) and the whole assembly (right-bottom).

The liquid level is monitored during the condensation process by observing the photomultipliers signals due to a ^{57}Co γ-ray source (122 keV) placed below the chamber bottom, under its canter. A sharp increase of the amplitude, by about a factor two, is observed when the liquid level is high enough to cover the entrance window of the respective photomultiplier. Condensing is continued for a while, allowing the liquid surface to rise well above the photomultiplier windows.

Figure 96: portable purification system

The chamber was operated at a xenon vapour pressure of 2.5 bar. During operation, the temperature of the helix condenser is always about –100 ºC and the temperature of the chamber was maintained stable by the dripping in xenon. The gas could be circulated, either directly or through the purification system, so that it can be permanently purified before returning to the condenser and chamber.

Each acquisition channel was calibrated with respect to the PMT gain at the operating temperature, using a short light pulse (<300 ns) from a green LED and acquiring the corresponding single electron spectra. The LED was placed in the vacuum shell outside the liquid xenon chamber, close to the electrical feedthroughs, so that the light emitted by the diode could penetrate into the chamber through the ceramic insulators. The calibration was periodically checked during measurements.

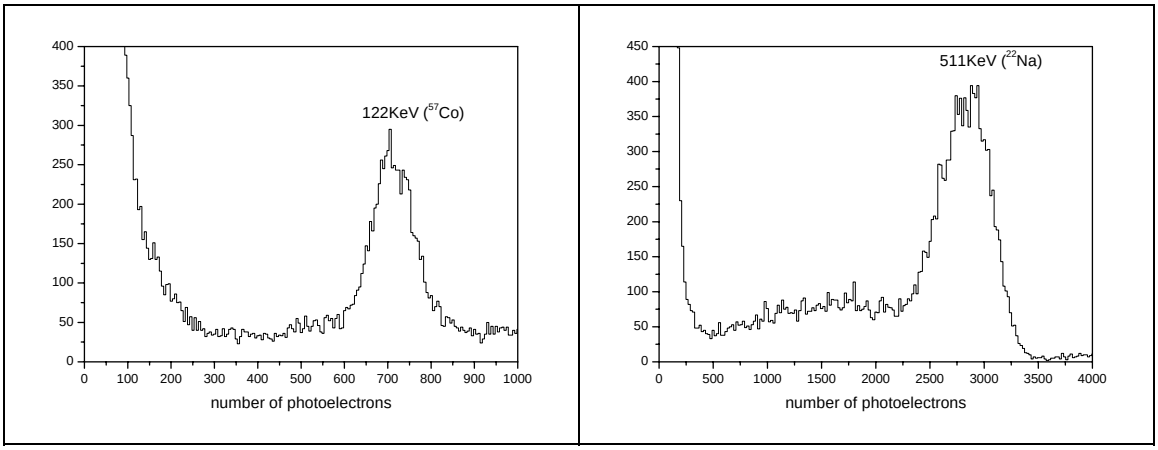

Figure 97: Pulse height spectra due to 122 keV (left) and 511 keV (right) γ-rays.

Some examples of the pulse height spectra measured with the LXe test module are shown in Figure 97 and Figure 98. The signals from all photomultiplier tubes were recorded, provided that a trigger occurred. The trigger was generated at the condition that at least two out of the seven PMTs produced signals with the amplitude above a threshold, which was set somewhat above the amplitude of single electron signal. Offline, after calibration, the PMT amplitudes are converted to number of photoelectrons and added with equal weights. An energy resolution (FWHM) of about 18% and 22% was obtained for 122 keV and 511 keV, respectively. From these measurements we arrive at an overall conversion efficiency of ~5.5 photoelectrons per 1 keV of deposited energy. This corresponds to a collection of about half the emitted VUV photons, assuming that the mean energy required to produce one photon is W_s = 20 eV and the quantum efficiency is 20% for all PMTs.

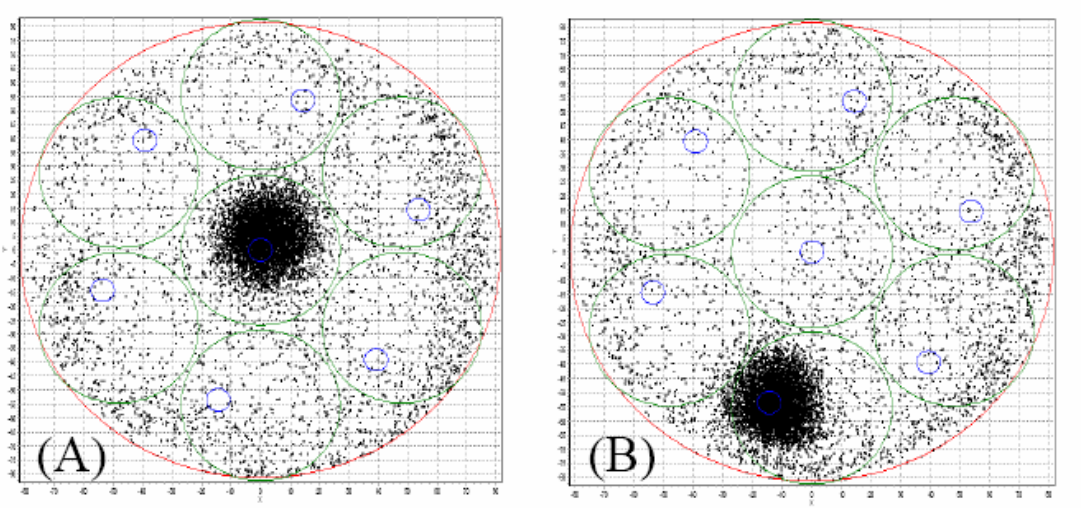

Figure 98: Reconstructed position of the scintillation events due to 122 keV γ-rays from a ^{57}Co source, placed at the bottom of the chamber below the central collimator hole (a), and below a non-central position (b). The large circle corresponds to the active volume of the liquid xenon scintillator, medium circles outline the photomultipliers and the small circles indicate the holes in the collimator, all in scale.

The time resolution was measured with 511 keV γ-rays, requiring the coincidence with the BaF_2 detector which gives the START signal for the TDC. The STOP signal is provided by the trigger signal of the chamber. The time resolution was determined as a function of the energy deposited by Compton scattering in the active volume. The results are shown in Table 10.

Table 10: Time resolution (FWHM) as a function of the deposited energy

Energy range [keV]	**Time resolution [ns]**
75 to 105	3.0
50 to 70	3.6
35 to 50	4.2
20 to 35	4.4

The chamber response has been measured by placing the ^{57}Co source at different positions under the chamber bottom. A lead mask with 7 holes of 8 mm diameter was attached to the chamber bottom, in this experiment. The holes were located under each photomultiplier tube, rotated by 15º around the chamber axis. The (x,y) position of each interaction has been

determined using our reconstruction algorithm. The result shows that most of the interaction positions are correctly reconstructed (see Figure 98). The uniform background is due to Compton scattering in the stainless steel chamber bottom, as it was shown by correlating event position and pulse amplitude. Selecting only those events that have their reconstructed (x,y) coordinates within a circle centered at the corresponding hole of the lead mask, it was possible to remove most of the low energy background in the pulse height spectrum of ^{57}Co.

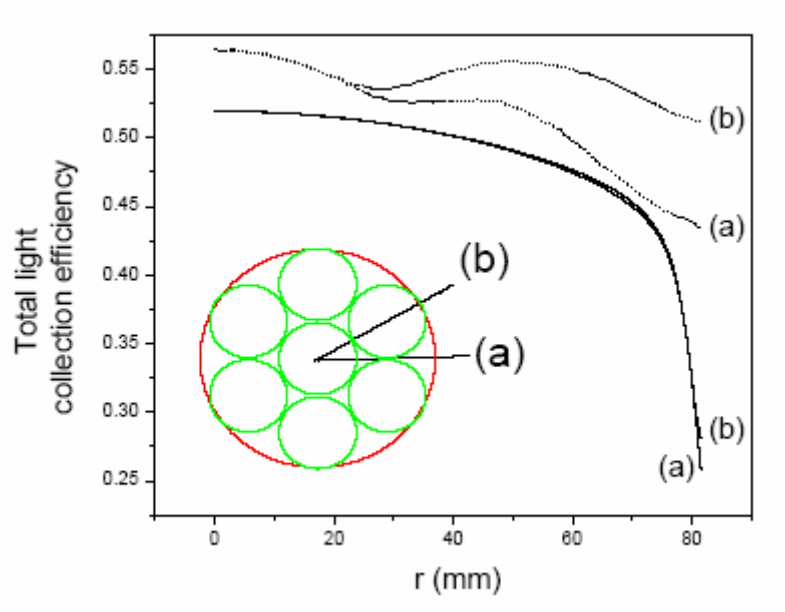

Figure 99: Light collection efficiency, obtained by Monte Carlo simulation, as a function of the distance to the chamber axis along the radial paths (a) and (b) indicated in the insert. Solid lines are for z = 0 (the chamber bottom, where the results for the two paths practically coincide) and dashed lines are for z = 39 mm (see Figure 93).

The total light collection as a function of the distance to the chamber axis has been studied by Monte Carlo simulation, both at the chamber bottom and at z =39 mm (see Figure 99). Two independent Monte Carlo models were developed. The first model is a detailed Monte Carlo simulation of the detector and of the experimental setup, based on Geant4. It includes the generation of γ-rays from the ^{57}Co source, their interactions with the detector medium, the production and propagation of the resulting scintillation photons in the liquid xenon. For the treatment of γ-ray interactions, the low-energy electromagnetic processes of Geant4 are used. The propagation of the scintillation photons in liquid xenon and their interaction with the various elements of the chamber is simulated using the optical processes, also from Geant4, in particular Rayleigh scattering, light absorption and refraction/reflection.

The other model is a standalone simulation of light propagation within the active volume of the detector. It takes into account the Rayleigh scattering and the light absorption in the liquid, as well as the refraction and reflection at the optical surfaces, too, but uses independent (non GEANT4) subroutines for those processes.

Both simulations were performed with the mean energy required to produce a scintillation photon being W_s = 20 eV and the quantum efficiencies of all PMTs set to 20%. The PTFE reflectivity, as well as the absorption and scattering lengths, λ_{abs} and λ_{scat}, respectively, for the VUV photons have been varied. The absorption and scattering lengths for the VUV photons in liquid xenon are not known, at present. However, several authors have reported a value of about 30 to 40 cm for the total attenuation length. Using λ_{tot}=35 cm, which sets the constraint $1/\lambda_{tot}=1/\lambda_{scat}+1/\lambda_{abs}$, and assuming that $\lambda_{tot}=\lambda_{scat}$ (i.e. no absorption), we adjusted the total

number of simulated photoelectrons to the value obtained experimentally, thus arriving to a lower limit for the PTFE reflectivity of 0.87±0.03. This value is compatible with results reported in the literature.

In a similar way, but setting the PTFE reflectivity to 1 and λ_{tot}=35 cm, we tried to estimate limits for λ_{abs} and λ_{scat}, which would make the simulation to agreed with experimental data. The result is a lower limit for the absorption length of about 40 cm and an upper limit for the scattering length of about 200 cm. The important result, however, is that such agreement requires the existence of Rayleigh scattering in the liquid xenon for its own scintillation light. The above estimates were confirmed using the standalone Monte Carlo model. In this case, the ratio of the simulated total number of photoelectrons for two positions of the ^{57}Co source (see Figure 96) was adjusted to the one observed experimentally. The advantage of such approach is that this ratio is independent of the values set for the quantum efficiency and W_s, as the number of photoelectrons at each source position is proportional to their product. The result for a lower limit for the PTFE reflectivity and the limits for the absorption and scattering lengths are in excellent agreement with those obtained with the GEANT4 based model.

A good agreement has therefore been achieved between the results of bench tests with γ-rays and those obtained from simulations. This fact gives us confidence on the simulation tools and on the values of input parameters used in our computations. Moreover, several important parameters related with the propagation of the scintillation light in the liquid xenon chamber have been obtained. Thus, we conclude that this method can be applied to trustfully predict the performance of a full-scale LXe gamma cascade calorimeter.

Tests with a neutron beam

With the aim of studying the response of the module to neutrons and γ-rays simultaneously, the LXe module has been exposed to neutrons at the tandem accelerator of the Demokritos Research Centre, in Athens, Greece. The energy of neutrons used in the tests was 6 MeV and 8 MeV. The module performed well under a flux of incident neutrons of $2{\cdot}10^5$ to $7{\cdot}10^5$ n/s (calibrated with a BF_3 counter) and gammas $>2{\cdot}10^5$ γ/s (estimated from Compton peak in the TOF spectrum with γ-rejection OFF), respectively. The issues addressed in these tests were: a) observation of the signals due to both γ-rays and neutrons, simultaneously; b) measurement of the scintillation decay time for γ-rays and xenon recoils due to elastic scattering of neutrons in xenon; c) measurement of the suppression factor of LXe scintillation efficiency for nuclear recoils and for γ-rays (also known as quenching factor); d) observation of possible activation effects; e) validation of the developed MC simulation models; f) operation of the liquid xenon module and the associated systems in a harsh environment.

Among the results obtained we highlight the following: i) The observable decay for γ-rays and xenon recoils time was measured to be 47±7 ns and 30±4 ns, respectively, for energies from roughly 5 to 150 keV. No energy dependence was observed within the errors. Thus, this indicates that the discrimination is in principle possible although its efficiency was not yet evaluated. ii) The suppression factor of liquid xenon scintillation efficiency for nuclear recoils with respect to γ-rays was measured in the nuclear recoil energy range between 5 and 30 keV. iii) Assessment of the light collection efficiency over the whole sensitive volume of the chamber. iv) Indication of occurrence of activation of ^{52}Cr ($t_{1/2}$=3.79 min); stainless steel is about 20% Cr and the abundance of ^{52}Cr in natural chromium is about 84%.

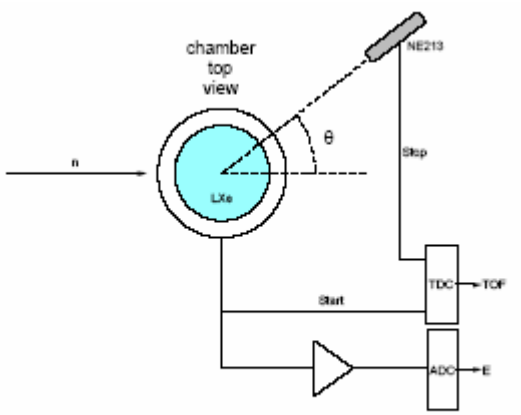

Figure 100: Layout of the experiment with the neutron beam.

Monte Carlo simulation of the LXe calorimeter

Detailed Monte Carlo simulations have been implemented using the Geant 4 library in order to study the aspects relevant to the performance of a calorimeter for detecting γ-ray cascades in neutron capture experiments, notably at n-TOF. The following issues have been addressed: i) simulation of the hadronic processes occurring both in the target and in the detection volume (in particular elastic and inelastic scattering as well as neutron capture); ii) generation of the γ-ray cascades; iii) interactions of the neutrons and γ-rays in the detection medium; iv) propagation of the scintillation light throughout the vessel, up to the photomultiplier tubes.

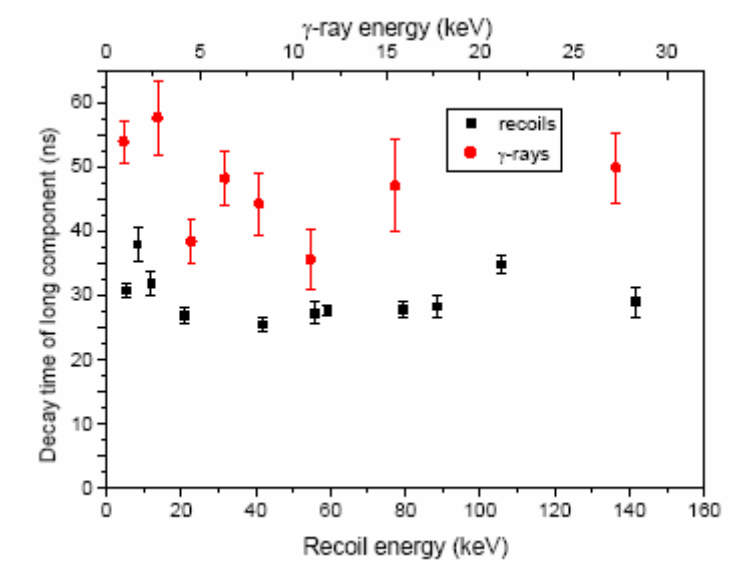

Figure 101: decay time of LXe scintillation due to γ-rays and Xe recoils.

We considered a detector consisting of a cylindrical vessel filled with liquid xenon, with a length of 150 cm, and radii 15 and 45 cm, internal and external respectively, surrounded by an array of photomultipliers (see Figure 93). The inner surface was covered with PTFE to increase light collection.

The physical parameters used in the simulation were set to values extracted from the data collected with the prototype chamber, both in bench tests with γ-rays and from measurements

at the neutron beam. They are summarized in Table 11. This was of utmost importance since there are few (or no) previous measurements of these parameters reported in the literature.

Table 11: Parameters used in the simulations.

Parameter	Value
PTFE reflectivity	94%
Quenching factor	0.2
Absorption length	87 cm
Scattering length	58 cm

From the simulations we estimate that ~60% of the cascades coming from ^{197}Au are fully contained by this quantity of xenon, and in ~99% of the cases at least one gamma deposits energy in excess of 2.5 MeV in the vessel. In the outer region of the cylinder, the volume has been segmented in cells of 15×15 cm^2×15 cm, each equipped with an array of PMTs, using walls made of thin PTFE sheets to improve the light collection uniformity while maintaining good collection efficiency (see Figure 101). The PTFE walls separate the cells only partially as shown in Figure 102. In fact, the simulations show that the light collected from a scintillation hit is strongly dependent of its radial position, in the case there are no such walls. On the other hand, full segmentation of the volume introduces a significant reduction in the light collection. The trade-off between the two effects pointed to the partial separation of the cells to about half of the LXe thickness, starting from the outer side.

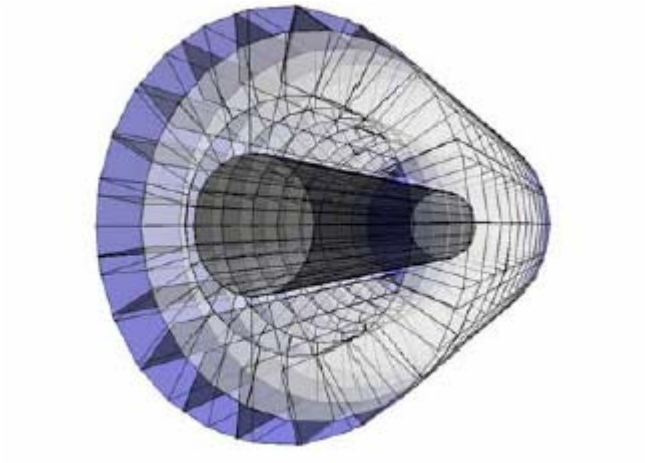

Figure 102: Geometry of the simulated LXe calorimeter.

For the purpose of this study we considered a ^{197}Au target. The cascades have been generated from evaluated data files produced at Karlsruhe. As for the *n*-capture in xenon, we used the data files produced by the Geant team.

The main background is expected to come from the capture, by xenon nuclei, of neutrons scattered at the target sample. The signal to noise ratio is therefore strongly dependent on the energy of the neutrons, according to the capture cross-section of the various xenon isotopes. Aiming at reducing this background, we considered the possibility of isotope separation, having simulated both natural xenon and xenon containing only isotopes of mass above 129. The effect of including a neutron absorber, e.g. ^{6}LiH, placed around the target is also being considered.

The neutrons have been assumed to come all along the cylinder axis, the target being positioned at the centre of the setup, with energies corresponding to the n-TOF measuring "decades": i) E<10 eV, ii) 10 eV<E<100 eV, iii) 100 eV<E<1 keV, , iv) 1 keV<E<10 keV, and v) 10 keV<E<100 keV. The results are shown in Figure 103 and Figure 104.The time structure of the neutron beam was not considered.

Table 12: Signal to noise ration of the LXe calorimeter.

Neutron energy	Natural Xe	A > 129 only
0 – 10 eV	7.23	275
10 – 100 eV	1.12	127
100 – 1000 eV	1.15	8.6
1 -10 keV	0.27	0.9
10 – 100 keV	0.18	0.5

The energy resolution for cascade events fully contained in xenon is estimated to be ~7% FWHM. The segmentation of the active volume might allow the offline reconstruction of the scintillation point in each cell, thus allowing further improvement in the energy resolution.

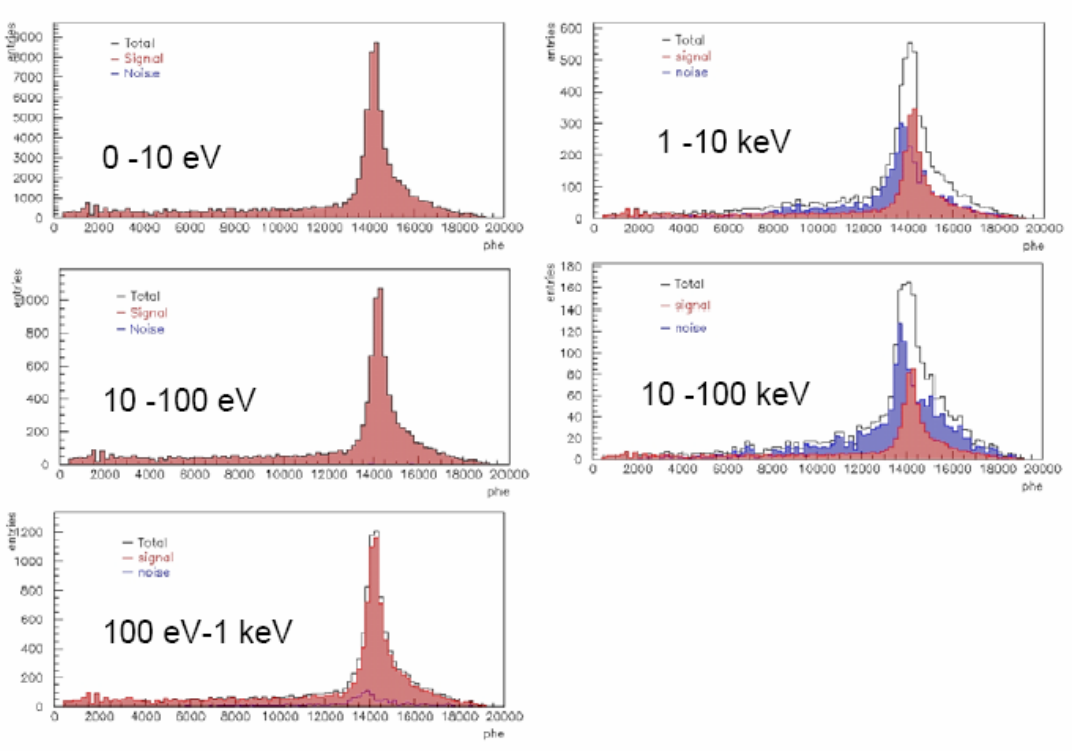

Figure 103: Monte Carlo simulated spectra of γ-ray cascades from a ^{197}Au target for different energies of the incident neutrons obtained with the LXe calorimeter filled with natural xenon. In red - the contribution from ^{197}Au γ-ray cascades; in blue – that due to the neutrons scattered in the target and captured by Xe isotopes.

This technique has been demonstrated experimentally with the prototype chamber. The signal to noise ratio, integrated for energy depositions in excess of 2.5 MeV, is shown is Table 3 for ^{197}Au, both for natural xenon and for A>129. This ratio should improve considerably if a *n*-absorber is used, so that the energies of the neutrons entering the xenon volume be shifted away from the resonances of the Xe *n*-capture cross-sections. From the spectra of Figure 103

and Figure 104 we might be able to subtract much of the remaining background, provided the background spectrum be evaluated for various energies of the neutrons, for example using well measured target nuclei to send neutrons into the vessel.

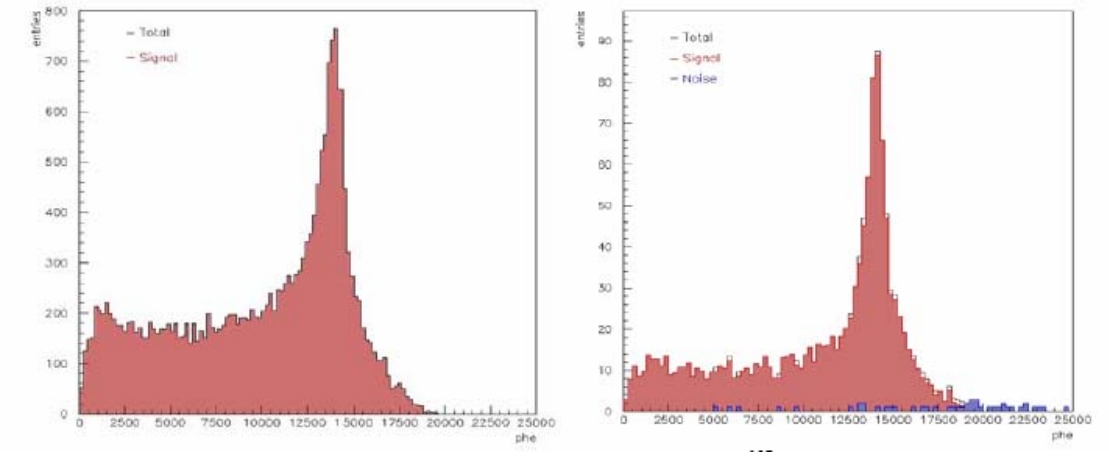

Figure 104: Monte Carlo simulated spectra of γ-ray cascades from a ^{197}Au target for different energies of the incident neutrons obtained with the LXe calorimeter filled with distilled xenon (see text). In red - the contribution from ^{197}Au γ-ray cascades; in blue – that due to the neutrons scattered in the target and captured by Xe isotopes.

Activities performed at Democritos

Contributed by *P Assimakoupoulos* (Ioannina University, Ioannina, Greece)

The experimental line for neutron production at the 5.5 MV TANDEM accelerator laboratory of the NCSR "Democritos" is shown in Figure 105. The facility includes a deuterium gas cell with remote control or a solid titanium tritiated 5 Ci source at the end of the line. The holder of the tritiated source is constructed from Al-6061 after MCNP simulation for minimum scattering and activation. A cold air jet is used for cooling the neutron production source. Neutron flux is monitored with a BF_3 detector. The mean neutron energy is determined from the reactions' kinematics, taking into account of the deuteron energy loss in the window of the gas cell or the titanium target, as well as the differential cross section of the reactions. A typical neutron beam energy profile obtained under these conditions is contained in Figure 106.

Neutron threshold reactions were used for flux normalization in the irradiations. Initially, several combinations with different target support materials and distances from the neutron production target were investigated through Monte Carlo calculations and test measurements. The optimal conditions with the minimum background and acceptable energy resolution were produced by placing a thin aluminium target holder in 3 - 4 cm from the neutron production target. In the case of the tritium source, the aluminium holder was placed at a distance of 1.5 cm from the neutron source in order to increase the neutron flux.

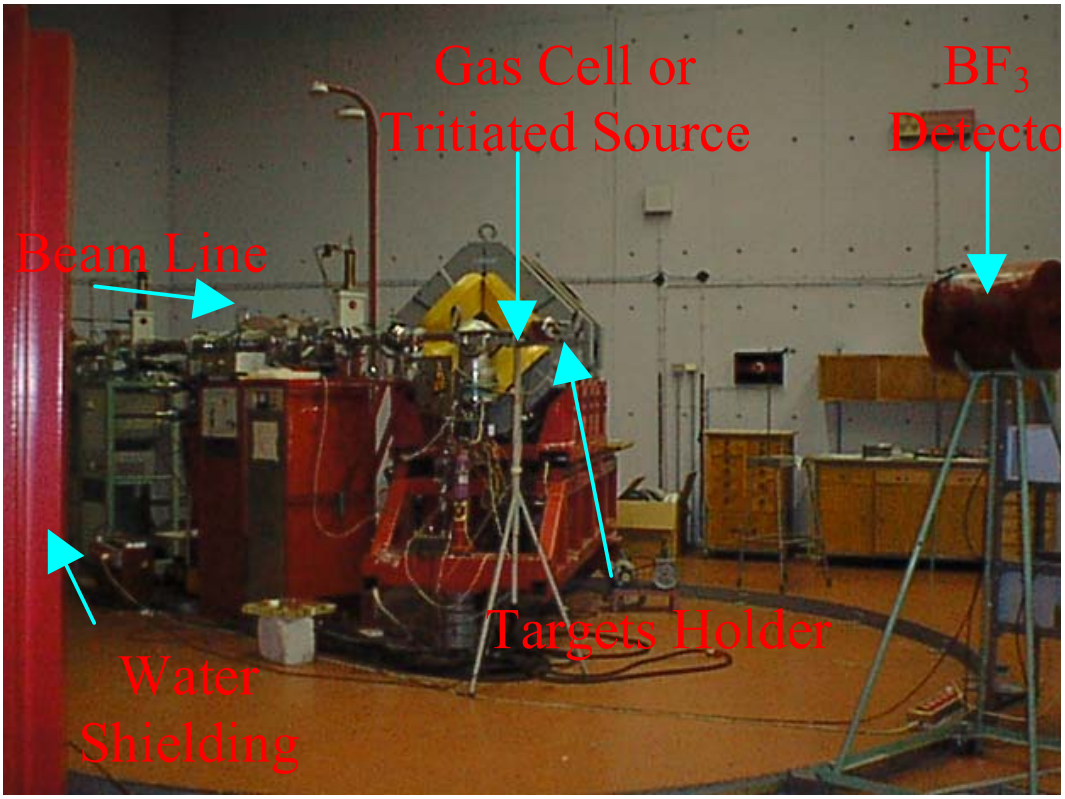

Figure 105: Experimental beam line for neutron production at the TANDEM accelerator laboratory of the NCSR "Democritos".

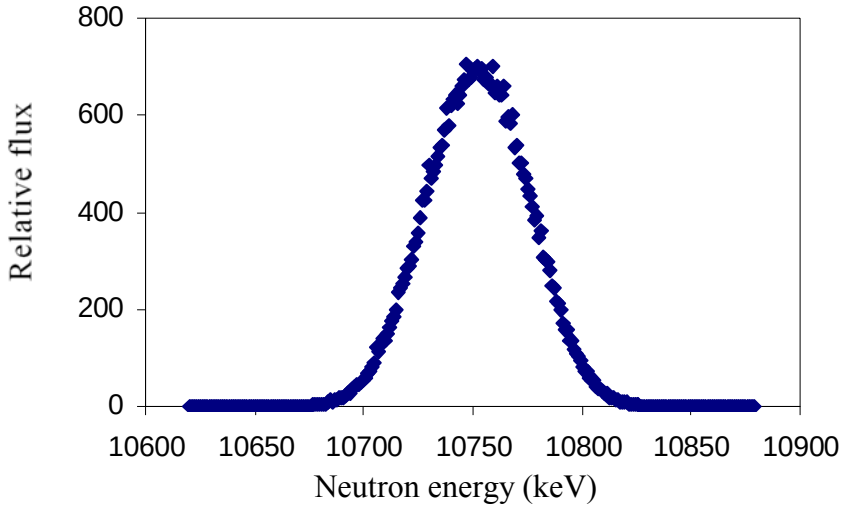

Figure 106: Monte Carlo simulation of the neutron beam energy profile at nominal beam energy 10.75 MeV.

Measurement of the ^{232}Th(n,2n)^{231}Th reaction cross section

Fifteen deuteron beam energies were selected with currents up to 5 μA. Two Th targets (0.5 mm and 0.155 mm thick and surface of 1x1 cm^2) of high purity (99.5 % ^{232}Th, from Goodfellow SARL), were used. The Thorium samples were placed between two Fe foils and/or two Al foils and secured with thin Al rings. In a few points (especially in the higher energy part of the data), a niobium foil was also included in the sandwich arrangement. The assembly was irradiated at 0° with respect to the deuteron beam; the duration of the irradiation varied between a few hours and more than 60 hours near the threshold and at the high energy region. During the irradiation, the neutron flux was monitored with a BF_3 detector. After each irradiation, the intensity of the γ-ray lines emitted by the de-excitation of the produced nuclei, was measured with γ spectroscopy. A 20 % reverse-electrode coaxial germanium detector (GR2018, Canberra) was used for the activity measurements of the iron or aluminium foils and an 80 mm^2 Si(Li) detector for the low energy line of ^{231}Th. A typical γ spectrum of a ^{232}Th sample after neutron irradiation is shown in Figure 107. The photopeak areas were determined by means of the PAW program.

The efficiency of the detectors was determined with several point-like sources prior to irradiation and the simulation codes GEANT3.21 and MCNP4B. Neutron background from the (d,n) reactions on the cell structural materials was determined at different deuteron energies within the studied energy range by MCNP simulation and evacuating the gas cell and irradiating aluminium, iron, niobium, gold or thorium foils. Prior to the determination of the ^{232}Th(n,2n)^{231}Th reaction cross section, it was assured that the measured 25 keV line came exclusively from the ^{231}Th nucleus produced. This was accomplished by considering all candidate nuclei and fission fragments and calculating the produced ^{231}Th nuclei and their subsequent decay as a function of time (n-TOF/APC Internal Note 01-03, June 2001). It was thus determined that the ^{231}Th decay constant had the value given in the literature.

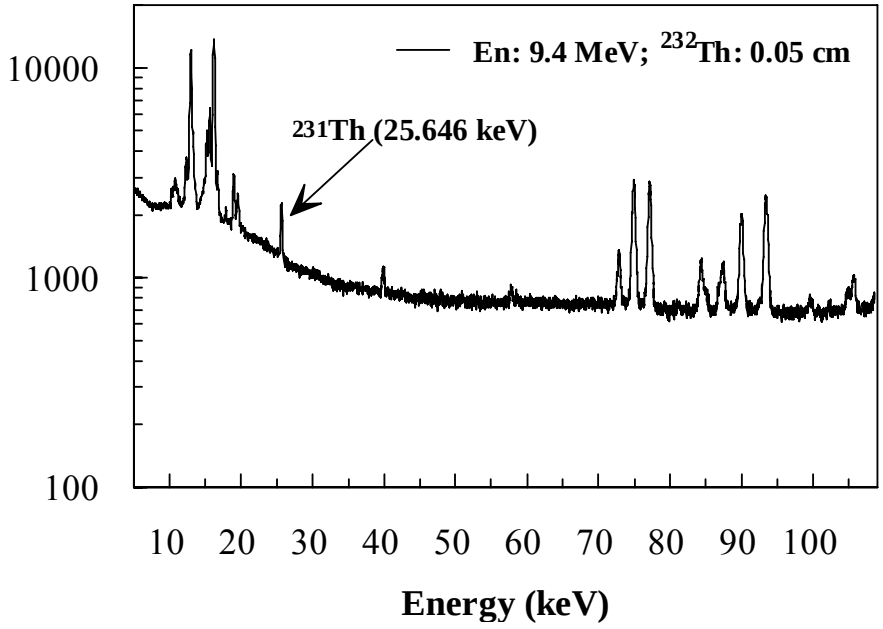

Figure 107: Typical gamma spectrum of a ^{232}Th sample after irradiation.

The ^{232}Th(n,2n)^{231}Th reaction cross section relative to the ^{56}Fe(n,p)^{56}Mn or the ^{27}Al(n,a)^{24}Na reaction cross sections was determined from the relation:

$$\frac{\sigma_{n,2n} < E_n >}{\sigma_{n,p(a)} < E_n >} = \frac{N^{Fe(Al)}}{N^{Th}} \cdot \frac{N_{Act-Th}}{N_{Act-Fe(Al)}} \cdot \frac{\sum_i \varphi_i (1 - e^{-\lambda_{Mn(Na)}(t_{i+1} - t_i)}) \cdot (e^{-\lambda_{Mn(Na)}(T_{irr} - t_{i+1})})}{\sum_i \varphi_i (1 - e^{-\lambda_{Th}(t_{i+1} - t_i)}) \cdot (e^{-\lambda_{Th}(T_{irr} - t_{i+1})})}$$

where $<E_n>$ is the mean neutron energy in the sample, N the number of atoms in the samples, N_{Act} the number of activated nuclei and the sums are introduced to account for any variation in the neutron flux. Since an accurate determination of the reaction cross section relies on the precise knowledge of each term in the above equations, these were determined both experimentally and through simulations. Furthermore, the absolute efficiency of the Ge and Si(Li) detectors was determined with point-like sources and extensive Monte Carlo simulations. Activities had to be corrected due to the flux variation during each run and this was done through the neutron flux rate of the BF_3 detector. In the d + d reaction, the contribution of neutrons produced in the cell structural materials (e.g. the Mo entrance window, the stainless steel cell and the Pt beam stopper) was evaluated by deuteron bombardment of an evacuated cell and examination of the activation of different metallic foils in the same arrangement as the thorium-metallic monitoring foils. MCNP simulations were also performed.

Through the analysis described above, the values of the ^{232}Th(n,2n)^{231}Th reaction cross section for the energies studied were determined and are shown in Figure 108. In the same figure, the corresponding cross sections extracted from the different evaluated data files as well as the most recent experimental data of Raics et al. (Phys. Rev. C 32 (1986) 87) are also included. The overall error in the values was between 5 to 14 % and was mainly introduced

from the statistical errors in the photopeak area determination. These errors varied between 1.5 and 3.5 % for the activated iron or aluminium foils and between 2.4 and 9.2 % for the thorium foils.

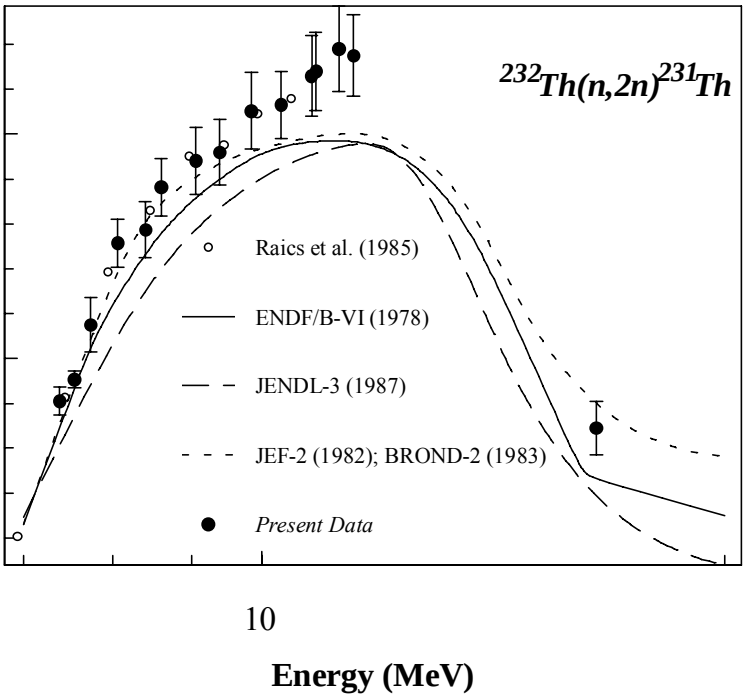

Figure 108: ^{232}Th(n,2n) reaction cross section results obtained here, compared to existing evaluated data in the four major libraries of neutron data and some recent measurements.

The results of the present work indicate that the values of the ^{232}Th(n,2n)^{231}Th reaction cross section follow the JEF-BROND database values up to 9 MeV of neutron energy but are higher than those of all databases in the maximum of the cross section. Moreover, they are in agreement with the older experimental results of Raics et al. and a recent evaluation (V. Maslov, Nuclear Physics A 743 (2004) 236).

Measurements of the ^{241}Am(n,2n)^{240}Am reaction cross section

The cross section of the ^{241}Am(n,2n)^{240}Am reaction was measured at four neutron energies from 9.7 up to 17.1 MeV. The neutron beam was produced via the reaction ^{2}H(d,n)^{3}He, for the energies of 9.7, 10.5 and 10.6 MeV by using a deuterium filled gas cell, while for the energy of 17.1MeV, the beam was produced via the ^{3}H(d,n)^{4}He reaction, with a 5Ci Tritiated Titanium target on silver backing. The flux variation of the neutron beam, during the 100 h of continuous irradiation, was monitored by using a BF_3 detector, whose spectra were stored at 100 sec time intervals. The absolute flux of the beam was obtained with respect to reference reactions ^{27}Al(n,α), ^{197}Au(n,2n) and ^{93}Nb(n,2n), whose cross sections were taken from the IRDF-2002 data base.

The Americium target consisted of a 37 GBq ^{241}Am disk shaped source with a diameter of 2.5 cm, encapsulated in stainless steel. For safety reasons and in order to reduce the counting rate on the detector due to the high activity of the source itself, the target was additionally enclosed in a 3 mm thick lead container. Disk shaped reference foils of materials with the same diameter as the Americium target – Al (65.8 mg/cm^2), Au (9.4 mg/cm^2) and Nb (86.9 mg/cm^2) - were placed in front of the target and irradiated under the same conditions in order to determine the neutron flux.

Table 13: ^{241}Am(n,2n) reaction cross section data.

Energy (MeV)	*Cross Section (mb)*	*Error (%)*
9.7	148	*8*
10.5	220	13
10.6	229	13
17.1	200	27

The activity of the irradiated targets was measured off line by using a 56% HPGe detector, for about 2-3 half lives each. Self absorption and geometry effects for the targets were taken into account in all measurements and the appropriate corrections were applied. The resulting activity was corrected for decay during the irradiation by taking into account the neutron beam variations with the BF_3 monitor spectra. Furthermore, corrections were applied for the time interval between the target irradiation and the activity measurement. The preliminary results for cross section values are contained in Table 13 and the graph in Figure 109. Additional measurements for energies around 11.5, 8.5, and 15 MeV are planned for 2005.

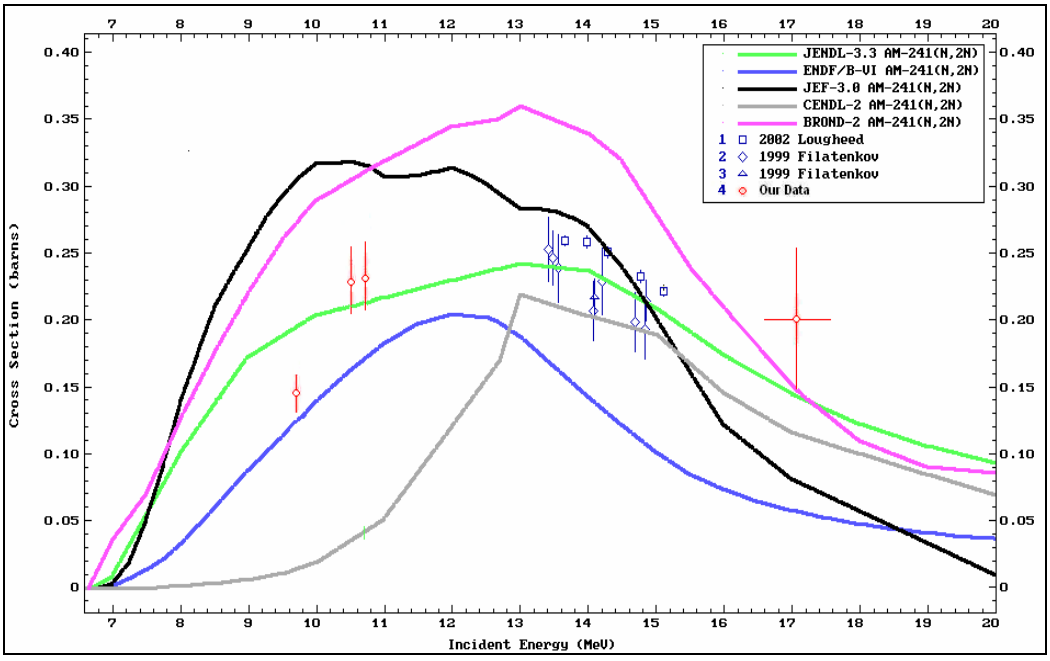

Figure 109: ^{241}Am(n,2n) reaction cross section results obtained here, compared to existing evaluated data in the four major libraries of neutron data and some recent measurements.

Measurements of neutron-induced fission cross section ratios ^{232}Th/^{nat}U at neutron energies below 10 MeV.

Neutron-induced fission cross sections have been measured for ^{232}Th relative to natural U at neutron energies 7.5, 8.5 and 9.5 MeV. With a deuterium gas target, neutrons were produced via the ^{2}H(d,n)^{3}He reaction. During the whole run the neutron flux was monitored using a BF_3 detector placed at a distance of 2.2 m from the neutron source. Two fissionable material targets were used; a 1.0247 mg/cm^2 ^{232}Th and a 0.9516 mg/cm^2 natural U for the reference reaction.

The sensor for detecting the fission products was an arrangement of two silicon detectors or two plastic track detectors (lexan), placed in close contact with the fissionable materials irradiated for a few hours under the same conditions. Additional irradiation measurements were carried out, without fissionable targets, in order to perform background corrections.

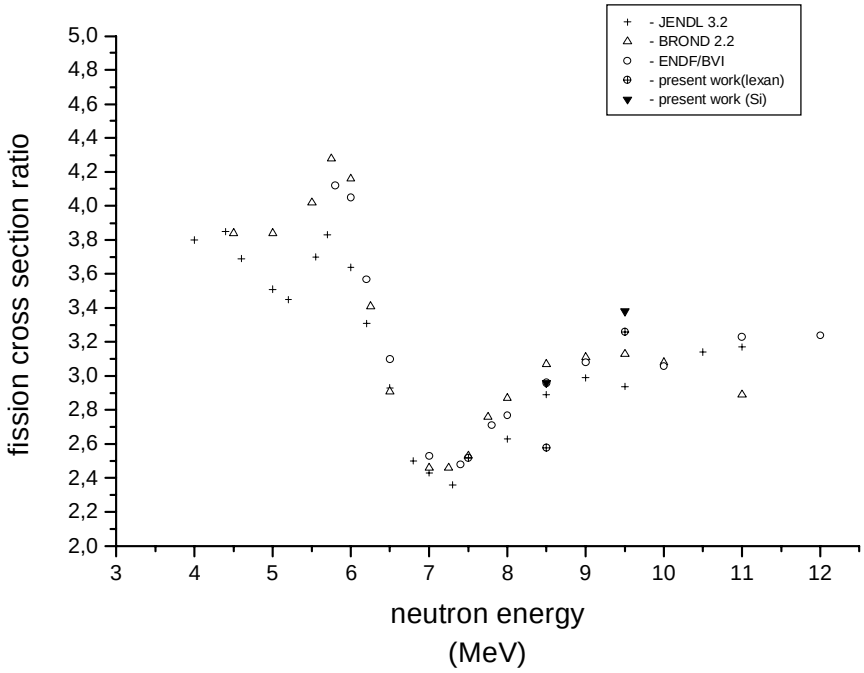

Figure 110: Fission cross section ratios for ^{nat}U/^{232}Th obtained here, compared to existing evaluated data in the four major libraries of neutron data.

For the silicon detectors, the total number of counts, after background subtraction, representing the total number of fission fragments, was used to obtain the cross section values of ^{232}Th relative to natural U. For the plastic detectors, the fission fragment tracks were

revealed, following a proper etching process with a chemical solution of NaOH (25% w/w) at a temperature of 50 ^{o}C for six hours. The procedure resulted in the enlargement of the fission fragment tracks to sizes that can be viewed and counted with an ordinary optical microscope. The total number of tracks per cm^2 was used to calculate the fission cross section ratio between ^{232}Th and natural U.

• Table 14: Fission cross section ratios for ^{nat}U/^{232}Th.

E_n(MeV)	Cross section ratio (Si)	Cross section ratio (lexan)
9.5	3.38 ± 0.059	3.26 ± 1.09
8.5	2.96 ± 0.08	2.58 ± 0.56
7.5	-	2.52 ± 1.3

The results of the ^{nat}U / ^{232}Th fission cross section ratio are contained in Table 14 and Figure 110, along with previous evaluated data of ENDF/B-VI, JENDL-3.2 and BROND-2.2. The data obtained here, are in good agreement with most previous measurements, except for the case of lexan detector at neutron energy of 8.5 MeV, where the value obtained here differs by a small amount.

Modeling and Nuclear Data Evaluation Activities

Contributed by: *H Leeb* (TUW, Wien)

Modeling as well as Nuclear Data Evaluation is an important component of a coherent Nuclear Data project. According to the available task force the activities were restricted to specific topics which are important either from the performed experiments or as a basis of complete forthcoming evaluations. Following this concept the modeling part has been focused on the improvement of the dispersive optical model and the description of (n,xn) reactions and their determination via prompt γ-spectroscopy. In the evaluation part two key issues were treated: (i) the determination of covariance information and their inclusion in the EXFOR library; (ii) the generation of evaluated nuclear data files for ^{151}Sm and ^{232}Th. The choice of isotopes is related to the impact of available completely analyzed experimental data measured at n_TOF at CERN. In addition different methods have been used for the evaluation. The evaluated file for ^{151}Sm is based on semi-microscopic approaches in the energy region between 1keV and 30MeV, while the ^{232}Th is a complete evaluated data file up to 150MeV generated via standard methods. The novel feature of the ^{232}Th file is the inclusion of covariance information and the extension in energy to 150MeV. In the following the main activities are outlined and some details are presented.

Modeling

The knowledge of the relevant (n,xn) cross sections is important to reliably determine the neutronics of a reactor system. For most nuclei the (n,xn) cross section data are scarce and often contradictory. Therefore nuclear models are extensively used for the generation of evaluated data files. Usually the classical exciton model or statistical calculations are applied with good success. In order to gain in predictive power we aimed at a more microscopic description and applied the multistep direct reaction mechanism of Tamura, Udagawa and Lenske [1] for the first step and evaporation processes for the further steps. In addition the multistep compound reaction mechanism [2] has been taken into account. Both are included in the program package EMPIRE-II [3]. Especially, we have evaluated the ^{207}Pb(n,2n) cross section [4] to give a guideline to the experiments via prompt γ-spectroscopy going on at IRMM at Geel. In Figure 111 the results of the calculation are compared with the data of Vonach et al. [5]. In the right part of Figure 111 the ^{207}Pb(n,2nγ) cross section for the transition from the first 2^+ state to the ground state is displayed. The measured cross section for this transition lies within the uncertainties of our calculation. In addition, calculations with the exciton model included in TALYS [6] lead to similar results for the ^{207}Pb(n,2n) cross sections.

Similar calculations have also been performed with EMPIRE-II for ^{232}Th(n,3n). However, the results are less reliable because the fission channel is not properly included in the published version of EMPIRE-II.

The determination of (n,xn) cross sections via prompt γ-spectroscopy is usually restricted to reactions leading to residual nuclei with even mass number. In these nuclei almost the complete cascade decays through the lowest lying 2^+ and 4^+ states. Odd mass nuclei do not show this simple level scheme. However, within the project we could show that for several odd mass nuclei the method can also be applied if the sum over certain transitions is taken [7].

A major goal of the modeling activities was focused on the dispersive optical model which is based on the analyticity of the optical potential. Taking into account this basic property provides a significant improvement of the quality of phenomenological optical potentials. In a

first step closed-form solutions of the dispersion relations in the nucleon-nucleus optical model have been derived for both standard Woods-Saxon volume and surface contributions [8] using the energy dependence of the imaginary parts suggested by Brown and Rho [9] and Delaroche et al. [10]. Using these expressions a code for the calculation of the dispersion relation between real and imaginary parts of the nuclear optical model potential has been developed within the project [11]. The use of this package in optical model parameter search codes allows for an efficient and consistent dispersive analysis. As an example a first complete analysis of neutron-^{27}Al scattering has been made with this dispersive optical model [12]. Extensions to deformed nuclei, e.g. actinides, are in progress in order to provide a consistent coupled-channel optical model potential. A first application of the approach is expected in the forthcoming evaluation of ^{234}U [13].

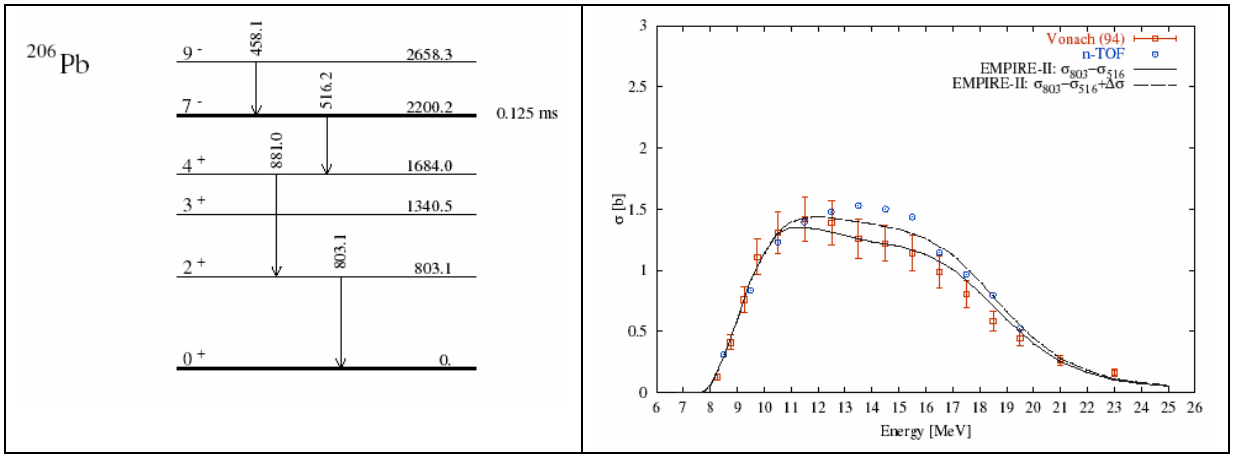

Figure 111: Level scheme of ^{206}Pb and the calculated γ-transitions (left figure). Prompt ^{207}Pb(n,2nγ) cross section for the E_γ=803 keV transition in ^{206}Pb calculated with EMPIRE-II using the microscopic Hartree-Fock-BCS level densities (right figure). The experimental data are from Vonach et al. [5] and the preliminary results obtained within the n_TOF-ND-ADS project. Two extrem assumption regarding the unknown branching ratios have been made, i.e.(i) all transitions are trapped in the isomeric 2^+ state (dashed line) and (ii) all transitions are prompt into the ground state (solid line).

Evaluation

Considerable effort was devoted to the generation of covariance matrices for the capture experiments with C_6D_6 detectors at the n_TOF facility in order to provide nuclear cross sections with complete covariance information for the EXFOR library. This task of the n_TOF-ND-ADS experiment presents a novelty although the procedure for covariance determination is well known and straightforward and should be performed for each experiment. Nevertheless the given information is restricted in most cases to the mean standard deviation of the statistical and systematic uncertainties. In principle the inclusion of covariance information is foreseen in the EXFOR-format, but it has actually never been used in practice so far.

A complete covariance analysis for the measurements of the ^{151}Sm(n,γ)- and the ^{232}Th(n,γ)-cross sections in the energy region between 1keV and 1MeV was performed [14,15]. Both measurements apply the total energy detector technique using an experimentally validated Pulse Height Weighting Technique. The determination of the covariance matrix of uncertainties $\left\langle \Delta\sigma_\gamma^s(E)\Delta\sigma_\gamma^s(E')\right\rangle$ must follow the method of analysis and the applied corrections. An essential part of the analysis is a proper correction of the background. Performing additional measurements with empty sample holder, with a carbon sample and a

lead sample the ambient background as well as the background contributions due to the sample holder, the in-beam γ-rays and scattered neutrons were determined and the capture yield appropriately corrected. In addition, corrections for multiple scattering and self absorption, isotopic composition and inelastic scattering contributions have been applied. In case of ^{232}Th(n,γ) one had in addition to account for the radioactivity of the sample and the beam fraction incident on the sample. With the complete information from the analysis the determination of the covariance matrix is straightforward. In principle one has to distinguish between systematic and statistical errors, where the latter are directly related to the count rates of the detectors and contribute only to the diagonal of the covariance matrix. Systematical errors stem typically from normalisations and the corrections as discussed above. In order to account properly for the uncertainties of the correction terms either count rates of additional experiments or parametrized forms of the correction terms including covariances have been determined.

In Figure 112 and 5.1.3 the final results of the covariance analysis of the ^{151}Sm(n,γ) and ^{232}Th(n,γ) cross sections are shown. In the left part of the figures the cross sections with the total uncertainties are shown. For ^{151}Sm(n,γ) the total error is in the order of 6%, where the major part stems from the systematics errors (~4-5%), while the statistical errors are varying between 1% at 3keV and about 4% in the energy region above 100keV. For the measurement of the ^{232}Th(n,γ) the systematic errors are about 6% and the statistical uncertainties typically about 1.5%. The normalized covariance matrices are shown on the right hand side of the figure using the quantity

$$C(E,E') = \frac{\left\langle \Delta\sigma_\gamma^s(E)\Delta\sigma_\gamma^s(E') \right\rangle}{\sqrt{\left\langle \left(\Delta\sigma_\gamma^s(E)\right)^2 \right\rangle \left\langle \left(\Delta\sigma_\gamma^s(E')\right)^2 \right\rangle}} \quad , \qquad (0.0.1)$$

where the number of the mesh point in energy is given on the x- and y-axis. In this representation the diagonal elements C(E,E) are always 1.

The difference in the analyses of the capture experiments of ^{151}Sm and ^{232}Th shows up in the covariance matrix and is related to the treatment of the neutron flux. For the determination of the ^{151}Sm(n,γ) cross section a reference measurement to Au was performed in the energy region between 5 and 200 keV, thus avoiding a precise determination of the incident neutron flux. Due to the reference measurement some systematic errors cancel, but on the other hand statistical uncertainties due to the Au-measurement have to be added. For the analysis of the ^{232}Th(n,γ) data the energy dependence of the neutron flux measured by the PTB group has been used as a standard. The corresponding normalization constant was determined by the comparison with the double peak of saturated resonances at about 20 eV. In order to check the cross section values also a comparison with a reference measurement with Au was performed and satisfactory agreement found. Due to the normalization of the PTB flux the covariance matrix exhibits large nondiagonal elements as can be seen Figure 112 (b).

Evaluated nuclear data files have been generated for ^{232}Th and ^{151}Sm including the new data obtained within the n_TOF-ND-ADS project. The two evaluation follow a different concept. Due to the scarcity of data the evaluation of ^{151}Sm is based on semi-microscopic approaches [16], while the evaluation of ^{232}Th makes use of standard techniques [17]. At present the re-evaluation of ^{232}Th is of great interest because a proper description of the reaction cross sections of ^{232}Th is a requirement for the critical evaluation of the Thorium-Uranium fuel cycle and the design of corresponding reactor systems. Therefore, the generation of a complete evaluated data file for this isotope has been performed [17] which covers the whole energy region from thermal energies up to 150MeV and includes not only the available n_TOF data, but also experimental data from other groups which have become available recently. The latter data are essentially neutron total [18], capture [19,20] and fission cross sections [21], as well as the neutron and charged-particle emission spectra and particle yields [22,23] which have been used for improvements of theoretical models. Above the resonance

region the evaluations are based on the deformed optical model, statistical calculations using the GNASH code and the Kalbach-Mann model for the double-differential emission cross sections for neutrons and charged particles. In addition the ALICE-IPPE code is used to describe the emission cross sections for deuterons, tritons and α-particles. Applying the method of unrecognized error estimation a complete statistical analysis has been performed and covariance matrices for the most important reactions have been determined.

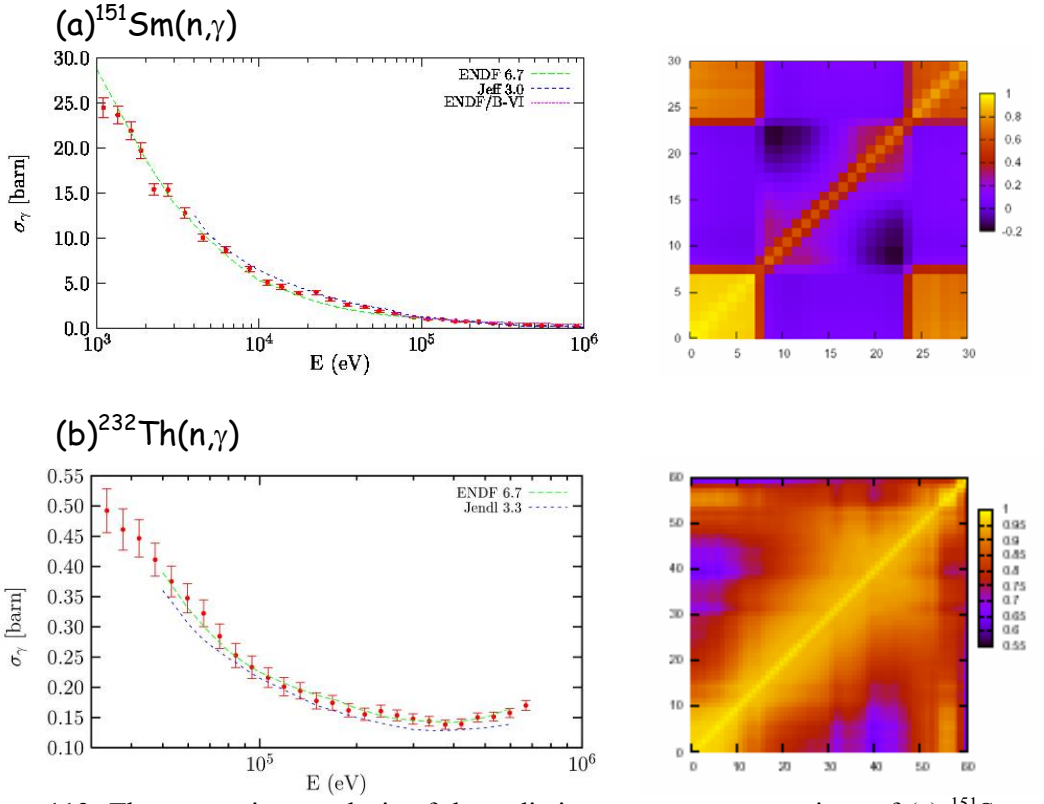

Figure 112: The uncertainty analysis of the radiative capture cross sections of (a) ^{151}Sm and (b) ^{232}Th. The left figure gives the cross section data with the total uncertainties and a comparison with the available evaluated nuclear data file. The right figure shows the covariance matrix normalized to the diagonal elements (for details see text). The scale gives the number of the mesh point of the energy.

A major effort of this re-evaluation has been devoted to describe the total and elastic scattering cross sections via a coupled-channel optical model. Using a standard parametrized ansatz of the coupled-channel optical potential, the parameters have been adjusted to reproduce the available experimental neutron and proton cross section data for the whole actinide region. The inclusion of the recent high precision measurements [18] of the total cross sections for ^{232}Th and ^{238}U in the optimization procedure is of great importance. The parameters differ only little from previous values, but result in an essential reduction of the uncertainties of the evaluation. An essential improvement could be achieved for the radiative capture cross section, where rather discrepant experimental data were available. The recent measurements at the n_TOF facility at CERN and at Geel [19] resolve these discrepancies and coincide with the values from evaluations. A comparison of the new evaluation with experimental data is given in Figure 113 The recently measured ^{232}Th(n,2n) cross sections [24] represent another important input into the re-evaluation of ^{232}Th. The discrepancies between different experimental are particularly striking for this reaction. The results for ^{232}Th(n,2n) are displayed in Figure 114. The experimental determination of the ^{232}Th(n,3n) and ^{232}Th(n,5n) cross sections performed at Louvain-la-Neuve within the n_TOF-ND-ADS project would present the first data on these reactions. A further important input to the re-evaluation, especially at higher energies, are the novel fission data measured at the n_TOF

facility at CERN. Here, even at energies below 20 MeV where sufficient data are available there are still

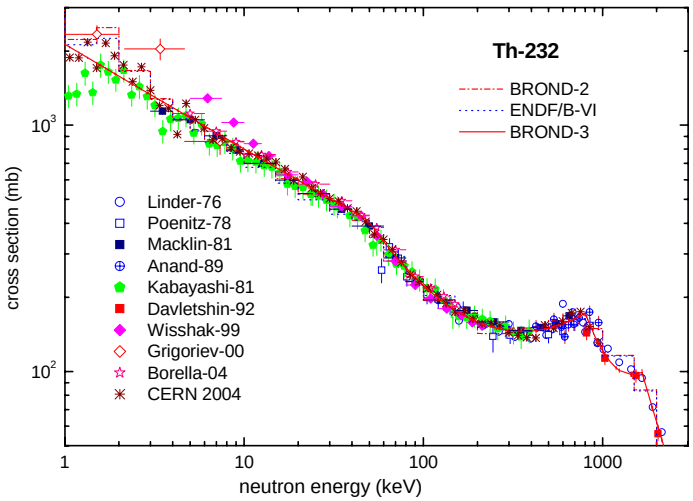

Figure 113: Comparison of the experimental radiative capture cross section of ^{232}Th with the recent re-evaluation (BROND-3), the old BROND-2 and the ENDF/B-VI evaluation.

some open questions which should be clarified by the measurements within the project. However, at present it is too early to make any conclusions because the first raw and uncorrected data from the PPAC chambers show a much more pronounced structure related to next chance fission than previous experiments (see Figure 115). Whether this is true physics or an artefact of the novel detector has still to be verified. An analysis including recent measurements of the prompt fission multiplicity [25] as well as a more realistic evaluation of fission neutron spectra has been performed.

The present re-evaluation of ^{232}Th, however, can only be considered as a first version because the n_TOF experiments on fission cross section as well as the capture measurements in the resonance region were not analyzed in time to be included in this evaluation. A first analysis of the capture data obtained at the n_TOF facility at CERN indicates that their inclusion will significantly improve the description of the resonance region. In the present version the resonance region is based on the BROND-3 evaluation and no separate analysis of the resonance region has been performed. An update of the file will be performed when all n_TOF data can be included.

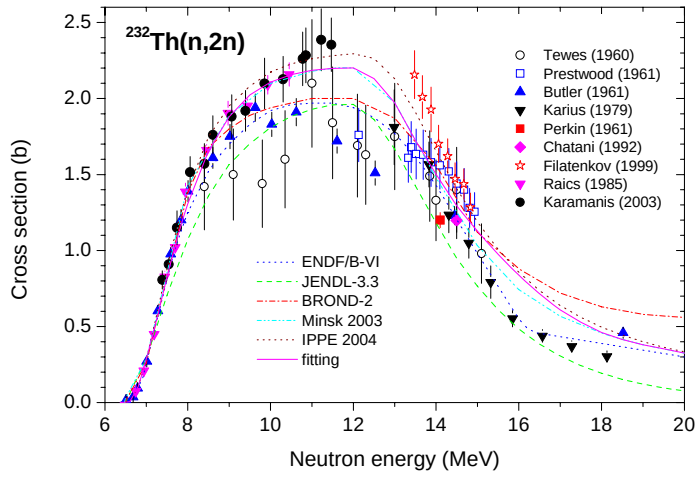

Figure 114: Comparison of the experimental ^{232}Th(n,2n) cross section with different evaluations. The new re-evaluation is here denoted by IPPE2004.

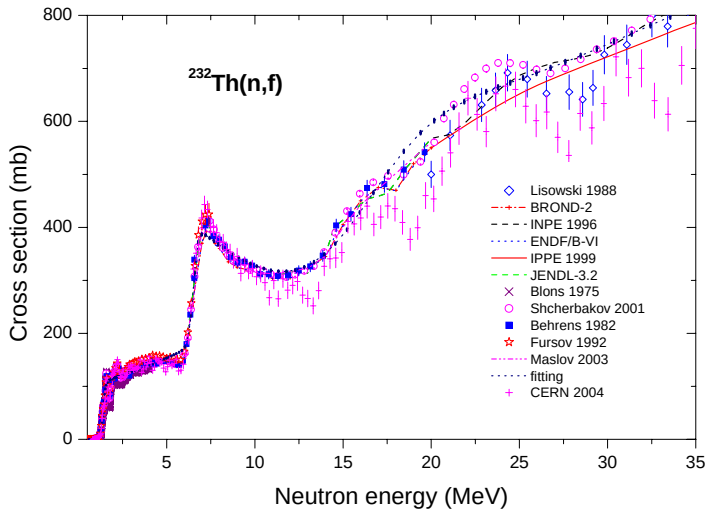

Figure 115: Comparison of the raw fission data based on the ratio of the count rates of the ^{232}Th and ^{235}U loaded PPAC chambers with available experimental data. For comparison the evaluations of fission cross section are also shown.

The evaluated data file for ^{151}Sm is based on a relatively small amount of experimental data. Therefore an evaluated file [16] suited for activation calculation has been generated on the basis of realistic microscopic models. In particular the specific nuclear structure of the Sm-isotopes had to be taken into account properly. The file covers the energy range between 1keV and 30MeV and includes all relevant reaction channels. The reaction calculations are based on a deformed semi-microscopic and Lane consistent nucleon-nucleus optical potential which has been obtained by folding the nuclear density of the nucleus with an effective nucleon-nucleon interaction [26] obtained from Brückner-Hartree-Fock calculations in nuclear matter. The axially deformed nuclear density has been obtained from Hartree-Fock-Bogoliubov calculations [27] using the Gogny D1S interaction [28]. This deformed optical potential has been used in coupled-channel calculations in ECIS with 5 coupled channels in order to evaluate the transmission coefficients as well as the total, elastic and non-elastic cross sections. For the calculation of reaction cross sections the TALYS code [6] has been used with averaged transmission coefficients. The optical models for composite particles (d, t, ^{3}He, α) have been obtained via folding of the nucleon-nucleus potential with the projectile density. The files MF=3, 8 and 10 have been generated for all relevant channels. In Figure 116 the radiative capture cross section and the inelastic scattering cross sections for ^{151}Sm are displayed. In order to reproduce the experimental data measured at the n_TOF facility the parameters Γ_γ=123meV and average level distance D_0=1,12eV had to be chosen. The Γ_γ-value fits well to the experimental finding, where Γ_γ-values between 40 and 150meV with an average value of Γ_γ=98meV were extracted from experiment. The average spacing is slightly lower than the experimentally obtained value D_0=1,48eV. Finally, it should be remarked that this semimicroscopic evaluation is fully consistent with a recent semimicroscopic evaluation of Eu-isotopes [29].

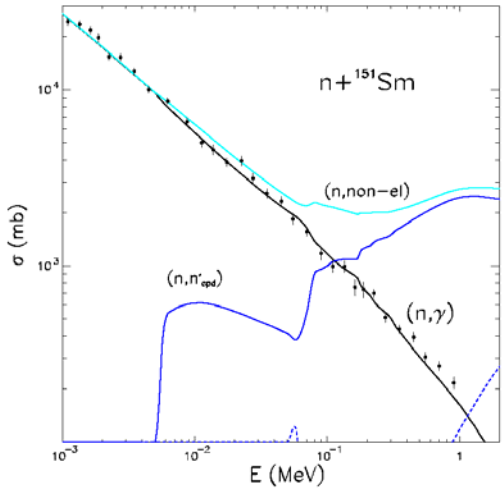

Figure 116: Microscopically based evaluated radiative capture, inelastic and total non-elastic cross sections for neutron scattering on ^{151}Sm. For comparison the measured values of the radiative capture cross sections measured in the n_TOF-ND-ADS project are shown.

The extension of the energy range of evaluated nuclear data files requires due to scarce data sets the extensive use of nuclear models. This is also true for nuclei which are not accessible to experiment. In the past the deficiencies of evaluated data could be compensated by extensive testing. Today one increasingly relies on simulation, however, which require for their reliability the knowledge of uncertainties of nuclear data and their associated covariances. The determination of covariance matrices for experimental data is straightforward. However, there exists no standard technique for covaraince determination if only few data are available and extensive modeling is required for the generation of an evaluated data file. This problem has been addressed within the project n_TOF-ND-ADS as many nuclei in the actinide region are not accessible to experiment. Based on a previous work on uncertainties in optical model calculations three types of contributions to the uncertainty of model evaluations have been identified, i.e. (i) the parameter uncertainties, (ii) the numerical uncertainties and (iii) the model deficiency. While (i) and (ii) are well under control, the contribution of the model deficiency is undefined. A procedure for a reliable estimate of the covariance matrix for integral cross sections [30] was suggested. The method has been successfully applied to the determination of the covariance matrix for several reactions on Fe.

In summary, the essential goal of a fast transfer of the data measured within the n_TOF-ND-ADS project has been built up and first EXFOR- as well as ENDF-Files have been generated for those data available within the time constraints. Improvements are expected with the inclusion of the fission and capture data (in the resonance region) in the evaluated file of ^{232}Th. An update of the evaluated files of ^{233}U and ^{234}U is foreseen within the Co-ordinated Research Project (CRP) on Thorium-Uranium cycle elements [13] which will include the ^{233}U and ^{234}U capture and fission data measured at CERN n_TOF. The developments on optical potential as well as covariances represent an important basis for future evaluations.

References

[1] T. Tamura, T. Udagawa, and H. Lenske, Phys. Rev. C **26**, 379 (1982).

[2] H. Nishioka, J.J.M. Verbaarschot, H.A. Weidenmüller, and S. Yoshida, Ann. Phys. **172**, 67 (1986).

[3] M. Herman, EMPIRE-II, http://www-nds.iaea.org/empire/.

[4] Raskinyte and H. Leeb, *The ^{207}Pb(n,2n) reaction within EMPIRE-II*, ATI-NDC-2004-01.

[5] H. Vonach, A. Pavlik, M.B. Chadwick, R. Haight, R.O. Nelson, S.A. Wender, and P.G. Young, Phys. Rev. C **50**, 1952 (1994).

[6] A.J. Koning, S. Hilaire, and M.C. Duijvestijn, TALYS: Comprehensive nuclear reaction modelling, Proceedings of the International Conference on Nuclear Data for Science and Technology – ND2004, Sep. 26-Oct. 1, 2004, Santa Fe, USA, to be published.
[7] M. Tutz, *Neue Methoden zur Bestimmung von (n,xn)-Wirkungsquerschnitten bei schweren Kernen*, Diplomarbeit, TU Wien, October 2000.
[8] J.M. Quesada, R. Capote, A. Molina, M. Lozano, and J. Raynal, Phys. Rev. C **67**, 067601 (2003).
[9] G.E. Brown and M. Rho, Nucl. Phys. **A372**, 397 (1981).
[10] J.P. Delaroche, Y. Wang, and J. Rapaport, Phys. Rev. C **39**, 391 (1989).
[11] J.M. Quesada, R. Capote, A. Molina, M. Lozano, Computer Physics Communications **153**, 97 (2003).
[12] A. Molina, R. Capote, J.M. Quesada, and Lozano, Phys. Rev. C **65**, 034616 (2002).
[13] Co-ordinated Research Project on Thorium-Uranium Cyle Elements, Nuclear Data Section of the International Atomic Energy Agency, Vienna (2003-2005).
[14] M.T. Pigni, H. Leeb and the nTOF Collaboration, *Covariance analysis for ^{151}Sm(n,□) at the n_TOF facility at CERN*, ATI-NDC-2004-02.
[15] M.T. Pigni, H. Leeb and the nTOF Collaboration, *Covariance analysis for ^{232}Th(n,□) at the n_TOF facility at CERN*, ATI-NDC-2004-03.
[16] E. Bauge, P. Dossantos-Uzaralde, C. Le Luel, H. Leeb, M.T. Pigni and the nTOF Collaboration, *An Activation File of ^{151}Sm Based on Microscopic Calculations*, ATI-NDC-2005-02.
[17] A.V. Ignatyuk, E.V. Gai, V.P. Lunev, Yu.N. Shubin, N.N. Titarenko, A. Mengoni, H. Leeb, *Re-evaluation of Neutron Cross Sections for Th-232 on the basis of n_TOF measurements*, ATI-NDC-2005-01.
[18] W.P. Abfalterer et al. Phys. Rev. C **63**, 044608 (2004).
[19] A. Borella, A. Brusegan, K. Volev et al., submitted to Nucl. Phys. A (2004).
[20] A. Aerts, E. Berthoumieux, F. Gunsing, and L. Perrot, Internal Report DAPNIA-04-125 (2004).
[21] O. Scherbakov, A. Donets, A. Evdokimov et al., in Nuclear Data for Science and Technology (Tsukuba 2001), E. K. Shibata, JAERI, 2002, v. 1, p. 230.
[22] E. Raeymackers, S. Benck, N. Nica et al., Atomic Data and Nuclear Data Tables 87, 231 (2004).
[23] V. Blideanu et al., Proceedings of the TRAMU-2003 Meeting, GSI Darmstadt, September 2003, http://www-wnt/gsi.de/tramu/blideanu.pdf .
[24] D. Karamanis, S. Andiamonje, P.A. Assimakopoulos et al., Nuclear Instruments and Methods A **505**, 381 (2003).
[25] O.I. Batenkov et al., Report on ISTC Project 1145 (2003).
[26] E. Bauge, J.P. Delaroche, and M. Girod, Phys. Rev. C **58**, 1118 (1998).
[27] E. Bauge, J.P. Delaroche, M. Girod, G. Haouat, J. Lachkar, Y. Patin, J. Sigaud, and J. Chardine, Phys. Rev. C **61**, 034306 (2000).
[28] J.F. Berger, M. Girod, and D. Gogny, Comput. Phys. Commun. **63**, 365 (1990); J. Dechargé and D. Gogny, Phys. Rev. C **21**, 1568 (1980).
[29] E. Bauge, NEA/OECD, JEFF-Doc 951.
[30] H. Leeb, M.T. Pigni and I. Raskinyte, *Covariances For Evaluations Based On Extensive Modelling*, Proceedings of the International Conference on Nuclear Data for Science and Technology – ND2004, Sep. 26-Oct. 1, 2004, Santa Fe, USA, to be published.

Nuclear Data dissemination Platform

Contributed by *A Mengoni and V Vlachoudis* (CERN)

Introduction

Neutron data libraries presently in use are derived from evaluations based on experimental data or from nuclear models, used where experimental data are lacking or inconsistent. The reliability of design and safety studies for the development of advanced nuclear technologies is critically dependent on the availability of complete evaluations of basic nuclear data with high accuracy and energy resolution. Some of the evaluations currently in the nuclear databases fall well below the required standard. Two examples may illustrate the point

- Resonance cross sections are difficult to evaluate from experimental data, and they cannot be predicted by theory to the required level of accuracy by the present day understanding of nuclear physics;
- Nuclear data format allows the specification of the uncertainty in the data evaluation, but this information is basically absent from the evaluated data files. The numerical values given in these data files are expectation values for use in applications without an estimation of their statistical significance.

In parallel to the experimental activity, a specific activity performed within the framework of the n_TOF-ND-ADS Project addressed the need to develop a software environment to allow the efficient and coherent storage, retrieval and processing of nuclear data in their various formats. This proposal aimed at designing and implementing the tools to provide high quality and up-to-date nuclear reaction information for applications. The environment takes advantage of the latest development of the programming languages addressing the need and capabilities of modern computers. Emphasis is put on how cross-sections and other quantities coming from the experiment and nuclear model codes are categorised and stored. Accordingly, a comprehensive discussion on the data processing and reduction methods to obtain cross sections, and the features of the data format used so far, have taken place during the period in which the project has been active.

Data processing and dissemination of the results for the n_TOF project

The n_TOF experiment produced a large quantity of high-quality data. It is important to consider, as an example, that the operation of the n_TOF Total Absorption Calorimeter used for capture cross section measurements required a data transfer and storage capabilities of 2.5TB/day (2.5×10^{12} bytes/day). In order be able to store, retrieve and manipulate these data efficiently, the CERN infrastructure (CASTOR) has been used, with ad-hoc built software exploiting the ROOT code system developed at CERN. ROOT a sophisticated extensible OO package that a group of CERN scientists has developed in the recent years designed to store and retrieve efficiently large data sets and to perform data analysis, manipulation and visualization operations.

As they are produced, all the results of experimental measurements have to be gathered in an appropriate data base for convenient access by users: general availability and accessibility of the data is, next to scientific publications, the most important product of any experiment.

Two different strategies for the dissemination of the results of the measurements performed within the n_TOF-ND-ADS Project have been considered. The first one consisted in the development of a database based on the Object Oriented programming technique. The aim of this development is to offer an efficient and state-of-the-art data repository for the data, which alleviates or solve all the problems connected with the data formats. This development would allow backward compatibility, but, at the same time, allow the evolution of the data format without damaging running codes based on the old format or on this new format.
The second option considered a web-based interface providing to the evaluation programs either via ASCII files or directly via a set of calls accessible via FORTRAN or C++. Check and comparison tasks will be implemented so that they will become integral part of the n_TOF database and can be highly automated.
The second of these options has been adopted in consideration of the fact that most of the results of the measurements performed within the framework of the project became available only at the end of the project itself and therefore the need for an immediate diffusion through a web-based interface is considerable more efficient for this purpose. In the next section we describe the technical details of this new proposed format.

The n_TOF Dissemination Web Interface

A web-based dissemination platform has been built and is presently (January 2006) running on the n_TOF main web server (http://www.cern.ch/ntof). The web interface runs on two different modes:

- an editing mode, reserved for experimentalists and with restricted access, which is used in input the information necessary to fully describe an experiment
- a browsing/retrieving mode which allows users to gather all the information available in the database concerning a given measurement.

Numerical data can be downloaded directly from the server. The most used format for storing the numerical data is free-format ASCII but other formats can be used as well. For example, ROOT files or histogram files to be used by people doing the data analysis can be stored as well.

A screenshot of the main page of the n_TOF dissemination web interface is shown in the Figure xx below. The database can be browsed from the navigation tool on the left-hand side of the page. The measurements performed have been classified into three categories: “capture”, “fission”, and “others” for easy access.

The database is continuously updated by the n_TOF collaborators working on the experimental data analysis. As most of the experiments performed during the course of the project have been completed only recently, the database contains at present a subset of all the available entries. However, it is expected that the inclusion of the results of all the measurements performed within the framework of the project will be included into the database, together with the related documentation.

One important point to consider here is that the n_TOF Collaboration Board has established a strict policy concerning the priorities in the dissemination of the results obtained. Very briefly, the priority in the dissemination task is given to the publication

of a paper in a wide-diffusion journal in which the results of a given measurement are presented. After the publication of a paper, the data related to a given measurement can be released to the community for further reference. For example, as soon as the paper related to a given measurement has been published, the data are distributed for compilation into the EXFOR data library following the commitments of the project. Of course, the preferred mean for the diffusion of the numerical data as well as of all the related documentation of a given measurement is the n_TOF Dissemination web-interface on the main n_TOF web-server, as discussed in this report.

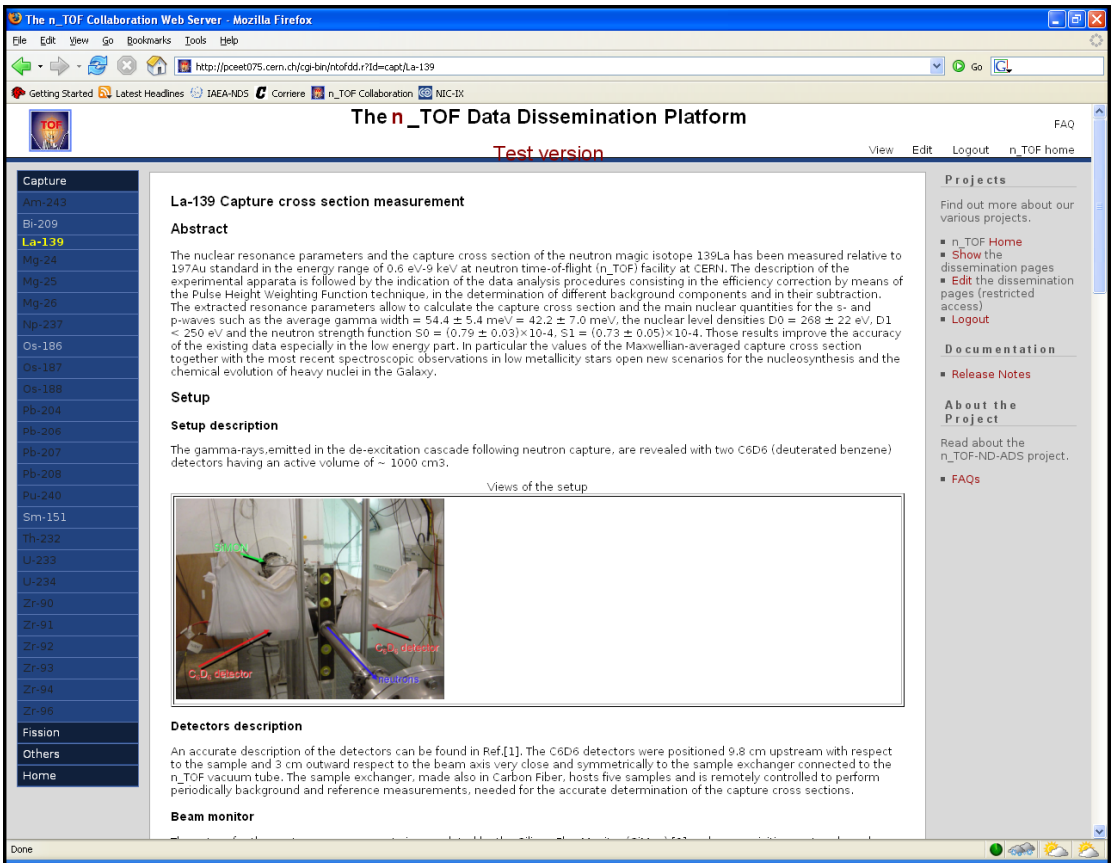

Figure 117: Screenshot of one of the pages of the the n_TOF Data Dissemination Platform website. The web address of the site is: http://www.cern.ch/ntof/DataDiss.

Annex

PhD & Master Theses

In connection with the n_TOF-ND-ADS Project, a considerable amount of activity has been produced within the framework of PhD and/or for Master Theses. These are listed here below.

PhD Theses

[1] Misure di sezioni d'urto neutroniche per La-139 e Np-237 ad n_TOF
R. Terlizzi
Universita' degli Studi di Bari, Italy. February 2006.

[2] Mesure de la section efficace de capture neutronique du ^{232}Th à n_TOF au CERN
G. Aerts
Universite de Paris XI, UFR Scientifique d'Orsay, France, September 2005.

[3] Mesures de sections efficaces de fission induites par neutrons
L. Ferrant
Universite de Paris Sud, Orsay, France, Septermber 2005.

[4] Measurement of the ^{234}U(n,f) cross section with PPAC detectors at the n_TOF facility
C. Paradela Dobarro
Universidade de Stantiago de Compostela, Spain, June 2005.

[5] New radiative neutron capture measurements of ^{207}Pb and ^{209}Bi
C. Domingo Pardo
Universidad de Valencia – CSIC, Valencia, Spain, December 2004.

[6] Mesure de sections efficaces de réactions (n,xn) par spectroscopie gamma prompte auprès d'un faisceau à très haut flux instantané
S. Lukic
Université Louis Pasteur de Strasbourg, France. October 2004.

[7] Trasmutation of Nuclear Waste in Accelerator Driven Systems
A. Herrera-Martínez
University of Cambridge, UK. September 2004.

[8] Détection de neutrons avec un détecteur de type Micromegas: de la Physique nucléaire à l'imagerie
J. Pancin
Universite Bordeaux I, France. June 2004.

[9] Μέτρηση της Ενεργού διατομής σύλληψης νετρονίου από το ασταθές καίσιο 135, (Neutron capture studies on unstable Cs-135 for nucleosynthesis and transmutation)
N. Patronis
Department of Physics, The University of Ioannina, Greece. March 2004.

[10] Mesures et analyses des sections efficaces neutroniques totales et de capture radiative des Iodes 127 et 129 de 0.5 eV à 100 keV
G. Noguere
Université Louis Pasteur de Strasbourg, France. December 2003.

[11] Calculo del potencial optico nucleon-nucleo para reacciones nucleares de interes en la transmutacion de residuos radiactivos
A. Molina Coballes
Universidad de Sevilla, Spain. September 2003.

[12] Measurements of neutron capture cross sections at the n_TOF facility at CERN
S. Marrone
Universita' degli Studi di Bari, Italy. September 2002.

In preparation

[1] Mesure de la section efficace de capture neutronique du l' ^{234}U par le calorimètre 4π de n_TOF au CERN pour les réacteurs de génération IV
W. Dridi
Université d'Evry Val d'Essonne, France. To be submitted in November 2006.

[2] The 187Re/187Os pair: galactic evolution and cosmo-chronometry
M. Mosconi
University of Karlsruhe, Germany. To be submitted in 2006.

[3] Πειραματική μελέτη της ενεργού διατομής σχάσης νετρονίου σε U-234 και Th-232
(Experimental investigation of neutron induced fission on U-234 and Th-232)
D. Karademos
Department of Physics, The University of Ioannina, Greece. To be submitted in 2006.

[4] Μελέτη της αντίδρασης ^{241}Am(n,2n)
(Study of the ^{241}Am(n,2n) reaction)
G.Perdikakis
National Technical University of Athens, Greece. To be submitted in 2006.

[5] Τροποποίηση των χαρακτηριστικών της δέσμης (0.025 eV – 1 GeV) και πειράματα ενεργού διατομής σύλληψης νετρονίου υψηλής ακριβείας στην εγκατάσταση n_TOF του CERN
(Modification of the neutron beam features (0.025 eV - 1 GeV) and high precision measurements of neutron capture cross sections, at the n_TOF facility at CERN).
T. Papaevangelou
Aristotle University of Thessaloniki, Greece. To be submitted in 2006.

[6] Μέτρηση ενεργών διατομών αντιδράσεων νετρονίων με το 4π TAC (Θερμιδόμετρο Ολικής Απορρόφησης) στην εγκατάσταση n_TOF του CERN και με ανιχνευτή πυριτίου στον επιταχυντή TANDEM του ΕΚΕΦΕ «Δημόκριτος»
(Neutron induced reactions cross sections measurements, with the 4π Total Absorption Calorimeter, TAC, at the n_TOF facility (CERN) and with silicon detectors at the TANDEM accelerator - NCSR, Demokritos)
C. Lampoudis
Aristotle University of Thessaloniki, Greece. To be submitted in 2006.

Master Theses

[1] Il calorimetro γ di n_TOF: misure di sezioni d'urto neutroniche di interesse astrofisico, per la trasmutazione di scorie nucleari e la produzione di energia
C. Massimi
Tesi di Laurea, Universita' degli Studi di Bologna, Italy, 2004.

[2] Determinação da secção eficaz de captura neutrónica do ^{94}Zr utilizando o espectrómetro TOF no CERN.
L. Marques
Estágio Profissionalizante da Licencitura em Engenharia Física (Master Thesis), Lisbon, Portugal, December 2004.

[3] Studio di sezioni d'urtro neutroniche presso la facility n_TOF: il caso del Sm-151
D. Muzzolini
Universita' degli Studi di Trieste, Italy, Anno Accademico 2001/2002.

[4] Entwicklung eines optimierten C6D6-Detektors zur Messung von stellaren (n,gamma)-Querschnitten am CERN n_TOF-Spektrometer
R.. Plag
Diploma thesis, University of Karlsruhe, February 2001

n_TOF Winter schools

Two schools have been organized by the n_TOF Collaboration during the course of the project. A first school took place in “Les Houches”, France, during the winter of 2003 (see Figure 118, top panel).

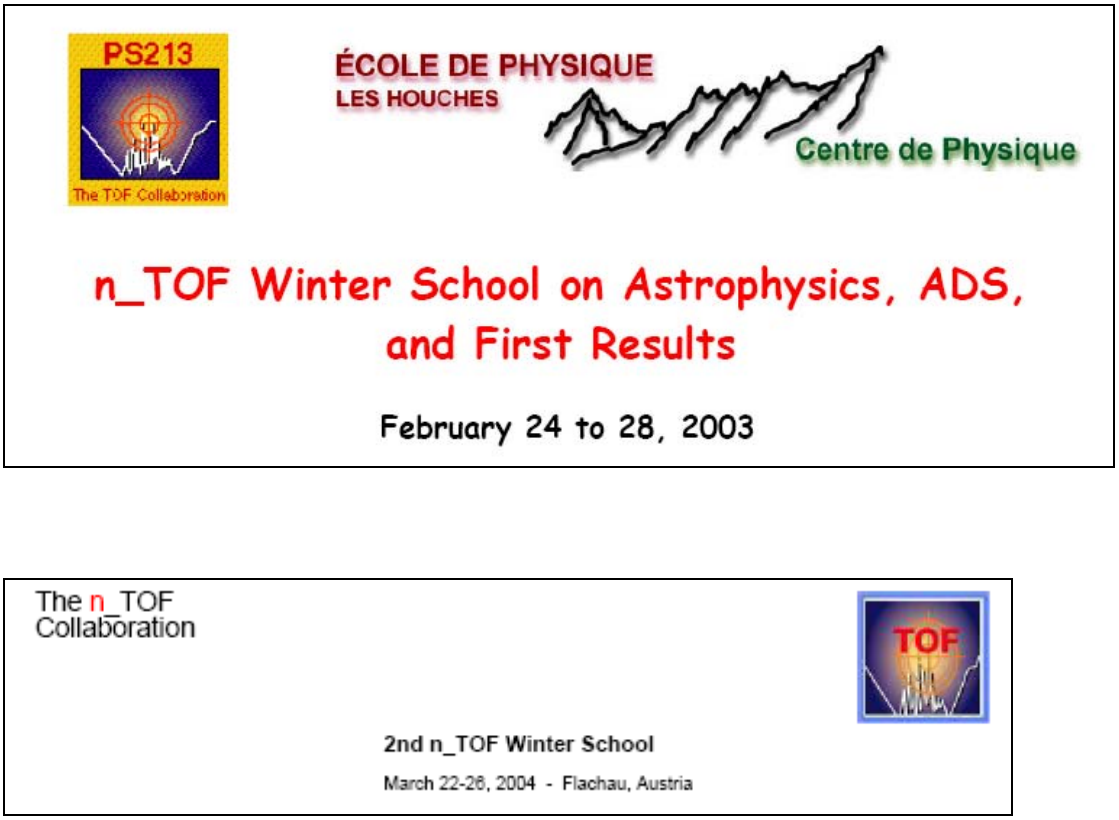

Figure 118: announcements of the two n_TOF winter schools held in 2003 and 2004.

The Second n_TOF winter school took place in “Flachau”, Austria, during the winter of 2004. The participation to both schools included, in addition to members of the n_TOF Collaboration participating actively to the experimental activities, also students, young researchers and others from the nuclear physics and astrophysics communities.

Publications

We report here only the list of full papers published in international journals. The full list of publications with all the papers published in Conference Proceedings is available on the n_TOF main webserver at the link www.cern.ch/ntof in the "Documents" section.

[1] *First results from the neutron facility (n_TOF) at CERN*
C. Borcea, S. Buono, P. Cennini, M. Dahlfors, V. Dangendorf, A. Ferrari, G. Garcia-Munoz, Y. Kadi, V. Lacoste, R. Nolte, E. Radermacher, C. Rubbia, F. Saldana, V. Vlachoudis, T. Weierganz, L. Zanini.
Applied Physics A**74** (2002) S55-7.

[2] *Measurement of the n_TOF beam profile with a micromegas detector*
J. Pancin et al.
Nuclear Instruments and Methods in Physics Research Section A: Accelerators, Spectrometers, Detectors and Associated Equipment, Volume **524**, Issues 1-3, 21 May 2004, Pages 102-114.

[3] *Results from the commissioning of the n_TOF spallation neutron source at CERN*
C. Borcea, P. Cennini, M. Dahlfors, A. Ferrari, G. Garcia-Muñoz, P. Haefner, A. Herrera-Martínez, Y. Kadi, V. Lacoste, E. Radermacher, F. Saldaña, V. Vlachoudis, L. Zanini, C. Rubbia, S. Buono, V. Dangendorf, R. Nolte and M. Weierganz.
Nuclear Instruments and Methods in Physics Research Section A: Accelerators, Spectrometers, Detectors and Associated Equipment, Volume **513**, Issue 3, 11 November 2003, Pages 524-537.

[4] *An optimized C6D6 detector for studies of resonance-dominated (n,g) cross-section*
R. Plag, M. Heil, F. Käppeler, P. Pavlopoulos, R. Reifarth, and K. Wisshak, and The n_TOF Collaboration.
Nuclear Instruments and Methods in Physics Research Section A: Accelerators, Spectrometers, Detectors and Associated Equipment, Volume **496**, Issues 2-3, 11 January 2003, Pages 425-436.

[5] *Pulse shape analysis of liquid scintillators for neutron studies*
S. Marrone, D. Cano-Ott, N. Colonna, C. Domingo-Pardo, F. Gramegna, E. Gonzalez-Romero, F. Gunsing, M. Heil, F. Kaeppeler, P.F. Mastinu, P.M. Milazzo, T. Papaevangelou, P. Pavlopoulos, R. Plag, R. Reifarth, G. Tagliente, J.L. Tain, K. Wisshak, and The n_TOF Collaboration.
Nuclear Instruments and Methods in Physics Research Section A: Accelerators, Spectrometers, Detectors and Associated Equipment, Volume **490**, Issues 1-2, 1 September 2002, Pages 299-307.

[6] *Neutron cross-section measurements in the Th-U cycle by the activation method*
D. Karamanis, S. Andriamonje, P. A. Assimakopoulos, G. Doukellis, D. A. Karademos, A. Karydas, M. Kokkoris, S. Kossionides, N. G. Nicolis, C. Papachristodoulou, C.T. Papadopoulos, N. Patronis, P. Pavlopoulos, G. Perdikakis, R. Vlastou, and The n_TOF Collaboration.
Nuclear Instruments and Methods in Physics Research Section A: Accelerators, Spectrometers, Detectors and Associated Equipment, Volume **505**, Issues 1-2, 1 June 2003, Pages 381-384.

[7] *A low background neutron flux monitor for the n_TOF facility at CERN*
S. Marrone, P.F. Mastinu, U. Abbondanno, R. Baccomi, E. Boscolo Marchi, N. Bustreo, N. Colonna, F. Gramegna, M. Loriggiola, S. Marigo, P.M. Milazzo, C. Moreau, M. Sacchetti, G. Tagliente, R. Terlizzi, G. Vannini, G. Aerts, E. Berthoumieux, D. Cano-Ott, P. Cennini, C. Domingo-Pardo, L. Ferrant, E. Gonzalez-Romero, F. Gunsing, M. Heil, F. Kaeppeler, T. Papaevangelou, C. Paradela,P. Pavlopoulos, L. Perrot, R. Plag, J.L. Tain, H. Wendler, and The n_TOF Collaboration
Nuclear Instruments and Methods in Physics Research Section A: Accelerators, Spectrometers, Detectors and Associated Equipment, Volume **517**, Issues 1-3, 21 January 2004, Pages 389-398.

[8] *New Experimental validation of the Pulse Height Weighting Technique for Capture cross-section measurements*
U. Abbondanno, et al. (The n_TOF Collaboration)
Nuclear Instruments and Methods in Physics Research Section A: Accelerators, Spectrometers, Detectors and Associated Equipment, Volume **521**, Issues 2-3, 1 April 2004, Pages 454-467.

[9] *Time-energy relation of the n_TOF neutron beam: energy standards revisited*
G. Lorusso, et al. (The n_TOF Collaboration)
Nuclear Instruments and Methods in Physics Research Section A: Accelerators, Spectrometers, Detectors and Associated Equipment, Volume **532**, Issue 3, 21 October 2004, Pages 622-630.

[10] *The data acquisition system of the neutron time of flight facility n_TOF at CERN*
U. Abbondanno et al. (The n_TOF Collaboration).
Nuclear Instruments and Methods in Physics Research Section A: Accelerators, Spectrometers, Detectors and Associated Equipment, Volume **538**, Issues 1-3, 11 February 2005, Pages 692-702.

[11] *Neutron Capture Cross Section Measurement of Sm-151 at the CERN Neutron Time of Flight Facility (n_TOF)*
U. Abbondanno et al. (The n_TOF Collaboration).
Physical Review Letters **93**, 161103 (2004).

[12] *Neutron capture studies on unstable Cs-135 for nucleosynthesis and transmutation*
N. Patronis, S. Dababneh, P.A. Assimakopoulos, R. Gallino, M. Heil, F. Käppeler, D. Karamanis, P.E. Koehler, A. Mengoni, R. Plag, and the n_TOF Collaboration
The Physical Review C **69**, 025803 (2004).

[13] *Measurement of the ^{241}Am(n,2n) reaction cross section, by the activation method*
G. Perdikakis, C. T. Papadopoulos, R. Vlastou, A. Lagoyannis, A. Spyrou, M. Kokkoris, S. Galanopoulos, N. Patronis, D. Karamanis, Ch. Zarkadas, G. Kalyva, S. Kossionides, and the n TOF Collaboration.
The Physical Review C. Submitted for publication (2006).

For a full account see: U. Abbondanno *et al.* (The n_TOF Collaboration), *Performance Report*, CERN, INTC-2002-037.
Available online at the link: www.cern.ch/ntof.

CERN n_TOF: Basic Parameters

Proton beam

Proton beam momentum:		**20 GeV/c**
Beam size at the target position		
σ (horizontal)		7.8 mm
σ (vertical)		5.6 mm
Intensity	dedicated	7×10^{12}
[proton/pulse]	parasitic	4.5×10^{12}
Repetition frequency (typical)		1pulse/2.4s
Pulse width		6 ns (rms)
n/p		300

The Lead target

Dimensions	
X, Y, Z (external dimensions)	80x80x60 [cm^3]
Niche dimension	55x20x20 [cm^3]
beam direction (Z-axis)	coplanar in YZ plane 10º in X-direction
Window	
Material	Aluminum alloy
Diameter	80 cm
Thickness	1.6 mm
Grid thickness	40 mm
Equivalent mass thickness	6.17 mm
Cooling & Moderation	
Material	H2O
Thickness in the exit face	5 cm

The TOF tube

Sector-Material	Thickness [mm]	Length [m]	Internal Diameter [cm]
1-Al Alloy	8.0	4.135	80
2-Stainless Steel	7.9	65.75	80
3-Stainless Steel	6.4	68.35	60
4-Stainless Steel	4.8	61.372	40
TOTAL LENGTH:		**199.607**	

CERN n_TOF: Basic Parameters

Collimators

First collimator			
Segment-Material	**Internal-External radius [cm]**	**Length [m]**	**Initial co-ordinate [m]**
1-Iron	5.5 - 25.0	1	135.54
2-Concrete	5.5 - 25.0	1	136.54
Second collimator: capture mode			
Segment-Material	**Internal- External radius [cm]**	**Length [m]**	**Initial co-ordinate [m]**
1-Borated polyethylene 5%	0.9 - 20.0	0.5	175.35
2-Iron	0.9 - 20.0	1.25	175.85
3-Borated polyethylene 5%	0.9 - 20.0	0.75	178.10
Second collimator: fission mode			
Segment-Material	**Internal- External radius [cm]**	**Length [m]**	**Initial co-ordinate [m]**
1-Borated polyethylene 5%	4.0 - 20.0	0.5	175.35
2-Iron	4.0 - 20.0	1.25	175.85
3-Borated polyethylene 5%	4.0 - 20.0	0.75	178.10

The neutron beam profile in EAR-1 (collimator for capture mode)

Energy range		**x-dimension [mm]**	**y-dimension [mm]**
1 eV - 100 eV		7.6 ± 0.5	7.2 ± 0.4
100 eV - 1 keV		7.4 ± 0.8	7.3 ± 0.6
1 keV - 100 keV		7.4 ± 1.4	7.6 ± 1.2
10 keV - 100 keV		7.9 ± 2.6	7.4 ± 2.0
100 keV - 1 MeV		7.5 ± 0.9	7.0 ± 0.7
1 MeV - 10 MeV		6.6 ± 0.5	6.4 ± 0.4
10 MeV - 30 MeV		6.4 ± 0.7	6.1 ± 0.6

CERN n_TOF: Basic Parameters

The neutron fluence in EAR-1

Energy range	Uncollimated [n/pulse/cm2]	Capture mode [n/pulse]	Fission mode [n/pulse]
< 1 eV	**2.0E+05**	**3.1E+05**	**2.0E+06**
1 eV - 10 eV	2.7E+04	4.5E+04	2.9E+05
10 eV - 100 eV	2.9E+04	4.7E+04	3.1E+05
100 eV - 1000 eV	3.0E+04	5.1E+04	3.3E+05
1 eV - 1 keV	**8.6E+04**	**1.4E+05**	**9.3E+05**
1 keV - 10 keV	3.2E+04	5.4E+04	3.6E+05
10 keV - 100 keV	3.9E+04	7.1E+04	4.7E+05
100 keV - 1000 keV	1.1E+05	2.3E+05	1.5E+06
1 keV - 1 MeV	**1.8E+05**	**3.5E+05**	**2.3E+06**
1 MeV - 10 MeV	8.3E+04	2.4E+05	1.7E+06
10 MeV - 100 MeV	2.8E+04	7.2E+04	5.1E+05
> 100 MeV	4.4E+04	1.2E+05	5.6E+05
1 MeV - > 100 MeV	**1.6E+05**	**4.4E+05**	**2.7E+06**
Total	**6.2E+05**	**1.2E+06**	**8.0E+06**

Note: 1 pulse is 7E+12 protons. Collimated fluence (fission and capture modes) is integrated over the beam surface.

Energy resolution @ 187.5 m (collimator for capture mode)

Neutron Energy	p-beam pulse width FWHM [cm]	moderation FWHM [cm]	ΔE/E
1 eV	0.0	3.0	3.0E-04
10 eV	0.1	3.0	3.2E-04
100 eV	0.2	3.3	3.5E-04
1 keV	0.6	5.1	5.5E-04
10 keV	2.0	7.9	8.7E-04
30 keV	3.4	10.2	1.1E-03
100 keV	6.2	18.0	2.0E-03
1 MeV	19.5	34.1	4.2E-03
10 MeV	61.7	16.9	6.8E-03
100 MeV	195.0	14.5	2.1E-02

The n_TOF Collaboration (*)

U. Abbondanno[20], G. Aerts[7], H. Álvarez[35], F. Alvarez-Velarde[31], S. Andriamonje[7], J. Andrzejewski[26], P. Assimakopoulos[16], L. Audouin[12], G. Badurek[1], P. Baumann[10], F. Bečvář[6], E. Berthoumieux[7], F. Calviño[33], D. Cano-Ott[31], R. Capote[3,36], A. Carrillo de Albornoz[27], P. Cennini[37], V. Chepel1[28], E. Chiaveri[37], N. Colonna[19], G. Cortes[33], A. Couture[41], J. Cox[41], M. Dahlfors[37], S. David[9], I. Dillmann[12], R. Dolfini[23], C. Domingo-Pardo[32], W. Dridi[7], I. Duran[35], C. Eleftheriadis[13], M. Embid-Segura[31], L. Ferrant[9], A. Ferrari[37], R. Ferreira-Marques[28], L. Fitzpatrick[37], H. Frais-Koelbl[3], K. Fujii[20], W. Furman[30], C. Guerrero[31], I. Goncalves[28], R. Gallino[22], E. Gonzalez-Romero[31], A. Goverdovski[29], F. Gramegna[18], E. Griesmayer[3], F. Gunsing[7], B. Haas[8], R. Haight[39], M. Heil[12], A. Herrera-Martinez[37], M. Igashira[25], S. Isaev[9], E. Jericha[1], Y. Kadi[37], F. Käppeler[12], D. Karamanis[16], D. Karadimos[16], M. Kerveno[10], V. Ketlerov[29,37], P. Koehler[40], V. Konovalov[30,37], E. Kossionides[15], M. Krtička[6], C. Lamboudis[13], H. Leeb[1], A. Lindote[28], I. Lopes[28], M. Lozano[36], S. Lukic[10], J. Marganiec[26], L. Marques[27], S. Marrone[19], P. Mastinu[18], A. Mengoni[3,37], P.M. Milazzo[20], C. Moreau[20], M. Mosconi[12], F. Neves[28], H. Oberhummer[1], S. O'Brien[41], M. Oshima[24], J. Pancin[7], C. Papachristodoulou[16], C. Papadopoulos[14], C. Paradela[35], N. Patronis[16], A. Pavlik[2], P. Pavlopoulos[11], L. Perrot[7], R. Plag[12], A. Plompen[5], A. Plukis[7], A. Poch[33], C. Pretel[33], J. Quesada[36], T. Rauscher[38], R. Reifarth[39], M. Rosetti[17], C. Rubbia[23], G. Rudolf[10], P. Rullhusen[5], J. Salgado[27], L. Sarchiapone[37], I. Savvidis[13], C. Stephan[9], G. Tagliente[19], J.L. Tain[32], L. Tassan-Got[9], L. Tavora[27], R. Terlizzi[19], G. Vannini[21], P. Vaz[27], A. Ventura[17], D. Villamarin[31], .C. Vincente[31], V. Vlachoudis[37], R. Vlastou[14], F. Voss[12], S. Walter[12], H. Wendler[37], M. Wiescher[41],and K.Wisshak[12].

[1]Atominstitut der Österreichischen Universitäten,Technische Universität Wien, Austria,
[2]Institut für Isotopenforschung und Kernphysik, Universität Wien, Austria,
[3]International Atomic Energy Agency (IAEA), NAPC, Nuclear Data Section, Vienna, Austria
[4]Fachhochschule Wiener Neustadt, W iener Neustadt, Austria,
[5]CEC-JRC-IRMM, Geel, Belgium,
[6]Charles University, Prague, Czech Republic,
[7]CEA/Saclay - DSM, Gif-sur-Yvette, France,
[8]Centre National de la Recherche Scientifique/IN2P3 - CENBG, Bordeaux, France,
[9]Centre National de la echerche Scientifique/IN2P3 - IPN, Orsay, France,
[10]Centre National de la Recherche Scientifique/IN2P3 - IReS, Strasbourg, France,
[11]Pôle Universitaire Léonard de Vinci, Paris La Défense, France,
[12]Forschungszentrum Karlsruhe GmbH (FZK), Institut für Kernphysik, Germany,
[13]Aristotle University of Thessaloniki, Greece,
[14]National Technical University of Athens, Greece
[15]NCSR, Athens, Greece,
[16]University of Ioannina, Greece,
[17]ENEA, Bologna, Italy,
[18]Istituto Nazionale di Fisica Nucleare(INFN), Laboratori Nazionali di Legnaro, Italy,
[19]Istituto Nazionale di Fisica Nucleare, Bari, Italy,
[20]Istituto Nazionale di Fisica Nucleare, Trieste, Italy,
[21]Dipartimento di Fisica, Università di Bologna, and Sezione INFN di Bologna, Italy,
[22]Dipartimento di Fisica, Università di Torino and Sezione INFN di Torino, Italy,
[23]Università degli Studi Pavia, Pavia, Italy,
[24]Japan Atomic Energy Research Institute, Tokai-mura, Japan,
[25]Tokyo Institute of Technology, Tokyo, Japan,
[26]University of Lodz, Lodz, Poland
[27]Instituto Tecnológico e Nuclear(ITN), Lisbon, Portugal,
[28]LIP - Coimbra & Departamento de Fisica da Universidade de Coimbra, Portugal,
[29]Institute of Physics and Power Engineering, Kaluga region, Obninsk, Russia,
[30]Joint Institute for Nuclear Research, Frank Laboratory of Neutron Physics, Dubna, Russia,
[31]Centro de Investigaciones Energeticas Medioambientales y Technologicas, Madrid, Spain,
[32]Istituto de Física Corpuscolar, CSIC-Universidad de Valencia, Spain,
[33]Universitat Politecnica de Catalunya, Barcelona, Spain,
[34]Universidad Politecnica de Madrid, Spain,
[35]Universidade de Santiago de Compostela, Spain,
[36]Universidad de Sevilla, Spain,

[37]*CERN, Geneva, Switzerland,*
[38]*Department of Physics and Astronomy - University of Basel, Basel, Switzerland,*
[39]*Los Alamos National Laboratory, New Mexico, USA,*
[40]*Oak Ridge National Laboratory, Physics Division, Oak Ridge, USA,*
[41]*University of Notre Dame, Notre Dame, USA.*

(*) as of December 2004.

Acknowledgements